ABSTRACT

Title of Dissertation: ESTIMATING THE SPATIAL AND TEMPORAL DISTRIBUTION OF SNOW WATER EQUIVALENT WITHIN A WATERSHED

Michael Charles Menoes, Doctor of Philosophy, 2003

Dissertation directed by: Associate Professor Kaye L. Brubaker
Department of Civil and Environmental Engineering

The goal of this research was to develop a spatial-temporal model to forecast the snow water equivalent (SWE) within a watershed. This model defined the relationship between the physical parameters of a watershed and the spatial distribution of SWE within that watershed. Many models of snowmelt runoff rely on snow depletion curves, which describe the seasonal decline of snow covered fraction and SWE, assuming some interannual uniformity of basin response. The null hypothesis associated with this research was that the spatial and temporal variability of SWE within a watershed is a random process that is independent of the physical characteristics of the watershed.

A conceptual model of spatially distributed SWE accumulation and depletion that can be calibrated and validated with spatially distributed observations was created. The effects of the physical variables and parameters on the SWE distribution within a watershed were demonstrated, and both significant and insignificant physical variables

and parameters were identified. How data were used in the calibration/validation of the model was demonstrated, including showing the benefit of additional data on model accuracy. Finally, the proper calibration and validation of the model using an actual watershed was demonstrated on three different watersheds.

Results of the research were mixed in terms of accepting or rejecting the null hypothesis. Created SWE maps and satellite images of the Upper Rio Grande Watershed visually suggested that similar SWE patterns exist for this watershed. An analysis of the data from the SNOTEL sites within the Upper Rio Grande Watershed also suggested the existence of similar interannual SWE patterns within the watershed. This analysis supports the Depletion Curve Theory.

However, an analysis of the SWE distributions for the three watersheds, performed utilizing the Kolmogorov-Smirnov Two-Sample Nonparametric Test, suggested that consistent interannual SWE patterns do not exist for the watersheds studied. This analysis contradicts the Depletion Curve Theory.

ESTIMATING THE SPATIAL AND TEMPORAL DISTRIBUTION OF SNOW WATER EQUIVALENT WITHIN A WATERSHED

by

Michael Charles Menoes

Thesis submitted to the Faculty of the Graduate School of the
University of Maryland at College Park in partial fulfillment
of the requirements for the degree of
Doctor of Philosophy
2003

Advisory Committee:

Associate Professor Kaye L. Brubaker, Chair
Professor Ralph C. Dubayah
Professor Richard H. McCuen
Associate Professor Glenn E. Moglen
Professor Rachel T. Pinker

DEDICATION

This dissertation is dedicated to my family and especially my wife, Sherri. Their encouragement, support and love have guided me through these past three years and have made the realization of this dissertation possible. Without their support, this endeavor would not have been possible.

ACKNOWLEDGEMENTS

I would like to acknowledge the guidance and friendship that Doctor Philip H. DeGroot has provided me over the years. He has helped shape me into the engineer that I am today, and it was his initial encouragement that brought me back to graduate school.

I would like to acknowledge and thank my advisor, Doctor Kaye L. Brubaker. I greatly appreciate the opportunity that she gave me by offering me an assistantship. Without the assistantship, my attendance at graduate school would not have been possible. Additionally, without her guidance, insight, support and friendship, the completion of this dissertation would not have been possible.

I would also like to acknowledge the assistance of my dissertation committee. The input, insight and friendship that I received from Drs. Richard McCuen, Glenn Moglen, Ralph Dubayah and Rachel Pinker were invaluable and greatly appreciated.

I would like to acknowledge and thank the National Science Foundation. This research was supported by the National Science Foundation grant number CMS-9733925.

TABLE OF CONTENTS

LIST OF TABLES

LIST OF FIGURES

LIST OF ABBREVIATIONS

ANOVA - standard analysis of variance

CDWR - California Department of Water Resources

cm - centimeter

Con - coniferous

CU - computational units

Dec- deciduous

DEM - digital elevation map

$\overline{e}$ - sample mean error

$\overline{e} / \overline{Y}$ - mean relative error

GIS - geographic information system

HEC - Hydrologic Engineering Center (of the Army Corps of Engineers)

HRU - hydrologic response unit

K-S - Kolmolgorov-Smirnoff

m - meters

mm - millimeters

NCDC - National Climatic Data Center

NOHRSC - National Operational Hydrological Remote Sensing Center

NRCS - Natural Resources Conservation Service

NWSRFS - National Weather Service River Forecast System

PCA - Principal Component Analysis

PRMS - Precipitation-Runoff Modeling System

SCA - snow-covered area

S_e - standard error of the estimate

SNOTEL - Snow Telemetry

SRM - Snowmelt Runoff Model

SSARR - Streamflow Synthesis and Reservoir Regulation

SWE - snow water equivalent

S_y - standard deviation of the measured data

UCSB - University of California at Santa Barbara

USDA-ARS - United States Department of Agriculture - Agriculture Research Service

USEPA - United States Environmental Protection Agency

USGS - United States Geological Survey

$\$_d$ - deviation sensitivity

$\$_r$ - relative sensitivity

MODEL PARAMETER NOTATION

Notation for Chapter 1

SWE - snow water equivalent

Notation for Chapter 2

SWE - snow water equivalent

Notation for Chapter 3

SWE - snow water equivalent

A_{REA} - watershed area (hectares)

C_{OVER} - relative ground roughness (unitless)

E_{LEV} - mean elevation (m)

F - forest cover (fraction)

T_{REE} - general type of tree (coniferous or deciduous) (unitless)

L_{AT} - mean latitude (degrees)

O_{RIENT} - orientation (degrees)

S_{LOPE} - mean slope (degrees)

T_{Avg} - daily air temperature (^{o}C)

R_{H} - relative humidity (fraction)

P_{T} - total precipitation (cm / day)

W_{S} - wind speed (m / s)

W_{O} - wind orientation (degrees)

C_C - cloud cover (fraction)

S_R - incoming solar radiation (cal / cm^2*day)

T_{Max} - maximum daily air temperature (^oC)

T_{Min} - minimum daily air temperature (^oC)

K_{CS} - received clear sky radiation (cal / cm^2*day)

A_{LB} - albedo of the snowpack (unitless)

S_h - shading factor used to reduce incoming solar radiation based upon surrounding topography (unitless)

$f_3(F)$ - factor dependent upon tree species (unitless)

C_{OUNT} - refers to the number of days since the last snowfall (days)

W_{CAN} - reduced wind speed due to forest canopy (m / s)

F_d - forest density (fraction)

R_T - portion of precipitation that occurs as rain (cm)

S_T - portion of precipitation that occurs as snow (cm)

S_{DENS} - the determined density of fresh snow (g / cm^3)

D_{EPTH} - the depth of snowpack (cm)

E_{NET} - net energy (cal / cm^2 day)

L_W - net received longwave radiation (cal / cm^2 day)

S_H - turbulent exchange of sensible heat with the atmosphere (cal / cm^2 day)

L_H - turbulent exchange of latent heat with the atmosphere (cal / cm^2 day)

P_{MELT} - advective energy derived from rain (cal / cm^2 day)

SO_H - conductive heat exchange with the underlying ground (cal / cm^2 day)

T_{SURF} - temperature of the surface of the snowpack (^{0} C)

SB - Stefan-Boltzmann constant (1.19 E^{-7} cal / cm^2 day K^4)

e_{SS} - emissivity of snow (0.97)

e_{at} - integrated effective emissivity of the atmosphere and canopy

e_a - near surface vapor pressure

c_a - heat capacity of air (0.24 cal / g ^{o}C)

r_a - mass density of air (0.0012 g / cm^3)

z_m - height at which the wind speed and air temperature are measured (cm)

z_0 - roughness height that depends on the irregularity of the snow surface (cm)

f_s - stability correction factor (unitless)

T_f - temperature factor defining the difference between the air temperature and the snow surface temperature (^{o}C)

r_w - density of water (assumed to be 1.0 g / cm^3)

c_w - heat capacity of water (1.0 cal./ /g ^{o}C)

T_{RAIN} - temperature of the rain (^{o}C)

l_f - latent heat of fusion (79.7 cal / g)

$Cold_C$ - cold content of the snowpack (cal / cm^2 day)

c_i - heat capacity of ice (0.502 cal./ /g ^{o}C)

T_{PACK} - average temperature of the snowpack (^{o}C)

MeltSWE - SWE lost from snowpack due to melt (cm of SWE)

SubSWE - SWE lost from snowpack due to sublimation (cm of SWE)

$WindSWE_{OUT}$ - SWE lost from snowpack due to wind transport (cm of SWE)

Perpwidth - perpendicular width (to the wind speed) along an HRU with which snow transport will occur (m)

$WindSWE_{IN}$ - SWE gained to a snowpack due to wind transport (cm of SWE)

H_{CRIT} - critical height of new snow (cm)

D_{ENS} - density of the existing snowpack (g / cm^3)

$AvalSWE_{OUT}$ - SWE lost from snowpack due to avalanching (cm of SWE)

$AvalSWE_{IN}$ - SWE gained to a snowpack due to avalanching (cm of SWE)

MAX_{INT} - maximum possible interception that can occur (cm of SWE)

S_{mean} - mean maximum snow load per unit area of branch (kg / m^2)

LAI - leaf area index (unitless)

Int_{SNOW} - amount of snow that is intercepted by a canopy (cm of SWE)

C_P - canopy-leaf contact area per unit area of ground (unitless)

InterSWE - amount of existing SWE that the canopy has currently intercepted (cm of SWE)

Int_{WIND} - amount of interception lost from the canopy due to wind transport (cm of SWE)

Int_{SUB} - amount of interception lost from the canopy due to sublimation (cm of SWE)

U - unloading rate coefficient (unitless)

t - time (days)

C- dimensionless loading coefficient (unitless)

Notation for Chapter 4

SWE - snow water equivalent

T_{MAX} - maximum daily air temperature (°C)

T_{MIN} - minimum daily air temperature (°C)

T_{AVG} - average daily air temperature (°C)

P_T - total precipitation (cm / day)

W_S - wind speed (m / s)

W_O - wind orientation (degrees)

S_R - incoming solar radiation (cal / cm^2*day)

R_H - relative humidity (fraction)

C_C - cloud cover (fraction)

S_{LOPE} - mean slope (degrees)

O_{RIENT} - orientation (degrees)

L_{AT} - mean latitude (degrees)

F - forest cover (fraction)

T_{REE} - general type of tree (coniferous or deciduous) (unitless)

T_{YPE} - refers to whether the HRU is an alpine or valley HRU

C_{OVER} - relative ground roughness (unitless)

Notation for Chapter 5

SWE - snow water equivalent

S_h - shading factor used to reduce incoming solar radiation based upon surrounding topography (unitless)

F_d - forest density (fraction)

$f_3(F)$ - factor dependent upon tree species (unitless)

T_f - temperature factor defining the difference between the air temperature and the snow surface temperature (^oC)

Notation for Chapter 6

SWE - snow water equivalent

S_h - shading factor used to reduce incoming solar radiation based upon surrounding topography (unitless)

F_d - forest density (fraction)

$f_3(F)$ - factor dependent upon tree species (unitless)

T_f - temperature factor defining the difference between the air temperature and the snow surface temperature (^oC)

Notation for Chapter 7

SWE - snow water equivalent

S_h - shading factor used to reduce incoming solar radiation based upon surrounding topography (unitless)

F_d - forest density (fraction)

$f_3(F)$ - factor dependent upon tree species (unitless)

T_f - temperature factor defining the difference between the air temperature and the snow surface temperature (^oC)

Notation for Chapter 8

SWE - snow water equivalent

S_h - shading factor used to reduce incoming solar radiation based upon surrounding topography (unitless)

F_d - forest density (fraction)

$f_3(F)$ - factor dependent upon tree species (unitless)

T_f - temperature factor defining the difference between the air temperature and the snow surface temperature (^oC)

P_T - total precipitation (cm / day)

T_{Max} - maximum daily air temperature (^oC)

T_{Min} - minimum daily air temperature (^oC)

W_S - wind speed (m / s)

C_C - cloud cover (fraction)

R_H - relative humidity (fraction)

S_R - incoming solar radiation (cal / cm^2*day)

Notation for Chapter 9

SWE - snow water equivalent

Notation for Chapter 10

SWE - snow water equivalent

K_{CS} - received clear sky radiation (cal / cm^2*day)

A_{LB} - albedo of the snowpack (unitless)

S_h - shading factor used to reduce incoming solar radiation based upon surrounding topography (unitless)

$f_3(F)$ - factor dependent upon tree species (unitless)

C_C - cloud cover (fraction)

T_{SURF} - temperature of the surface of the snowpack (^{0} C)

T_f - temperature factor defining the difference between the air temperature and the snow surface temperature (^{o}C)

W_{CAN} - reduced wind speed due to forest canopy (m / s)

F_d - forest density (fraction)

f_s - stability correction factor (unitless)

F - forest cover (fraction)

P_T - total precipitation (cm / day)

CHAPTER ONE

INTRODUCTION

1.1 IMPORTANCE OF SNOWMELT

This research is inspired by the fact that snowmelt accounts for 50% - 80% of the annual stream flow in many areas of the world, including the Sierra Nevada, the Rockies, the Alps, the Andes, and the Himalayan Mountains (Ferrris and Congalton, 1989). Large quantities of snow, associated with rapid melting is often associated with severe flooding, while a small snowpack often results in summer water shortages. By monitoring and estimating the spatial and temporal variation of the snow pack until the end-of-winter snow accumulation, and through the ablation period, it is possible to construct worst case scenarios of spring floods, or summer water shortages early in the season. Thus, to better be able to forecast these events, a means of estimating the snow content during the accumulation season and through the melt season is needed.

In addition, water derived from snowmelt is being used for the generation of hydropower, irrigation, and domestic and industrial water supply. In the western United States, in 1980, the annual value of snowmelt water was estimated between six and sixty billion dollars (Castruccio et al., 1980). This same study indicated that a mere 1.5 percent increase in Colorado River forecast accuracy would result in a net economic benefit of 5.1 million dollars.

Two important concepts that will appear throughout this dissertation shall be defined at this time. These two concepts are snow water equivalent, or SWE, and snow-

covered area, or SCA. SWE can be defined as the depth of water that would result from the complete melting of the snow water covering a unit area. By definition, SWE involves the measurement of a three-dimensional quantity. However, it is recorded as a depth. SCA can be defined as the portion of the unit area that is covered by snow. SCA involves the measurement of only a two-dimensional quantity. Consequently, SCA is an easier quantity to observe than SWE.

1.2 EXISTING SNOWMELT MODELS

Empirical snowmelt runoff models have traditionally been used for operational runoff volume forecasts. However, these models supply little information on the timing, rate, or magnitude of discharge. In addition, these models often are of little use in situations outside of the original conditions for which they were set up. Attempts to more accurately predict runoff associated with snowmelt have led to the development of physically based, spatially distributed snowmelt models. These models require information concerning the spatial distribution of snowpack water storage. As Elder (1989) points out, however, a widely suitable method does not currently exist to directly map SWE within a watershed. Konig and Sturm (1998) also concluded that it is currently practical to use remote sensing (aerial photography and satellite imagery) to determine the extent of snow, or SCA, but not the depth of snow, or SWE. A spatially distributed model should be calibrated and validated with spatially distributed data, and the lack of knowledge as to the necessary snow cover data required to perform this task remains a significant obstacle.

Several snowmelt runoff models, such as the Snowmelt Runoff Model (SRM), utilize the depletion curve theory. Depletion curve theory describes the seasonal decline of snow covered area (SCA) as a function of time or accumulated melt. A consequence of using snowmelt runoff models which utilize the depletion curve theory is that assumptions must be made as to the degree of uniformity of basin response from year to year. These assumptions have yet to be properly addressed in terms of relevance and accuracy.

The spatial distribution of snow cover can be measured with the aid of remote sensing tools. However, as Cline (1998) points out, direct measurement of SWE by remote sensing is not yet possible. As a result, the measurement of the spatial distribution of SWE and total snow volume within a basin must be performed by intensive field sampling to capture the large spatial variability that exists in basin snowpacks. Economic and safety limitations generally restrict the number of field samples that may be obtained (Elder, 1989). Consequently, the task of determining the volume and distribution of SWE within a watershed remains difficult.

1.3 ADVANCING THE STATE OF THE ART

In order to advance the field of physically based, spatially distributed snowmelt models, new developments in the estimation of SWE are required. These advances should be based upon the physical parameters of the watershed in study and should be able to define the heterogeneous snow pack of the watershed, which changes markedly in time and space.

The successful development of a model capable of accomplishing the objectives, as described in the abstract, will hopefully progress the state of the art in the field of snowmelt-runoff forecasting in two ways. The first way will be accomplished by attempting to provide the spatially distributed snowmelt models with a more accurate depiction of the spatial and temporal distribution of SWE and total snow volume within a watershed, thus allowing for more accurate predictions from these snowmelt models.

Second, models can provide insight into how the spatial distribution of SWE affects watershed response by providing estimates of runoff volume, over time, based on projected depletions from different portions of the watershed. Because both SWE and energy are nonuniform, the delivery of meltwater to the soil and as surface runoff is also nonuniform. Just as the spatial distribution of rainfall affects watershed response, so does the spatial distribution of melt water input.

CHAPTER TWO

LITERATURE REVIEW

2.1 INTRODUCTION

This chapter provides an overview of current literature addressing the spatial and temporal distribution of SWE within a watershed. The following pages provide a brief summary of recent work being performed in this field, which will provide the reader with an introduction to pertinent concepts regarding the objectives and methodology associated with this study. The topics discussed in the following sections relate to the goals of the proposed research and indicate current practices involved in the methodology of snow modeling.

2.2 CONCEPTUAL MODELS OF SWE DISTRIBUTION

The goal of the proposed research was to develop a spatial-temporal model to forecast the snow water equivalent (SWE) within a watershed. The following paragraphs describe current undertakings aimed at accomplishing this same task. An understanding of these current efforts will help in the formulation of the proposed model.

Liston (1999) noted that models used to simulate snowmelt commonly represent study areas by a collection of finite areas or grid cells. He maintained that within each grid cell, three fundamental features are required to describe the evolution of seasonal snow cover from the end of winter through spring melt. These are the within-grid SWE

distribution, the gridcell melt rate, and the within-grid depletion of snow covered area. Liston noted that this relationship is borrowed from Cline (1998), and demonstrated how knowledge of any two of them allows generation of the third. Liston also indicated that numerous studies have noted that the depletion of snow-covered area is strongly related to runoff, and that such an accounting for the snowmelt volume within each grid cell could be used directly as input for sophisticated snowmelt models.

Skaugen (1999) developed theoretical means to estimate the mean SWE over an area by analytically combining the frequency of precipitation events and information from satellite images. He reported that the mean areal SWE can be estimated by modeling the snow accumulation process in time and space as sums of random gamma distributed variables. He stated that from snow pillows and precipitation gauges, the value of daily accumulated precipitation/snow has been found to be well represented by a two-parameter gamma distribution.

Luce, Tarboton, and Cooley (1998) presented and tested a physically based lumped model of snowpack evolution for a small watershed that uses a depletion curve parameterization to relate the basin-averaged SWE to SCA. They also presented a method for deriving the depletion curve from snowpack measurements at peak accumulation. Their work showed that through the use of an areal depletion curve, it was possible to obtain lumped snowmelt model simulations that agree well with distributed models and observed data.

Swamy and Brivio (1996) used Landsat Multispectral Scanning System and Thematic Mapper in order to evaluate the SCA variation within an alpine catchment.

DEM, slope and aspect parameters were developed as part of their analysis. The Landsat Multispectral Scanning System has a spatial resolution of about 79 meters, while the Thematic Mapper has a spatial resolution of 30 meters. Five sets of data were analyzed covering the April to July period. A second-order polynomial was used to approximate the depletion of SCA and to estimate the daily areal extent of SCA. The results indicated that approximating snow depletion curves for various elevation zones using a second-order polynomial fit was encouraging.

Cline, Bales, and Dozier (1998) presented a modeling approach that couples information about SCA from remote sensing with a distributed energy balance model to calculate the spatial distribution of SWE in a mountain basin at the peak of the accumulation season. They borrowed upon the earlier work of Martinec and Rango (1981) to define a mathematical relationship between SWE and energy exchange as

$$SWE_i = f(D,E) \tag{2-1}$$

where SWE_i is the snow water equivalent associated with grid cell i, D is the duration of snow cover at grid cell i, and E is the energy exchanges occurring at grid cell i. The modeling approach presented here produced an estimate of the magnitude and distribution of SWE in the test basin at peak accumulation that compared well to field measurements that had been obtained as part of an earlier study.

Konig and Sturm (1998) presented a descriptive method for mapping the end-of-winter snow distribution in the arctic using aerial photographs taken during the melt. They believed that the photos show a distinctive number of snowmelt patterns that arise reliably year after year, and demonstrated that data and results from an energy balance

melt model indicate that the patterns are not caused by differential melt but instead represent areas of distinctive end-of-winter snow depth. The results indicated that these snowmelt patterns can be used to map the end-of-winter snow distribution for any basin, providing that the basin has sufficiently smooth topography.

2.3 EFFECTS OF PHYSICAL VARIABLES ON SWE

One of the objectives of the proposed research was to demonstrate the effects of the physical variables and parameters on the SWE distribution within a watershed. The following paragraphs describe research relating physical properties of a watershed with the distribution of SWE. A better understanding of this relationship could ultimately lead to better accuracy for snow distribution modeling.

Donald, Kouwen, and Pietroniro (1995) looked to create a model for land cover-based snow depletion curves for short grass, ploughed fields, and deciduous forests. The basin being studied was divided into different subunits based upon homogeneous land cover. To develop the model theory, they drew upon previous studies that have indicated that maximum accumulation depth is a function of vegetation, elevation, and topography. They also noted that these same studies indicate the tendency of the snowpack to follow consistent patterns from year to year.

Copland (1998) evaluated snow cover on an alpine glacier. He states that the improved evaluation of snowpack conditions may be possible by combining terrain zonation (division of the glacier into areas of similar terrain) with elevation-based regression predictions. He used a digital elevation model (DEM) to calculate the terrain

parameters of elevation, slope angle, aspect, profile curvature, and planform curvature. He anticipated that these terrain topographic features will help to control the snow cover distribution. His study shows that in terms of estimating SWE, elevation is the most important terrain parameter.

Elder, Dozier, and Michaelsen (1989) discussed the relationship between snow accumulation and terrain features and vegetation. They drew upon past studies that had shown snow accumulation to be dependent on vegetation and topographic roughness from small-scale localized effects to large-scale terrain features such as ridges and valleys.

Konig and Sturm (1998) believed that abrupt changes in snow depth arose from two basic processes: flow separation of wind from the ground and the snow-holding capacity of the landscape. They argued that topography is the primary factor that controls the snow distribution, and thus, snow patterns should remain the same from year to year, assuming that the wind direction does not change significantly.

Derksen et al. (1999) sought to relate North American prairie snow cover to archived atmospheric teleconnections (climatic anomaly that is a distant consequence of another climatic anomaly, such as the El Nino-Southern Oscillation). Using a rotated principal components analysis (PCA) of pentad resolution imagery, they hoped to identify a relationship between atmospheric patterns and prairie SWE and SCA. This study produced no evidence to support snow cover as a forcing variable on atmospheric circulation. The study also explored time lagged correlations between SWE distribution, SCA extent, and atmospheric teleconnections. Their study concluded that

total prairie SWE and SCA are poorly autocorrelated over time (based upon a monthly time series).

Hellstrom (1999) developed a pragmatic procedure for measuring and modeling the effects of forest cover on snow depth. He explored the magnitude of longwave and shortwave radiation, precipitation, and wind speed beneath different types of forest cover. Based upon his findings, Hellstrom developed sub-models for simulation of sub-canopy radiation, wind speed, and precipitation, which can be incorporated into remote sensing image interpretation and numerical models.

Shook, Gray and Pomeroy (1993) used fractal geometry as a basis for developing a relationship for the area-frequency and perimeter-area characteristics of soil and snow patches that form during ablation. They concluded that snow patches were not random and that their size distribution is predictable, such that the perimeter-area ratio of the soil and snow patches decreased with increased patch size.

Yamazaki and Kondo (1992) developed a snowmelt and heat-balance model in forested areas. They developed a two-layer model. The first layer described the effect of canopy on the heat balance and wind-speed profile, and the second layer incorporated this information into determining snowmelt.

Liston and Sturm (1998) developed a snow-transport model which described the interactions between wind, vegetation and topography, and their effect on the distribution of SWE. Their model attempts to divide the domain into blowing-snow source and sink regions based on topography and vegetation characteristics. They warn that their model does not take into account the affects that tree stands have on blowing

snow, and thus indicate that the model is not applicable to forested areas.

2.4 DETERMINATION OF THE EXTENT OF REQUIRED DATA

Another one of the objectives of the proposed research was to show the benefit of additional data on model accuracy and when and where to collect the data. The following paragraphs describe studies which dealt directly with the amount of spatial and temporal data required for accurate research results. A better understanding of the types and amount of required data will help in model formulation.

Liston (1999) noted the interactions among weather, climate, hydrology, and ecosystems. He maintained the importance of daily observations of atmospheric and hydrologic processes and their affects on SCA. In this regard, Liston stated that "data obtained at frequencies less than daily still are valuable but will contribute to errors resulting from accumulation and ablation events that occur at higher frequencies."

Skaugen (1999) used snow courses as a data source for his research. He briefly discussed some previous studies that made recommendations for snow course sampling. These suggestions included: sampling with at least 50 meter to 100 meter intervals in order to avoid redundant information; in order to double the precision of the mean, approximately five times the number of sampling points is needed; and snow courses which are surveyed as a straight line or as a circle produce the smallest standard error.

Konig and Sturm (1998) mapped the end-of-winter snow distribution in the arctic based upon a number of distinctive snowmelt patterns that were associated with topography. They determined that the snow depths in individual patterns did not

correlate well with one another. As a result, they decided that direct snow depth measurements in each type of identified pattern was necessary to assign values to patterns for each year.

Williams and Tarboton (1999) developed an energy driven snowmelt model that is topographically dependent. Their model differs from most other models in that it used direct measurements of melt to drive the model, rather than utilizing meteorological variables to estimate melt. For their model simulations of a hypothetical basin, five index points (to collect melt data) were deemed sufficient for their small study area (~ 40 Ha.). The authors go on to say that they have not yet determined the index point density required for larger study areas. They claim that this is a question for further research related to the scale and variability of snow accumulation and melt.

2.5 CALIBRATION AND VALIDATION OF MODELS

An additional research objective was to calibrate/validate the proposed model using an actual watershed. The following paragraphs discuss calibration efforts taken during several studies. A better understanding of the different calibration/validation methodology could allow for greater model flexibility.

Skaugen (1999) calibrated his model using an existing model called HBV. The HBV- model is a commonly used rainfall-runoff model in the Nordic countries and includes a snowfall routine that accounts for the development of the snowpack. Skaugen claimed that previous studies had calibrated the HBV-model for all of the catchments within his study basin.

Donald, Kouwen, and Pietroniro (1995) performed snow surveys of the their study area. The surveys were conducted on sixteen different days during the course of two separate winters. The data were used to establish empirical snow cover distribution curves to which the modeled snow cover depletion curves were compared.

Elder, Dozier, and Michaelsen (1989) performed an extensive field program to measure SWE within their study basin. The program resulted in hundreds of depth measurements used to validate the results of the developed accumulation model.

Cline, Bales, and Dozier (1998) chose to study the same basin as had Elder, Dozier, and Michaelsen (1989). As a result, Cline et al. calibrated their model based upon the field data that had been collected for the earlier study and compared the modeled total basin volume of runoff to the volume of runoff predicted using Elder's model.

Liston and Sturm (1998) developed end-of-winter snow distribution maps that were a combination of ground-based depth and density measurements and aerial photographs. Three sets of aerial photographs were taken for each study year. For each of the three sets, maps were drawn outlining the snow-vegetation boundaries, to which the SWE observations were added. Analysis showed that the map could be used to extrapolate snow depth data where no direct measurements had occurred. This map was used to compare the accuracy of model simulation results.

2.6 INPUTTING THE SWE MODEL INTO AN EXISTING WATERSHED RUNOFF MODEL

Ultimately, it is hoped that the proposed SWE model will act as a more accurate input for runoff models predicting stream discharge. The following paragraphs discuss efforts taken to incorporate more accurate SWE information into runoff models.

Swamy and Brivio (1997) developed a model to approximate snow depletion and to estimate daily snow cover areal extent for three different elevation zones within their study basin. This model was then used as input for the Snowmelt Runoff Model (SRM) to predict stream flows.

Although not actually proceeding in this manner, Liston (1999) discussed that the calculated snowmelt volume within each model grid cell could provide the meltwater inputs to a land surface hydrology model. He stated that the resulting hydrographs could be compared to observed river and stream discharges, providing a validation tool for assessing the snow evolution simulation.

2.7 THE TREATMENT OF SNOW IN CURRENT FORECAST MODELS

The National Weather Service River Forecast System models snow accumulation and ablation by means of the SNOW-17 snow model. The SNOW-17 operation is a snow accumulation and ablation model developed by the Hydrologic Research Laboratory of the Office of Hydrology (Anderson, 1973). The model is conceptual, each physical process affecting snow accumulation and snowmelt is mathematically represented in the model. The current version of the model is

essentially the same as that described by Anderson (1973).

There are six major parameters in the snow cover model, the most important of which is the areal depletion curve which is not a single-valued parameter. There are also six minor parameters in the snow model. The user's manual for this model suggests that most of the effort during calibration should be devoted to determining the proper value of the major parameters. The model uses air temperature as the index to snow cover energy exchange. The manual explains that the two reasons for this are: 1) air temperature data are normally readily available from both climatological and operational hydrometeorological networks; and 2) it has been shown in many studies that air temperature is probably the best single index to areal snow cover energy exchange.

In the SNOW-17 snow model, the excess liquid-water is first lagged and then attenuated. Lag is a function of the water-equivalent of the ice portion of the snow cover, and the excess liquid-water. The attenuation part of the liquid-water transmission process uses a withdrawal rate which is the portion of the excess liquid-water which drains from storage within the snow cover during a given time interval. The manual states that the functional forms of the equations used to determine lag and attenuation were developed by plotting experimental data and using regression analysis.

Although the manual states that each of the physical processes affecting snow accumulation and snowmelt is mathematically represented in the model, there are several physical processes not explicitly included in the model. These processes are: water vapor transfer, interception of snow, and redistribution of snow. The manual

reports that these processes were not included in the model because an adequate quantification of these processes would require additional data that may be difficult to obtain. The manual also claims that utilization of the areal depletion curve helps to incorporate the effects of these processes.

The manual also describes some of the shortcomings of the SNOW-17 snow model. One such example is : if a watershed is subdivided into too many parts, it becomes difficult to determine reasonable unique parameter values based solely from a single output hydrograph. Additionally, the manual states that the model gives best results when day to day and year to year variability in meteorological conditions affecting snow cover accumulation and energy exchanges are small. The following quote from the manual indicates this fact.

> "The distribution of the snow cover during the accumulation period is influenced by topography, vegetation cover, storm type, and wind conditions. Because these factors are stationary or similar from year to year, the snow cover accumulation patterns are also similar. Snowmelt patterns are influenced by topography, vegetation cover, and weather conditions and are also similar from year to year. Because of these similarities in snow accumulation and melt patterns, each area should have a reasonably unique areal depletion curve."

This quote implies that there exist interannual similarities in the distribution of SWE from year to year within a watershed. However, the literature does not adequately address this topic as to the validity of the statements made by the user's manual.

2.8 COMMON THEMES THROUGHOUT THE LITERATURE

Several themes emerge from the literature review that have a direct bearing on the proposed research. The first theme is that new methods are being developed to

increase the accuracy of SWE estimations within a basin. An important note, however, is that these methods provide information on the spatial distribution of SWE after the end of the melt season. Since these studies, such as the ones performed by Liston (1999), Konig and Sturm (1998), and Cline, Bales, and Dozier (1998) do not provide the critical SWE information during the accumulation and ablation period, these methods provide little use in present year forecasting.

One of the goals of many of these new methods was to provide past data that could possibly be used in future forecasting. This can be summed up in a quote from Cline (1998): "Although the post facto determination of SWE distributions might appear to be too late for forecasting the timing, rate and magnitude of snowmelt runoff, it is conceivable that similarities in SWE patterns within basins from year to year would make back-calculated SWE estimates from previous years useful for current forecasting."

A second theme involves the collection of data. The necessity of an abundance of spatially distributed data to describe the spatial and temporal variability of SWE within a watershed is acknowledged. The difficulty in acquiring this data is also acknowledged. From a spatial standpoint, efforts are made to minimize the amount of field surveying required. Some studies, such as the one performed by Cline (1998), perform no surveys at all. The sources of data for Cline's study was a time series of SCA from remote sensing measurements, a meteorological record during the snowmelt season, and a DEM of the watershed. Some studies, such as the one performed by Elder, Dozier, and Michaelsen (1989), limit the amount of snow surveying required by

limiting the size of the watershed in study. Some studies, such as the one performed by Luce, Tarboton, and Cooley (1998), select watersheds that have been the site of many previous hydrologic investigations.

A third theme is that the studies indicate some consistency in the spatial distribution of snow, or SWE from year to year within a variety of study areas. As a result of the research performed by Donald, Kouwen, and Pietroniro (1995), it was concluded that the snowpack at Waterloo, Ontario, had a tendency to follow consistent patterns from year to year. These findings, they argued, were consistent with a study performed in 1991 by Burkard that indicated that a significant difference did not exist in same-type land unit snow cover distributions from site to site in southern Ontario.

In addition, the spatial variability of SWE is, to some undetermined degree, affected by the surrounding physical parameters of the study area. Studies performed by Hellstrom (1999), Copland (1998), Konig and Sturm (1998), and Donald, Kouwen, and Pietroniro (1995) showed that the topography of the study area directly affects the snow cover distribution.

CHAPTER THREE

MODEL DEVELOPMENT

3.1 INTRODUCTION

As previously mentioned, the goal of this research is to develop a spatial-temporal model to predict the spatial distribution of SWE within a defined region, such as a watershed. This chapter presents the design goals of the model, pertinent information regarding the theory behind the model development, and the derivation of the equations that define the model.

3.2 MODEL DESIGN GOALS

The design goals of the model are: simplicity, physically based, and distributed over a study area or watershed. The main goal of the model is simplicity, in terms of both required data input and operation. An attempt has been made to limit the required input to readily accessible meteorological data so that the model can be easily used without being restricted by unavailable data. Additionally, an attempt has been made to simplify the complex physical processes responsible for the spatial and temporal variability of SWE within a watershed. Simplifying these processes will reduce the required number of input variables, while not necessarily compromising the accuracy of the model. This last point is often discussed in the literature and summed up well by McCuen (2000): “Yet, studies have shown that accuracy is not highly correlated with model complexity. Increasing the complexity of a model does not necessarily imply that

the prediction accuracy increases significantly."

The second design goal is that the model should be physically based so that the model becomes applicable to all watersheds while minimizing the need to calibrate a large number of parameters at each location. This characteristic helps to reduce the uncertainty that may be introduced during calibration, from such processes as subjective optimization.

The final design goal is that the model must allow inputs that are spatially distributed over a watershed. A distributed model is required to account for the spatial variability within the watershed. This characteristic is required to help test the hypothesis that spatial and temporal patterns of SWE exist within the watershed, and these patterns remain similar from year to year.

3.3 BACKGROUND

It is important to emphasize the drivers of spatial variability in SWE (spatially varying snowfall, redistribution of snow, spatially varying melt, etc.). Part of this variability may be explained by fixed features of the watershed (topography, vegetation, etc.) while part may be explained by the directionality of weather systems (precipitation, wind, etc.). The former can be assumed to be fixed, at least on a seasonal time scale, and the latter is likely to follow certain patterns typical of weather systems for a given region and season. There will still be some pure randomness in the SWE distribution, but ample evidence of certain basic patterns will be evident.

The conceptual model describes the response of the snowpack to these drivers. The model output will be of a nature that it can be calibrated and validated with spatially-distributed observations of SWE. The model will not be calibrated by inputting its results into an existing runoff model and comparing streamflow totals. As Bloschl discusses (1998), the common practice of calibrating a model with a large number of free parameters to a single observed variable, such as streamflow, can produce the correct answer for the wrong reasons, and can mask physically unrealistic treatments or compensating errors in the mathematical model.

The model will need to work in the forecast mode. It is likely that only large-scale average precipitation and temperature forecasts would be available; therefore, the model must contain provisions for downscaling or distributing the forecast to the spatially-distributed watershed subunits. The method for performing this task will be discussed in a later chapter.

As previously mentioned, Liston (1999) has noted that models used to simulate snowmelt commonly represent study areas by a collection of grid cells. This approach will also be utilized in the development of the model. The model will be based upon hydrologic response units (HRUs), that are flexible in shape and scale. Donald et al. (1995) define an HRU as a region in a watershed that is considered to be homogeneous, having a distinct hydrological response. Based upon this definition, it is proposed that a watershed be discretized into elements that shall be sized to accomplish the following: (1) to be approximately homogeneous in vegetation and topography, and (2) to allow for an approximately nonvarying value of SWE within each element. The topographic

features of the watershed will help determine the element size based upon the first criterion, while both topographic and meteorological parameters will help determine the element size based upon the second criterion. Since topographic characteristics will remain constant in time, under the model, once a network of elements have been established for a specific watershed, they can remain constant from year to year.

Although topographic characteristics of a watershed remain constant in time, the model will be capable of simulating some land use changes. Additionally, forecasting could also be performed to model the effects of some land use changes on snow accumulation and ablation within a watershed. Deforestation is a good example of such a land use change.

The next step in model development is to formulate the equations governing the accumulation and ablation of SWE over a unit area. The model will be based upon a mass balance approach. A three-dimensional mass balance equation will need to be solved to determine the SWE within each element. This equation will include the effects of precipitation, sublimation, transport, and surplus water input. The general form of the equation can be written as follows:

$$dSWE / dt = f(precipitation, sublimation, transport, surplus\ water\ input) \quad (3\text{-}1)$$

where *precipitation* includes both rain and snow, *transport* includes wind effects and avalanching, and *surplus water input* includes both infiltration and runoff. The concept of surplus water input is described by Dingman (1994) as largely determining the amount and timing of streamflow and ground-water recharge. Figure 3-1 shows the mass balance of a general element.

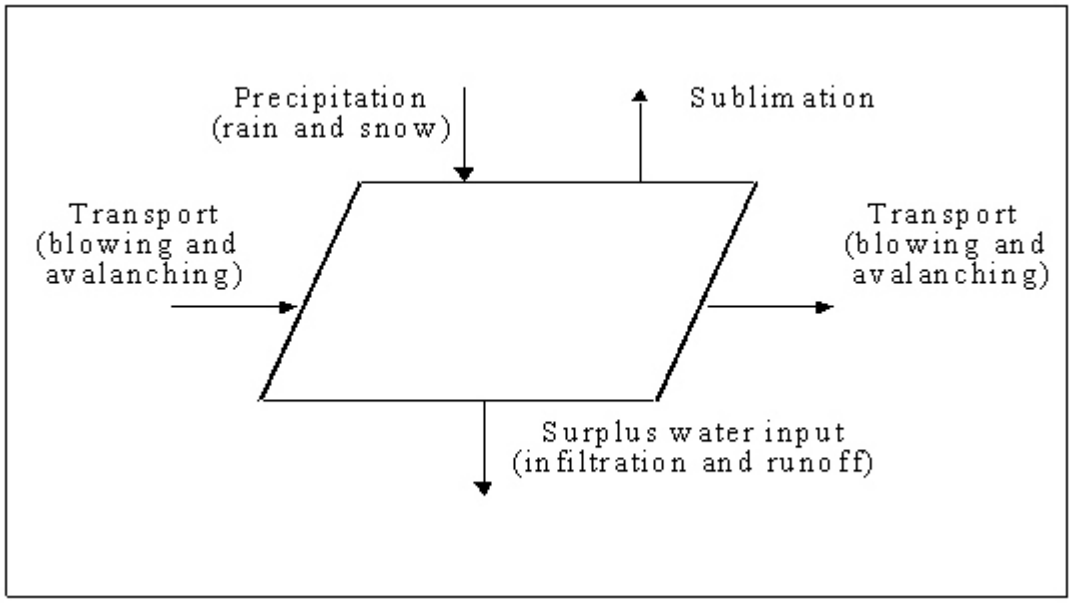

Figure 3-1. Mass Balance of a Hypothetical HRU

To solve Eq. (3 - 1), additional equations must be included for each of the predictor variables found in this equation. As an example, the generalized equation for transport is as follows:

$$transport = f(wind\ speed\ and\ direction,\ vegetative\ cover,...) \quad (3\text{-}2)$$

The complexity of these additional equations includes determining the number of significant predictor variables, realizing that these predictor variables can be functions of both space and time, and that additional equations may need to be developed for some of these predictor variables. Energy exchange is an example of this last point. This parameter will be a predictor variable required to estimate surplus water input, and itself is made up of many predictor variables such as cloud cover, snow albedo, etc.

Once the equations defining SWE have been developed, the simulation model will be constructed. This model will produce a time series of SWE maps for a particular watershed. These maps will demonstrate the spatially varying SWE distributions within the watershed for different time periods.

3.4 THE HRU SUBDIVISION PROCESS

Recent research has incorporated the concept of HRU subdivisions for the purpose of watershed analysis. The methods used to subdivide watersheds as part of these studies shall provide structure for the methodology used by the proposed model.

Jeton and Smith (1994) indicate that digital data were used to develop a GIS data base and HRU classification for the American River and Carson River basins. The following criteria were used by the authors in delineating HRUs: (1) Data layers are hydrologically significant and have a resolution appropriate to the watershed's natural spatial variability, (2) the technique for delineating HRUs accommodates different classification criteria and is reproducible, and (3) HRUs are not limited by hydrographic-subbasin boundaries. The article points out that HRUs so defined are spatially noncontiguous.

For the Jeton and Smith study, HRUs were delineated assuming that watershed properties could be grouped according to hydrologically significant characteristics even if the corresponding areas do not lie within contiguous areas. The watershed was first divided into 100-by-100-meter areas or representative cells, and all possible combinations of five data layers (altitude, land cover, soil, slope, and aspect) for a given

basin were identified and tabulated. Each cell was then characterized by a pattern or combination of the five data layers.

The study indicates that to determine the sensitivity of hydrologic response to watershed characteristics, an analysis of individual HRU water and energy budgets is required. Such issues as the optimum resolution of source data, and determining the minimum number of HRUs required to model basinwide hydrologic processes need to be addressed by further research.

Mashriqui and Cruise (1997) used the modeling strategy of the "grouped response unit" concept whereby land classes were identified within similar regions and used as hydrologic and sediment response units. These grouped response units were called computational units. The computational units (CUs) were defined on the basis of homogeneity of topography and soil characteristics using frequency histograms of relevant parameters as objective criteria. The CUs were based on topographic and climatological similarities.

The authors suggested that perhaps the most important step in the modeling process was the determination of the computation units. The subdivision process began with the basic soils map. This map was then modified by deleting the minor secondary soil series that occurred within an area of a dominant soil type. The soils and slope images were then overlayed. The goal was to use these images to divide the Rosario Basin into a minimum number of homogeneous computation units. The authors indicate that this was done interactively using the Map II software system. Frequency histograms of slope values were then computed for each CU in order to determine the

distribution of slopes across the CU. The goal was to obtain histograms that were distributed about the dominant slope value with a minimum amount of variance.

Gorokhovich, et al. (2000) indicated that one of the main types of GIS models used in hydrology include hydrologic response units (HRUs). They went on to define HRUs as hydrologically similar areas derived by overlaying land use properties and soil properties. Hydrologic properties for this study were runoff and infiltration, derived from combinations of land use classes and hydric soil groups. All spatial analysis was done using ARCINFO, produced by ESRI.

Creation of HRUs required an overlay procedure to combine several datasets: soils, land use, and slope. The resulting dataset looked like a mosaic consisting of multiple HRU planes, each with a single runoff value. Precipitation data was then paired to each HRU to estimate runoff from each HRU.

Kouwen, et al. (1993) utilized the methodology of subdividing a watershed by grouping hydrologic response units that have similar response characteristics on the basis of classified land-cover maps. These are regions that have a locally uniform hydrologic response to meteorologic stimuli. The authors went on to point out that the number of HRUs required for a watershed varies with basin characteristics.

The authors argued that, in practice, the number of HRUs that can be used is limited by data availability. For example, prediction of a hydrograph using a sparse rain gauge network is unlikely to improve by applying uncertain interpolated rainfall estimates to a collection of HRUs no matter how well defined they are. In fact, the forecast may degrade due to model errors arising from calibrations with limited data.

Davis, et al. (1992) used ground-based field estimates to estimate regional fluxes and biophysical conditions by subdividing the study area into HRUs and extrapolating field measurements. The study region was stratified into 14 different terrain units based on land use and land cover and topographic variables that were hypothesized to have strong influence on surface biophysical properties. The authors stated that the stratification of land surfaces for climatological studies requires classification of the terrain into surface strata that are relatively uniform in terms of surface fluxes of energy and matter.

The authors developed various site stratification methodologies to attempt to determine the optimal way to subdivide the study area. Standard analysis of variance (ANOVA) techniques were used to test the significance of the variance reductions produced by four different site stratifications of increasing complexity.

In summary, various spatially distributed physical properties of a watershed or study area have been used in the delineation of smaller, similar response units. Some issues, such as determining the optimum resolution of source data and the minimum number of HRUs required to model a basin, need to be addressed by further research. Several studies have indicated that the subdivision process produces HRUs that can be spatially noncontiguous; the approach used in the present study required HRUs to be contiguous.

3.5 REQUIRED INPUT DATA

3.5.1 Required HRU Topographical and Land Use Data

The proposed model requires the following topographic data from each of the HRUs within the watershed: area - A_{REA} (hectares), relative ground roughness - C_{OVER} (unitless), mean elevation - E_{LEV} (m), forest cover - F (fraction), general type of trees (coniferous or deciduous) - T_{REE} (unitless), mean latitude - L_{AT} (degrees), orientation - O_{RIENT} (degrees), and mean slope - S_{LOPE} (degrees).

A_{REA} is required to determine the volume of SWE that may be transported into or out of an HRU by means of wind transport or avalanching. A_{REA} is also required to help determine the limiting size of an HRU. As previously mentioned, HRUs will be sized to allow for an approximately nonvarying value of SWE to be maintained within the HRU. Significant wind deposition within an HRU is not possible, because it will produce significant variations of SWE within the HRU. Therefore, HRUs must be sized to accommodate the average distance of snow transport for that particular terrain. Various terrain will accommodate differing snow transport distances. For example, snow transport in mountainous regions is greatly limited by topography, unlike snow transport through a prairie. Without properly sizing the HRUs, snow transport becomes inconsequential with larger size HRUs. Gray and Male (1981) provide just such distances. For mountainous terrain, Gray and Male (1981) indicate that snow transport due to blowing wind can be limited to 50 meters or less, whereas for prairies or relatively flat terrain, snow transport due to blowing snow can occur for up to 1.5 kilometers.

Relative ground roughness is required to help determine if an avalanche within an HRU is possible. Both Armstrong and Williams (1986) and McClung and Schaerer (1993) provide rules of thumb for the minimum snow depth required for avalanching to occur, which depend on the average surface roughness. The model ensures that this minimum snow depth is satisfied before avalanching can occur. Relative ground roughness is primarily determined by vegetative and soil composition. Relatively smooth ground cover requires a snow depth of 0.3 m, average terrain with some boulders and shrubs requires a depth of 0.6 m, and rough terrain with large boulders and tree stumps require a snow depth of 1.0 m.

The mean elevation is required because both the total precipitation and the temperature depend on elevation. Many literature examples, such as Elder, Dozier, and Michaelsen (1989) and Cline, Bales, and Dozier (1998) cited orographic effects on total precipitation and temperature. Tarboton and Luce (1996) discussed the importance of subdividing a watershed into elevation zones as recommended by a review of eleven different snowmelt runoff models by the World Meteorological Organization in 1986.

Forest cover, F, is a significant characteristic of an HRU. Buttle and McDonnell (1987), Davis et al. (1997), Hedstrom and Pomeroy (1998), and Hellstrom (1999), among others, discussed the effects of canopy cover on the distribution of SWE. Hellstrom (1999) indicated that modeling and field studies suggest that forest cover generally decreases received shortwave radiation at the forest floor, increases incoming longwave radiation, decreases wind speed leading to reduced turbulent heat exchanges and wind-driven snow transport, and decreases precipitation accumulation at the forest

floor.

Along with forest density, the general type of trees within the forest can be significant. Tree type refers to the species of tree and allows the modeler to differentiate between, as an example, balsam fir and jack pine. Hedstrom and Pomeroy (1998) and Pomeroy et al. (1998) discussed the importance of tree type on the maximum and actual interception totals, and canopy sublimation rates.

The mean latitude and orientation are important factors in estimating the incoming solar radiation. Dingman (1994) discussed the importance of latitude and orientation when estimating incoming solar radiation. The watershed orientation is also important in determining SWE transport caused by the prevailing wind direction. Copland (1998) examined the effect that orientation has on the snow cover over an alpine glacier.

The mean slope can have a significant impact on many processes regarding SWE distribution. Slope affects incoming solar radiation. Dubayah and Rich (1995) discussed how variability in ground slope can create strong local gradients in solar radiation. Slope can also affect variations in snow depth induced by wind drift. Additionally, slope is the most important topographic factor in determining avalanche possibility. As Armstrong and Williams (1986) point out, a 26^0 slope represents the angle of repose for granular substances such as sand and dry, unbonded snow; therefore, this is the minimum ground slope in which an avalanche can occur.

3.5.2 Required Meteorological Data

The model was designed to be driven by meteorological inputs of average daily air temperature T_{Avg} (°C), relative humidity R_H (fraction), total precipitation P_T (cm / day), wind speed W_S (m / s), wind orientation W_O (degrees), cloud cover C_C (fraction), and incoming solar radiation S_R (cal / cm^2*day).

Some meteorological stations report maximum daily air temperature, T_{Max} (°C) and minimum daily air temperature, T_{Min} (°C), rather than the average daily air temperature. When this is the case, average daily air temperature is computed as follows:

$$T_{Avg} = (T_{Max} + T_{Min}) / 2 \qquad (3-3)$$

If average daily air temperature is available, the model bypasses Eq. 3-3.

Many meteorological stations do not record relative humidity. When these data are not available, the model estimates relative humidity by means of the following equation:

$$RH = \frac{6.11 \times Exp((17.3TMin) / (TMin + 237.3))}{6.11 \times Exp((17.3TAvg) / (TAvg + 237.3))} \qquad (3-4)$$

This equation comes from Thornton et al. (1997), in which the assumption is made that T_{Min} is a reasonable surrogate for the dew-point temperature. If relative humidity data are available, the model bypasses Eq. 3-4.

Many meteorological stations also do not record incoming solar radiation. When these data are not available, the model estimates incoming solar radiation by

means of the following equation:

$$SR = Sh \times K_{cs} \times (0.355 + (0.68 \times (1 - CC))) \times Exp\left(-2 \times f3(F)\right) \times \left(1 - ALB / 100\right) \quad (3\text{-}5)$$

where S_R is in (cal / cm^2 day), K_{CS} is the received clear sky radiation, A_{LB} is the albedo of the snowpack, S_h is a shading factor used to reduce incoming solar radiation based upon surrounding topography, $f_3(F)$ comes from Dunne and Leopold (1978), and is a continuous function dependent upon tree type which relates forest canopy density, F, to the ratio of solar radiation received under forest to that in the open. K_{CS} comes from standard equations for celestial geometry accounting for attenuation of diffuse and direct solar radiation in the atmosphere. K_{CS} takes into account the time variable transmissivity of the clear sky, which is dependent upon the near surface vapor pressure (e_a). Dingman (1994) provides a complete derivation of K_{CS}. If incoming solar radiation data are available, the model bypasses Eq 3-5.

Albedo is defined as the ratio of the reflected radiation to the incident radiation. The albedo governs the amount of radiant energy absorbed by a snowpack and ultimately influences the rate of melt. Gray and Male (1981) made a distinction between the albedo for a deep mountain snowpack and a shallow, prairie snowcover. They borrowed on previous work performed by the Army Corps of Engineers which showed that gradual changes in albedo occur on a deep mountainous snowpack while rapid changes in snowpack albedo occur on a shallow, prairie snowpack. This difference is a result of the exposed ground associated with patchy snowcover. Gray and Male (1981) provided a figure with plots of albedo data for both a deep mountain

snowpack and a shallow prairie snowcover. This figure was copied and used to derive the formulas for the albedo that the model uses. Figure 3-2 shows the copied plots of the albedo data and the curve fitting involved in formula derivation. Curve fitting was accomplished by means of Microsoft Excel Solver, which uses a generalized reduced gradient nonlinear optimization code.

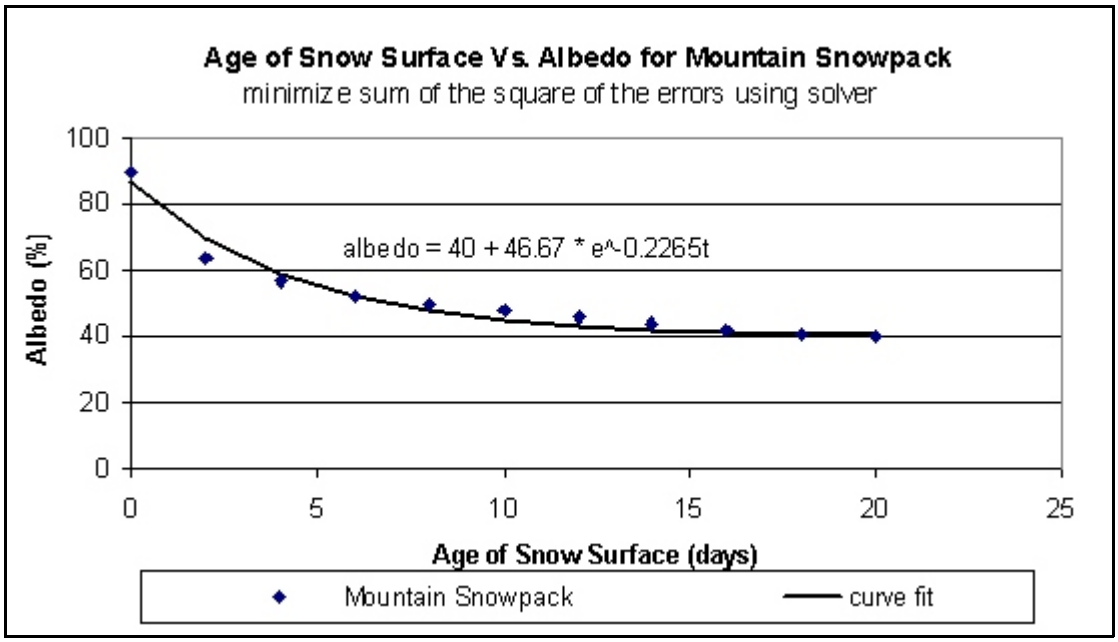

a)

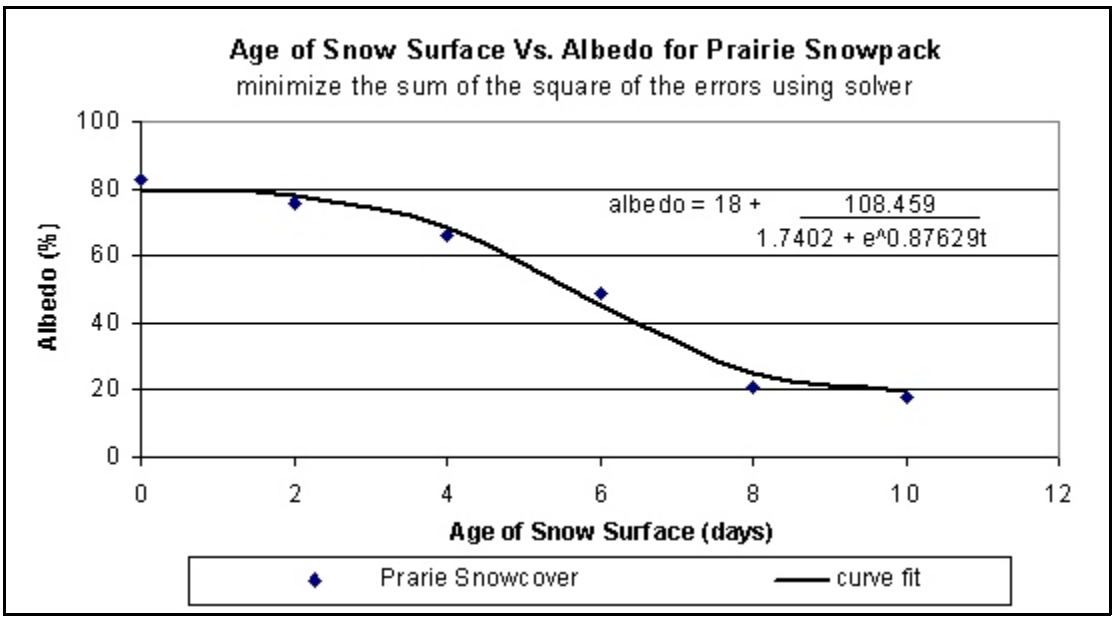

b)

Figure 3-2 Determination of snowpack albedo as per Gray and Male (1981):
a) for a mountain snowpack and b) for a prairie snowcover

A review of Figure 3-2a shows that the albedo range for a mountain snowpack is approximately 40 to 87. These values are consistent with findings for deep snowpacks presented in Maidment (1993). The equation used by the model to estimate snowpack albedo for an alpine region in Figure 3-2a is:

$$ALB = 40 + 46.67 \times Exp(-0.2265COUNT) \quad (3\text{-}6)$$

where C_{OUNT} refers to the number of days since the last snowfall. A review of Figure 3-2b shows that the albedo range for a prairie or valley snowpack is approximately 18 to 80. Again, these values are consistent with findings for prairie snowpacks presented in

Maidment (1993) and Gray and Male (1981). The equation used to estimate snowpack albedo for a prairie in Figure 3-2b is:

$$ALB = 18 + \frac{108.459}{1.7402 \times Exp(0.87629 COUNT)} \qquad (3-7)$$

where C_{OUNT} is as defined above. Since valleys are prone to patchy snow cover, similar to that of a prairie, an assumption has been made that the snowcover properties (depth, etc.) for a valley would be more similar to that of a prairie than that of an alpine region. The model defines HRUs as being either alpine or prairie/valley, and then uses the appropriate albedo equation.

A new variable, W_{CAN}, is calculated to take into account the effect of forest canopy on wind speed. As Dingman (1994) points out, wind speed measurements (W_S) are generally recorded in fields or clearings and must be adjusted for forest canopy. Dingman (1994) presents an equation for calculating this effect that he borrows from Dunne and Leopold:

$$WCAN = (1 - 0.8F \times Fd)WS \qquad (3-8)$$

where F_d is the forest density (dimensionless). If the HRU lacks a forest cover, W_{CAN} (m / s) equals W_S. Table 3-1 contains a summary of required input data for each HRU.

Table 3-1. Summary of the Required Input Data for Each HRU.

Topographic and Land Use Data	Meteorological Data
area	average daily air temperature
relative ground roughness	relative humidity
mean elevation	total precipitation
forest cover	wind speed
conifer versus deciduous	wind orientation
mean latitude	cloud cover
orientation	incoming solar radiation
mean slope	
alpine versus valley/prairie	

3.6 MODEL MODULES

3.6.1 Introduction

The model will be broken up into several modules. Each module will define one of the processes pictured in Figure 3-3. The daily results of each module will represent the amount of SWE entering or leaving an HRU based upon the process that is defined by that particular module. As seen in Figure 3-3, all modules will be summed on a daily basis to determine the net increase or decrease of SWE for each HRU.

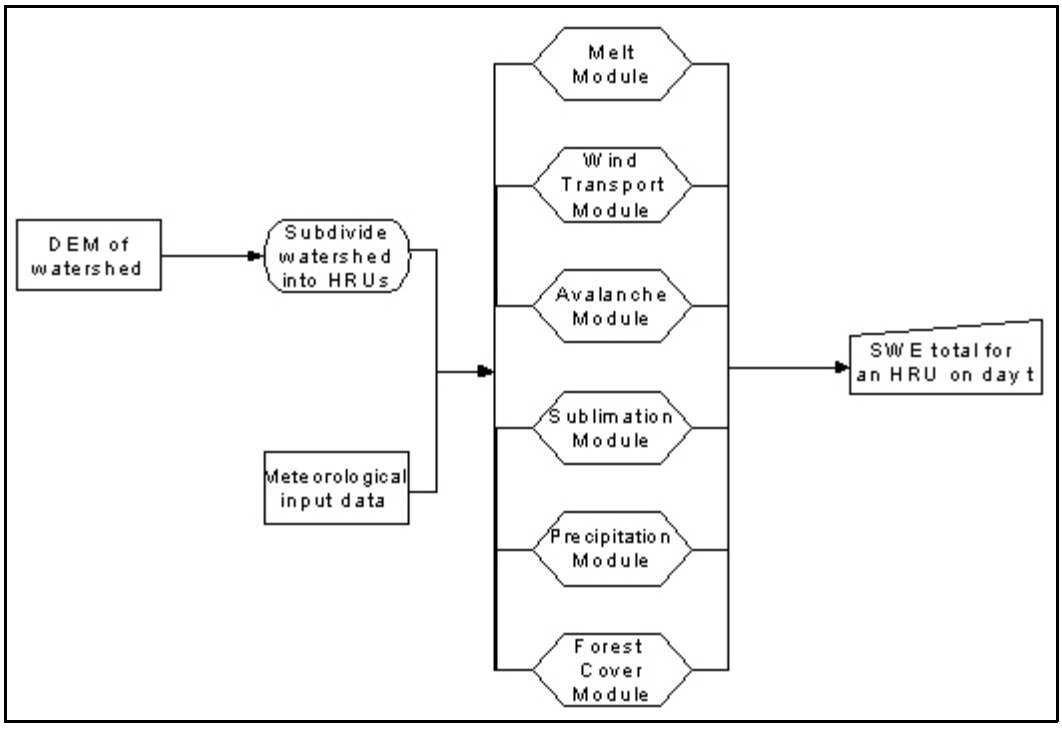

Figure 3-3. Simplified schematic of the model operation

3.6.2 Precipitation Module

When precipitation occurs, it generally falls as either rain or snow. If snow occurs, SWE accumulation occurs, and the resulting total SWE value is dependent upon the total snow accumulation and the density of the newly fallen snow. If rain occurs, energy received is added to the snowpack. If the snowpack is not yet ripe, the rain results in SWE accumulation equal to the depth of rainfall while bringing the snowpack closer to a ripe condition. If the snowpack is already ripe, the rain does not increase SWE accumulation, but does increase the snowpack melt rate, thus causing SWE ablation. The concept of a ripe snowpack will be discussed in more detail in the next section. Figure 3-4 depicts a simplified schematic of the precipitation module.

The phase in which precipitation occurs is temperature dependent. The equations used to make this determination are used by many models, such as the Utah Energy Balance Snow Accumulation and Melt Model (Tarboton and Luce, 1996), and are borrowed from the equations developed by the Army Corps of Engineers (1956). These equations are as follows:

$$R_T = P_T \qquad \text{if } T_{AVG} \geq 3\ ^0\text{C}$$

$$R_T = P_T(T_{AVG} - (-1)) / (3 - (-1)) \qquad \text{if } -1\ ^0\text{C} < T_{AVG} < 3\ ^0\text{C} \qquad (3\text{-}9)$$

$$R_T = 0 \qquad \text{if } T_{AVG} \leq -1\ ^0\text{C}$$

$$S_T = P_T - R_T \qquad (3\text{-}10)$$

where P_T (cm) is the amount of total precipitation, R_T (cm) is the portion of precipitation that occurs as rain, S_T (cm) is the portion of precipitation that occurs as snow.

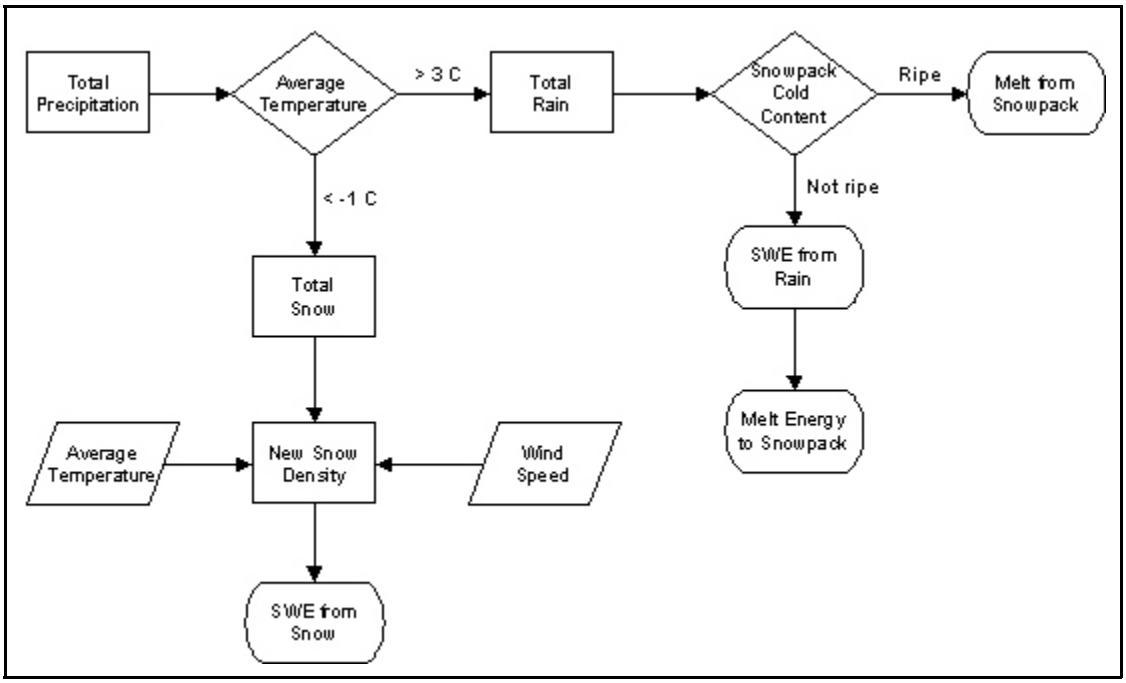

Figure 3-4. Simplified schematic of the precipitation module

If snow has occurred, and the measurement of the snow has been given in cm of depth, a method of converting snowfall depth to an equivalent value of SWE is required. As earlier mentioned, this requires determining the density of the newly fallen snow. Many studies, such as Sevruk (1985), Schmidt (1980), and Hedstrom and Pomeroy (1998), have shown that the density of fresh snow is dependent upon the wind speed and air temperature. The model uses the following equation, which draws upon a study performed by Sevruk (1985), to estimate the new snow density based upon the wind speed and air temperature:

$$S_{DENS} = 0.0768 + 0.0106 W_{CAN} + 0.0017 T_{AVG} \qquad \text{if } T_{AVG} \leq -2.5\ ^{0}\text{C}$$

$$S_{DENS} = 0.0959 + 0.01 W_{CAN} - 0.004 T_{AVG}^{\ 2} \qquad \text{if } T_{AVG} > -2.5\ ^{0}\text{C} \qquad (3\text{-}11)$$

where S_{DENS} is the determined density of the fresh snow (g / cm^3), and W_{CAN} and T_{AVG} are as previously defined. These equations were developed from figures presented by Sevruk (1985) by again utilizing the Microsoft Excel Solver. While Sevruk's results were developed from data collected in the Swiss Alps, his findings follow the generally accepted principles that new snow density increases with rising temperature and greater wind speed. Additionally, because of a general lack of other published data regarding this topic, this equation will be used by the model and applied to watersheds outside of Sevruk's study area. Since Sevruk's results do coincide with accepted beliefs regarding the relationship between air temperature, wind speed, and new snow density, it is believed that using these equations for watersheds outside of the Swiss Alps region will still provide rational and useful results.

If snowfall has been reported in terms of depth, once a new snow density has been determined, the depth of snowfall can be converted to SWE by the following equation:

$$SWE_{snow} = SDENS \times DEPTH \tag{3-12}$$

where SWE_{snow} (cm) is the amount of SWE resulting from the new snowfall, and D_{EPTH} is the depth of the new snowfall.

As previously mentioned, if rain falls on a snowpack that is not ripe, the depth of rainfall is added to the SWE total, as defined by the following equation:

$$SWE_{rain} = RT \tag{3-13}$$

where SWE_{rain} (cm) is the amount of SWE resulting from the new rainfall. If rain falls on a snowpack that is ripe, no additional SWE accumulation results. The net energy effect caused by rainfall shall be discussed in the following section.

3.6.3 Melt Energy Module

The period of general increase in the SWE of a snowpack is commonly referred to as the accumulation period. During this time, the net input of energy to the snowpack is generally negative, which causes an increase in the cold content of the snowpack and a decrease in the average temperature of the snowpack. The melt period of a seasonal snowpack typically begins when the net input of energy to the snowpack becomes continually positive. The positive net energy input first acts to warm the snowpack, thus reducing the cold content to zero and raising the average temperature of the snowpack also to $0\ ^0$C. Once the snowpack becomes isothermal at $0\ ^0$C, the snowpack becomes

ripe. Further positive input of net energy causes melt to occur and a release of surface water input. Figure 3-5 depicts a simplified schematic of the melt energy module, as discussed in this section.

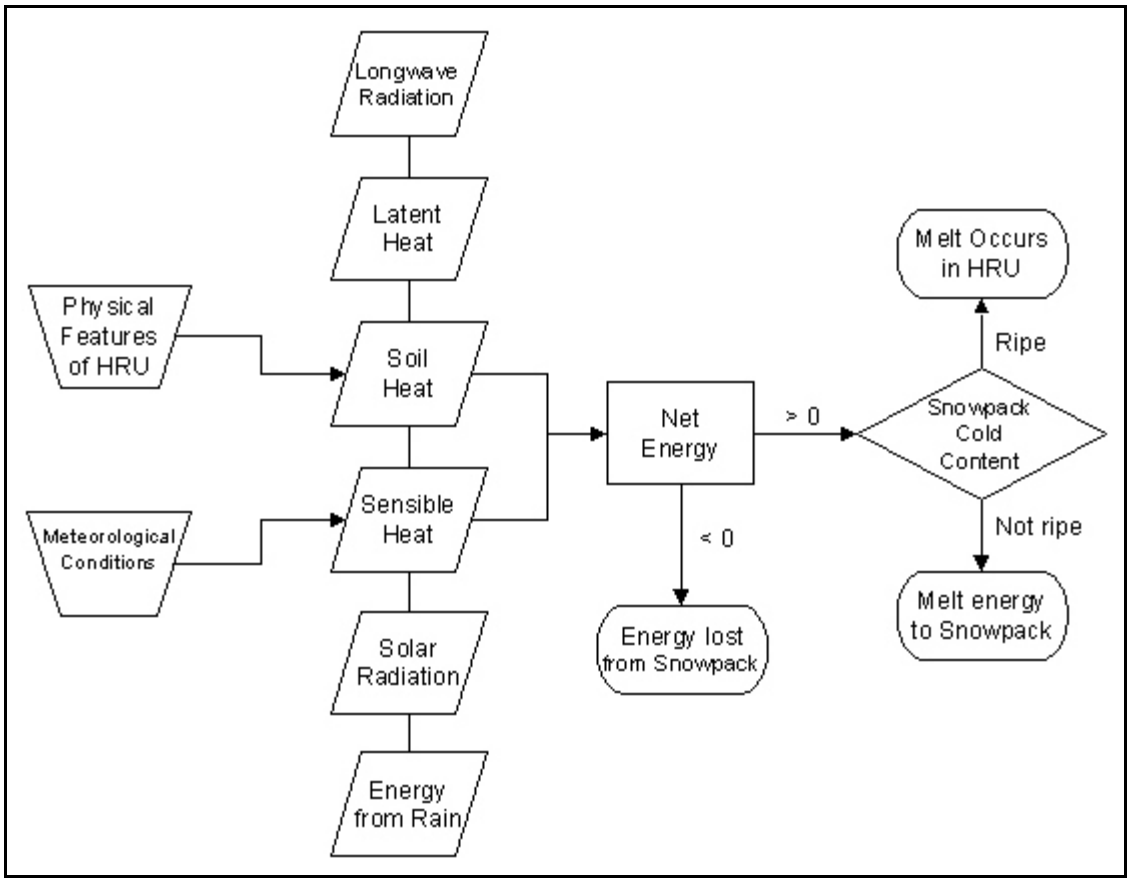

Figure 3-5. Simplified schematic of the melt energy module

The energy exchanges that determine the progress of snowmelt include the following processes: shortwave (solar) radiation, longwave radiation, sensible heat, latent heat, advective (rain) energy, and conductive heat exchange with the ground. Thus the equation for net energy is as follows:

$$E_{NET} = S_R + L_W + S_H + L_H + P_{MELT} + SO_H \quad (3\text{-}14)$$

where E_{NET} (cal / cm^2 day) is net energy, L_W (cal / cm^2 day) is the net received longwave radiation, S_H (cal / cm^2 day) is the turbulent exchange of sensible heat with the atmosphere, L_H (cal / cm^2 day) is the turbulent exchange of latent heat with the atmosphere, P_{MELT} (cal / cm^2 day) is the advective energy derived from rain, and SO_H (cal / cm^2 day) is the conductive heat exchange with the underlying ground.

Longwave radiation is the energy flux emitted by all matter, and is frequently referred to as terrestrial radiation. The net input of longwave energy is the difference between the incident flux emitted by the atmosphere, clouds and overlying forest canopy, and the outgoing radiation from the snowpack. The equation for estimating longwave radiation is as follows:

$$LW = \left(\varepsilon at \times SB \times TAVG^4\right) - \left(\varepsilon ss \times SB \times TSURF^4\right) \quad (3\text{-}15)$$

where T_{SURF} (^{0}C) is the temperature of the surface of the snowpack, SB is the Stefan-Boltzmann constant (1.19 E^{-7} cal / cm^2 day K^4), ε_{SS} is the emissivity of snow (0.97), and ε_{at} is the integrated effective emissivity of the atmosphere and canopy. The following equation from Dingman (1994) can be used to estimate ε_{at}:

$$\varepsilon at = \left(1 - F\right)\left(0.53 + 0.065 ea^{0.5}\right)\left(1 + 0.4CC\right) + F \quad (3\text{-}16)$$

where e_a is the near surface vapor pressure.

The following equation from Dingman (1994) can be used to estimate e_a:

$$e_a = 6.11 RH \times Exp\left(\frac{17.3 TAVG}{TAVG + 237.3}\right) \tag{3-17}$$

Sensible heat can be defined as the turbulent flux of energy exchanged at the surface of the snowpack due to a difference in temperature between the snowpack surface and overlying air. In terms of the energy balance of the snowpack, a positive value for the sensible heat flux indicates heat being transferred into the snow. Dingman (1994) defines sensible heat by the following equation:

$$S_H = c_a \rho_a \times \frac{W_{CAN}}{6.25\left[\ln\left(\frac{z_m}{z_o}\right)\right]^2} \times \left(T_{AVG} - T_{SURF}\right) \tag{3-18}$$

where c_a is the heat capacity of air (0.24 cal / g °C), ρ_a is the mass density of air (0.0012 g / cm^3), z_m (cm) is the height at which the wind speed and air temperature are measured, and z_0 (cm) is the roughness height, which depends on the irregularity of the snow surface.

Dingman (1994) indicates that wind speed and air temperature readings are typically taken at a height of 2 meters. He also states that the roughness height can be highly variable both spatially and temporally. As a result, Dingman (1994) suggests using a value of 0.15 cm for z_o. Making the same assumptions as Dingman and substituting all of these values into Eq. 3-18 yields a more direct expression for sensible

heat:

$$S_H = 7.69 W_{CAN}(T_{AVG} - T_{SURF}) \tag{3-19}$$

Several authors, including Dingman (1994) and Tarboton and Luce (1996), indicated that Eqs. 3-18 and 3-19 apply strictly to conditions of neutral atmospheric conditions. These authors define neutral atmospheric conditions as occurring when the actual temperature gradient in the air near the snow surface equals the adiabatic lapse rate. The authors go on to state that these conditions typically exist when the air temperature is less than the temperature of the snowpack surface. For cases in which the air temperature is greater than the temperature of the snowpack surface, the authors suggest using a stability correction factor. This factor will reduce turbulent heat exchange with the snowpack mimicking the results of having a temperature gradient less steep than the adiabatic lapse rate. Dingman (1994) defined this factor as:

$$f_s = 1 + \frac{9810 z_m (T_{AVG} - T_{SURF})}{(T_{AVG} + 273.2) W_{CAN}^2} \tag{3-20}$$

where f_s is unitless.

Utilizing the stability correction factor yields the final equation for sensible heat:

$$S_H = 7.69 W_{CAN}(T_{AVG} - T_{SURF}) \qquad \text{if } T_{AVG} < T_{SURF}$$

$$S_H = \frac{7.69 W_{CAN}(T_{AVG} - T_{SURF})}{f_s} \qquad \text{if } T_{AVG} \geq T_{SURF} \tag{3-21}$$

Latent heat can be defined as the turbulent flux of energy exchanged at the surface of the snowpack due to vapor movement as a result of a vapor pressure difference between the snowpack surface and the overlying air. In estimating latent heat, it is important to note that two phase changes may be involved. If the vapor-pressure gradient is away from the snowpack, water vapor will move from the snow to the air and evaporation will occur. If the vapor-pressure gradient is towards the snowpack, water will move from the air to the snow and condensation will occur. Evaporation represents a loss of latent heat from the snowpack, while condensation represents a gain of latent heat to the snowpack. Dingman (1994) defines latent heat flux for these two phases as follows:

$$L_H = 11.8 W_{CAN}(e_{ss} - e_a) \qquad \text{if } T_{AVG} > T_{SURF} \qquad (3\text{-}22)$$

$$L_H = -13.3 W_{CAN}(e_{ss} - e_a) \qquad \text{if } T_{AVG} < T_{SURF}$$

where e_{ss} is the vapor pressure at the snow surface. Eq. 3-22 also features the same assumptions as does Eq. 3-21. The vapor pressure at the snow surface can be estimated as follows:

$$e_{ss} = 6.11 RH \times Exp\left(\frac{17.3 \times TSURF}{TSURF + 237.3}\right) \qquad (3\text{-}23)$$

As with the sensible heat flux, the same authors also recommend using the stability correction factor at those times when the air temperature is greater than the snow surface temperature. Applying this factor to Eq. 3-22 yields the following

equation to estimate latent heat flux:

$$LH = \frac{11.8 W_{CAN}(e_{ss} - e_a)}{f_s} \qquad \text{if } T_{AVG} > T_{SURF} \qquad (3\text{-}24)$$

$$LH = -13.3 W_{CAN}(e_{ss} - e_a) \qquad \text{if } T_{AVG} < T_{SURF}$$

In order to estimate values for sensible and latent heat fluxes, a method for estimating the temperature of the snowpack surface is required. Although many references cite the need to determine the temperature of the snowpack surface, few references provide procedures for actually estimating this variable. When the air temperature is above the freezing mark, many snowmelt models utilizing an energy balance approach, such as HEC-1, Streamflow Synthesis and Reservoir Regulation (SSARR), and the National Weather Service River Forecast System (NWSRFS), assume that the snowpack surface temperature is at freezing (0 ^{o}C). This assumption will also be used in the model.

For times when the air temperature is below the freezing mark, it will be assumed that the equation for the snowpack surface is as follows:

$$T_{SURF} = T_{AVG} - T_f \qquad (3\text{-}25)$$

where T_f is a temperature factor defining the difference between the air temperature and the snow surface temperature. This relationship was borrowed from a study performed in Vermont by Brubaker, Rango, and Kustas (1996) where measured snow surface temperature data were available. The result of their research showed that $T_f = 2.5$ for the study area. Applying this equation to watersheds outside of the Vermont area will

most likely introduce error. As a result, it is proposed that a sensitivity analysis be performed on this variable to determine its importance on a watershed by watershed basis.

When rain falls on a snowpack that is ripe, the rainwater is cooled to the snowpack temperature, and the heat given up by the rainwater is used to melt the snowpack. For this particular case, the rainfall component to the energy balance can be computed as follows:

$$P_{MELT} = \rho_w c_w R_T \times T_{RAIN} \tag{3-26}$$

Where P_{MELT} is in units of cal / cm^2 day, ρ_w is the density of water (assumed to be 1.0 g / cm^3), c_w is the heat capacity of water (1.0 cal./ /g ^oC), and T_{RAIN} (^oC) is the temperature of the rain. As per Dingman (1994), Maidment (1993), Tarboton and Luce (1996) among others, rain temperature is almost always assumed to be equal to the air temperature. Making this substitution into Eq. 3-25 yields:

$$P_{MELT} = \rho_w c_w R_T \times T_{AVG} \tag{3-27}$$

When rain occurs on a snowpack that is not yet ripe, the rain will first be cooled to the freezing point, giving up sensible heat, and then freeze, releasing latent heat. For this particular case, the rainfall component to the energy balance can be computed as follows:

$$P_{MELT} = \left(\rho_w c_w R_T \times T_{RAIN} \right) + \left(\rho_w \lambda_f R_T \right) \tag{3-28}$$

where λ_f is the latent heat of fusion (79.7 cal / g). Once again, the assumption will be made that air temperature is a reasonable approximation for the rain temperature. This substitution into Eq. 3-28 will yield:

$$P_{MELT} = \left(\rho_w c_w R_T \times T_{AVG}\right) + \left(\rho_w \lambda_f R_T\right) \tag{3-29}$$

Combining Eqs. 3-27 and 3-29 yields the final equation for estimating the rainfall component to the energy balance:

$$P_{MELT} = \rho_w c_w R_T \times T_{AVG} \quad \text{if } Cold_C = 0 \tag{3-30}$$

$$P_{MELT} = \left(\rho_w c_w R_T \times T_{AVG}\right) + \left(\rho_w \lambda_f R_T\right) \quad \text{if } Cold_C > 0$$

In order to estimate the melt energy provided by rain, another variable, $Cold_C$, must first be estimated. $Cold_C$ represents the cold content of the snowpack. Gray and Male (1981) point out that it was the Army Corps of Engineers, in 1956, that first introduced the idea of a snowpack cold content to monitor the energy change in a snowpack. These authors defined cold content as the amount of heat required per unit area to raise the temperature of the snowpack to 0 ºC.

For the case where a snowpack does not exist, $Cold_C$ also does not exist (or equals 0). For the case where the snowpack is comprised entirely of the most recent snow, $Cold_C$ can be computed as follows:

$$Cold_C = -c_i \rho_w SWE \times T_{PACK} \tag{3-31}$$

where $Cold_C$ is in units of cal / cm^2 day, c_i is the heat capacity of ice (0.502 cal./ /g ºC), SWE (cm) is the snow water equivalent of the snowpack, and T_{PACK} is the average

temperature of the snowpack. T_{PACK} is assumed to be equal to T_{AVG} for this particular case. For the case where a snowpack already exists, $Cold_C$ can be calculated from the following equation:

$$Coldc = Coldc_{t-1} - E_{NET} \tag{3-32}$$

where $Cold_{Ct-1}$ represents the value of the cold content on the previous day. Combining the three cases produces the following equation for $Cold_C$:

$$Coldc = 0 \qquad \text{if SWE} = 0$$

$$Coldc = -ci\rho wSWE \times T_{AVG} \qquad \text{if } SWE_{t-1} = 0 \text{ and } S_T > 0 \tag{3-33}$$

$$Coldc = Coldc_{t-1} - E_{NET} \qquad \text{if } SWE_{t-1} > 0$$

where SWE_{t-1} represents the snow water equivalent of the snowpack on the previous day.

The final term in the net energy Eq. 3-14 involves the energy exchange between the snowpack and the underlying soil by heat conductance. Dingman (1994), Gray and Male (1981), Maidment (1993), among others, point out that the ground heat flux is typically the smallest component of the daily energy balance and that its effect on total snowmelt can be ignored. Tarboton and Luce (1996) provided an expression for determining the ground heat flux in their Utah Energy Balance Snow Accumulation and Melt Model. This model also indicates that, if the required soil data are not available to estimate the ground heat flux, this variable should be set equal to 0. Based upon the above statements and keeping with the design goal of model simplicity, SO_H will be set equal to 0 to avoid the need for soils data input into the model.

Once E_{NET} has been calculated, the amount of melt that has occurred for a specific day can be determined. If a snowpack does not exist, melt obviously equals 0. If a snowpack exists, but the snowpack is not ripe ($Cold_C > 0$), then melt also equals 0. If a snowpack both exists and is ripe, but the net energy for the day is negative (heat energy is being lost by the snowpack), melt will still equal 0. Only when a ripe snowpack exists and the net energy for a particular day is positive (heat energy is being added to the snowpack), will melt occur on that day. When this occurs, melt can be determined by the following equation:

$$MeltSWE = \frac{E_{NET}}{\rho_w \lambda_f} \qquad \text{if SWE} > 0,\ Cold_C = 0 \text{ and } E_{NET} > 0 \qquad (3\text{-}34)$$

where MeltSWE has units of cm of SWE. For all other cases described above, MeltSWE equals 0.

3.6.4 Sublimation Module

Sublimation can be defined as the change in phase from ice directly to water vapor. Maidment (1993), Pomeroy and Essery (1999), and Pomeroy et al. (1998) discuss that sublimation is primarily a function of the following three factors: air temperature, wind speed and relative humidity. In general, sublimation increases as wind speed increases, air temperature increases, and relative humidity decreases. Figure 3-6 shows a simplified schematic of the sublimation module, as discussed in this section. Maidment (1993) demonstrates the relationship between sublimation and wind speed, air temperature and relative humidity. The following equation for estimating

sublimation was borrowed from Maidment (1993):

$$SubSWE = 0.1\left(0.1 + 10^{(0.100102 W_{CAN}) + (0.040735 T_{AVG}) - (1.3708\, RH) + 0.031508}\right)$$

for $W_{CAN} > 5$ m/s (3 - 35)

$$SubSWE = 0$$ for $W_{CAN} \leq 5$ m/s ____ (3-36)

where SubSWE is in units of cm.

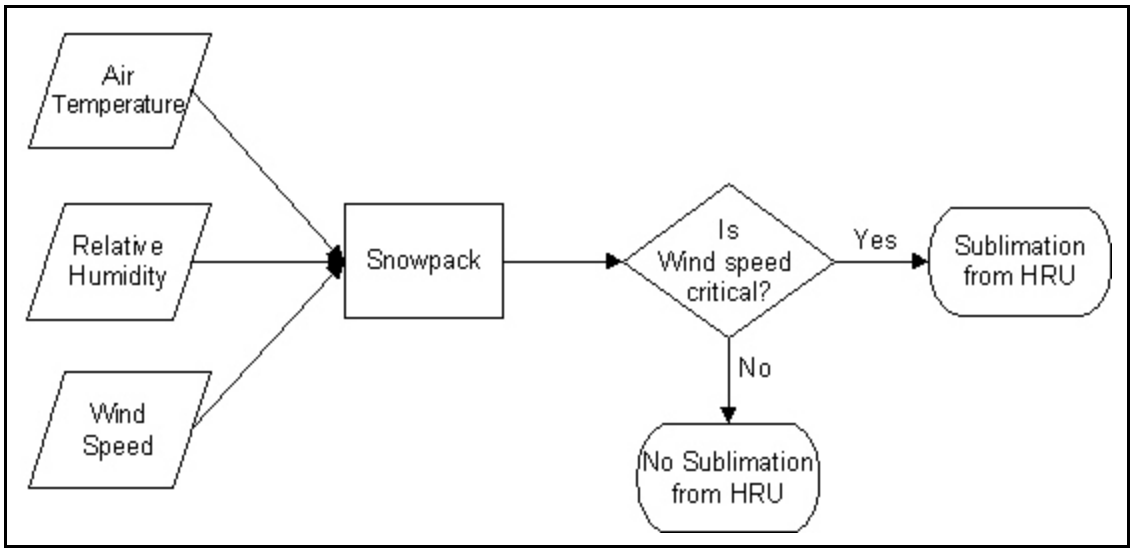

Figure 3-6. Simplified schematic of the sublimation module

Eqs. 3-35 and 3-36 indicate that a threshold wind speed (5 m/s) is required for sublimation to occur. Consequently, on days where the average daily wind speed does not exceed this threshold speed, the model will predict that no SWE is lost from a snowpack due to sublimation. The question that arises is how realistic is this? On days where the daily average wind speed equals 4.5 m/s, it seems highly likely that for some portion of the day the wind speed will actually be greater than the threshold value, but

the model will still predict that no sublimation has occurred. This problem has been experienced by other snow-transport models. One such example is the snow-transport model for complex terrain created by Liston and Sturm (1998). Their model also operates on a daily time step and simulates three-dimensional snow-depth evolution over topographically variable terrain. Among the required meteorological data are average daily wind speed. The authors conclude that "If the meteorological inputs fail to resolve brief but intense periods of snowfall or high wind, then the actual drift accumulation or erosion will not be simulated." This quote indicates that more frequent wind data would most likely increase model accuracy, but the trade-off would be increased computational time, if decreasing the model time step, or increased data requirements.

A proposed method to increase model accuracy without the above mentioned negative implications is to utilize conditional probability on the input data. Conditional probability can be defined as : P(A | B) = the probability of A occurring, given that B has already occurred, or

$$P(A \mid B) = \frac{P(A \cap B)}{P(B)} \tag{3-37}$$

where $P(A \cap B)$ is the probability of the intersection of A and B, and *P(B)* is the probability of B occurring. For the above hypothetical situation in which the average daily wind speed is 4.5 m/s, *P(B)* would be equal to 1.0 because it is known that the daily average wind speed is less than 5.0 m/s. Additionally, $P(A \cap B)$ can be

determined by examining the hourly wind data to determine how many hourly values are greater than the threshold value, given that the daily average is 4.5 m/s. The model then could estimate sublimation occurring for that portion of the day that the wind speed was determined to be greater than the threshold wind speed based upon conditional probability. The use of conditional probability will be incorporated into the model in an attempt to increase the accuracy of sublimation totals.

3.6.5 Wind Transport Module

Most hydrologic studies regarding wind transport, such as Li and Pomeroy (1997), Liston and Sturm (1998), Schmidt (1980), and Schmidt (1984), have focused on the redistribution of snow and the effect on the spatial variability in SWE. Wind transport typically comprises three components: creep, saltation, and suspension. Creep refers to the movement of large, heavy snow particles that roll along the snowpack surface. Maidment (1993) indicated that creep typically is a very small portion of the amount of snow that is transported by wind. Saltation refers to the movement of snow particles by jumping along the snow surface. The transport rate of saltating snow typically depends upon the vertical distribution of wind, the texture of the snowpack surface, the fetch distance, and the existence of vegetation or other elements protruding from the snow surface. A typical jump may be 1 cm high and 20 cm long. Suspension refers to the movement of snow particles suspended in the airstream above the snowpack surface. The concentration of suspended snow is typically highest just above the saltation layer and decreases with height at a rate that is dependent upon the wind

speed. Figure 3-7 shows a simplified schematic of the wind transport module.

Figure 3-7. Simplified schematic of the wind transport module

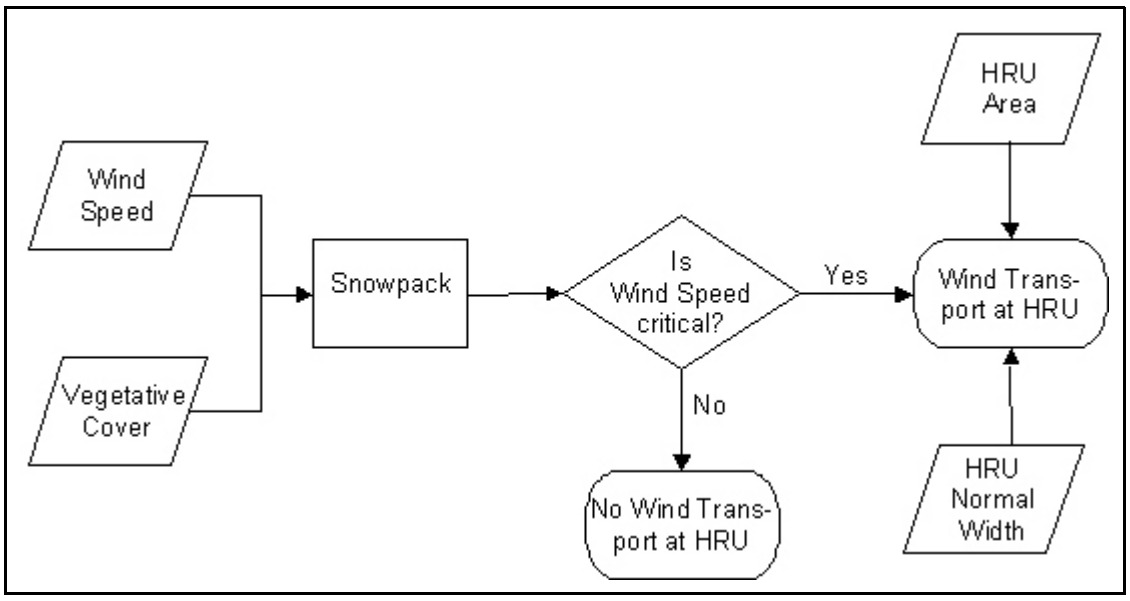

Equations were borrowed from Maidment (1993) to estimate wind transport. The following equation is used by the model to estimate wind transport out of an HRU in alpine regions:

$$WindSWE_{OUT} = 0.000066529\, Perpwidth\left(W_{CAN} - 5\right)^3 / AREA \qquad \text{(3-38)}$$

if $W_{CAN} > 5$ m / s

where $WindSWE_{OUT}$ is in units of cm of SWE, and Perpwidth (m) refers to the perpendicular width (to the wind speed) along an HRU with which snow transport will occur. The following equation is used by the model to estimate wind transport out of an HRU in a prairie region:

$$WindSWE_{OUT} = \left(0.0000019008\, Perpwidth \times W_{CAN}^{4.04}\right) / AREA \qquad \text{(3-39)}$$

if $W_{CAN} > 6.5$ m / s

For the model development, it is assumed that valley regions of an alpine watershed are more represented by Eq. 3-39 than by Eq. 3-38. Studies indicated that threshold wind speeds are greater for alpine regions than for prairies due to the greater surface roughness.

Studies by Li and Pomeroy (1997), Liston and Sturm (1998), Schmidt (1980), and Schmidt (1984) have also noted the importance of a threshold wind speed that must be exceeded before wind transport can occur. This theme is also represented in Eqs. 3-38 and 3-39. Since these equations utilize a threshold wind speed, the model also incorporated conditional probability to better estimate wind transport based upon the same setup as for sublimation.

The model also estimated the amount of wind transport that will enter an HRU, $WindSWE_{IN}$ (cm). This value was determined by the model by means of first calculating all values of $WindSWE_{OUT}$ for all HRUs, and then, based upon the wind orientation, W_{OR}, determine how much wind transport leaving an HRU was directed toward the various adjacent HRUs.

3.6.6 Avalanching Module

An avalanche is a rapid downslope movement of a large mass of snow. The essential elements for avalanches are deep snow and steep slopes, but variations of snow, terrain conditions and meteorological conditions affect the form and sizes of avalanches.

Armstrong and Williams (1986), and McClung and Schaerer (1993) explained that the start of an avalanche is the outcome of the relationship between the stress and strength within the snowpack on an incline. Failure occurs when the stress exceeds the strength at some point. Stresses in a snowpack are increased by the weight of additional snowfall, the accumulation of drifting snow, or the weight of rainfall. Decreases in snowpack strength most frequently result from a significant rise in air temperature or a "rain on snow" event.

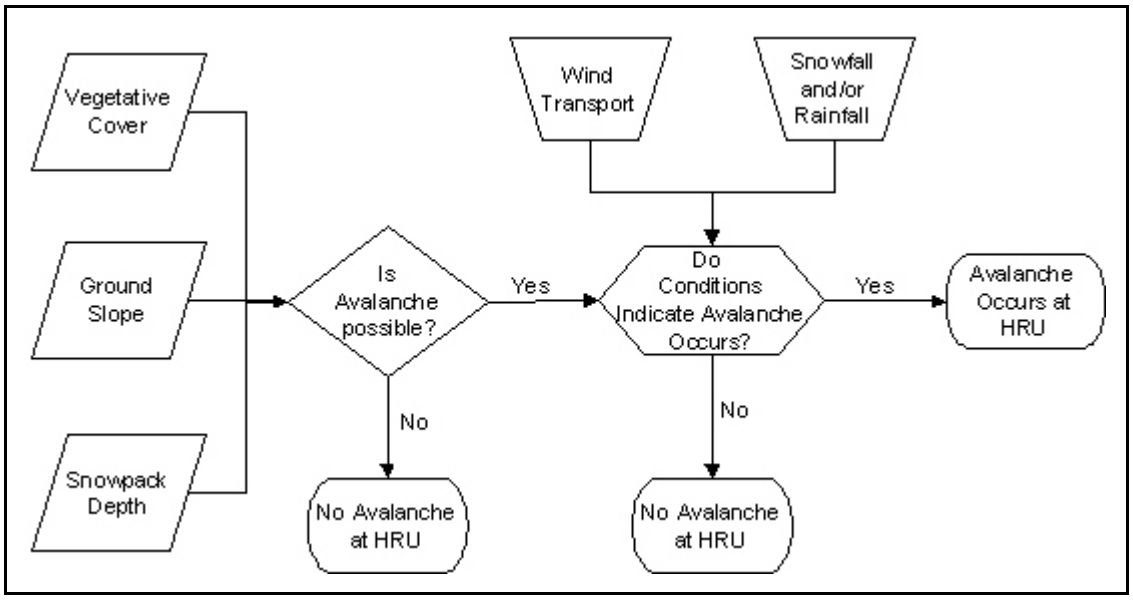

Figure 3-8. Simplified schematic of the avalanche module

Armstrong and Williams (1986), McClung and Schaerer (1993), Sulakvelidze and Dolov (1973), Fohn, et al (1977), and Hopfinger and Tochon-Danguy (1991) made reference to the fact that the process of avalanching is random. The contention is that two identical snowpacks under the same meteorological conditions may or may not

respond identically in terms of avalanching. The consequence of this contention is that modeling the process of avalanching with meteorological data creates a stochastic process as opposed to a deterministic process. This is undesirable in terms of the model development because the proposed model should be able to create reproducible results. To deal with the stochastic element of avalanching, the model will be developed so that a specific combination of physical conditions of the HRU and meteorological conditions will always produce an avalanche. Conversely, if these conditions are not met, the model will predict that no avalanche occurs. Figure 3-8 shows a simplified schematic of the avalanche module.

The three physical parameters of the HRU that affect avalanching are slope, forest cover and surface roughness. As previously mentioned, a 26^0 slope represents the angle of repose for granular substances such as sand and dry, unbonded snow, therefore this is the minimum ground slope in which an avalanche can occur. Forest cover is important in terms of providing an anchor against avalanching. Armstrong and Williams (1986) stated that "A dense stand of trees can easily provide enough anchors to prevent avalanches from releasing." The model will require that an HRU has an F_d (forest density fraction) less than 0.7 in order for an avalanche to occur. As previously mentioned, both Armstrong and Williams (1986), and McClung and Schaerer (1993) discussed the importance of surface roughness. Both discussed that the rougher the ground surface, the greater the depth of snow on the ground that is required to cover the ground anchors (such as boulders and large rocks). Both provide the following rules of thumb for the minimum depth of ground snow required for an avalanche to occur under

various surface conditions: less than 9 inches of snow (not SWE) seldom produces an avalanche; 9 inches to 15 inches of snow can produce small slides on relatively smooth ground cover; 15 inches to 27 inches can produce large slides on average terrain containing some brush and boulders; and 27 inches to 36 inches can produce large slides on rough terrain with many boulders and tree stumps. The model will require an HRU, based upon its C_{OVER} (relative ground roughness) parameter, to have a minimum snow depth that corresponds to the above values.

The three meteorological parameters that most significantly affect avalanching are snowfall (total depth and intensity), rainfall and wind transport. Hopfinger and Tochon-Danguy (1991) indicated that more than 80% of all avalanches occur during or shortly after a storm. In addition, Armstrong and Williams (1986) stated that a snowfall intensity of 1 inch / hour or greater, that is sustained for ten or more hours, is generally a "red flag" indicating avalanche danger. Armstrong and Williams (1986) also discussed that "rain on snow" events often trigger avalanches because the rain provides additional weight to the avalanche slope but does not provide additional strength to the snowpack. McClung and Schaerer (1993) discussed the significance of wind transport in determining avalanches. They reported that significant snow deposition due to wind transport can often start avalanches because a great amount of weight can be added to the snowpack in a relatively short period of time, more than offsetting the strength added to the snowpack. The model will require that any one of the three following meteorological conditions exist in order for an avalanche to occur within an HRU: total snowfall (depth not SWE) for the current day is greater than 25 cm, total rainfall for the

current day is greater than 5 cm, or $WindSWE_{IN}$ for the current day is greater than 1.5 cm of SWE.

The model will first check the HRU parameters to see if they are in compliance with the requirements for an avalanche occurring. If the HRU parameters indicate that an avalanche cannot occur, the model will bypass the rest of the code dealing with avalanching. If the HRU parameters indicate that an avalanche can occur, the model will next check the meteorological parameters. If the meteorological parameters indicate that an avalanche cannot occur for that day, the model will bypass the remainder of the avalanching code. If the meteorological parameters indicate that an avalanche does occur for that particular day, the model will continue with the avalanche code by calculating the volume of SWE associated with the avalanche.

The next step of the model would be to determine the amount of SWE lost from an HRU because of an avalanche. Sulakvelidze and Dolov (1973) provided a method for determining the volume of an avalanche. The first step of their method is to determine the height of the existing snow. The model determines the height of the existing snow by means of the variable D_{EPTH} (cm). The D_{EPTH} of snow on a given day is based upon the snowpack depth from the day before, taking into account that the snowpack density generally increases through settlement and compaction, the total amount of snow that may have fallen on that day, and the depth of snow that may have been lost due to melt. The model uses the following equation to determine the snowpack depth for a given day:

$$DEPTH_t = \left(0.995\, DEPTH_{t-1}\right) + ST - \left(10\, MeltSWE\right) \quad \text{if SWE} > 0 \tag{3-40}$$

where D_{EPTHt} refers to the depth of the snowpack on day t, and $D_{EPTHt-1}$ refers to the depth of the snowpack on day t-1. The second step of Sulakvelidze and Dolov's (1973) method is to calculate the critical height of the new snow. The model performs this task by means of the following equation:

$$HCRIT = \left(\left(\frac{\cos(SLOPE) - 3.6\sin(SLOPE)\cos^2(SLOPE)}{4.3 \times DENS}\right)^2 + \frac{2.9\cos^2(SLOPE)}{DENS^2}\right)^{0.5} + \frac{\cos(SLOPE) - 3.6\sin(SLOPE)\cos^2(SLOPE)}{4.3 \times DENS} \tag{3-41}$$

where H_{CRIT} is the critical height of new snow (cm), and D_{ENS} is the density of the existing snowpack (g / cm^3). The model determines the density of the snowpack based upon the following equation:

$$DENS = SWE \div DEPTH \tag{3-42}$$

The final step of Sulakvelidze and Dolov's (1973) method is to determine the volume of the avalanche. The model accomplishes this by utilizing the following equation:

$$AvalSWEOUT = 0.00075 \times \left(DEPTH \times HCRIT\right)^{1.56} \times DENS \tag{3-43}$$

where $AvalSWE_{OUT}$ is the amount of SWE leaving an HRU due to an avalanche (cm).

In addition to SWE leaving an HRU due to avalanching, SWE may enter an HRU due to avalanching if the adjacent HRU is capable of producing an avalanche. All

values of $AvalSWE_{OUT}$ leaving HRUs will be recorded by the model and then the model will determine which HRUs these SWE values will enter as $AvalSWE_{IN}$ (cm).

3.6.7 Forest Cover Module

As previously mentioned, forest cover results in decreased received shortwave radiation at the forest floor (Eq. 3-5), increased incoming longwave radiation (Eq. 3-15), decreased wind speed (Eq. 3-8) leading to reduced turbulent heat exchanges (Eqs. 3-21 and 3-24) and wind driven snow transport (Eqs. 3-38 and 3-39), and decreased precipitation accumulation at the forest floor as compared to open areas. This final point will be examined in greater detail.

Pomeroy et al. (1998) helped demonstrate the significance of properly modeling snow interception through the following quote: past studies in forest snow interception and sublimation suggest that in "boreal, montane and subalpine forests over one-half of cumulative seasonal snowfall can remain intercepted in midwinter, and 25 - 45% of the annual snowfall can sublimate from snow intercepted in the canopy."

Figure 3-9 shows a simplified schematic of the forest cover module discussed in this section. The first step in modeling forest snow interception and sublimation is to determine the maximum amount of snow interception that can occur based upon forest conditions. Hedstrom and Pomeroy (1998) provided a method of estimating the maximum possible interception by means of the following equation:

$$MAXINT = 0.1 S_{mean}\left(0.27 + \frac{0.046}{S_{DENS}}\right) LAI \qquad (3\text{-}44)$$

where MAX_{INT} is the maximum possible interception that can occur (cm of SWE), S_{mean} is the mean maximum snow load per unit area of branch (kg / m^2), and LAI is the leaf area index (unitless).

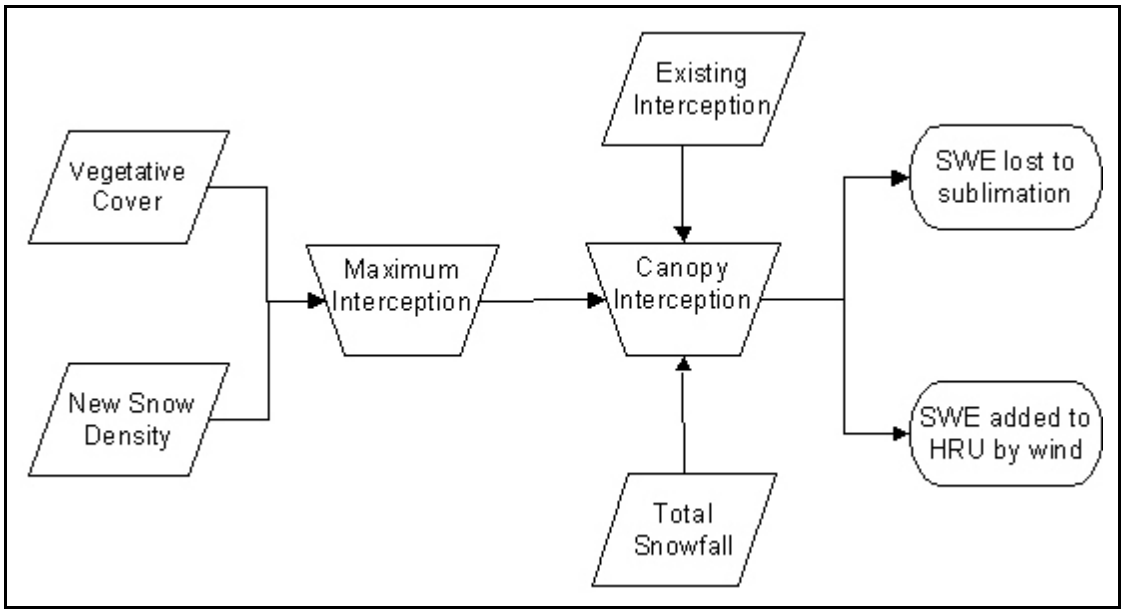

Figure 3-9. Simplified schematic of the forest cover module

Hedstrom and Pomeroy (1998) estimated that S_{mean} for conifers is 6 kg / m^2 and use an average value of 3 for estimating the LAI for conifers. A review of the literature did not yield analogous values for deciduous trees, but logic indicates that both values will be significantly smaller for deciduous trees than for conifers because leaves fall from deciduous trees during the winter. For deciduous trees, the model uses a value of 1.5 kg / m^2 when estimating S_{mean}, and a value of 0.5 when estimating LAI. Sensitivity analysis will be performed for these two parameters to determine the effect that parameter uncertainty has on model output.

The next step in modeling forest snow interception and sublimation was to estimate the total snowfall that is intercepted by the canopy during a snow event on a particular day. Hedstrom and Pomeroy (1998) provided a method of estimating daily interception by means of the following equation:

$$IntSNOW = 0.1\left(MAXINT - InterSWE\right)\left(1 - e^{\frac{-CpSrSDENS}{MAXINT}}\right) \quad (3\text{-}45)$$

where Int_{SNOW} (cm of SWE) is the amount of snow that is intercepted by a canopy, C_P (unitless) is the canopy-leaf contact area per unit area of ground, InterSWE (cm of SWE) is the amount of existing SWE that the canopy has currently intercepted. Hedstrom and Pomeroy (1998) suggested that C_P be set equal to 1 if the wind speed through the canopy, W_{CAN}, is greater than 2 m / s, and equal to forest density, F_d, if the wind speed through the canopy is less than 2 m / s.

Now that methods have been presented for estimating maximum interception and actual interception that occurs over a canopy during a snow event, a summation of total interception must be kept during a complete accumulation and ablation season. The model does this through the variable InterSWE by means of the following equation:

$$InterSWE_t = InterSWE_{t-1} + Int_{SNOW} - Int_{WIND} - Int_{SUB} \quad (3\text{-}46)$$

where $InterSWE_t$ (cm of SWE) is the amount of interception that exists on day t, $InterSWE_{t-1}$ is the amount of interception that exists on day t-1, Int_{WIND} (cm of SWE) is the amount of interception lost from the canopy due to wind transport, and Int_{SUB} (cm of SWE) is the amount of interception lost from the canopy due to sublimation. If Eq. 3-

46 yields a negative value, $InterSWE_t$ is set equal to 0 cm of SWE.

Hedstrom and Pomeroy (1998) estimated Int_{WIND} by means of the following equation:

$$IntWIND = InterSWE \times e^{-(U \times t)} \tag{3-47}$$

where U is an unloading rate coefficient, and t is time (days). These authors went on to define a dimensionless loading coefficient, C, as follows:

$$C = e^{-(U \times t)} \tag{3-48}$$

Additionally, Hedstrom and Pomeroy (1998) determined a mean value of 0.678 for C for a weekly time period. Determining a corresponding daily value of C (by dividing the mean value for a weekly time period by 7 days) and substituting this value back into Eq. 3-47 yields the following equation:

$$IntWIND = 0.0969 \times InterSWE \tag{3-49}$$

Snow that is lost from the canopy because of wind transport, Int_{WIND}, will be added to the underlying snowpack total of SWE.

Hedstrom and Pomeroy (1998), Lundberg, Calder and Harding (1998), Pomeroy, et al. (1998), and Yamazaki and Kondo (1992) have all studied the complexity of sublimation rates which occur from a canopy. In an attempt for modeling simplicity, the model incorporates the following equation to estimate daily sublimation from a canopy:

$$\begin{aligned} Int_{SUB} &= 0.24 \text{ cm / day} && \text{for InterSWE} > 0.24 \text{ cm} \\ Int_{SUB} &= 0 && \text{for InterSWE} < 0.24 \text{ cm} \end{aligned} \tag{3 - 50}$$

This equation is based upon a quote from Pomeroy, et al. (1998) who stated that previous studies have measured or estimated a long term average sublimation rate from a snow covered canopy of approximately 0.1 mm / hr (or 0.24 cm / day).

3.6.8 Final SWE Module

The ultimate goal of the model is to determine the SWE on the ground within an HRU throughout the accumulation and ablation period of a snow season. The model performs this task by means of the following equation:

$$SWE_t = SWE_{t-1} + (AvalSWE_{IN} - AvalSWE_{OUT}) + (WindSWE_{IN} - WindSWE_{OUT}) + PrecipSWE + Int_{WIND} - MeltSWE - SubSWE \quad (3\text{-}51)$$

CHAPTER FOUR

DATA ACQUISITION AND MODEL SETUP

4.1 INTRODUCTION

The following three watersheds have been chosen for analyzing the proposed model: the Upper Rio Grande Watershed in Colorado, the Reynolds Creek Watershed in Idaho, and the Emerald Lake Watershed in California. These watersheds have been chosen for several reasons. First, all three watersheds are known to have a continuous seasonal snowpack, which is essential if a spatial and temporal pattern of SWE distribution is to be established. Second, measured and recorded data are available. These data are required to perform the calibration/validation of the developed model. Third, the watersheds differ in size by several orders of magnitude, which will help to test the issue of scaling. Bloschl (1998) notes the difference in the scale of physical processes from wind drift at hillslopes, significant to the nearest meter, to differences in climatic conditions, significant to tens of kilometers. Does model accuracy depend upon watershed size? This research aims to address this question.

4.2 UPPER RIO GRANDE WATERSHED

4.2.1 Description

The Rio Grande River originates in Colorado, flows through New Mexico and Texas, and eventually to the Gulf of Mexico. Approximately 75% of the average annual flow is the result of snowmelt. The headwaters of the basin are located to the east of the

continental divide in Colorado. The portion of the watershed examined for this study includes only those headwaters upstream of Del Norte. The watershed is centered at approximately 107^0 W, 37^0 7' N, and has an area of approximately 3,450 square kilometers. The basin is bounded on the east by the San Luis Valley and Sangre De Cristo Mountains. The elevation range is from approximately 2432 m to 4215 m. The terrain is fairly rugged, with an average slope of 15 % (Dubayah, 1994).

Annual precipitation ranges from 25 cm in the foothills to 130 cm in the high mountains, over 60 % of which occurs as snowfall. Roughly 60 % of the region is forested. The alpine regions have dense forests consisting chiefly of pine, fir and aspen. The subalpine zone is composed largely of spruce-fir trees. Alpine vegetation consists predominantly of meadows and grasslands (Dubayah, 1994). Figure 4-1 shows the location of the watershed.

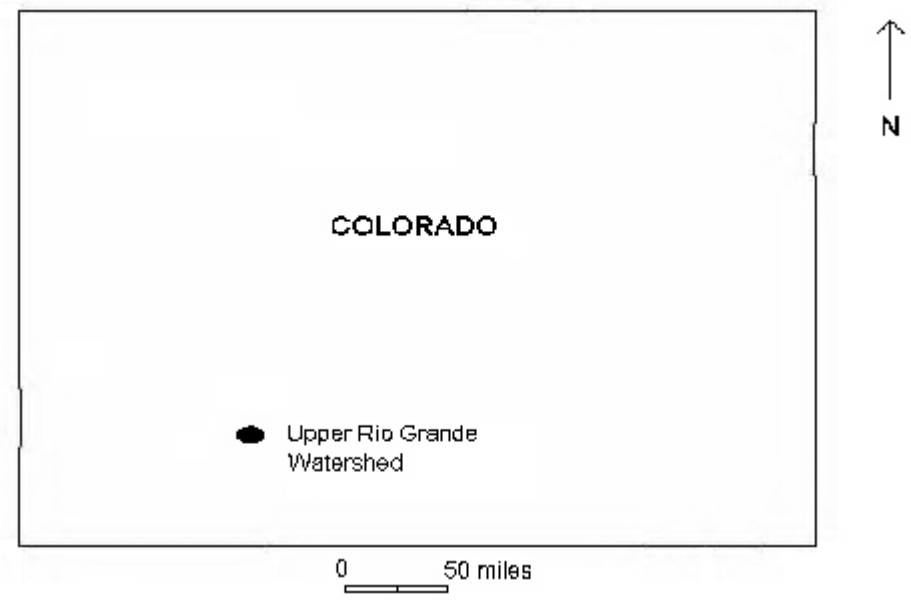

Figure 4-1. Location of Upper Rio Grande Watershed

4.2.2 Creating HRUs Based on DEM and Watershed Data

Digital elevation map (DEM) data were gathered from the United States Geological Survey (USGS, 2003). DEMs used from this site have a 30-m resolution. A geographic information system program (GIS), ArcView, utilized the watershed DEMs to help determine the land slope and orientation of each pixel contained within the watershed. Land use data from 1998 for the watershed were gathered from the United States Environmental Protection Agency (USEPA, 2003). This data were used to determine forest cover, type (conifer or deciduous) and extent, throughout the watershed.

Based upon the DEM and watershed data, the watershed was subdivided into HRUs. As previously mentioned, the rationale behind the subdivision process is to produce subunits where it is reasonable to assume that the average SWE value is representative of the entire subunit for any given day.

The first step of the process of subdividing the watershed into HRUs was to utilize the "Blockstats" command in ArcView to combine single pixels into groupings of (35 pixels x 30 pixels) 1050 pixels. The grouping size of 1050 pixels was selected subjectively. ArcView was then used to determine the required physical parameters for each grouping. For the elevation, slope and forest density parameters, values were determined by ArcView utilizing the mean value of all 1050 pixels. For the area parameter, values were determined by ArcView as the sum of the areas of all of the pixels. For the orientation parameter, values were determined by ArcView based upon the median value of all of the pixels.

Ideally, each of these groupings could have become separate HRUs. This was not feasible for two reasons. The first reason has to do with the creation of input files. Each grouping had an area of 0.945 square kilometers. Based upon the watershed being approximately 3,450 square kilometers, the total number of HRUs would be approximately 3,651. Each HRU needs an input file defining the physical parameters of the watershed as well as potentially 9 yearly input files defining the required meteorological parameters (T_{MAX}, T_{MIN}, T_{AVG}, P_T, W_S, W_O, S_R, R_H, and C_C). Given that the proposed model will run for 8 years for this particular watershed, a total of nearly 266,500 input files would potentially need to be created for this watershed. The second reason has to do with the limited availability of calibration data. Although it is logical to assume that smaller HRUs will produce more accurate results, not enough field measurements exist to determine if subdividing the watershed into smaller and smaller HRUs increases the model accuracy.

The procedure of combining these groupings into the final HRUs was based primarily upon the elevation and forest cover of the 1050 pixel groupings. Tarboton and Luce (1996) point out that in 1986, the World Meteorological Organization compared 11 different snowmelt models from several countries. Among the conclusions of the study were: (1) subdivision of basins into elevation zones is very important, and (2) the recognition of snow interception is important, especially to forecast land change effects. A map of the watershed showing the groupings of the 1050 pixels was created along with a table of the physical parameters of the pixel groupings. The map was inspected, and the physical parameters of each adjacent pixel grouping were examined. Based

upon the two primary criteria of elevation and forest cover, adjacent pixel groupings were subjectively combined if their elevations did not differ by more than 200 m and their forest cover was approximately equal. The physical parameters of the subdivided HRUs were calculated in a manner similar to that of the 1050 pixel groupings. Based upon the above procedure, the watershed was subdivided into 83 HRUs. Note that the above procedure is subjective and that the final creation of HRUs is not unique. Possible automated procedures for subdividing a watershed into HRUs is the subject of further research, and are discussed in Chapter 10. Since this procedure is subjective, sensitivity analysis was performed on the procedure regarding the subdivision of HRUs. This analysis determined the effect that the subjective decisions regarding the subdivision of HRUs had on model output. Table 4-1, found in Appendix A, contains a listing of HRUs created for the Upper Rio Grande Watershed and their pertinent physical parameters . The HRUs are treated as homogeneous units in the model. Pixel properties were analyzed for each HRU to demonstrate that the hydrologically and climatologically important physical characteristics cluster fairly closely around their mean values in the HRUs. Plots shown in Appendix B depict the range of values for the created HRUs. One of the plots in Appendix B depicts equivalent latitude. The formula for computing equivalent latitude is given by the following equation:

$$\Lambda eq = \sin^{-1}\left(\sin\beta\cos\alpha\cos\Lambda + \cos\beta\sin\Lambda\right) \qquad (4\text{-}1)$$

where β is the angle of inclination of the slope (positive downward), α is the azimuth of the slope (clockwise from north), and Λ is the actual latitude (Dingman 1994). An inspection of the plots found in Appendix B indicate that the slope distribution is more skewed than the other plots. The reason for this is that slope was considered the least important of the physical characteristics of the watershed during the process of combining pixels. Figure 4-2 contains a depiction of the watershed divided into HRUs with numbering corresponding to the Table 4-1.

4.2.3 Collecting Meteorological Data

Temperature, precipitation, and SWE data for this watershed were downloaded from the Colorado Snow Telemetry (SNOTEL) site, operated by the Natural Resources Conservation Services (NRCS, 2003) . Data were gathered from four sites within the watershed: Beartown, Upper Rio Grande, Middle Creek, and Wolf Creek Summit. Figure 4-3 shows the location of the SNOTEL sites in relationship to the watershed. Summary information regarding the SNOTEL sites is contained in Table 4-2.

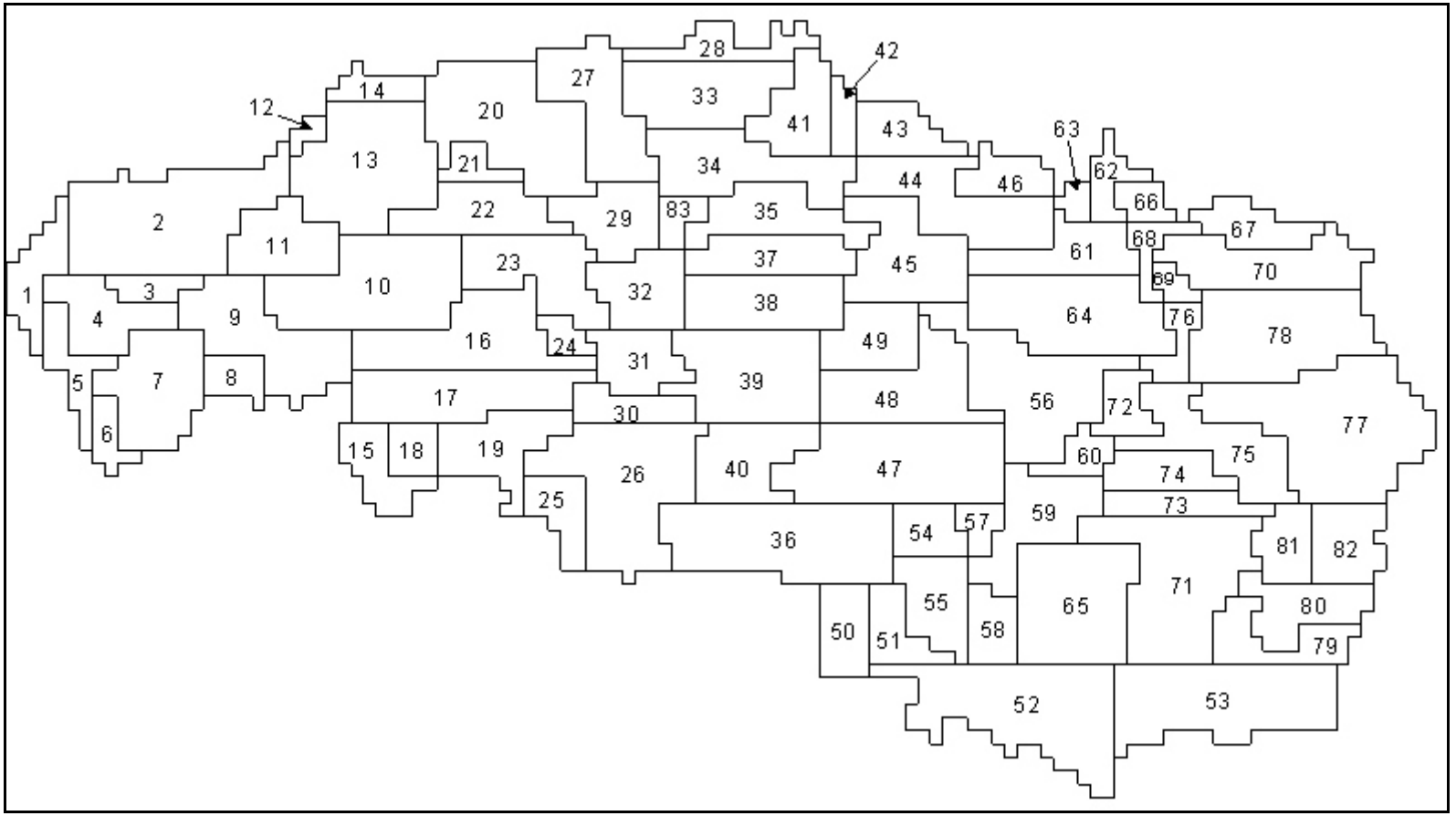

Figure 4-2. Delineation of HRUs for the Rio Grande Watershed

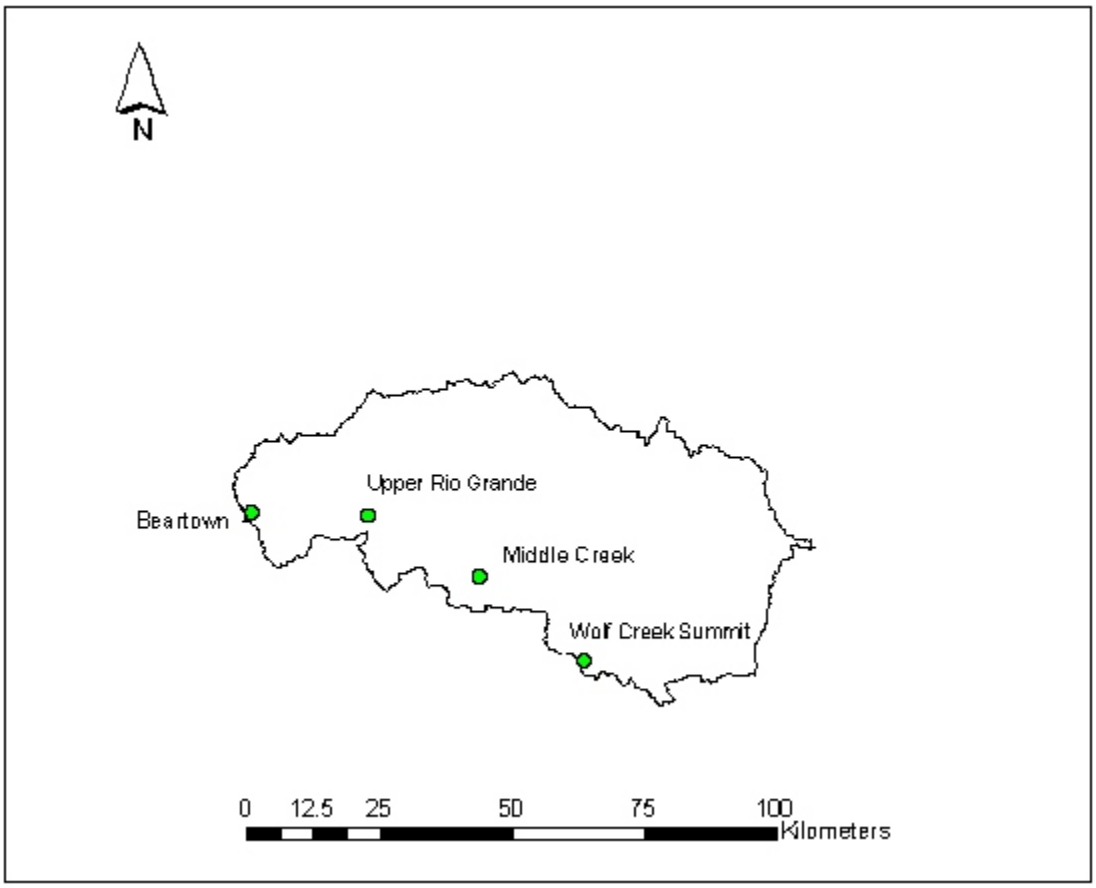

Figure 4-3. Location of SNOTEL sites in the Upper Rio Grande Watershed

Table 4-2. Summary of the SNOTEL sites used for the Upper Rio Grande Watershed

Site ID	SNOTEL ID No.	SNOTEL Station Name	Elevation (m)	Annual Average Precipitation (cm) for 1993 - 2001
1	07M32S	Beartown	3536	106.5
2	07M21S	Middle Creek	3529	105.8
3	07M16S	Upper Rio Grande	2865	59.9
4	06M17S	Wolf Creek Summit	3353	135.9

A review of the SNOTEL website showed temperature, precipitation and SWE data available as far back as the 1930s for some of the stations. However, a closer inspection of the stations included in Table 4-2 showed that the data records are mostly incomplete through the early 1990s, often missing up to two months worth of data in any given year. The inspection helped determine that temperature, precipitation, and SWE data records were nearly complete for the water years 1993 through 2000 (a water year begins on October 1 of the preceding year) . As a result, it was decided to operate the proposed model for the Upper Rio Grande Watershed for these water years.

Sporadic data were missing from these water years for the stations listed in Table 4-2. The largest number of missing temperature data for the 8-year study period was 15, with the average number of missing data being 9. To estimate values for the missing temperature data on a particular day, the arithmetic average value was determined for that day from the remaining years of existing data. This average value was then used as the unknown temperature value.

The largest number of missing precipitation data for the 8-year study period was 18, with the average number of missing data being 7. To estimate values for the missing data, the "normal-ratio method" (McCuen, 1989) was applied. The general formula for computing a missing data point is given by the following equation:

$$\hat{P} = \sum_{i=1}^{n} w_i P_i \qquad (4\text{-}2)$$

where $\hat{P}$ is the unknown data point, P_i is the parameter value at station I, and w_i is the

weight given to station I. Each station weight is determined by the following equation:

$$wi = \frac{Ax}{nAi} \tag{4-3}$$

where A_i is the average annual parameter value at station I, A_x is the average annual parameter value at the station with the missing data, and n is the number of stations. McCuen (1989) states that the normal-ratio method is preferred in areas when "the average annual catches differ by more than 10%," such as locations where orographic effects are present, as is the case for this watershed. A review of the average annual precipitation values for the four SNOTEL sites in Table 4-2, indicate that a difference of more than 10% does exist between most of the stations.

Wind data were not available at the SNOTEL sites, but were downloaded from the National Climatic Data Center (NCDC, 2003). Wind data were collected at the four closest stations to the Upper Rio Grande watershed, which are: Alamosa Municipal Airport, Durango / La Plata, Gunnison, and Telluride Regional Airport. Summary information regarding the NCDC sites is contained in Table 4-3. Figure 4-4 shows the location of the NCDC sites in relationship to the watershed.

Table 4-3. Summary of the NCDC sites used for the Upper Rio Grande Watershed

Site ID	NCDC ID No.	NCDC Station Name	Elevation (m)
1	724620	Alamosa Municipal Airport	2299
2	724625	Durango / La Plata	2038
3	724677	Gunnison	2339
4	724627	Telluride Regional Airport	2769

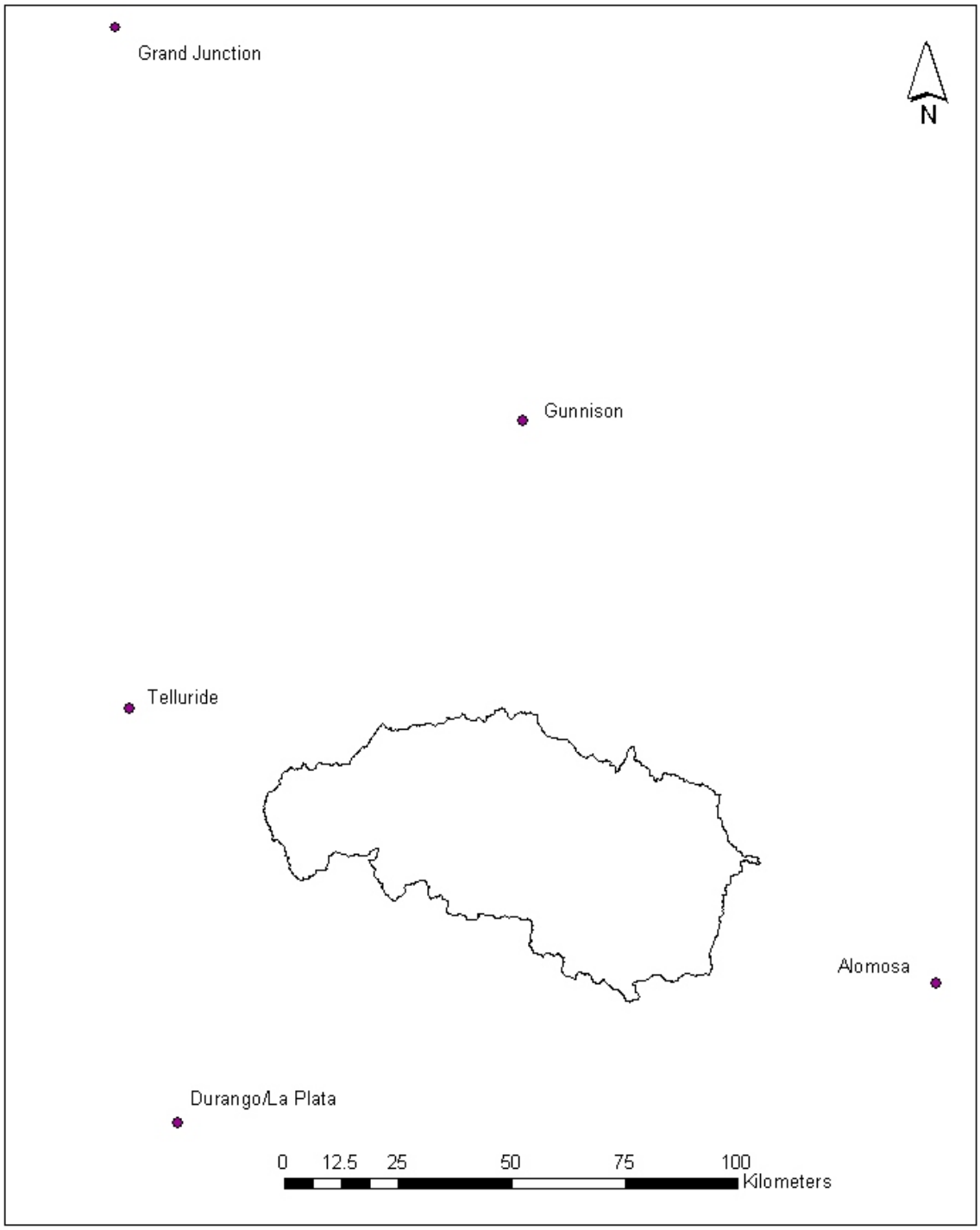

Figure 4-4. Location of the NCDC sites in relationship to the Upper Rio Grande Watershed.

A review of Figure 4-4 indicates that most of the available wind data for this watershed originate from 50 to 75 kilometers outside of the watershed, and are recorded at elevations much lower than those found throughout the watershed. At these distances, it is questionable whether or not the wind speed data recorded at the four NCDC sites approximates the actual wind speeds within the watershed. A deviation sensitivity analysis will be performed on the wind data to determine the potential error to SWE estimates due to the data uncertainty.

Sporadic daily wind data were missing from the NCDC sites listed in Table 4-3. No effort was made to estimate the missing data since the literature does not provide estimation methods similar to those for precipitation. As a result, on days that wind data were missing from a particular station, data were substituted from the other stations in which data existed for that particular day.

Cloud cover data were also downloaded from NCDC (2003). Most NCDC sites do not collect cloud cover data, so finding these data in proximity to the watershed was problematic. Cloud cover data were collected from the Alamosa Municipal Airport for the time span of October 1996 through July 2001, and from Grand Junction for the span of October 1993 through October 1996. The NCDC station at Grand Junction is approximately 180 kilometers northwest of the watershed (see Figure 4-4). Similarly to the wind data, the actual cloud cover conditions occurring at the watershed may be quite different from the available data. Again, a deviation sensitivity analysis will be performed on this data to determine the potential error to SWE estimates due to the data uncertainty.

Solar radiation and relative humidity data were not available within close proximity to the watershed. Consequently, the proposed model will estimate these values utilizing Eq. 3-5 to determine incoming solar radiation, and Eq. 3-4 to calculate relative humidity. The model is designed to accept remotely sensed solar radiation data, such as the data that can be found at http://www.atmos.umd.edu/~srb/gcip/webgcip.htm, when this data are available. Data correction for elevation differences may be required.

4.2.4 Spatially Distributing Meteorological Data to the HRUs

Temperature data were spatially distributed from the SNOTEL sites to the 83 HRUs by means of the nearest-neighbor approach with a lapse rate adjustment for elevation. McCuen (1989), Gray and Male (1981) and many others cite the relationship between elevation and temperature. Based upon the literature, a lapse rate of 0.722^0 C / 100 m was used in estimating temperature data for the HRUs.

Precipitation data were spatially distributed from the SNOTEL sites to the 83 HRUs by means of the hypsometric method as described in Dingman (1994). This method is appropriate for regions in which orographic effects are important, where precipitation for the period of interest is a strong function of elevation. Additionally, this method requires a relationship between precipitation and station elevation and generally takes the linear form of:

$$\hat{P}(z) = a + bz \qquad (4\text{-}4)$$

where $\hat{P}$ is the estimated precipitation value (cm), z is the station elevation (m), and a

and b represent the intercept and slope of the line, respectively. Precipitation data were plotted against station elevation for the Upper Rio Grande watershed for the years of interest (Figure 4-5).

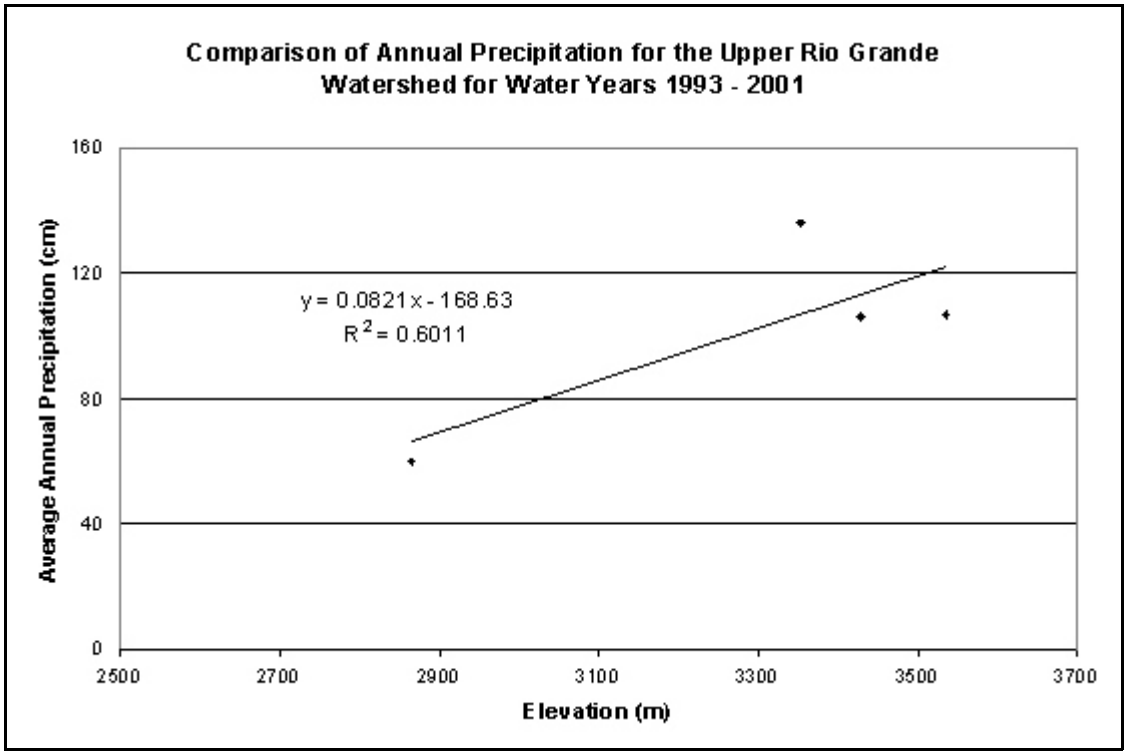

Figure 4-5. Establishing the relationship between precipitation and station elevation for the SNOTEL sites within the Upper Rio Grande Watershed

A review of Figure 4-5 indicates that the slope of the line is 0.08. This indicates that there is an approximate increase of 82 mm in precipitation per 100 m increase in elevation. The intercept of the line is -168.63 cm of precipitation, which is irrational. Consequently, the developed relationship should be limited to a range of station elevations used in developing the equation (2850 m to 3550 m). Although the sample number is small (n = 4) and the coefficient of determination has a moderate value

($R^2 = 0.6011$), Singh and Singh (2001) report that the linear relationship and slope of the relationship, as shown in Figure 4-5, is consistent with several previous studies conducted in this watershed regarding precipitation.

Dingman (1994) states that in some cases, the relationship between precipitation and elevation may vary systematically with a region, for example, the windward side of a mountainous region that may have a more rapid elevational increase in precipitation than the leeward side. In these instances, it is suggested to apply the hypsometric method separately for each identified subregion. Unfortunately, this last point could not be tested for this watershed. A review of Figure 4-3 and the NCDC wind data, shows that all SNOTEL sites within the watershed are located on the windward side of the watershed. This may suggest more accurate precipitation and thus SWE predictions for the HRUs on the windward side of the watershed than the leeward side.

Wind data were spatially distributed from the SNOTEL sites to the 83 HRUs by means of the nearest-neighbor approach. This simple approach was chosen because the literature does not provide any more sophisticated means of spatially distributing wind data. Luce and Tarboton (2000) point out that interpolation of the wind field in mountainous terrain is difficult and in practice seldom done.

Cloud cover data were assumed constant over the entire watershed. This approach was taken for two reasons. First, on any specific day, cloud cover data were available at only one site. Second, the literature again does not provide any more sophisticated means of spatially distributing cloud cover data. Remote sensing satellite images form the National Operational Hydrological Remote Sensing Center (NOHRSC,

2003) could provide more accurate cloud cover data, however, these images are typically only available for approximately 20 days out of the water year.

4.2.5 Creating Required Input Files

Once the physical parameters of the HRUs had been determined and the meteorological data had been spatially distributed, input files required to run the proposed model were created. An input parameter file was created for each HRU, containing values that remained constant from year to year. This input file consisted of six values: S_{LOPE}, O_{RIENT}, L_{AT}, F, T_{REE}, and T_{YPE}. The T_{YPE} parameter refers to whether the HRU is an alpine or valley HRU, and affects the albedo calculation. The parameter, C_{OVER}, was not required for the Upper Rio Grande input files because the transport of snow between HRUs by avalanching became inconsequential for such large size HRUs. This was demonstrated by the fact that several 1050 pixel groupings had an average slope value greater than the required 26 degrees. However, once these groupings were combined to form the 83 HRUs, the average slopes of all HRUs were less than 26 degrees.

For each HRU, meteorological input files were created for T_{MAX}, T_{MIN}, T_{AVG}, $W_{S,}$ and P_T, for each of the study years. These files contained daily values for each variable. Input files were not created for S_R and R_H as these data were not available and were internally estimated by the model by means of Eqs. 3-5 and 3-4, respectively. Input files were not created for W_O because uniform wind transport from an HRU is negligible due to the large size HRUs, as per Gray and Male (1981). Although wind transport from

HRU to HRU would occur along HRU borders, the simplified approach was taken, and it was assumed that wind transport would only occur within the HRUs and would not significantly alter a spatially uniform SWE value throughout the HRU.

4.2.6 Conditional Probability Analysis on Wind Data

As discussed in section 3.5.4, conditional probability analysis was performed on the wind data to increase the accuracy of the sublimation predictions. The purpose of the analysis was to determine the probability that the required threshold wind speed (4.8 m / s) was exceeded on an hourly interval given that the daily average wind speed was less than the threshold wind speed. Hourly wind data were downloaded from the Alamosa Municipal Airport and the Durango/La Plata NCDC sites. A sample of four years, two years from both sites, of hourly data were analyzed and the number of hours in a particular day that the threshold wind speed was exceeded was recorded along with the average daily wind speed. Table 4-4 (Appendix C) contains a summary of the results of the conditional probability analysis for the daily average wind speed, based upon the hourly wind data.

The values from Table 4-4 will be incorporated into the proposed model to more accurately estimate sublimation on days that the average daily wind speed does not exceed the threshold value. The model will accomplish this task in two steps. First, the total sublimation for the day will be estimated as if the threshold wind speed had been exceeded. Then, the total sublimation estimate will be multiplied by the probability value found in Table 4-4, depending on the actual average daily wind speed. As an

example, if the daily average wind speed on day t was determined to be 3.2 m / s, the model would calculate the total sublimation (by means of Eq. 3-35) as if the average wind speed was greater than the threshold wind speed (4.8 m / s). Next, based upon Table 4-4, the model would multiply this total sublimation value by 0.31 to determine the actual sublimation total that occurred on day t. This method assumes that the threshold wind speed is exceeded for a fraction of the day, as estimated by the probabilities found in Table 4-4. For days in which the average wind speed exceeds the threshold wind speed, the model will calculate the sublimation total based upon Eq. 3-35. Additional discussion of conditional probability and its effect on threshold processes can be found in Chapter 10.

4.3 REYNOLDS CREEK WATERSHED

4.3.1 Description

Reynolds Creek is a third-order perennial stream that drains north to the Snake River. The watershed is approximately 239 square kilometers and is located in the Owyhee Mountains of southwestern Idaho, approximately 80 kilometers southwest of Boise, Idaho. Elevations within the watershed range from 1101 m at the outlet to 2241 m. Precipitation varies from about 23 cm at the northern lower elevations, to over 110 cm in the higher regions at the southern and southwestern watershed boundaries where 75 % or more of the annual precipitation occurs as snowfall (Slaughter et al., 1998).

Sagebrush-grasslands dominate most of the watershed, while mountain sagebrush, aspen, sub-alpine fir, and Douglass fir trees are found in areas of higher

snow accumulation. Soils derived from volcanic and lake sediments are present on the watershed and range from shallow, desertic soils at lower elevations to deep organic soils at the higher elevations, which are dominated by forests (Slaughter et al., 1998). Figure 4-6 shows the location of the watershed.

4.3.2 Creating HRUs Based on DEM and Watershed Data

The Reynolds Creek watershed is a government-sponsored experimental watershed under the auspices of the United States Department of Agriculture - Agricultural Research Service (USDA-ARS). Hydrologic data and geographic data are publicly available and can be accessed at the USDA-ARS (2003). Included as part of these data is a 30-m DEM of the watershed derived from USGS contour and land use shapefiles. The DEM and forest cover shapefiles were downloaded and used to subdivide the watershed into HRUs. The process used to create the HRUs is the same process as used for the Upper Rio Grande Watershed. Table 4-5 (Appendix A) contains a summary of the physical parameters of the 28 HRUs created for the Reynolds Creek Watershed. Plots shown in Appendix D depict the range of values for the created HRUs.

Figure 4-6. Location of the Reynolds Creek Watershed

Again, due to the time constraint involved with creating a large number of input files and lack of additional SWE data, 1050 pixel groupings were recombined to create the HRUs. Consequently, this process will again prevent analyzing wind transport and avalanching between HRUs for this watershed. Figure 4-7 contains a depiction of the watershed divided into HRUs with numbering corresponding to the above table.

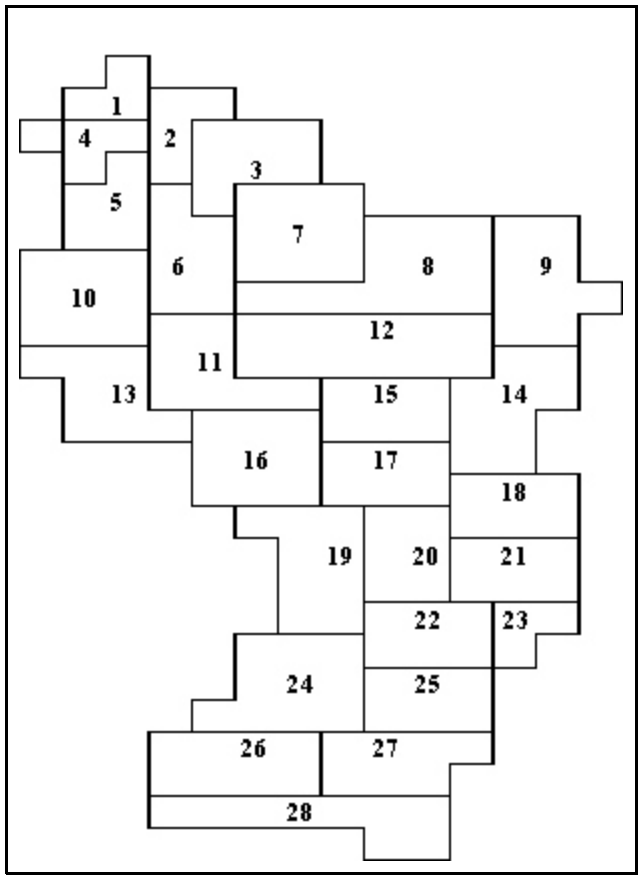

Figure 4-7. Delineation of HRUs for the Reynolds Creek Watershed

4.3.3 Collecting Meteorological Data

All necessary meteorological data were obtained from climate stations within the Reynolds Creek Watershed. Three stations record daily and hourly values for maximum and minimum air temperature, hourly values for relative humidity, hourly values for solar radiation, and daily and hourly values for wind speed and wind direction. A review of the available data indicated that all required data were available for the water years 1988 through 1996. As a result, the proposed model was operated for these years. Slaughter et al. (1998) describe the methodology that was used to estimate missing data

from these stations. Figure 4-8 shows the climate stations within the watershed, and Table 4-6 contains summary information regarding the climate stations.

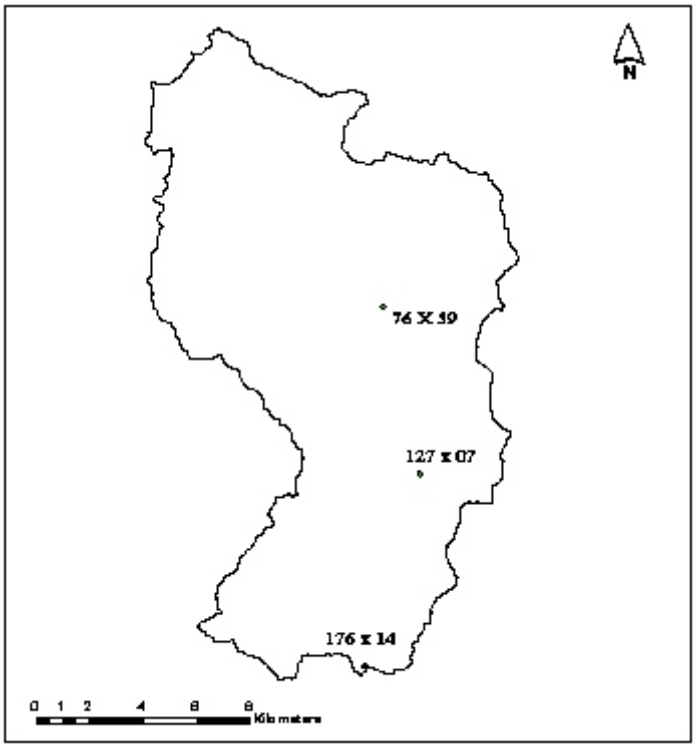

Figure 4-8. Location of the climate stations within the Reynolds Creek Watershed

Table 4-6. Summary of the climate stations used for the Reynolds Creek Watershed

Site ID	Station Designation	Elevation (m)	Beginning of Station Records
1	076 x 59	1202	1/1/64
2	127 x 07	1653	1/1/67
3	176 x 14	2097	1/1/67

Precipitation data were gathered from a more extensive network of sites within the basin. The watershed originally had 53 precipitation gauges, however, only 16 of them were operating through 1996 (Slaughter et al., 1998). Of the 16 precipitation gauges that operated through 1996, data were gathered from six of these sites. The sites were chosen due to the fact that the gauges have the longest active record (35 years) and that Slaughter et al. (1998) used these sites to develop the spatial and temporal precipitation characteristics within the watershed. This previous study will be utilized to spatially distribute precipitation from the gauges to the HRUs. In addition, Slaughter et al. (1998) describe that missing daily and hourly precipitation data from these gauges were estimated based upon data from nearby sites. Summary information regarding the precipitation gauges is included in Table 4-7. Additionally, Figure 4-9 identifies the six precipitation gauges within the watershed used for data collection.

Table 4-7. Summary of the precipitation gauges used for the Reynolds Creek Watershed.

Site ID	Station Designation	Elevation (m)	Annual Precipitation (cm)
1	057 x 96	1188	23.6
2	076 x 59	1207	27.5
3	116 x 91	1459	47.1
4	155 x 07	1654	71.2
5	163 x 20	2170	112.3
6	176 x 07	2061	99.4

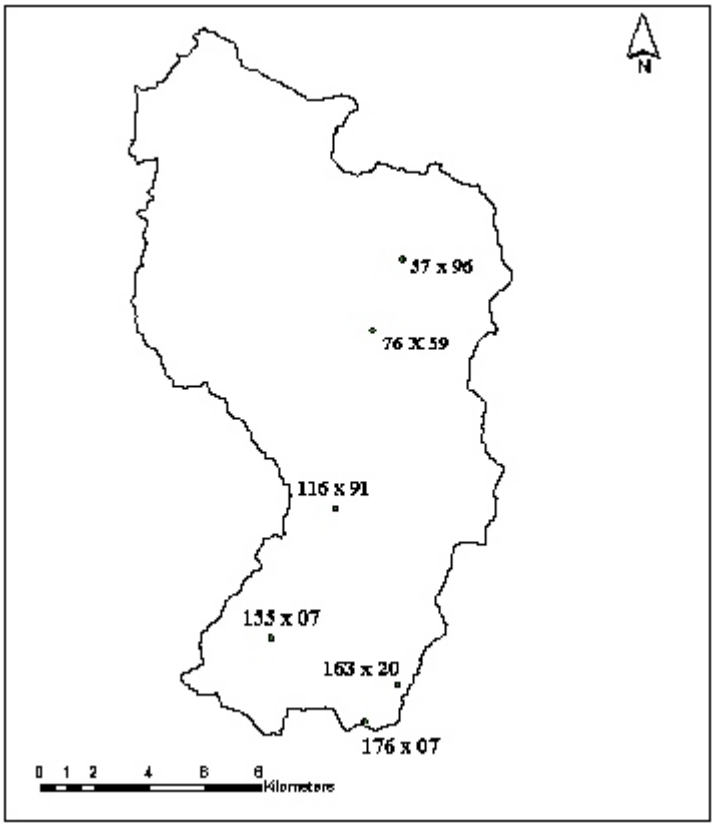

Figure 4-9. Location of the precipitation gauges within the Reynolds Creek Watershed

For calibration purposes, SWE data were collected from five different locations within the watershed. These locations can bee seen on Figure 4-10. Of the five SWE measurement sites, only data collected at two of them were used. Slaughter et al. (1998) state that the SWE measurements taken at: 144 x 62, 163 x 98 and 176 x 07 are in close proximity to areas of significant localized snow-drifting. Due to this reason, it is believed that measurements taken at these sites will not accurately represent the surrounding vicinity and thus these sites will not be used in the calibration process.

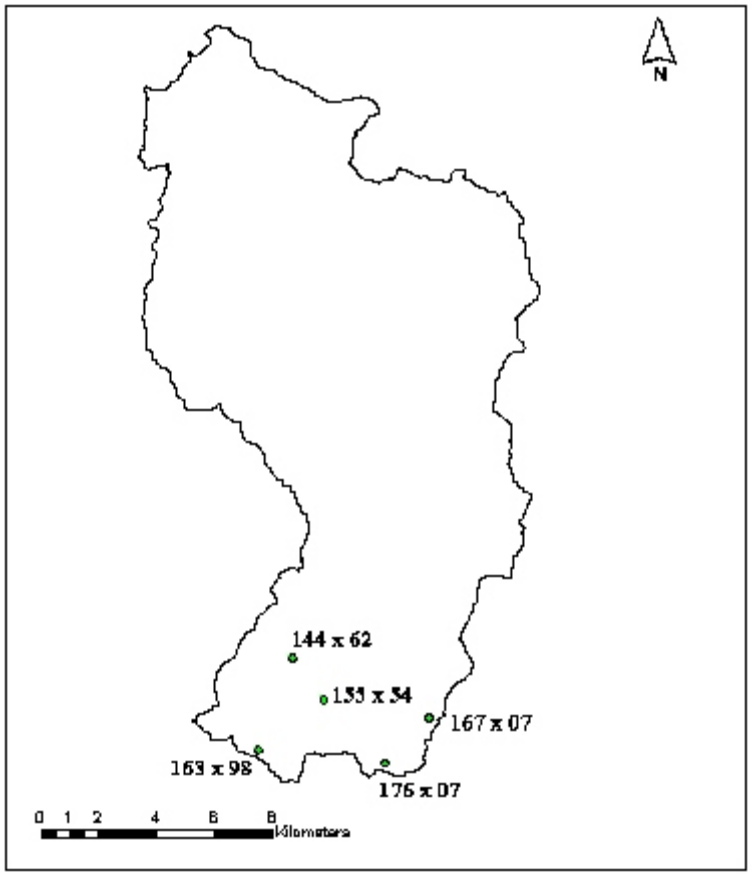

Figure 4-10. Location of SWE measurement sites within the Reynolds Creek Watershed

4.3.4 Spatially Distributing Meteorological Data to the HRUs

Temperature data were spatially distributed from the climate stations to the 28 HRUs in the same manner as previously described for the Upper Rio Grande Watershed. Wind data were also spatially distributed from the climate stations to the HRUs in the same manner as described for the Upper Rio Grande Watershed.

In addition, solar radiation and relative humidity data were spatially distributed from the climate stations to the HRUs by means of the nearest-neighbor approach. Solar radiation data were collected on a hourly time step, and these data were converted

to daily values by summing the hourly values that comprised a particular day. Relative humidity data were also collected on an hourly time step. These data were converted to daily values by taking the arithmetic mean of the 24 hourly values that comprised a particular day.

Precipitation data were spatially distributed from the climate stations to the 28 HRUs in the same manner as previously described for the Upper Rio Grande Watershed. For the Reynolds Creek Watershed, however, a new relationship had to be determined between gauge elevation and precipitation. This analysis was performed by Slaughter et al. (1998) and is given by the following equation:

$$\hat{P}(z) = -755.81 + 0.855z \tag{4-5}$$

where $\hat{P}$ is the estimated precipitation value (cm) and z is the station elevation (m).

This relationship was developed from data from six sites with a correlation coefficient equal to 0.92.

The relationship shown in Eq. 4-4 indicates that precipitation increases at a rate of approximately 86 mm per increase in station elevation of 100 m. Although not mentioned in the analysis performed by Slaughter et al. (1998), it must be assumed that the relationship presented in Eq. 4-4 is applicable only for the range of station elevations (1188 m to 2170 m) used to perform this analysis. The range of precipitation stations approximates the range of ground elevations found within the watershed (1101 m to 2241 m).

Similar to the Upper Rio Grande Watershed, cloud cover data were assumed constant over the entire watershed. This assumption was made for the same reasons described earlier. Cloud cover data were obtained from the regional airport at Salt Lake City, Utah.

4.3.5 Creating Required Input Files

Input files were created for the Reynolds Creek Watershed in the same manner as described for the Upper Rio Grande Watershed. An input parameter file was created for each of the 28 HRUs that remained constant from year to year. The input file consisted of six values: S_{LOPE}, O_{RIENT}, L_{AT}, F, T_{REE} and T_{YPE}. As was the case with the Upper Rio Grande Watershed, the parameter, C_{OVER}, was not required for these input files because the transport of snow between HRUs by avalanching became inconsequential for such large HRUs. Additionally, a review of Table 4-5 indicates that no HRU has a large enough ground slope to initiate avalanching.

For each HRU, meteorological input files were created for T_{MAX}, T_{MIN}, T_{AVG}, W_S, R_H, $S_{R,}$ and P_T, for each year. These files contained daily values for each variable. Input files were not created for WindOrient. As was the case with the Upper Rio Grande Watershed, uniform wind transport from an HRU was assumed negligible due to the large HRUs.

4.3.6 Conditional Probability Analysis on Wind Data

As discussed in section 4.2.6, conditional probability analysis was performed on the wind data to increase the accuracy of the sublimation predictions. A sample of four years of hourly wind data was gathered from the three climate stations located within the watershed. Table 4-8 (Appendix E) contains a summary of the results of the conditional probability analysis for the daily average wind speed, based upon the hourly wind data. The results of this analysis have been incorporated into the proposed model to improve the accuracy of the sublimation estimates. The method to accomplish this task is the same as described for the Upper Rio Grande Watershed.

4.4 EMERALD LAKE WATERSHED

4.4.1 Description

The Emerald Lake Watershed is located in California in the Sequoia National Park along the western slope of the Sierra Nevada. The watershed is centered at approximately 36^0 35' N, 118^0 40' W and has an area of 120 hectares. Elevations within the watershed range from approximately 2800 m at the outlet to 3416 m. The terrain is rugged, composed mainly of granite with steep slopes, averaging 31 degrees (Sierra Nevada Watershed Group, 1999).

Precipitation in the basin is strongly seasonal, with snowfall accounting for most of the deposition. Avalanching from the steep slopes onto the lake is a common occurrence. Typically, snow cover disappears by mid June, but may persist until mid July or early August when unusually large snowpacks exist. Vegetation is sparse

throughout the watershed, consisting of scattered conifers, low woody shrubs, and grasses (Sierra Nevada Watershed Group, 1999). Figure 4-11 shows the location of the watershed.

4.4.2 Creating HRUs Based on DEM and Watershed Data

As with the Upper Rio Grande Watershed, digital elevation model (DEM) data were gathered from the United States Geological Survey (USGS, 2003) and land use data for the watershed were gathered from the United States Environmental Protection Agency (USEPA, 2003). The process used to create the HRUs is the same process as described for the previous two watersheds but with one difference. Whereas the "BlockStat" command in ArcView combined 1050 pixels into groupings for the first two watersheds, this command combined sixteen pixels into groupings for the Emerald Lake Watershed. This smaller number could be used for pixel groupings due to the small size of the watershed. Table 4-9 contains a summary of the physical parameters of the 8 HRUs created for the Emerald Lake Watershed. A review of Table 4-9 indicates that HRU sizes are small enough and slopes are steep enough for both wind transport and avalanching to be significant at this scale. Figure 4-12 contains a depiction of the watershed divided into HRUs with numbering corresponding to Table 4-9 (Appendix A). Plots shown in Appendix F depict the range of values for the created HRUs.

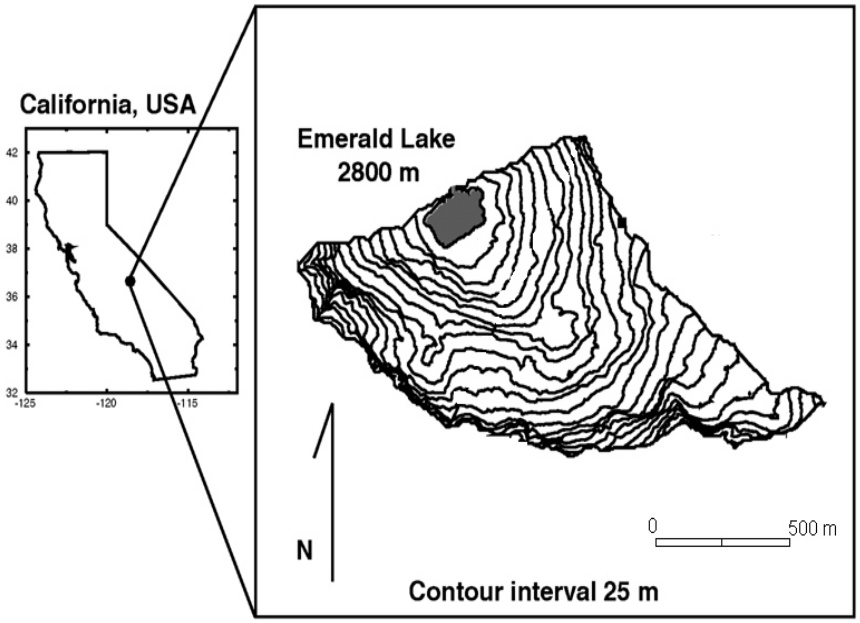

Figure 4-11. Location of the Emerald Lake Watershed (Sierra Nevada Watershed Group, 1999)

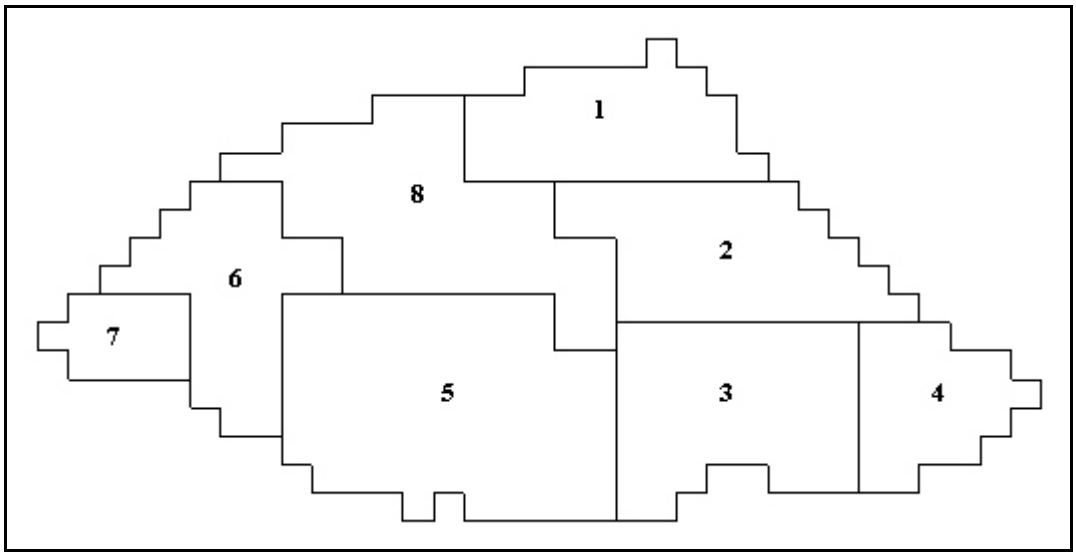

Figure 4-12. Delineation of HRUs for the Emerald Lake Watershed

4.4.3 Collecting Meteorological Data

Meteorological data for this watershed are part of a snow hydrology database that is maintained by the University of California at Santa Barbara (UCSB, 2003). All such data were obtained, with permission, from UCSB (2003). Within the watershed, one primary meteorological station exists within close proximity to the lake. From this station, temperature, precipitation, and wind speed and direction data were gathered. Figure 4-13 shows the location of the meteorological station. A review of the available data indicates that complete records for the required data exists for the water years 1992, 1993, 1996, 1997, and 1998. As a result, the proposed model will be run for these years.

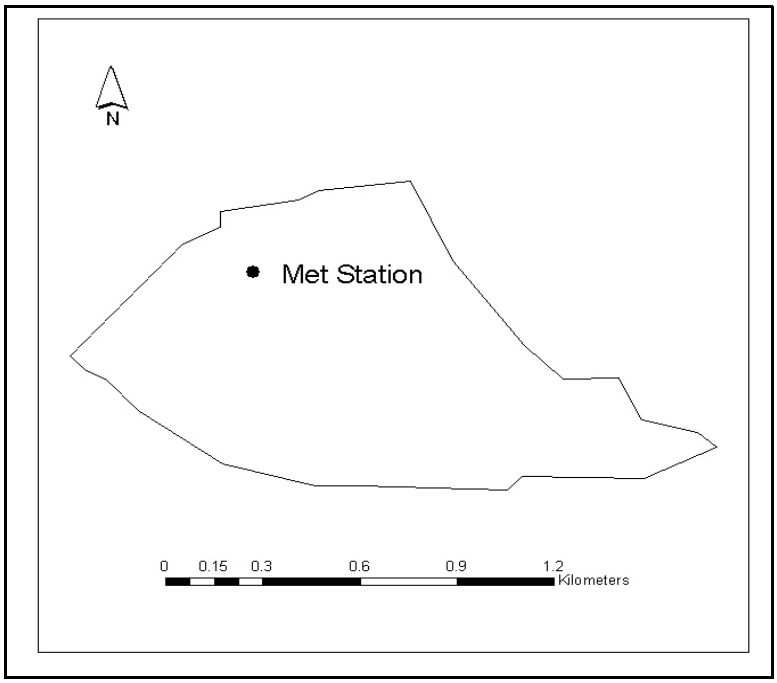

Figure 4-13. Location of Meteorological Station within the Emerald Lake Watershed

Cloud cover data were collected from the closest NCDC site, located at the Fresno Air Terminal. This site is approximately 100 km southwest of the Emerald Lake Watershed. Solar radiation and relative humidity data were not available for this watershed from the database. As a result, the proposed model will estimate these values by means of Eqs. 3-5 and 3-4, respectively.

Additional precipitation data were gathered from outside of the watershed from nearby precipitation gauges. These additional data were required to attempt to determine the relationship between gauge elevation and precipitation for the surrounding region. Precipitation data were gathered from five additional gauges operated by the California Department of Water Resources (CDWR, 2003). Figure 4-14 shows the location of these additional gauges in respect to the Emerald Lake Watershed. Table 4-10 contains a summary of the CDWR precipitation gauges used to estimate the relationship between gauge elevation and precipitation for the Emerald Lake region.

Table 4-10. Summary of the CDWR precipitation gauges used for the Emerald Lake Watershed

Gauge ID	CDWR Gauge Name	Elevation (m)	Annual Average Precipitation (cm) for 1990 - 2000
1	Ash Mountain	520.6	92.2
2	Bear Trap Meadow	2072.6	119.9
3	Big Meadow	2316.5	172.6
4	Grant Grove	2011.7	137.9
5	Lodgepole	2058.2	138.8

SWE measurements were taken at 5 random field locations throughout the watershed during the spring months and these field measurements were also downloaded. The location of these SWE measurement sites can be seen in Figure 4-15. The numbering of these sites corresponds with the number of the HRUs (Figure 4-12).

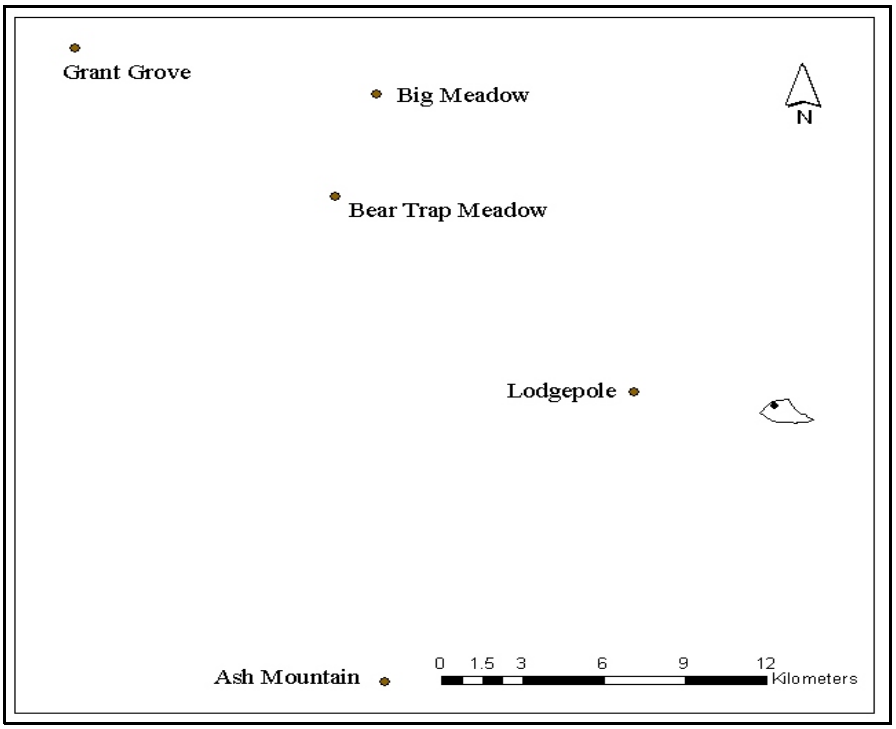

Figure 4-14. Location of the CDWR gauges in relationship to the Emerald Lake Watershed

4.4.4 Spatially Distributing Meteorological Data to the HRUs

Temperature data were spatially distributed from the meteorological station by means of a lapse rate as previously discussed. Cloud cover, wind speed, and wind orientation data were assumed to be equal for all HRUs. Precipitation data were

spatially distributed by means of a lapse rate, similar to the temperature data. The precipitation lapse rate was determined using the data from the CDWR gauges. These data were plotted to determine a linear relationship between gauge elevation and precipitation. This plot can be found on Figure 4-16.

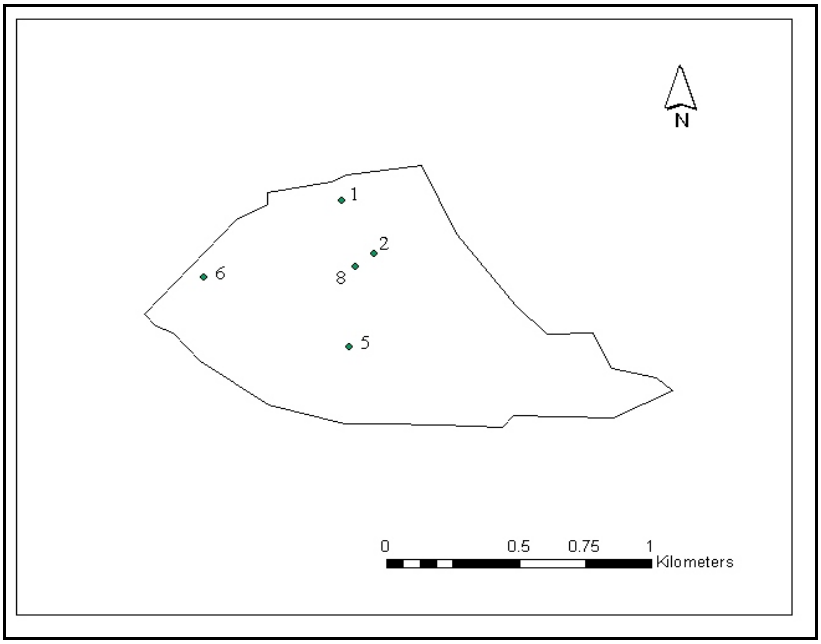

Figure 4-15. Location of SWE field measurement sites within the Emerald Lake Watershed

Although the sample number of gauges is small (n = 5), the coefficient of determination has a significant value ($R^2 = 0.7091$). A hypothesis test was performed on the R value to determine if this relationship is significant. The results of the hypothesis test indicate that it is for a level of significance of 0.01. The relationship determined in Figure 4-16 should be limited to the range of station elevations used in the regression. The slope of the regression line indicates that precipitation increases

approximately 34 mm for every station elevation increase of 100 m. Unlike the similar analysis performed for the Upper Rio Grande watershed, no other studies could be found in the literature to confirm the relationship.

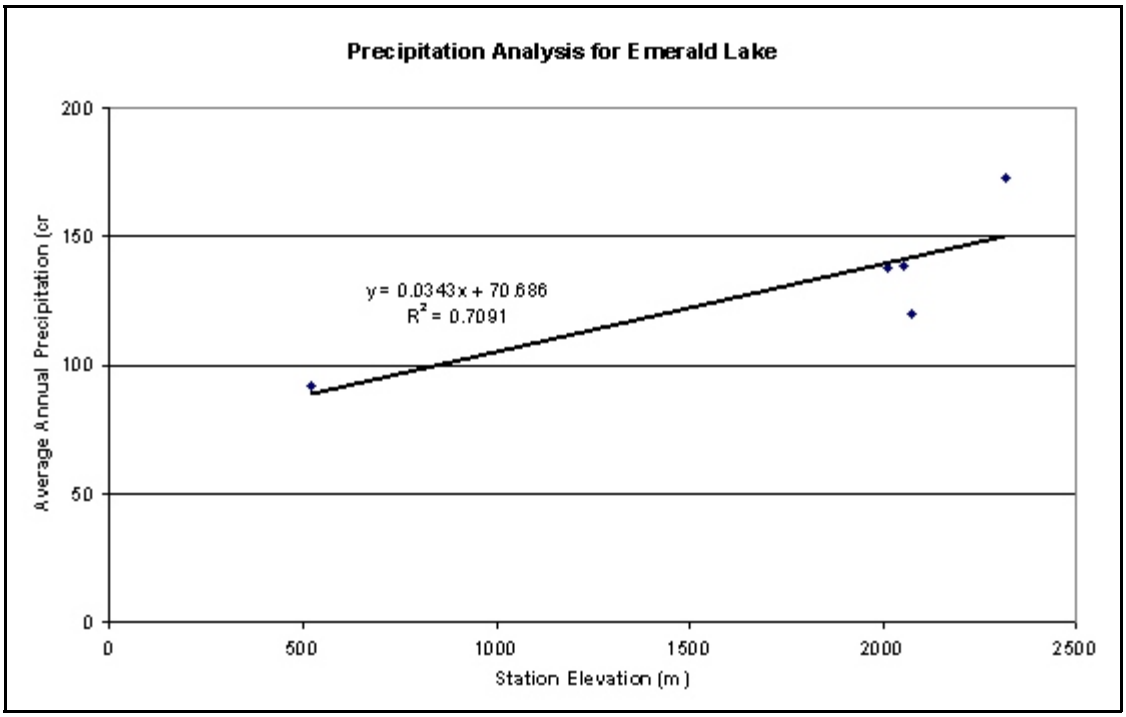

Figure 4-16. Establishing the relationship between precipitation and station elevation for the CDWR gauges surrounding the Emerald Lake Watershed

4.4.5 Creating Required Input Files

Input files were created for this watershed in the same manner as described for the earlier watersheds. An input parameter file was created for each of the eight HRUs that remained constant from year to year. Unlike the earlier watersheds, the input file consisted of seven values: S_{LOPE}, O_{RIENT}, L_{AT}, F, T_{REE}, $T_{YPE,}$ and C_{OVER}. A review of

Table 4-8 indicates that C_{OVER} was required for these HRUs since most had a ground slope of at least 26 degrees, which indicates the possibility of avalanching.

For each HRU, meteorological input files were created for T_{MAX}, T_{MIN}, T_{AVG}, W_S, $W_{O,}$ and P_T, for each year. These files contained daily values for each parameter. Unlike the earlier watersheds, input files for WindOrient were required to model wind transport between HRUs.

4.4.6 Conditional Probability Analysis on Wind Data

A wind speed analysis was performed on a sample of four years of hourly wind data gathered from the meteorological station located within the watershed. The rationale and procedure of the analysis have been discussed earlier. For this watershed, the analysis had to be extended to include both sublimation and wind transport. Table 4-11 (Appendix G) contains a summary of the results of the conditional probability analysis for the sublimation process in which the threshold wind speed is 4.8 m / s. All results from the conditional probability analysis will be incorporated into the model as discussed for the first two watersheds.

For wind transport, two separate analyses had to be performed. The reason for this is that the model differentiates between wind transport from an alpine HRU and a valley or prairie HRU. Table 4-12 (Appendix H) contains a summary of the results of the conditional probability analysis for the wind transport process for an alpine HRU in which the threshold wind speed is 5.0 m / s and Table 4-13 (Appendix I) contains the results for a valley or prairie HRU in which the threshold wind speed is 6.5 m / s.

CHAPTER 5

IMPLEMENTATION AND CALIBRATION OF THE MODEL FOR THE UPPER RIO GRANDE WATERSHED

5.1 INTRODUCTION

For the proposed SWE model, it is important to include an analysis that shows the accuracy of the model in which the parameters are set by information that is independent of the hydrologic data for that watershed. This is referred to herein as the pre-calibration phase. The accuracy of these cases can be compared using graphical results, standard goodness-of-fit statistics (such as the sample mean error and the mean relative error) and physically-based statistics, such as peak SWE for a water year.

The calibration process involves varying the model parameters to obtain an optimal agreement between the model output and the measured SWE data. This process should include a discussion of what type of calibration is being performed and why. It should also include a discussion of the goodness-of-fit criterion, the parameters to be optimized, and the rationale as to why the specific parameters were chosen for optimization. This is referred to herein as the subjective optimization process. The calibration process should also include an analysis that shows the improvement in model accuracy achieved as a result of the process by comparing modeled results with those obtained during the pre-calibration phase. This is referred to in this chapter as the post-calibration phase. The improvement in accuracy for these cases can be compared using the same measures as outlined for the pre-calibration phase.

Once a calibrated model has been developed, the reliability of the model must be confirmed or validated by running the model for a new data set (or several data sets). This task must be performed before the model can be used with confidence to make predictions. This is referred to herein as model validation.

5.2 PRE-CALIBRATION MODEL RESULTS

For the Upper Rio Grande Watershed, the model was initially run for the water year 1993, for the following three hydrologic response units (HRUs): 1, 40 and 50. These HRUs correspond to the SNOTEL sites: Beartown, Middle Creek, and Wolf Creek Summit, respectively. Meteorological data were initially collected from a fourth SNOTEL site, Upper Rio Grande. However, SWE data were unavailable at this site, so this site could not be included in the calibration process. The results of the initial model run for these HRUs are presented graphically in Figures 5-1 through 5-3.

Figures 5-1 through 5-3 are plots of model predicted SWE values along with SNOTEL SWE values for the three HRUs for the water year 1993. A visual inspection of Figures 5-1 through 5-3 indicates that the proposed model does not accurately match the SNOTEL SWE data. For Figures 5-1 and 5-2, which correspond to HRUs 1 and 40 respectively, the model severely under predicts the SNOTEL data. For both figures, the onset of melt occurs too early in the ablation period and the model predicts melt ensuing throughout portions of the ablation period that does not match the SNOTEL data. This occurrence is caused by an excess of net energy received during the accumulation period at these HRUs, which causes the snowpack to ripen, thus melt results too soon. For

Figure 5-3, which corresponds to HRU 50, the model accurately matches the SNOTEL SWE data to approximately the middle of March. After this time period, the model over predicts the peak SWE value and poorly matches the ablation period. This occurrence is caused by a deficit in the accumulation of net energy during the accumulation period at this HRU. This causes a delay in the ripening of the snowpack, which increases peak SWE and delays melt.

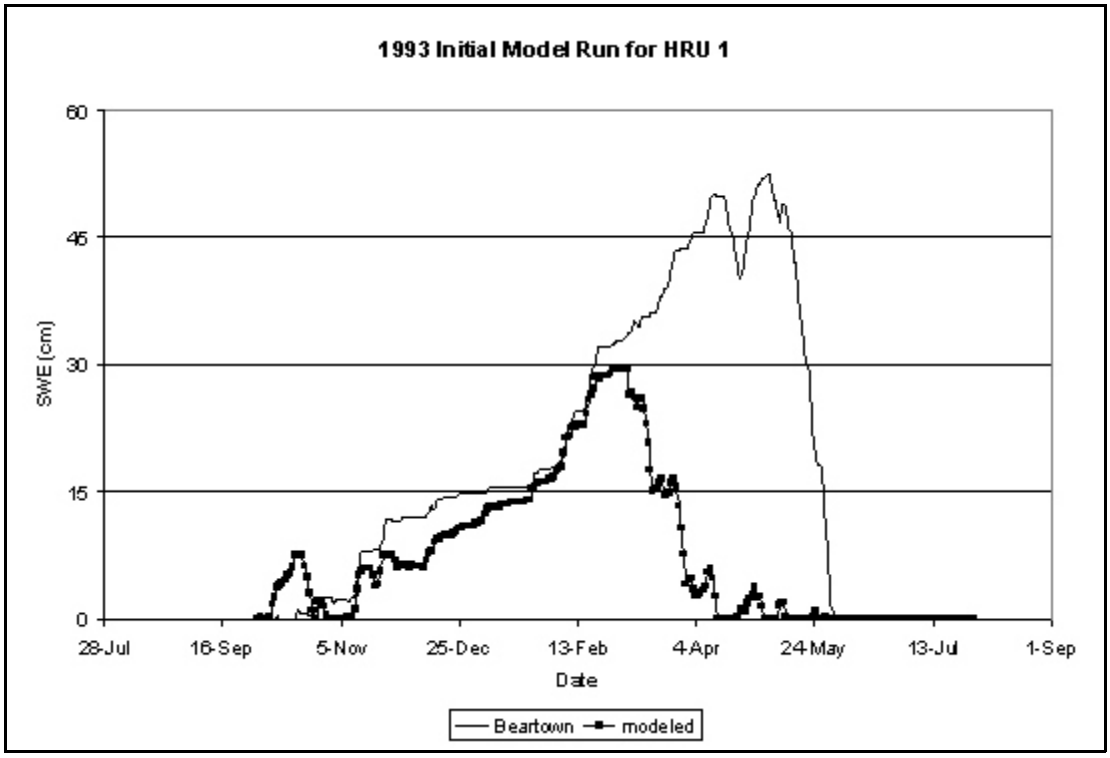

Figure 5-1. Initial model results for HRU 1 for 1993

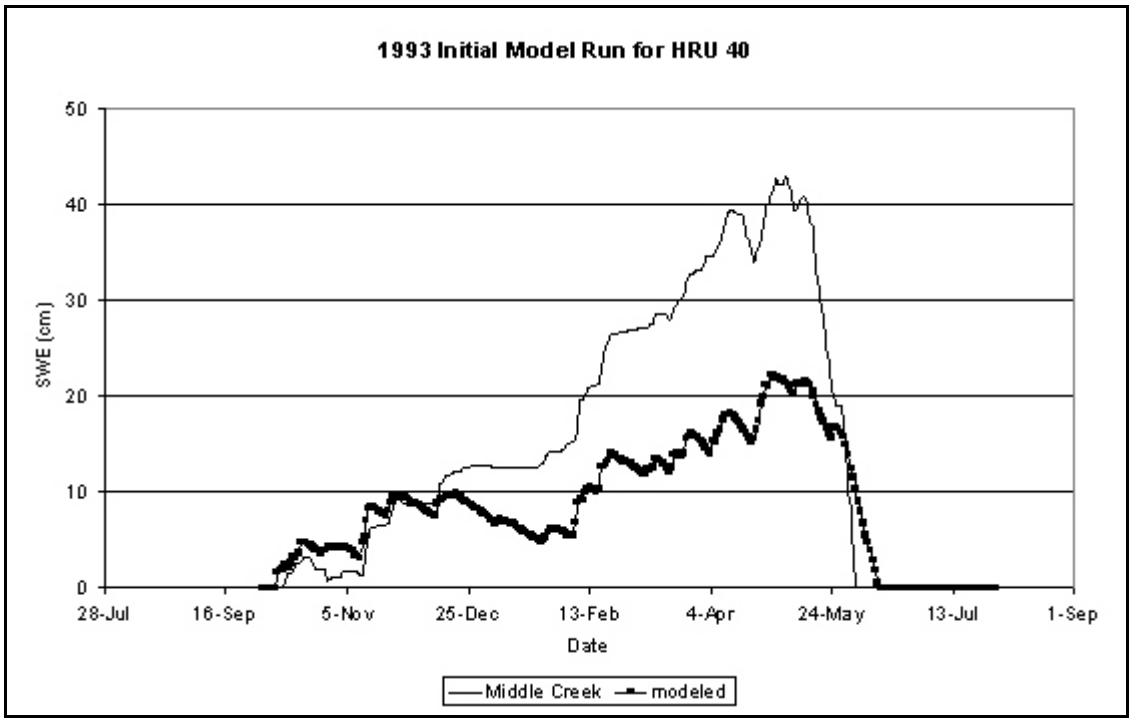

Figure 5-2. Initial model results for HRU 40 for 1993

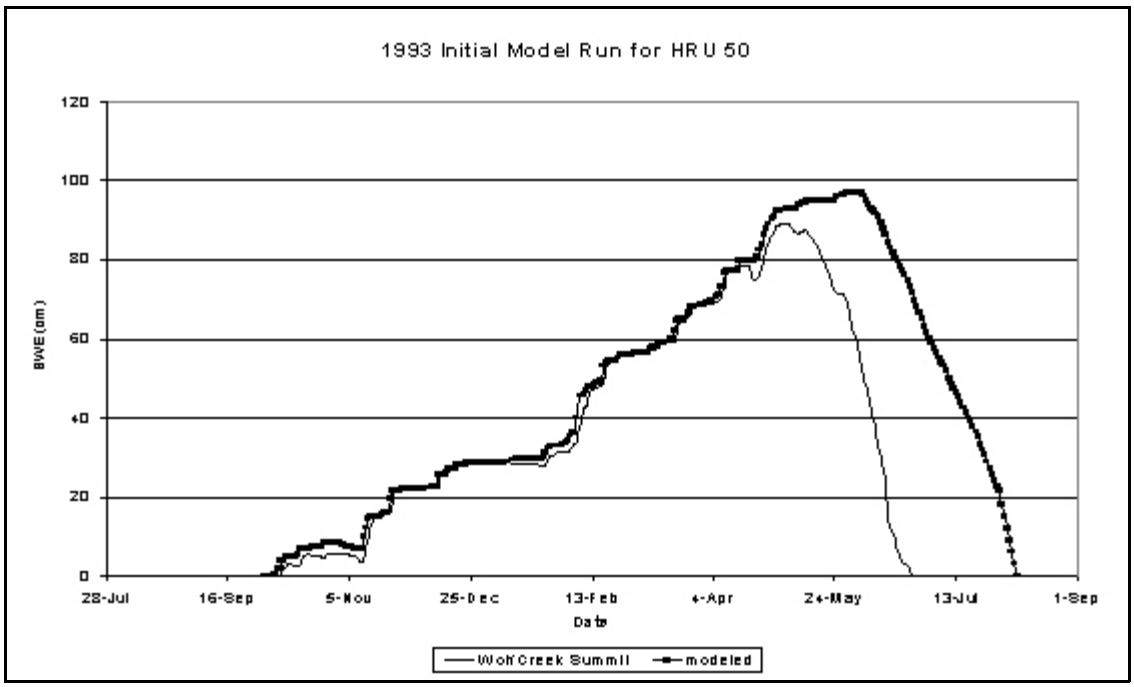

Figure 5-3. Initial model results for HRU 50 for 1993

In addition to a visual inspection, statistical analyses were performed on these initial runs to assess the accuracy of the proposed model for the measured SNOTEL SWE data. The statistical parameters computed include: the sample mean error ($\overline{e}$), the mean relative error ($\overline{e} / \overline{Y}$), the standard deviation of the measured data (S_y), the standard error of the estimate (S_e), and the ratio of the standard error of the estimate to the standard deviation of the measured data (S_e / S_y). Analyses were performed for the entire water year, the accumulation season, and the ablation season to help determine if the proposed model was more accurate for a specific part of the water year.

In addition to these statistical parameters, additional calculations were made to determine how accurately the proposed model matched physically significant values of the measured SNOTEL SWE data; comparing the algebraic and percent differences in the modeled peak SWE and measured SNOTEL SWE for the water year, comparing the difference in the date at which the snowpack becomes ripe with the date in which the model predicts that the snowpack becomes ripe, and comparing the difference in the length of the ablation period (defined as the time period from the date of snowpack ripening to date of snow disappearance) for each particular HRU. Comparing the peak modeled and measured SNOTEL SWE value is significant in that it provides a crude estimate for the approximate volume of runoff that may be generated during the ablation season. Comparing the date at which the snowpack becomes ripe is significant in that it gives an approximation to the date in which stream discharge becomes affected by snow ablation. Comparing the length of the ablation period for an HRU is significant because it can help identify severe discharge events. For the same snowpack, an

ablation season of 40 days could potentially trigger severe stream discharge events compared to an ablation period that lasts 120 days.

For the SNOTEL SWE data, the date in which the snowpack becomes ripe will be approximated by the day that the melt begins. No field data exists for these sites that directly indicates on which date the snowpack becomes ripe, but the onset of melt is generally accepted as a good approximation. This assumption was discussed by Gray and Male (1981) which cite a study performed by the Army Corps of Engineers in 1956. This study found that for watersheds with areas greater than 200 km^2, the lag time between the ripening of the snowpack and the beginning of melt can be ignored. Since this watershed is much greater in area than 200 km^2, this assumption should hold true. For the modeled results, the date at which the snowpack becomes ripe can be identified as the date in which the cold content of the snowpack becomes equal to 0.

The results of the pre-calibration statistical analyses can be found in Tables 5-1 through 5-3. These tables contain a summary of the goodness-of-fit statistics and the physically-based statistics discussed above for the entire water year, the accumulation period, and the ablation period respectively, for the water year 1993, for the HRUs 1, 40, and 50.

Table 5-1. Summary of the goodness-of-fit statistics for the water year 1993 for the HRUs 1, 40, and 50

Parameter	HRU 1	HRU 40	HRU 50
$\overline{e}$ (cm)	-13.5	-7.6	30.6
$\overline{e} / \overline{Y}$	-0.74	-0.51	0.86
S_e (cm)	22.4	11.4	26.1
S_e / S_y	1.11	1.05	0.89
Peak SWE modeled (cm)	29.5	18.2	96.9
Peak SWE measured (cm)	52.3	42.9	89.2
Δ Peak SWE (cm)	-22.8	-24.7	7.7
Δ Peak SWE / Peak SWE measured	-43.6%	-57.6%	8.6%
Modeled date of snowpack ripening	Feb. 28	April 12	May 30
Estimated date of snowpack ripening from SNOTEL SWE measurements	May 4	May 5	May 4
Δ Date of snowpack ripening (days)	-35	-23	26
Modeled length of snowpack ablation period (days)	74	62	70
Measured length of snowpack ablation period (days)	29	30	52
Δ length of snowpack ablation (days)	45	32	18

Table 5-2. Summary of the goodness-of-fit statistics for the measured accumulation period of the water year 1993 for the HRUs 1, 40, and 50

Parameter	HRU 1	HRU 40	HRU 50
$\overline{e}$ (cm)	-11.1	-7.9	17.5
$\overline{e} / \overline{Y}$	-0.52	-0.46	0.49
S_e (cm)	20.0	11.3	20.1
S_e / S_y	0.97	0.99	0.79

Table 5-3. Summary of the goodness-of-fit statistics for the measured ablation period of the water year 1993, for the HRUs 1, 40 and 50

Parameter	HRU 1	HRU 40	HRU 50
$\overline{e}$ (cm)	-32.1	-6.2	62.0
$\overline{e} / \overline{Y}$	-3.12	-0.67	1.79
S_e (cm)	35.7	10.6	65.6
S_e / S_y	1.25	1.64	1.65

A review of Table 5-1 indicates that the proposed model does not accurately fit the field data for any of the three HRUs. This fact can be seen by looking at the sample mean error values, which represents a systematic error or bias. These values indicate the average difference between the modeled SWE values and the measured SNOTEL SWE values for each day over the entire water year. All three of the absolute values are high indicating that the modeled values differ significantly from the SNOTEL values during the entire water year. The values for the mean relative error are also high. Large magnitudes, such as these, indicate that the mean error is nearly as large as the mean SNOTEL SWE value, which indicates poor accuracy. This fact can also be seen by the high values of S_e and S_e / S_y for each HRU. The S_e / S_y for all three HRUs are close to 1.0, which indicates that the model has not performed successfully and has not provided estimates more accurate than the mean SNOTEL SWE. The fact that the proposed model does not accurately fit the SNOTEL data is also evident from the high disparity between the modeled and measured values for the physically significant parameters. The difference in the peak modeled SWE and the peak SNOTEL SWE is significant for HRUs 1 and 40, while this difference is moderate for HRU 50. Attempts to estimate the

available runoff from these peak modeled SWE values will lead to significant errors and could have potentially devastating effects on downstream communities dependent upon snow melt. Additionally, the difference in the date of snowpack ripening is significant for all three HRUs. This can be seen in Table 5-1 by large values found for the difference in snowpack ripening. HRUs 1 and 40 predict snowpack ripening approximately one month earlier than is the case, while HRU 50 predicts snowpack ripening approximately one month later than what the SNOTEL SWE data indicates. An attempt to estimate when the stream discharge may be potentially affected by melt will be off by a significant length of time. Finally, Table 5-1 indicates that the length of the ablation period differs significantly for all three HRUs. Attempts to identify potential flooding events will prove difficult since the model predicts longer ablation period than what the SNOTEL SWE data actually indicate. Improvement in the goodness-of-fit and physically-based statistics is required before the proposed model can be considered accurate.

Tables 5-2 and 5-3 indicate that the proposed model does not accurately fit the measured SNOTEL SWE for either the accumulation period or the ablation period for the three HRUs during the water year 1993. The best indication of this is that the S_e / S_y values found in both tables are close to or greater than 1.0, which indicates that the model estimates are not better predictors than is the mean SNOTEL SWE.

A review of these tables also indicates that the goodness-of-fit statistics are better for the three HRUs during the accumulation period than during the ablation period. This is indicated by the improved mean relative error values and the S_e / S_y

values as determined during the accumulation period. This result was anticipated and indirectly supported by the literature. The distinction between these two periods (accumulation and ablation) is determined by the ability of the model to estimate the energy balance for each HRU within a watershed. Luce and Tarboton (2000), Gray and Male (1981), and Foster et al. (1996), among others, describe the difficulties involved in modeling the energy balance at each point in a basin. This difficulty leads to model uncertainty that ultimately causes errors in estimating SWE.

As discussed in the literature, net energy is typically negative during the accumulation period, while the cold content of the snowpack is typically greater than zero. During this time period, a significant error in estimating the energy balance at a point will still result in a negative value for net energy and greater than zero value for the snowpack cold content. Any precipitation that may occur during this time will add to the depth of SWE, and if precipitation does not occur, the SWE total will remain constant during this time. The end result of a significant error in the energy balance at a point during this time period has a minimal affect on the SWE total.

As also discussed in the literature, net energy is typically positive during the ablation period, while the cold content of the snowpack is typically zero, which indicates that the snowpack is ripe and melt is imminent. During this time period, a significant error in estimating the energy balance at a point, will result in too large or too small a positive value for net energy. This in turn could cause significant errors in estimates of melt, which would ultimately lead to errors in SWE estimates. If this pattern occurs regularly, significant errors in SWE estimates will occur during the

ablation period.

In addition to the earlier mentioned goodness-of-fit statistics, it was desired to determine if the model is significantly biased. In order to accomplish this, a hypothesis test using the "t" statistic was proposed. To perform this hypothesis test, the number of independent observations must be known. To determine this value, it must be determined if the time series of SWE values is autocorrelated. Haan (1976) indicates that in an autocorrelated series, each observation represents part of the information contained in the previous observation, and thus the observations are not independent. A correlogram was computed for the SWE values for 1993 for the Beartown SNOTEL site (Figure 5-4). Figure 5-4 indicates a very high level of autocorrelation between the SWE values even after a 20-day lag. As a result, a determination must be made as to the number of independent SWE observations if a hypothesis test is to be performed. Haan (1977) references the following equation:

$$n_e = \frac{n}{\frac{(1+\rho_1)}{(1-\rho_1)} - 2\rho_1 \frac{\left(1-\rho_1^{n}\right)}{n\left((1-\rho_1^{2})\right)}} \tag{5-1}$$

where n_e is the effective number of observations, n is the actual number of observations, and ρ_1 is the auotcorrelation value for a lag of 1. Using Eq 5-1 on the 1993 Beartown SWE data, the effective record length equals 1.5 observations. Due to the small effective record length, performing a hypothesis test using the "t" statistic was not feasible. Similar calculations performed for the Middle Creek and Wolf Creek Summit

SWE data also indicated an effective record length too small for conducting hypothesis tests. An effective record length of this size indicates that one predictor point can define an entire time series and that the bias experienced for that predictor point would be continuous for the entire time series. Erroneous conclusions could be drawn from reviewing this time series.

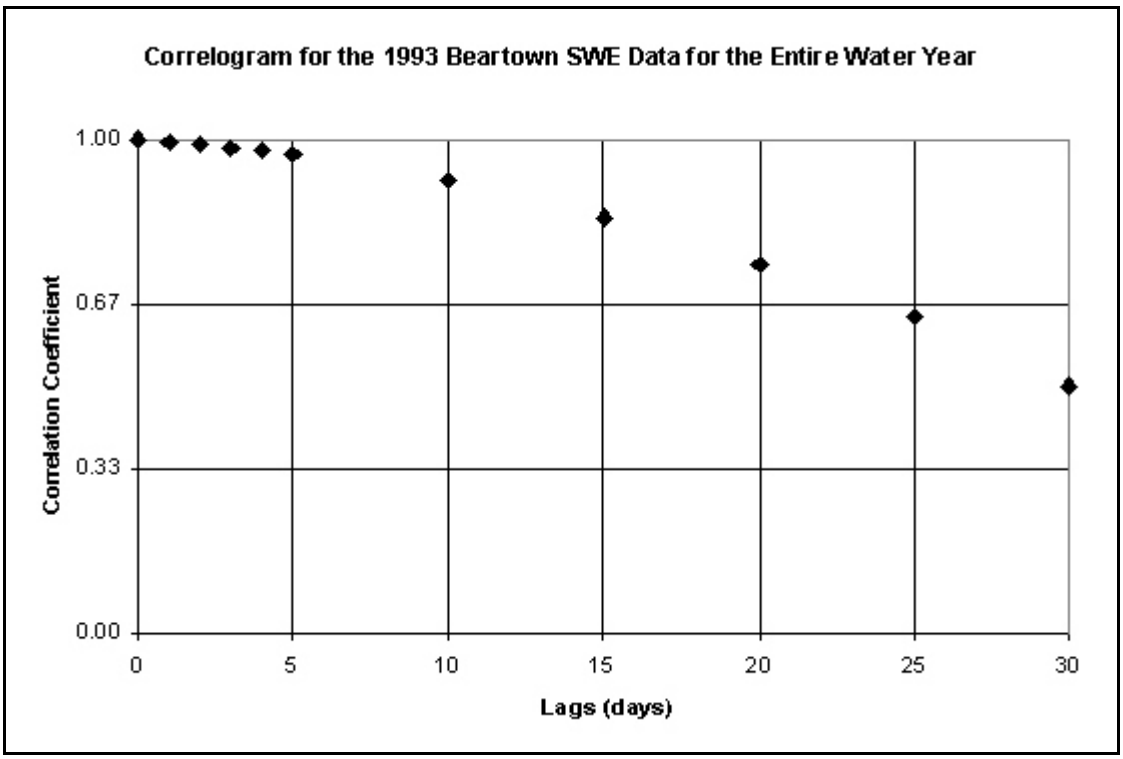

Figure 5-4. Correlogram for the Beartown 1993 SWE data

5.3 SUBJECTIVE OPTIMIZATION PROCESS

As discussed in Chapter 3, one of the design goals of the proposed model was that the model would be applicable to any watershed without having to be calibrated at each location. This design goal was desirable to help reduce the uncertainty that may be

introduced during calibration, especially if the model is calibrated by a subjective optimization process. Unfortunately, due to uncertainty in the values of some input data, subjective optimization must be used on the proposed model in order to attempt to minimize error output associated with the model.

The input parameters chosen to be modified are: S_h, F_d, $f_3(F)$, and T_f. These parameters were selected because of the uncertainty of their initial values. Whereas data was available for the other input parameters, the initial values for these parameters were derived from educated guesses. These parameters will be calibrated on a basin-wide approach and not calibrated for each HRU. S_h is a term found in the solar radiation equation (Eq. 3-5) used to reduce the amount of incoming solar radiation due to the shading caused by the surrounding topography. This value was estimated based upon the elevation and ground slope of an HRU and adjacent HRUs, during the initial run and needs to be adjusted during the calibration process. The range of values that this parameter may have is from 0 to 1.0. A value of 1.0 indicates that incoming solar radiation is not reduced by the shading factor, whereas a value of 0 indicates that no incoming solar radiation is being received at an HRU because of shading, although a value of 0 is not physically possible because of diffuse irradiance from the sky. Calibration of this term could perhaps be avoided by incorporating more sophisticated methods of estimating incoming solar radiation based upon topography, such as the model by Dubayah and Rich (1995).

F_d is a term that describes the density of a forest cover and is used in Eq. 3-8 to determine wind speed through a forested region. The land use data provided

information on forest cover but not on the density of forest cover. Two pixels that have both been identified as having only the same land use, "forest cover," could have very different forest densities. The range of values that this parameter may have is from 0 to 1.0. The greater the parameter value, the more dense the canopy. Aerial photography could be used to estimate this value for forested areas of a watershed. However, for a watershed the size of the Upper Rio Grande, this would be an expensive and time-consuming process.

The third calibration parameter, $f_3(F)$, is a term found in Eq. 3-5 and used to diminish incoming solar radiation based upon forest cover. The value for this term is based upon the specific tree type that comprises a forested region. Dingman (1994) provides values for $f_3(F)$ for various tree species, borrowed from Dunne and Leopold. These values indicate that $f_3(F)$ should range from approximately -1.6 for jack pine to approximately -3.6 for balsam fir. As was the case with F_d, typical land use data do not provide information regarding this term. The land use data indicate whether the forested region is coniferous, deciduous, or a combination, but the $f_3(F)$ term requires information regarding the type of coniferous forest such as balsam fir, jack pine, spruce, etc. This information is required because each tree species has an $f_3(F)$ value associated with it. If tree species are known within a watershed, $f_3(F)$ could be set to an exact value.

T_f is found in Eq. 3-25 to determine the surface temperature of the snowpack, based on near-surface air temperature. As discussed in Chapter 3, limited information exists in the literature about the estimation of the surface temperature of a snowpack.

Gray and Male (1981) indicated that the difference in temperature between the snow surface and surrounding air for most areas in the United States is typically 0-5 ^{0}C. In the preliminary application, T_f was set equal to 2.5 based upon previous work performed by Brubaker, Rango, and Kustas (1996). As mentioned also, this value, as determined by Brubaker, Rango, and Kustas (1996), was based upon measurements taken in Vermont and may not be suitable for the watersheds of this study. Typically, snow surface temperature measurements are only available for heavily instrumented, small research watersheds. Data could be collected regarding snowpack surface temperature from each watershed to better determine the relationship between air temperature and snowpack surface temperature. Due to this fact, it was not feasible to collect this data as part of this research.

Based upon Figures 5-1 through 5-3, an initial strategy was developed for adjusting these input parameters. As previously discussed, these figures show that the model tends to under predict SWE values for the Beartown and Middle Creek SNOTEL sites while the model over predicts SWE values for the ablation period for Wolf Creek Summit. As also previously mentioned, difficulties exist in estimating the energy terms that comprise the E_{NET} parameter (Eq. 3-14). The uncertainty in estimating the terms found in Eq. 3-14 lead to SWE prediction errors during the ablation period. Based upon these statements, the net energy should be decreased on HRU 1 (Beartown) and HRU 40 (Middle Creek), while the net energy should be increased on HRU 50 (Wolf Creek Summit). Initial changes to these parameters attempted to accomplish these objectives.

Now that the input parameters have been identified, the criterion for the subjective optimization procedure must be established. The criterion consisted of two parts. The first part was to optimize all previously discussed goodness-of-fit statistics and physically-based statistics. This objective was performed by means of utilizing systematic educated guesses. The second part was to ensure a physically realistic range of values for the input parameters, which is necessary to ensure that the calibration process does not yield physically unrealistic input parameters. Based upon these criteria, changes were made to the identified input parameters, model runs were conducted, and the resulting SWE values were recorded. From these SWE values, new goodness-of-fit statistics and physically-based statistics were calculated. These statistics were compared to determine if the model had improved in accuracy. No additional runs occurred when execution of the model failed to produce improvements in the goodness-of-fit and physically-based statistics. Table 5-4 provides a summary of pre-calibration and post-calibration values for the identified input parameters. Figures 5-5 through 5-7 show the post-calibration results for the water year 1993, for the HRUs 1, 40, and 50. A comparison of these figures with Figures 5-1 through 5-3 indicates the improvement due to calibration.

Table 5-4. Summary of the basin-wide pre-calibration and post-calibration values for the identified input parameters

Parameter	Physically realistic range of values	Pre-calibration value	Post-calibration value
S_h	0 to 1.0	0.90	0.83
F_d	0 to 1.0	0.90	0.80
$f_3(F)$	-3.6 to -1.6	-2.6	-1.6
T_f	0 to -5	-2.5	-1.2

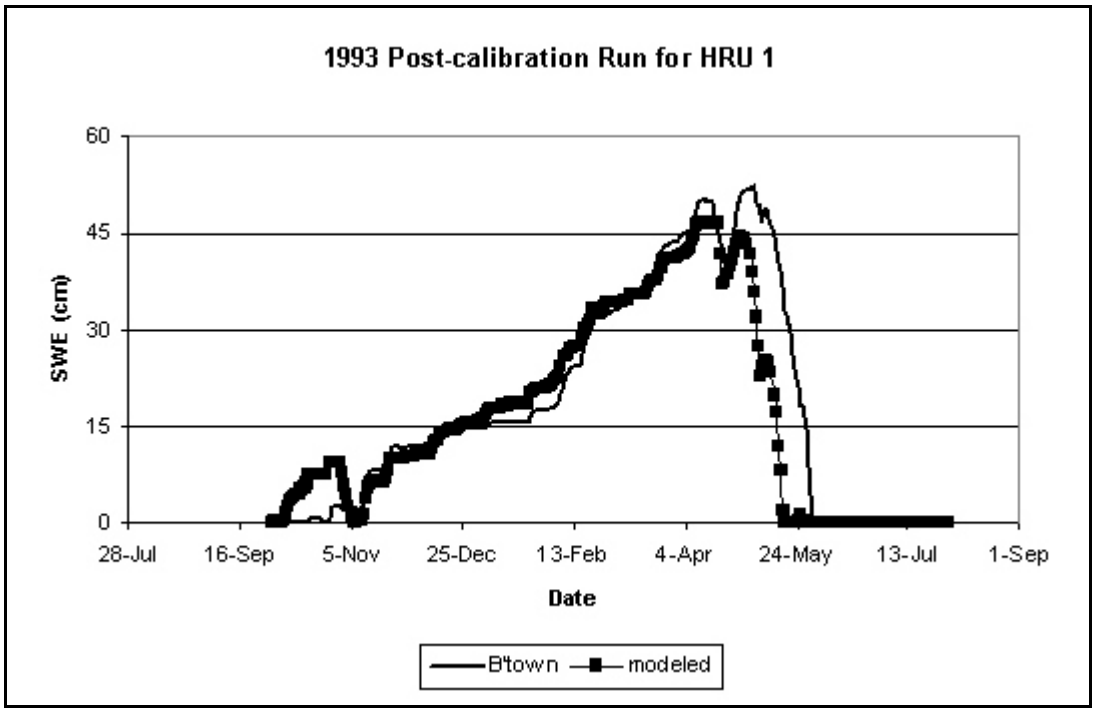

Figure 5-5. Post-calibration results for HRU 1 for 1993

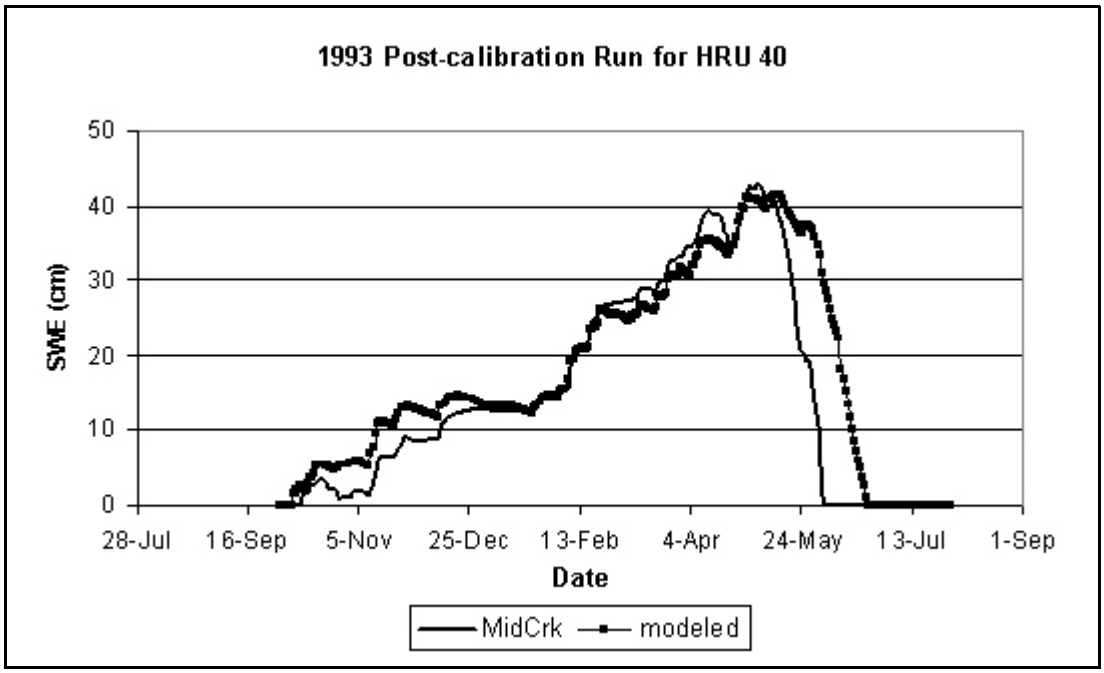

Figure 5-6. Post-calibration results for HRU 40 for 1993

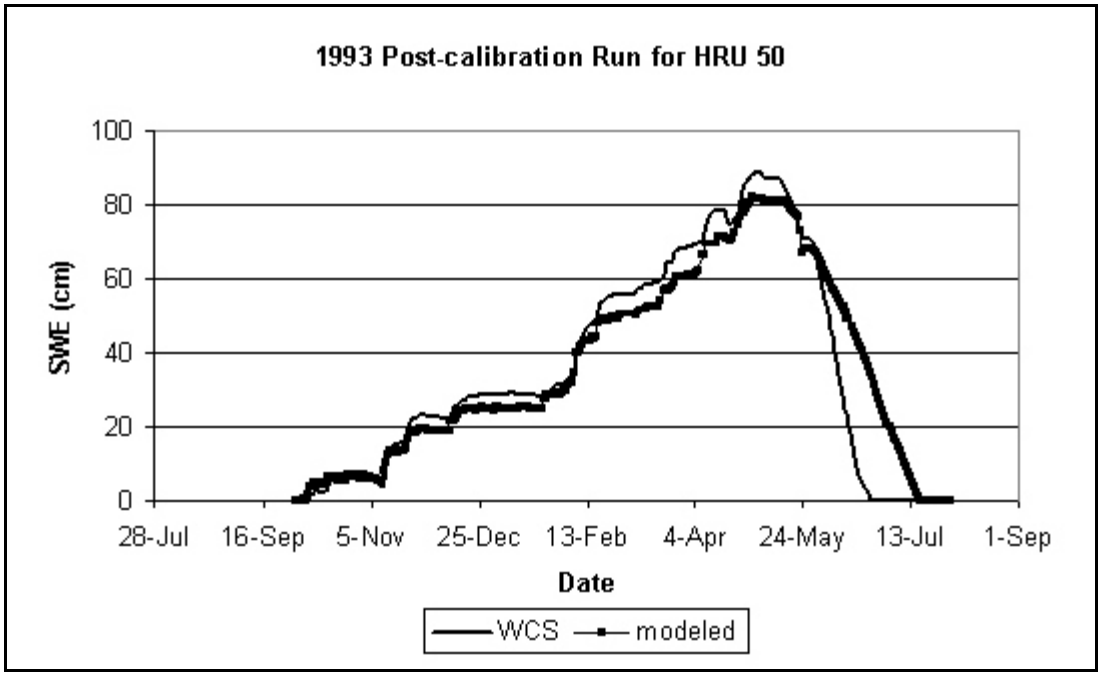

Figure 5-7. Post-calibration results for HRU 50 for 1993

Figures 5-5 through 5-7 show that visually, the proposed model matches the field data for 1993 for these sites much better than do the original model runs. To verify this, all statistics were recalculated for the post-calibration model runs and compared to the pre-calibration results (Table 5-5). Tables 5-6 and 5-7 contain a comparison of the goodness-of-fit statistics for the accumulation and ablation periods for the post-calibration and pre-calibration 1993 runs for the HRUs 1, 40, and 50. One potential problem seen in Figures 5-5 through 5-7 is that the model still shows a bias for all three HRUs during the ablation period. Further discussion of this will follow.

A comparison of Tables 5-1 through 5-3 with Tables 5-5 through 5-7 indicates that the post-calibration model is more accurate compared to the SNOTEL SWE data for this watershed than the pre-calibration model. The goodness-of-fit and physically-based statistics are significantly better for the post-calibration model runs, with the exception being the pre-calibration sample mean error and mean relative error values for the ablation period for HRU 40. Twelve trials were necessary to fit the model. The statistical values in Tables 5-5 through 5-7 represent the best run of the 12 trials.

Table 5-5. Comparison of the pre and post-calibration goodness-of-fit statistics for the water year 1993 for the HRUs 1, 40, and 50.

Parameter	HRU 1		HRU 40		HRU 50	
-------	Pre	Post	Pre	Post	Pre	Post
$\overline{e}$ (cm)	-13.5	-5.0	-7.6	2.9	30.6	0.5
$\overline{e}$ / $\overline{Y}$	-0.74	-0.27	-0.51	0.19	0.86	0.01
S_e (cm)	22.4	13.2	11.4	7.1	26.1	9.9
S_e / S_y	1.11	0.79	1.05	0.60	0.89	0.40
Peak SWE modeled (cm)	29.5	46.7	18.2	41.2	96.9	81.3
Peak SWE measured (cm)	52.3	52.3	42.9	42.9	89.2	89.2
Δ Peak SWE (cm)	-22.8	-5.6	-24.7	-1.7	7.7	-7.9
Δ Peak SWE / Peak SWE measured	43.6%	10.7%	57.6%	4.0%	8.6%	8.9%
Modeled date of snowpack ripening	Feb. 28	April 10	April 12	April 29	May 30	May 11
Estimated date of snowpack ripening from SNOTEL SWE measurements	May 4	May 4	May 5	May 5	May 4	May 4
Δ Date of snowpack ripening (days)	-35	-24	-23	-6	26	7
Modeled length of snowpack ablation period (days)	74	33	62	56	70	70
Measured length of snowpack ablation period (days)	29	29	30	30	52	53
Δ length of snowpack ablation (days)	45	4	32	26	18	17

Table 5-6. Comparison of the pre and post-calibration goodness-of-fit statistics for the measured accumulation period of the water year 1993, for the HRUs 1, 40 and 50.

Parameter	HRU 1		HRU 40		HRU 50	
--------	Pre	Post	Pre	Post	Pre	Post
$\overline{e}$ (cm)	-11.1	-1.5	-7.9	0.7	17.5	-3.2
$\overline{e} / \overline{Y}$	-0.52	-0.07	-0.46	0.04	0.49	-0.09
S_e (cm)	20.0	8.3	11.3	2.6	20.1	4.4
S_e / S_y	0.97	0.64	0.99	0.24	0.79	0.19

Table 5-7. Comparison of the pre and post-calibration goodness-of-fit statistics for the measured ablation period of the water year 1993, for the HRUs 1, 40 and 50.

Parameter	HRU 1		HRU 40		HRU 50	
--------	Pre	Post	Pre	Post	Pre	Post
$\overline{e}$ (cm)	-32.1	-31.1	-6.2	12.3	62.0	11.1
$\overline{e} / \overline{Y}$	-3.12	-3.02	-0.67	1.34	1.79	0.32
S_e (cm)	35.7	34.5	10.6	8.6	65.6	18.0
S_e / S_y	1.25	1.12	1.64	1.18	1.65	0.68

A review of Table 5-5 indicates that the model accurately fits the SNOTEL SWE data for HRU 50, as evident from the low values of the sample mean error, the mean relative error, and S_e / S_y. The sample mean error and mean relative error indicate that the modeled SWE values nearly match the SNOTEL SWE values for the entire water year. The model accurately approximates the date on which the snowpack ripens, with a difference of 7 days between the modeled and measured values. Using this information to predict the date on which snowmelt may affect stream discharge will provide a close

approximation. The model also produces an acceptable value for the peak SWE. The post-calibration value for predicted peak SWE is within 9% of the measured peak SWE value. The model, however, does not accurately predict the length of the ablation period. The model predicts an ablation period that is seventeen days longer than predicted with the SNOTEL SWE data, which would lead to an under estimate of the downstream stream discharge that results from snowmelt. This could have significant impact on downstream communities because the flood stage of severe discharges would be underestimated.

Based upon the goodness-of-fit statistics, Table 5-5 also indicates that the model matches the SNOTEL SWE data for HRU 40 moderately well. The sample mean error and the mean relative error indicate that predicted SWE values are close in magnitude to SNOTEL SWE values throughout the water year. However, the S_e / S_y value of 0.60 indicates that the predicted SWE values are only modestly better than the mean SNOTEL SWE values. The model accurately matches the peak measured SWE value, with the difference being only 4.0%. Estimates of potential snowmelt runoff should prove accurate based upon the close proximity of the peak values. The model also accurately predicts the date of snowpack ripening, with the difference between measured and modeled being six days. Using this information to predict the date in which snowmelt contributes to stream discharge will provide a close approximation. The model, however, does not accurately predict the length of the ablation period. The model predicts an ablation period that lasts 26 days longer than indicated by the SNOTEL SWE data, which would lead to significant under predictions of downstream

discharges that result from snowmelt.

Table 5-5 shows that the model inaccurately matches the SNOTEL SWE data for HRU 1. Although the sample mean error and mean relative error indicate that the predicted SWE values do not differ significantly from the SNOTEL SWE data, the S_e / S_y value of 0.79 indicates that the modeled results do not provide significant improvement in accuracy over the mean SNOTEL SWE. In addition, the calibrated model predicts the ripening of the snowpack at a significantly earlier time than which physically occurs. Using this information to predict the date on which snowmelt contributes to stream discharge will result in an error of approximately one month. This fact could have a significant impact on downstream communities. For example, crop planting based upon this early estimation may cause damage to the crops based upon a lack of streamflow from delayed snowmelt. The difference in the modeled peak SWE and SNOTEL SWE is 10.7%. Values over 10% could lead to significant error in estimating potential snowmelt runoff, again having significant impact on downstream communities relying on snowmelt. Surprisingly, the model matches the length of the ablation period well for this HRU, with the difference being only four days.

Tables 5-6 and 5-7 indicate that the model performs significantly better for all three HRUs for the accumulation period than for the ablation period, which as previously discussed, is not surprising. The sample mean errors (Table 5-7) indicate that the model significantly under predicts SWE for HRU 1 and over predicts SWE for HRU 40 and 50. These values indicate the existence of model bias during the ablation period, and the possibility that the model is neglecting an important physical process.

Suggestions for minimizing modeled output error during the ablation period will be discussed in Chapter 10.

5.4 MODEL VALIDATION

The model was calibrated using the SNOTEL SWE data from 1993. This year was chosen for calibration because the mean peak SWE value throughout the watershed was approximately equal to the average mean peak SWE value for the eight water years. The remaining seven years of data were used to validate the calibrated model. It was decided to validate the model with seven years of data to provide the largest possible sample size for determining model robustness. The calibrated model was run for the seven years using the finalized input parameters (Table 5-4) as determined by the subjective optimization process. All previously calculated goodness-of-fit and physically-based statistics (Tables 5-1 through 5-3) were determined for each of the seven years. Tables 5-8 through 5-10 contain the results of the statistical analyses for the three HRUs for the seven remaining water years. Within each table for each statistical parameter, three values are reported. These values correspond to the largest, smallest, and (seven year) average value determined for the particular parameter during the seven year period.

Table 5-8. Summary of the post-calibration average goodness-of-fit statistics for the water years 1994 - 2000 for the HRUs 1, 40, and 50.

Parameter	HRU 1			HRU 40			HRU 50		
---	Low	Mean	High	Low	Mean	High	Low	Mean	High
$\overline{e}$ (cm)	-0.6	4.9	6.1	-2.2	3.3	5.8	-3.1	3.2	4.9
$\overline{e} / \overline{Y}$	-0.11	0.30	0.44	-0.21	0.32	0.41	-0.33	0.16	0.33
S_e (cm)	7.8	15.6	21.9	5.9	9.4	12.5	5.7	9.0	12.6
S_e / S_y	0.44	0.69	0.79	0.43	0.56	0.71	0.26	0.34	0.42
Peak SWE modeled (cm)	72.8	77.6	80.8	52.1	56.0	60.4	85.1	90.0	96.5
Peak SWE measured (cm)	75.2	75.2	75.2	56.9	56.9	56.9	92.2	92.2	92.2
Δ Peak SWE (cm)	-2.4	2.4	5.6	-4.8	-0.9	3.5	-7.1	-2.2	4.3
Δ Peak SWE / Peak SWE measured (%)	-3.2	3.2	7.4	-8.4	-1.6	6.2	-7.7	-2.4	4.7
Modeled date of snowpack ripening	May 3	May 16	May 25	April 10	April 20	April 30	April 21	April 29	May 8
Estimated date of snowpack ripening from SNOTEL SWE measurements	April 23	April 23	April 23	April 18	April 18	April 18	April 26	April 26	April 26
Δ Date of snowpack ripening (days)	10	23	32	-8	3	13	-7	4	13
Modeled length of snowpack ablation period (days)	32	38	46	58	66	72	55	67	76
Measured length of snowpack ablation period (days)	52	52	52	47	47	47	50	50	50
Δ length of snowpack ablation (days)	-20	-14	-6	11	19	25	5	17	26

Table 5-9. Summary of the post-calibration average goodness-of-fit statistics for the measured accumulation period for the water years 1994 - 2000, for the HRUs 1, 40 and 50.

Parameter	HRU 1			HRU 40			HRU 50		
------	Low	Mean	High	Low	Mean	High	Low	Mean	High
$\overline{e}$ (cm)	-3.7	-2.4	0.7	-1.1	0.4	2.3	-1.8	0.2	2.3
$\overline{e} / \overline{Y}$	-0.27	-0.18	0.09	-0.17	0.10	0.25	-0.20	0.05	0.22
S_e (cm)	4.2	6.2	8.1	2.1	4.0	6.6	2.1	2.9	4.3
S_e / S_y	0.25	0.31	0.45	0.19	0.26	0.43	0.08	0.12	0.26

Table 5-10. Summary of the post-calibration average goodness-of-fit statistics for the measured ablation period for the water years 1994 - 2000, for the HRUs 1, 40 and 50.

Parameter	HRU 1			HRU 40			HRU 50		
------	Low	Mean	High	Low	Mean	High	Low	Mean	High
$\overline{e}$ (cm)	-5.6	24.2	33.5	6.7	11.6	17.3	5.8	11.4	17.2
$\overline{e} / \overline{Y}$	-0.59	2.17	3.07	0.78	1.24	1.69	0.22	0.41	0.69
S_e (cm)	22.5	31.6	39.8	11.2	16.5	23.4	14.1	16.3	20.7
S_e / S_y	1.06	1.58	2.21	1.02	1.41	1.92	0.50	0.59	0.74

A review of Table 5-8 indicates that most goodness-of-fit statistics and physically-based statistics, for the three HRUs for the remaining seven years of data, approximate the level of accuracy determined for the calibration year 1993. The one exception to this statement is the Δ peak SWE values. These values for all three HRUs are improved, with the improvement for HRUs 1 and 50 being significant. The mean values for this statistic for all three HRUs indicate that using the model to estimate the potential volume of snowmelt runoff should provide accurate results.

Tables 5-9 and 5-10 confirm that the model matches the accumulation period for all three HRUs much better than the model matches the ablation period for the HRUs. All of the goodness-of-fit statistics found in Table 5-9 suggest that the model works very well for all three HRUs for the remaining seven water years during the accumulation period. All of the goodness-of-fit statistics found in Table 5-10 show that the model poorly predicts during the ablation period for HRUs 1 and 40 for the remaining seven water years, and that the model shows moderate prediction accuracy during the ablation period for HRU 50 for the remaining water years.

A review of Figure 4-3 shows that all of the SNOTEL sites are located in the southwest quadrant of the watershed, or the windward side of the watershed. Greater uncertainty exists for that portion of the watershed in which no SNOTEL sites are located in close proximity. This could be especially problematic if a "rain shadow" is prevalent on the eastern (leeward) side of the watershed. If this is the case, extrapolating precipitation data as described in section 4.2.4 could introduce significant errors, without any means of measuring these errors. Ultimately, a greater level of confidence exist in the proposed model performance for the watershed region in which the SNOTEL sites exist.

5.5 BIAS ANALYSIS

Figures 5-5 through 5-7 support the existence of a significant bias in the ablation period. This bias indirectly points to a systematic error in the model that could possibly be corrected by adding an additional component to the model to better predict SWE

values during the ablation period. Further inspection into the model output suggests that this is not the case.

For HRU 1, the first reason for the significant bias that exist during the ablation period is the fact that the SWE time series has a high level of autocorrelation. As explained earlier, knowing that one SWE value is under predicted during the ablation period means that the likelihood is great that all SWE values will be under predicted during the ablation period.

For this HRU, the second reason for the significant bias that exists during the ablation period can be found by comparing the sample mean error from Table 5-7 (-31.1 cm), for the 1993 ablation period, to the sample mean error from Table 5-10 (24.2 cm), for the 1994 -2000 ablation periods. For the ablation period of 1993, the model results show that the SWE values are under predicted when compared to the SNOTEL SWE values. However, for the remainder of the years studied, the sample mean error associated with HRU 1 indicates that the model over predicts when compared to the SNOTEL SWE data during the ablation period. When the sample mean error is inspected for the ablation period for each of the water years, when compared to the SNOTEL SWE data, the modeled results over predicts for four of the water years, under predicts for two of the water years, and matches the data accurately for two of the water years. Figure 5-8 shows the model predicted SWE values along with SNOTEL SWE values for HRU 1, for the water year 1997. This figure clearly shows that the model is over predicting during the ablation period when compared to the SNOTEL SWE data. Figure 5-9 shows the model predicted SWE values along with

SNOTEL SWE values for HRU 1, for the water year 2000. This figure clearly shows that visually, the model accurately matches the SNOTEL SWE data during the ablation period. Although the sample size is small (n = 8), the results for these water years (for this HRU) seem to indicate that the residuals associated with the ablation period do not represent a systematic bias. As previously discussed, the bias that does exist is the result of modeling uncertainties regarding net energy.

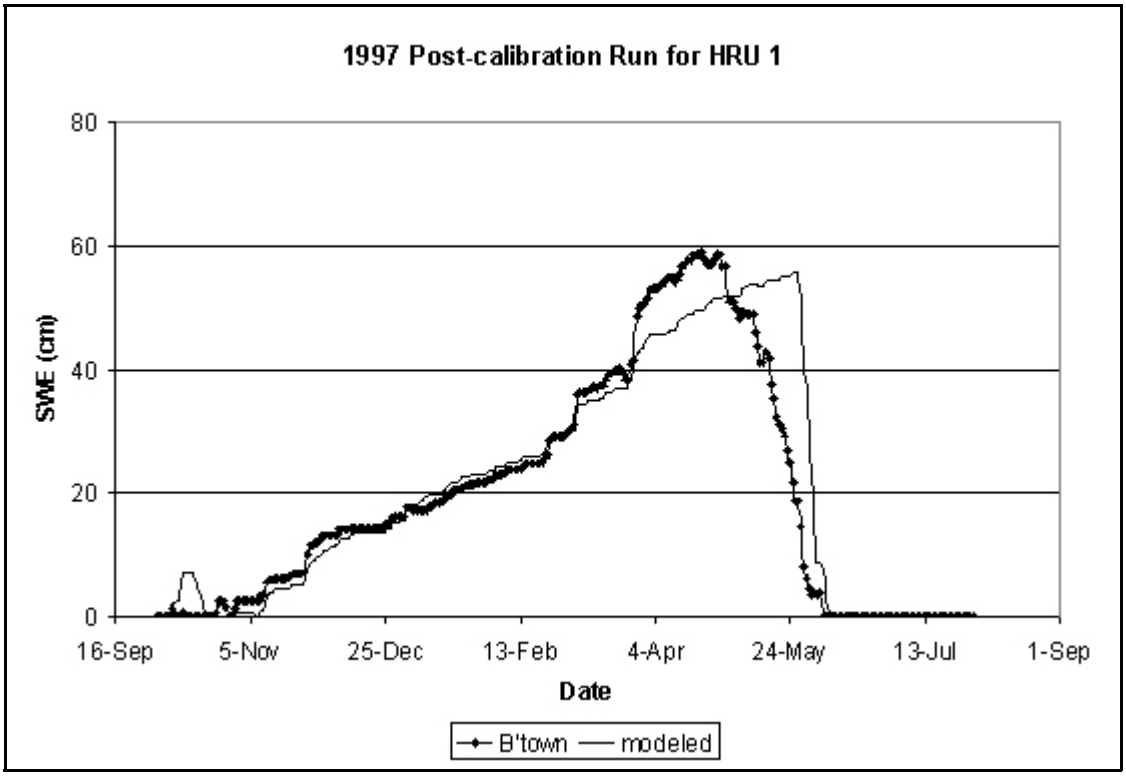

Figure 5-8. Validation results for HRU 1 for 1997

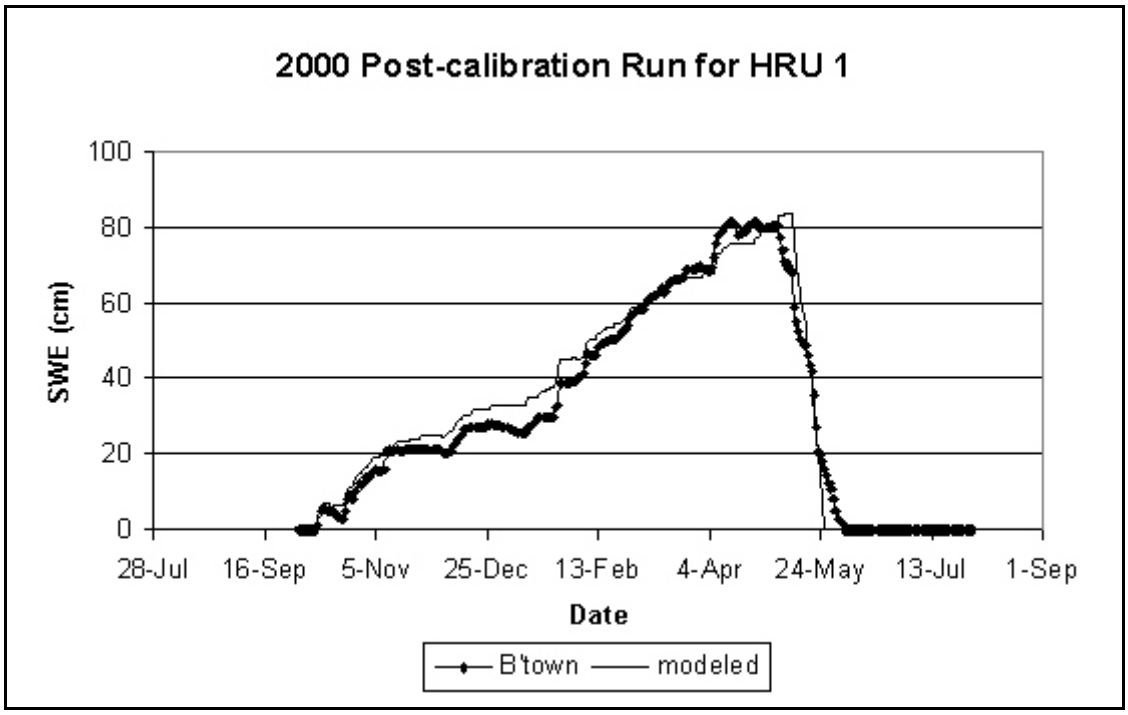

Figure 5-9. Validation results for HRU 1 for 2000

Unlike HRU 1, a review of the goodness-of-fit statistics for the studied water years does appear to indicate the presence of a systematic bias during the ablation period for both HRUs 40 and 50. The sample mean error for both of these HRUs indicates that the model significantly over predicts SWE values when compared to the SNOTEL SWE data, for all eight water years. Evidence of this can be found in Tables 5-7 and 5-10.

The contention is that this consistent over predicting during the ablation period does not represent a flaw in the model but actually indicates that the model is functioning properly. A review of Table 4-1 shows that HRU 1 has no forest cover, whereas HRUs 40 and 50 have complete forest cover. The SNOTEL sites in these HRUs are placed in such a location so as to measure and record data while minimizing

recording error from nearby obstruction, such as forest canopy. Figure 5-10 shows the SNOTEL site at Wolf Creek Summit (Santos, 2002). This figure shows that although some canopy exist in proximity to the SNOTEL station, the station has been placed in a relatively open location. This means that the SNOTEL data is representative of an HRU that has little or no canopy cover, which is not the case for HRUs 40 and 50.

The consequence of this fact for these two HRUs is that the SNOTEL SWE data are subjected to a net energy time series during the ablation period that is relatively canopy-free, whereas the modeled SWE values are subjected to a net energy time series during ablation that is completely canopy covered. This fact helps to explain why the canopy covered modeled results consistently over predict SWE when compared to the SNOTEL canopy-free data. Net energy received at the SNOTEL site will be greater during the ablation period than the net energy received at the remainder of the canopy covered HRU. This increase in net energy during the ablation period will result in melt occurring earlier and more rapidly at the SNOTEL station than for the remainder of the HRU, as predicted by the model.

The reason that the SNOTEL station receives a greater amount of net energy than does the remaining canopy covered HRU is that the wind speed through a canopy is reduced (Eq. 3-8). This reduction in wind speed effectively reduces both the latent and sensible heat exchange between the snowpack and the atmosphere. The net turbulent heat exchange is typically positive during the ablation period [Dingman (1994), Gray and Male (1981), Foster, et al. (1996)], indicating that the canopy cover reduces the positive net energy experienced at a point. Additionally, canopy cover reduces

incoming solar radiation, but this reduction is essentially offset by an increase in longwave radiation caused by canopy cover. For all water years studied, the model predicts a positive net turbulent heat exchange for the forest covered HRUs 40 and 50.

Figure 5-10. SNOTEL station at Wolf Creek Summit

5.6 COMPARISON OF MODEL RESULTS WITH SATELLITE IMAGERY

Previous work by Brubaker, Rango, and Menoes (2001) utilized satellite imagery of the Upper Rio Grande Watershed to help construct snow depletion curves. For their study, satellite images were obtained from the National Operational Hydrologic Remote Sensing Center (NOHRSC) for the water years 1990 through 1999. These satellite images have a pixel resolution of 1 km^2, and show the progression of

snow covered area throughout a water year by depicting the area within the watershed as either snow covered or snow free.

Appendix J contains a comparison of available satellite images (on the left side of the page) with modeled SWE results (on the right side of the page) for the water years 1993 through 1999. These years coincide with the intersection of years that the model was run for the Upper Rio Grande Watershed, 1993 through 2000, and the years that the satellite imagery were available, 1990 through 1999. The day refers to the day of year that the satellite image was taken and that the modeled SWE results represent. Day 1 refers to January 1, day 32 refers to February 1, etc.

For the satellite images, the limits of the watershed are outlined by the black border. Areas covered by snow within the watershed are depicted by the color white, and areas that are snow free are depicted by the color grey. For the modeled SWE results, the watershed is divided into HRUs as first depicted in Figure 4-2. If the model predicted SWE for a particular HRU on a particular day, the HRU has the color white, and if the model predicts no SWE for a particular HRU on a particular day, the HRU has the color grey.

A review of the figures in Appendix J show that similar ablation patterns exist for both the satellite images and the modeled SWE output. Ablation, for both sets of figures, typically begins in the lower elevations of the eastern region of the watershed near the outlet. As the melt season progresses, snow next typically recedes through the central stream valley with the center and eastern sections of the watershed becoming snow free. Typically, the higher elevations of the watershed found in the western

section and along the northern and southern borders of the watershed are the final areas to become snow free.

The similar ablation patterns that exist for the satellite imagery and modeled SWE results help support the research hypothesis that the spatial variability of SWE within a watershed can be defined by a system of physical variables defining the watershed. The physical variables defining the Upper Rio Grande Watershed help to create a temporal pattern of SWE within the watershed, and as can be seen in Appendix J, this pattern remains similar from year to year.

Table 5-11 contains a summary of the snow covered areas, as predicted by both the satellite imagery and the modeled SWE output for the available days for the water years 1993 through 1999. The results of the comparison found in Table 5-11 support the earlier claim that the model performs more accurately during the accumulation period than the ablation period. This can best be seen by the smaller differences in snow covered area between the satellite images and the modeled SWE results for the earlier days in each water year. These earlier days represent the accumulation period before the snowpack has ripened, and (except for 1996) the difference in SCA is typically 10% or less. Substantial differences exist for the days associated with the ablation period. The difference between SCA as seen on the satellite images and predicted by the model output is as great as 57%.

Model over prediction of SCA is to be expected due to the assumption of equal SWE across the HRU. The area of an HRU is considered "snow covered" if its SWE > 0. In actuality, as SWE approaches 0, a fraction of the HRU would be snow free. Many

snow accumulation and melt models use depletion curves to relate SWE to SCA. Adding depletion curves to this model would require the estimation of at least two additional parameters for each HRU.

Table 5-11. A comparison of snow covered area as predicted by satellite imagery and modeled SWE results for the water years 1993 through 1999.

Year	Day	% Snow Covered Area - Satellite Imagery	% Snow Covered Area - Modeled SWE Results	Difference % cover
1993	75	99.9	100	0.1
	91	91.8	90.8	-1.0
	98	83.6	90.8	7.2
	115	71.5	87.6	16.1
	130	53.2	84.5	31.3
	150	28.6	73.0	44.4
	171	11.2	38.9	27.7
	181	6.4	16.3	9.9
1994	63	87.7	90.9	3.2
	72	79.0	90.9	11.9
	90	76.9	85.9	9.0
	102	70.1	85.9	15.8
	128	49.8	81.8	32.0
	140	30.9	76.5	45.6
	149	21.3	47.7	26.4
1995	91	98.9	90.9	-8.0
	101	91.3	88.1	-3.2
	156	47.2	19.9	-27.3
	169	40.0	4.5	-35.5

Table 5-11. A comparison of snow covered area as predicted by satellite imagery and modeled SWE results for the water years 1993 through 1999, continued.

Year	Day	% Snow Covered Area - Satellite Imagery	% Snow Covered Area - Modeled SWE Results	Difference % cover
1995	177	19.2	3.9	-15.3
1996	79	71.3	91.9	20.6
	93	56.9	91.9	35.0
	107	48.0	88.0	40.0
	128	40.3	75.1	34.8
	144	11.5	68.9	57.4
	171	6.2	42.6	36.4
1997	72	100.0	90.9	-9.1
	84	99.6	90.9	-8.7
	126	59.5	86.6	27.1
	147	37.6	63.8	26.2
	165	28.1	46.3	18.2
	182	15.0	6.7	-8.3
1998	71	99.1	90.7	-8.4
	85	88.3	87.8	-0.5
	97	90.2	87.8	-2.4
	118	58.4	83.4	25.0
	132	40.4	76.7	36.3
	146	35.4	47.2	11.8
	167	25.3	44.5	19.2
	180	12.7	5.8	-6.9
1999	73	83.4	92.5	9.1
	82	81.9	87.6	5.7
	98	67.8	86.4	18.6

Table 5-11. A comparison of snow covered area as predicted by satellite imagery and modeled SWE results for the water years 1993 through 1999, continued.

Year	Day	% Snow Covered Area - Satellite Imagery	% Snow Covered Area - Modeled SWE Results	Difference % cover
1999	133	57.3	67.5	10.2
	140	53.3	67.5	14.2

5.7 CREATION OF SWE MAPS THROUGHOUT THE WATER YEAR

Within the ArcView program, SWE maps were created for each of the eight water years studied for the Upper Rio Grande Watershed. These maps depict the amount of SWE contained in each HRU throughout the watershed on a particular date. During the accumulation period, estimated to be from November 1 to May 1, maps were created every seven days. During the ablation period, estimated to be from May 2 to July 26, maps were created every five days. Appendix K contains these SWE maps, as well as a legend defining the color schematic for the maps.

As was seen with the satellite images, the SWE maps in Appendix K show that modeled results indicate that similar ablation patterns exist. Ablation typically begins in the eastern region of the watershed, then progresses through the central stream valley, and finally on to the western section and along the northern and southern borders of the watershed. The SWE maps found in Appendix K also show that modeled results indicate that similar accumulation patterns exists, which are typically the opposite of the ablation patterns.

The similar patterns that exist for the modeled SWE results again help support the alternative hypothesis of the research that the spatial variability of SWE within a watershed can be defined by a system of physical variables defining the watershed. The physical variables defining the Upper Rio Grande Watershed help to create a temporal pattern of SWE within the watershed, and as can be seen in Appendix K, this pattern remains similar from year to year.

5.8 SUMMARY OF RESULTS

The results presented in this chapter for the Upper Rio Grande Watershed indicate that the calibrated model performs very well during the accumulation period and provides accurate peak predictions when compared to the SNOTEL SWE data. This suggests that using the model to estimate potential runoff from a snowpack should provide an accurate estimate. The ability to accurately estimate potential runoff could prove significant in predicting potential downstream water shortages from a small seasonal snowpack or in planning a seasonal cropping strategy downstream of the snowpack.

The results from Tables 5-7 and 5-10, and the discussion from section 5-5 also show that the model does not perform accurately during the ablation period for the nonforested HRU. This implies the existence of a bias that is caused by the inability to accurately model net energy at a point. As a result, it is not recommended to use this model to make predictions during the ablation period, such as identifying possible severe stream discharge events based upon the length of the ablation period.

The results discussed in section 5-5 also imply that the spatial variability of SWE within a watershed is partially controlled by the physical characteristics of the watershed. The model results for the forested HRUs (40 and 50) show that two similar HRUs, differing only in forest cover, will consistently have different ablation periods associated with them. The effect of forest cover on the SWE distribution provides insight into what may occur from land use changes involving forest cover. The model implies that widespread deforestation could potentially result in more frequently occurring severe discharge events downstream by increasing net energy to the landscape, thus shortening the ablation period.

CHAPTER 6

IMPLEMENTATION AND CALIBRATION OF THE MODEL FOR THE REYNOLDS CREEK WATERSHED

6.1 INTRODUCTION

As discussed in Chapter 5, proper modeling technique should include an analysis that demonstrates the accuracy of the model in which the parameters are independent of the hydrologic data for a watershed. This analysis is referred to herein as the pre-calibration phase. The accuracy of the pre-calibration results can be compared using graphical results, standard goodness-of-fit statistics, and physically-based statistics.

Additionally, as discussed in Chapter 5, the subjective optimization process will be demonstrated as to what type of calibration is being performed and why, the goodness-of-fit criterion, the parameters to be optimized, and the rationale as to why the specific parameters were chosen for optimization. Next, a post-calibration analysis will include an analysis that shows the improvement in model accuracy achieved as a result of the subjective optimization process by comparing modeled results with those obtained during the pre-calibration phase. Finally, model validation will be assessed by determining the reliability of the model by running the model for a additional data sets. This task must be performed before the model can be used with confidence to make predictions.

6.2 PRE-CALIBRATION MODEL RESULTS

For the Reynolds Creek Watershed, the model was initially run for the water year 1988, for the following two HRUs: 26 and 28. These HRUs correspond to the SWE measurement locations: 155 x 54 and 167 x 07, respectively. The results of the initial model run for these HRUs are presented graphically in Figures 6-1 and 6-2. As can be seen in these figures, unlike the Upper Rio Grande Watershed, daily field measurements of SWE were not available. On average, bimonthly field measurements were made per water year at each of the two locations. The effect of having bimonthly SWE data as opposed to having daily SWE data on model performance and accuracy will be explored in more detail in Chapter 8 by means of sensitivity analysis.

A visual inspection of Figures 6-1 and 6-2 shows that the proposed model matches the SWE field measurements fairly accurately up through approximately the middle of March. After this date, the model diverges significantly from the SWE field measurements. At this time, the SWE field measurements become smaller in magnitude due to ablation, and the modeled SWE values continue to increase. This fact suggests that the model is under predicting the net energy received at these HRUs, causing a delay in the date of snowpack ripening, and thus a delay in the beginning of the melt season. These initial findings seem consistent with the results of the calibration process for the Upper Rio Grande Watershed, that the model matches the SWE field measurements more accurately during the accumulation period than during the ablation period, due to the model being more sensitive to errors in the net energy received during the ablation period than during the accumulation period.

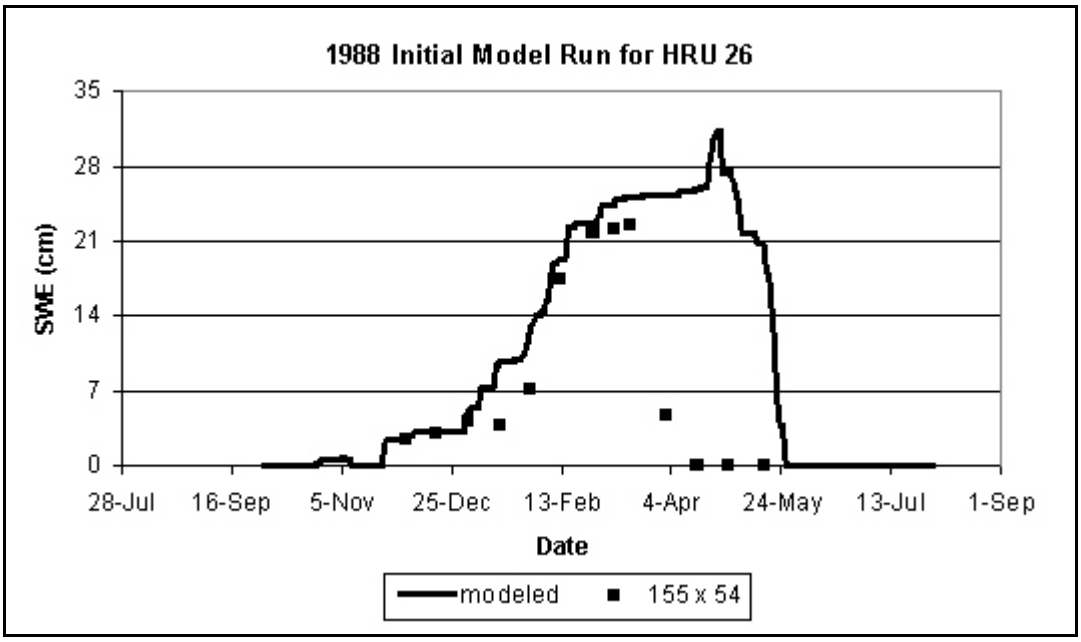

Figure 6-1. Initial model results for HRU 26 for 198

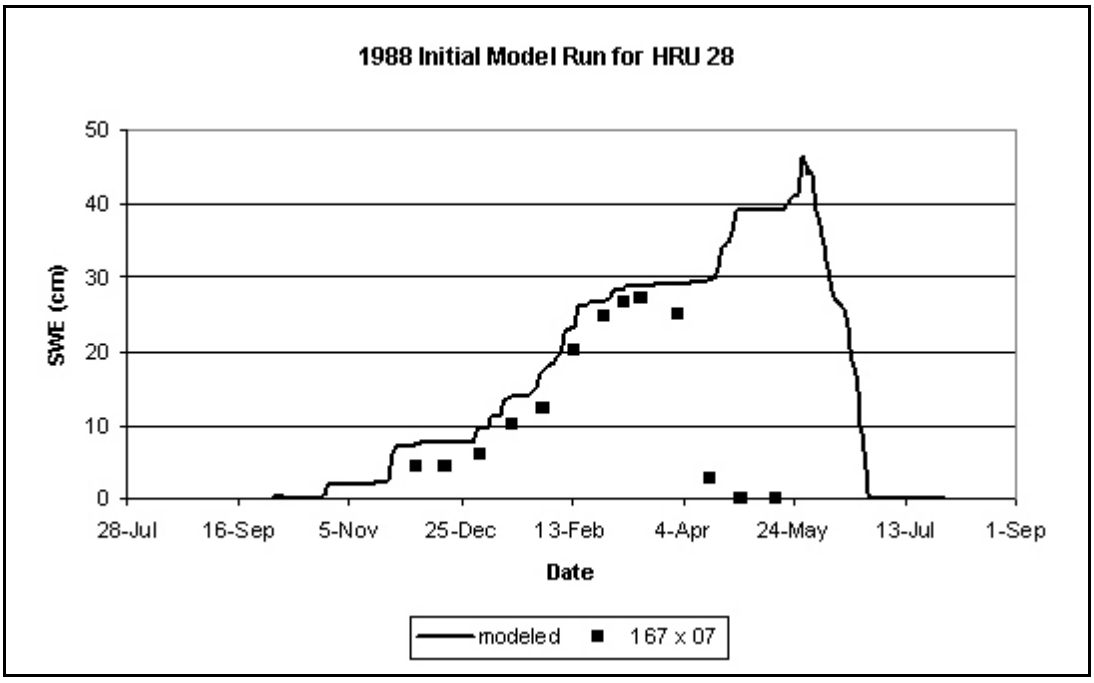

Figure 6-2. Initial model results for HRU 2 for 1988

Statistical analyses were performed on these initial runs to assess the accuracy of the proposed model for the measured SWE data. The same goodness-of-fit and physically-based statistics that were used for the Upper Rio Grande Watershed were also calculated for the Reynolds Creek Watershed. The analyses were also performed for the entire water year, the accumulation season, and the ablation season. Estimations of the date of snowpack ripening were accomplished by inspection of the field SWE data. Tables 6-1 through 6-3 contain a summary of the goodness-of-fit statistics for the entire water year, the accumulation period, and the ablation period respectively for the water year 1988, for the HRUs 26 and 28.

A review of Table 6-1 shows that the proposed model does not accurately match the field data for either of the HRUs. This fact can best be seen by the high values of S_e / S_y for each HRU. These values indicate that the model has not provided estimates more accurate than the mean measured SWE value. This fact can also be seen by examining the sample mean error values. These values are high indicating that the modeled SWE values differ significantly from the measured SWE values during the entire water year. There also exists a high disparity between modeled and measured values for most of the physically significant parameters. The difference between peak predicted and measured SWE is significant. Attempts to estimate potential runoff from snow melt will result in significant errors, which could have a detrimental impact downstream. Significant differences also exist in the estimation of snowpack ripening. The model predicts snowpack ripening much later in the year. Estimates of when stream discharge may be affected by melt will differ significantly.

Table 6-1. Summary of the pre-calibration goodness-of-fit statistics for the water year 1988, for the HRUs 26 and 28.

Parameter	HRU 26	HRU 28
$\overline{e}$ (cm)	8.8	10.4
$\overline{e} / \overline{Y}$	1.05	0.83
S_e (cm)	13.4	17.3
S_e / S_y	1.24	1.25
Peak SWE modeled (cm)	31.4	46.4
Peak SWE measured (cm)	22.6	27.2
Δ Peak SWE (cm)	8.8	19.2
Δ Peak SWE / Peak SWE measured	38.9%	70.6%
Modeled date of snowpack ripening	April 25	May 29
Estimated date of snowpack ripening from field SWE measurements	March 16	March 16
Δ Date of snowpack ripening (days)	40	74
Modeled length of snowpack ablation period (days)	32	30
Measured length of snowpack ablation period (days)	31	45
Δ length of snowpack ablation (days)	1	-15

Table 6-2. Summary of the pre-calibration goodness-of-fit statistics for the accumulation period of the water year 1988, for the HRUs 26 and 28.

Parameter	HRU 26	HRU 28
$\overline{e}$ (cm)	2.3	2.9
$\overline{e} / \overline{Y}$	0.20	0.19
S_e (cm)	3.1	3.1
S_e / S_y	0.35	0.32

Table 6-3. Summary of the pre-calibration goodness-of-fit statistics for the ablation period of the water year 1988, for the HRUs 26 and 28.

Parameter	HRU 26	HRU 28
$\overline{e}$ (cm)	23.5	27.3
$\overline{e} / \overline{Y}$	4.70	3.94
S_e (cm)	23.8	30.9
S_e / S_y	2.83	6.43

A review of Tables 6-2 and 6-3 indicate that the proposed model fits the measured data more accurately for the accumulation period for both HRUs. The values found in Table 6-2 indicate that the model performs very well for the accumulation period, indicating an accurate model. This fact can best be seen by the low values for S_e / S_y for each HRU. These values imply that the model has significantly improved the reliability of prediction over the mean measured SWE value. The sample mean error in Table 6-2 are also low, indicating that the predicted SWE values are close in magnitude to the measured SWE values during the accumulation period. Using model results to make any predictions regarding SWE accumulation during this period will provide accurate results. However, the values found in Table 6-3 indicate that the model does not accurately match the measured SWE data for the ablation period for the water year 1988. This is best shown by the fact that the S_e / S_y values for both HRUs during the ablation period are greater than 1.0. Additionally, the sample mean error for both HRUs are very high, signaling that the predicted SWE values differ significantly from the measured SWE values. Using model results to make any predictions regarding runoff from melt during this period will result in substantial error.

As was the case for the Upper Rio Grande Watershed, the high degree of autocorrelation between the time series of SWE values prevented a hypothesis test being performed to determine if the model is significantly biased. Using Eq 5-1 on the 1988 SWE data for HRUs 26 and 28 to determine the effective record lengths yields values of 2.1 and 2.3, respectively. These values indicate that two predictor points define the entire SWE time series and that the bias experienced by these two predictor points should be continuous for the entire time series. Due to the small effective record length, performing a hypothesis test using the "t" statistic was not feasible.

6.3 SUBJECTIVE OPTIMIZATION PROCESS

As for the Upper Rio Grande Watershed, the same subjective optimization process was performed for the Reynolds Creek Watershed. The same input parameters as identified and discussed earlier were chosen to be modified, and the same criterion was used for the subjective optimization procedure. Based upon Figures 6-1 and 6-2, attempts were made to increase net energy received at these HRUs so as to induce an earlier beginning to the modeled ablation period. This was accomplished by altering the selected parameters (which cannot be estimated directly from measurements or maps) accordingly. Table 6-4 contains a summary of the pre-calibration and post-calibration values for the previously identified input parameters. Figures 6-3 and 6-4 show the post-calibration results for the water year 1988, for the HRUs 26 and 28.

Table 6-4. Summary of pre-calibration and post-calibration values for the identified input parameters

Parameter	Physically realistic range of values	Pre-calibration value	Post-calibration value
S_h	0 to 1.0	0.90	0.85
F_d	0 to 1.0	0.90	0.78
f3(F)	-3.6 to -1.6	-2.6	-1.8
T_f	0 to -5	-2.5	-1.5

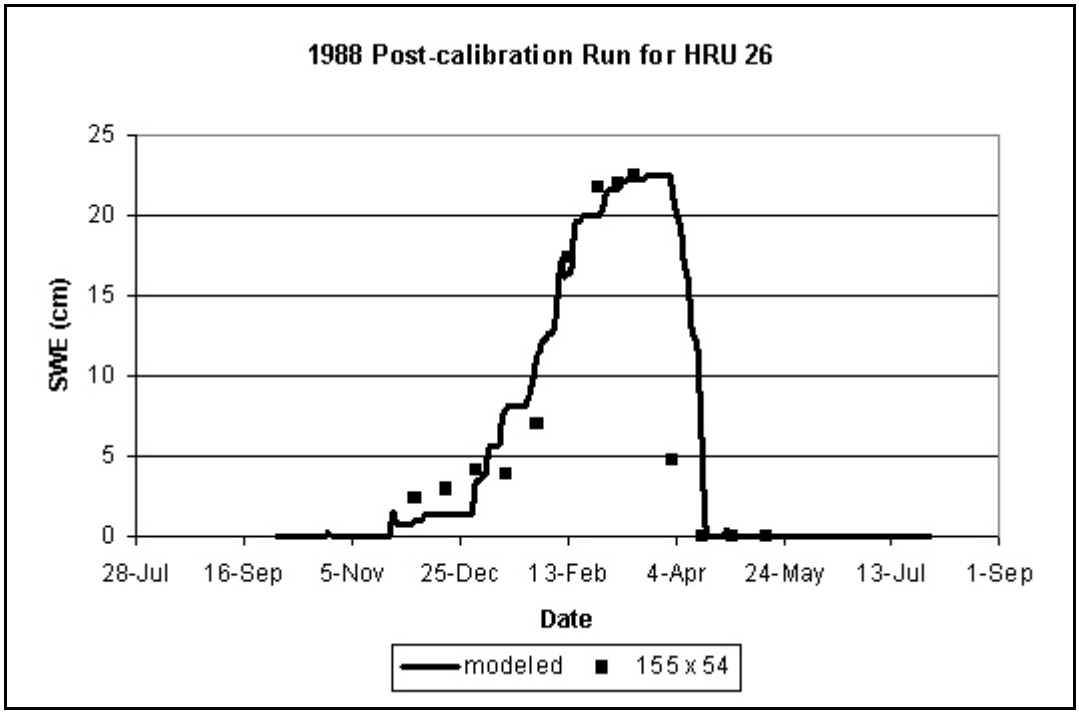

Figure 6-3. Post-calibration results for HRU 26 for 1988

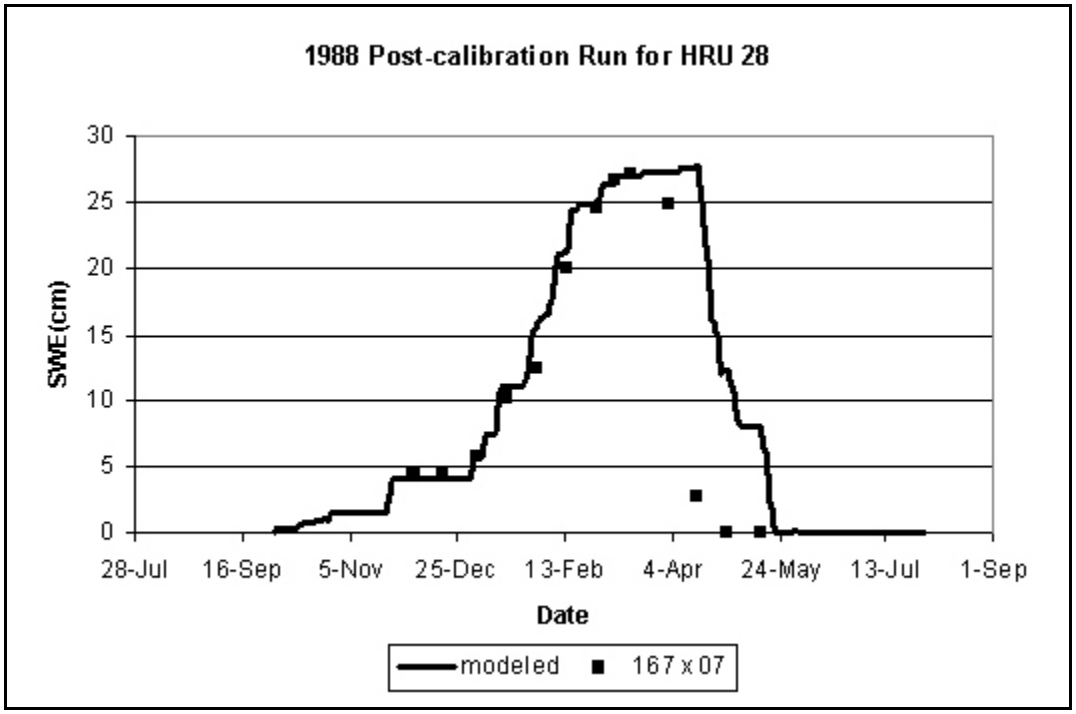

Figure 6-4. Post-calibration results for HRU 28 for 1988

A review of Figures 6-3 and 6-4 indicate that visually, the proposed model matches the field SWE data for 1988 for these HRUs more accurately than for the original model runs. These figures also show an apparent bias in the ablation period which will be further investigated. To verify model improvement, all statistics were recalculated for the post-calibration model runs. The results of these calculations, and the pre-calibration results can be found in Table 6-5. Tables 6-6 and 6-7 contain the summary of the goodness-of-fit statistics for the 1988 accumulation and ablation periods for the pre-calibration and post-calibration runs for HRUs 26 and 28.

An inspection of Tables 6-5 through 6-7 indicate that the post-calibration model fits the measured SWE data for this watershed more accurately than for the pre-

calibration model. The goodness-of-fit and physically-based statistics are significantly better for the post-calibration model runs. Fourteen trials were necessary to fit the model. The statistical values in Tables 6-5 through 6-7 represent the best run of the 14 trials.

A review of Table 6-5 shows mixed results in terms of model accuracy. The sample mean error values for both HRUs are low indicating that the modeled SWE values match the measured SWE values well during the water year. However, the S_e / S_y values are both moderately high, indicating that the predicted SWE value does not provide a significant improvement in accuracy over using the mean SWE value. The model does provide accurate predictions in approximating the peak SWE values for both HRUs for the water year. Estimating potential runoff from snow melt based upon modeled results should provide accurate values. This fact could provide crucial information to downstream communities when developing a water budget for the upcoming summer season. The model also provides accurate estimates for the length of the ablation period. The results for predicting the date of snowpack ripening are mixed. The model does an accurate job of predicting this date for HRU 26 (7 day difference), but does a poor job of predicting this date for HRU 28 (31 day difference). Table 6-5 also indicates that the model matches the measured SWE data for HRU 26 better than for HRU 28.

Table 6-5. Summary of the pre and post-calibration goodness-of-fit statistics for the water year 1988 for the HRUs 26 and 28.

Parameter	HRU 26		HRU 28	
----------	Pre	Post	Pre	Post
$\overline{e}$ (cm)	8.8	1.5	10.4	4.0
$\overline{e} / \overline{Y}$	1.05	0.18	0.83	0.27
S_e (cm)	13.4	5.2	17.3	8.1
S_e / S_y	1.24	0.61	1.25	0.79
Peak SWE modeled (cm)	31.4	22.6	46.4	27.9
Peak SWE measured (cm)	22.6	22.6	27.2	27.2
Δ Peak SWE (cm)	8.8	0	19.2	0.7
Δ Peak SWE / Peak SWE measured	38.9%	0%	70.6%	2.6%
Modeled date of snowpack ripening	April 25	March 23	May 29	April 16
Estimated date of snowpack ripening from field SWE measurements	March 16	March 16	March 16	March 16
Δ Date of snowpack ripening (days)	40	7	74	31
Modeled length of snowpack ablation period (days)	32	28	30	37
Measured length of snowpack ablation period (days)	31	31	45	44
Δ length of snowpack ablation (days)	1	-3	-15	-7

Table 6-6. Summary of the pre and post-calibration goodness-of-fit statistics for the accumulation period of the water year 1988, for the HRUs 26 and 28.

Parameter	HRU 26		HRU 28	
----------	Pre	Post	Pre	Post
$\overline{e}$ (cm)	2.3	0.1	2.9	0.5
$\overline{e} / \overline{Y}$	0.20	0.01	0.19	0.03
S_e (cm)	3.1	2.2	3.1	1.2
S_e / S_y	0.35	0.28	0.32	0.12

Table 6-7. Summary of the pre and post-calibration goodness-of-fit statistics for the ablation period of the water year 1988, for the HRUs 26 and 28.

Parameter	HRU 26		HRU 28	
----------	Pre	Post	Pre	Post
$\overline{e}$ (cm)	23.5	5.7	27.3	11.9
$\overline{e} / \overline{Y}$	4.70	1.14	3.94	1.72
S_e (cm)	23.8	9.7	30.9	14.6
S_e / S_y	2.83	1.05	6.43	1.65

The goodness-of-fit values found in Table 6-6 show that the model performs accurately during the accumulation period for both HRUs. The sample mean error and the mean relative error show that the predicted SWE values nearly match the measured SWE values during this period. In addition, the S_e / S_y values strongly suggest that the model has improved the reliability of prediction for the accumulation period over the mean measured SWE value. The goodness-of-fit values found in Table 6-7 show that the model does not perform accurately during the ablation period for both HRUs. The sample mean error and the mean relative error show that the predicted SWE values

differs significantly from the measured SWE values during this period. In addition, the S_e / S_y values are both greater than 1.0, which suggest that the model has not been successful in predicting SWE values during the ablation period.

As discussed above, and as was the case for the Upper Rio Grande Watershed, the proposed model performs significantly better for both HRUs for the accumulation period than for the ablation period. This fact initially points to the earlier discussion from Chapter 5 concerning the difficulty of measuring net energy for each of the HRUs, and that errors in net energy will cause more pronounced errors in SWE during the ablation period than during the accumulation period.

6.4 MODEL VALIDATION

The model was calibrated using the measured SWE data from 1988. This year was chosen for calibration because the mean peak SWE value throughout the watershed was approximately equal to the average mean peak SWE value for the eight water years The seven years of remaining data were used to validate the model results. It was decided to validate the model with seven years of data to provide the largest possible sample size for determining model robustness. The model was run for these years using the finalized input parameters (Table 6-4) and all previously calculated goodness-of-fit and physically-based statistics were determined for each of the seven years. Tables 6-8 through 6-10 contain the results of the statistical analyses for both of the HRUs for the seven remaining water years. Within each table for each statistical parameter, three values are reported. These values correspond to the largest, smallest, and (seven year)

average value determined for the particular parameter during the seven year period.

A review of Table 6-8 indicates that most goodness-of-fit statistics and physically-based statistics, for the two HRUs for the remaining seven years of data, approximate the level of accuracy determined for the calibration year 1988. The goodness-of-fit statistics determined during the validation period are similar to the post-calibration values for both HRUs. The range of sample mean error and the mean relative error values determined during the validation period are low indicating an accurate model, while the range of S_e / S_y values indicate only a modest improvement in predictive ability over the mean measured SWE value.

The validation and post-calibration physically-based statistics are comparable for HRU 26, but the same statistics show a significant improvement for HRU 28 for the validation period Δ date of snowpack ripening. The validation period range of values for this statistic indicate a significantly higher level of accuracy in predicting the date of snowpack ripening. Ultimately, these values again show that using the model to estimate potential runoff should provide accurate estimates, providing useful information for downstream communities. Additionally, using the modeled results to approximate the date of snowpack ripening, or the length of the ablation period should yield estimates that are useful to these same communities, but not as accurate as the potential volume of runoff.

Table 6-8. Summary of the post-calibration average goodness-of-fit statistics for the water years 1989 - 1995 for the HRUs 26 and 28.

Parameter	HRU 26			HRU 28		
---------	Low	Mean	High	Low	Mean	High
$\overline{e}$ (cm)	-2.1	1.3	3.7	-9.9	3.5	5.6
$\overline{e}$ / $\overline{Y}$	-0.18	0.10	0.28	-0.49	0.19	0.27
S_e (cm)	3.2	4.3	5.9	7.2	9.9	11.9
S_e / S_y	0.48	0.55	0.66	0.58	0.71	0.80
Peak SWE modeled (cm)	18.0	20.6	25.4	33.0	37.6	39.4
Peak SWE measured (cm)	22.1	22.1	22.1	34.5	34.5	34.5
Δ Peak SWE (cm)	-4.1	-1.5	3.3	-1.5	3.1	4.9
Δ Peak SWE / Peak SWE measured	-18.6%	-6.7%	14.9%	-4.3%	8.9%	14.2%
Modeled date of snowpack ripening	Feb. 9	Feb. 16	March 1	March 22	April 5	April 16
Estimated date of snowpack ripening from field SWE measurements	Feb. 22	Feb. 22	Feb. 22	March 25	March 25	March 25
Δ Date of snowpack ripening (days)	-13	-6	7	-3	11	22
Modeled length of snowpack ablation period (days)	48	58	66	39	50	58
Measured length of snowpack ablation period (days)	45	45	45	44	44	44
Δ length of snowpack ablation (days)	3	13	21	-5	6	14

Table 6-9. Summary of the post-calibration average goodness-of-fit statistics for the accumulation period for the water years 1989 - 1995, for the HRUs 26 and 28.

Parameter	HRU 26			HRU 28		
--------	Low	Mean	High	Low	Mean	High
$\overline{e}$ (cm)	-1.4	1.8	3.1	-0.8	3.7	4.5
$\overline{e} / \overline{Y}$	-0.17	0.15	0.28	-0.07	0.19	0.26
S_e (cm)	2.6	3.2	3.5	4.0	4.8	5.7
S_e / S_y	0.30	0.41	0.48	0.39	0.47	0.55

Table 6-10. Summary of the post-calibration average goodness-of-fit statistics for the ablation period for the water years 1989 - 1995, for the HRUs 26 and 28.

Parameter	HRU 26			HRU 28		
-------	Low	Mean	High	Low	Mean	High
$\overline{e}$ (cm)	-1.5	2.2	3.4	-1.1	8.7	9.5
$\overline{e} / \overline{Y}$	-0.37	0.44	0.53	-0.14	0.86	0.93
S_e (cm)	4.0	4.5	5.1	10.1	11.2	12.0
S_e / S_y	0.54	0.64	0.75	0.88	1.01	1.13

Tables 6-9 and 6-10 confirm that the model matches the measured SWE data more accurately for both of the HRUs during the accumulation period than for the ablation period. The difference, however, is not as significant as was found for the Upper Rio Grande Watershed. Tables 6-9 suggests that the model works moderately well during the accumulation period for both HRUs. The sample mean error for both HRUs are low during the accumulation period indicating that the predicted SWE values are close in magnitude to the measured SWE values. However, the S_e / S_y values for

both of the HRUs are between 0.4 and 0.5 suggesting that the model has improved the reliability of prediction over the mean measured SWE value only moderately. Table 6-10 shows that the proposed model works moderately well for HRU 26 during the ablation period, but predicts poorly for HRU 28 during the ablation period. The sample mean error for HRU 26 is low indicating accurate predictions during the ablation period for this HRU but an S_e / S_y value of 0.64 indicates only marginal improvement over using the mean measured SWE value. The sample mean error and the S_e / S_y value are both high for HRU 28 indicating that the model does not accurately fit the measured SWE data during the ablation period for this HRU.

As was the case with the Upper Rio Grande Watershed, both calibration sites, for the Reynolds Creek Watershed, exist in one section of the watershed. In this case, both sites are located at the southern end of the watershed indicating less certainty about model accuracy for the northern half of the watershed. It is hypothesized that the uncertainty is less for this watershed than for the Upper Rio Grande Watershed. The reasoning for this claim is that although no SWE data exists in the north sector of the watershed, meteorological and precipitation data were available. This was not the case for the Upper Rio Grande Watershed, where the input and validation data were all measured in the south/southwest sector of the watershed (see Figure 4-3).

6.5 BIAS ANALYSIS

A review of Figures 6-3 and 6-4 show that a bias exists in the ablation period for both HRUs, for the water year 1988. As was discussed for the Upper Rio Grande

Watershed, this bias could suggest a systematic error in the model that needs to be addressed. Further inspection into the model output for all of the water years, however, suggests that the error occurring during the ablation period is a random bias and not indicative of a shortcoming in the model.

For HRU 26, when the sample mean error is inspected for the ablation period for each of the water years, when compared to the field measured SWE data, the modeled results over predict for five of the water years, under predict for two of the water years, and match the measured SWE data accurately for one of the water years. Figure 6-5 shows the model predicted SWE values along with field measured SWE values for HRU 26, for the water year 1990. This figure clearly shows that the model is under predicting during the ablation period when compared to the field measured SWE data. The corresponding sample mean error for this period of the water year is -2.1 cm. Figure 6-6 shows the model predicted SWE values along with the field measured SWE values for HRU 26, for the water year 1992. This figure clearly shows that visually, the model accurately matches the field measured SWE data during the ablation period. The corresponding sample mean error for this period of the water year is 0.08 cm. Although the sample size is small (n = 8), the results for these water years (for this HRU) indicate that the residuals associated with the ablation period represent a random bias. As previously discussed for the Upper Rio Grande Watershed, this bias is the result of modeling uncertainties regarding net energy, or regarding total accumulation.

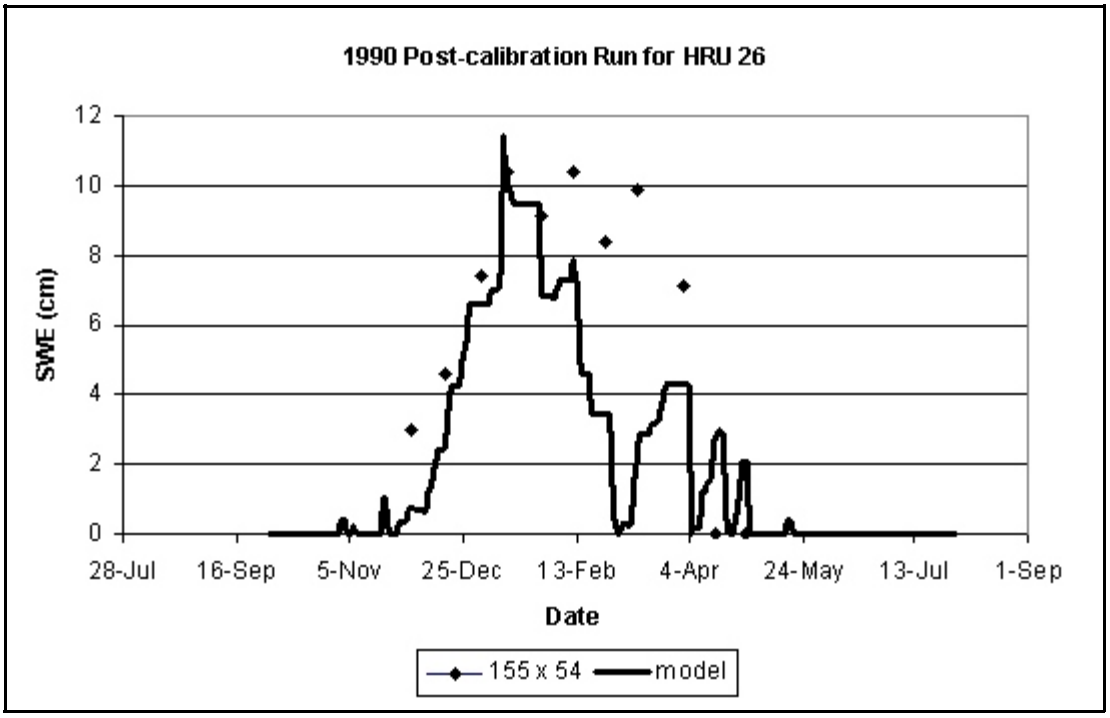

Figure 6-5. Post-calibration results for HRU 26 for 1990

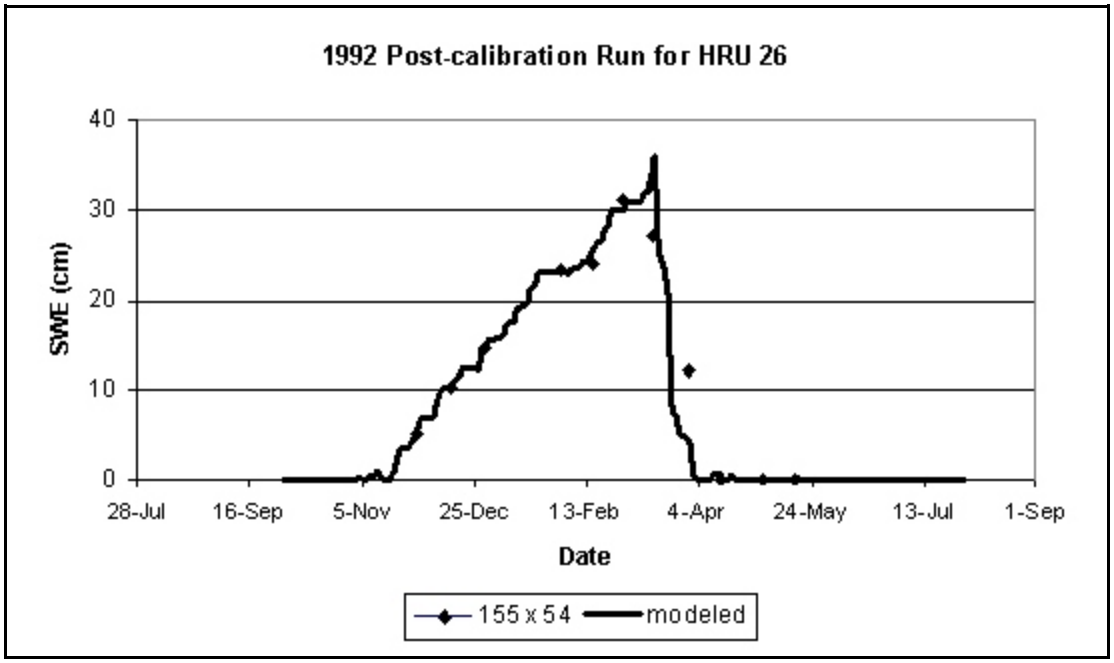

Figure 6-6. Post-calibration results for HRU 26 for 1992

A similar analysis can be performed for HRU 28. When the sample mean error is inspected for the ablation period for each of the water years, when compared to the field measured SWE data, the modeled results over predict for five of the water years, and under predict for three of the water years. Figure 6-7 shows the model predicted SWE values along with field measured SWE values for HRU 28, for the water year 1994. This figure clearly shows that the model is under predicting during the ablation period when compared to the field measured SWE data. The corresponding sample mean error for this period of the water year is -9.9 cm. Again, with a limited sample size (n = 8), the results for these water years (for this HRU) indicate that the residuals associated with the ablation period represent a random bias, again as a result of modeling uncertainties regarding net energy.

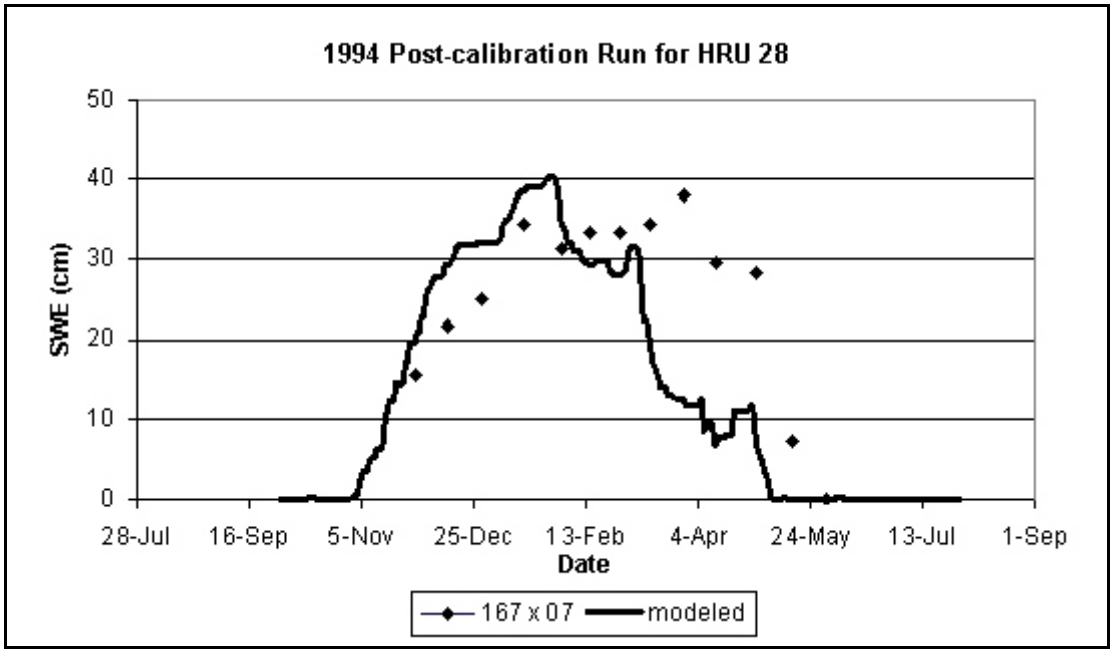

Figure 6-7.Post-calibration results for HRU 28 for 1994

A review of Table 4-5 indicates that both HRUs 26 and 28 are forested. This suggests that the results of this bias analysis should match the results performed for HRUs 40 and 50 (both forested) of the Upper Rio Grande Watershed (Section 5-5). However, this is not the case. The reason that the results are different for these forested HRUs is that the field measured SWE values were not isolated from canopy obstruction as were the SNOTEL measurements for the Upper Rio Grande Watershed. The SWE values obtained for the Reynolds Creek Watershed in HRUs 26 and 28 were representative of the entire HRU, unlike the SNOTEL SWE values. HRUs 26 and 28 are only partially forested and the forest type is a mixture of deciduous and coniferous (see Table 4-5), as opposed to the HRUs 40 and 50 from the Upper Rio Grande Watershed which were both completely forested by conifers (see Table 4-1).

6.6 SUMMARY OF RESULTS

The results presented in this chapter for the Reynolds Creek Watershed indicate that the model performs well during the accumulation period and provides accurate peak predictions when compared to the field measured SWE data. This suggests that using this model to estimate the volume of potential runoff from a snowpack should provide an accurate estimate. This could prove significant in predicting potential downstream water shortages from a small seasonal snowpack, or in predicting the potential generation of hydroelectric power downstream of the snowpack.

The results also show that the model does not perform accurately during the ablation period for the forested HRU. This implies the existence of a random bias that

is caused by the inability to accurately model net energy at a point. As a result, it is not recommended to use this model to make predictions during the ablation period, such as identifying possible severe stream discharge events based upon the length of the ablation period. Results were not available for nonforested HRUs, because both sites with field measured SWE data were forested, but it is highly probable that the results would mirror the results for the nonforested HRU for the Upper Rio Grande Watershed in which the model did not perform accurately during the ablation period, due to inaccuracies in modeling net energy at a point.

CHAPTER 7

IMPLEMENTATION AND CALIBRATION OF THE MODEL FOR THE EMERALD LAKE WATERSHED

7.1 INTRODUCTION

As discussed for the two previous watersheds, one of the objectives of the research is to demonstrate the proper calibration and validation of the model using data collected from various watersheds. This chapter will accomplish this task by discussing the implementation, calibration, and validation of the proposed model for the Emerald Lake Watershed. Pre-calibration results of the model will be compared using graphical results, standard goodness-of-fit statistics, and physically-based statistics. The subjective optimization procedure, as discussed in Chapter 5, used to improve upon the accuracy of the model results, will also be demonstrated. An analysis showing the improvement in model accuracy achieved as a result of the optimization process will be demonstrated by comparing modeled results with those obtained during the pre-calibration phase. This is referred to in this chapter as the post-calibration phase. The improvement in accuracy for these cases can be compared using the same techniques as outlined for the pre-calibration phase. Model validation will be performed by running the model with additional years of data. Finally, the model performance will be assessed.

7.2 PRE-CALIBRATION MODEL RESULTS

For the Emerald Lake Watershed, the model was initially run for the water year 1996, for the following HRUs: 1, 2, 5, 6 and 8. These HRUs correspond to the SWE measurement locations shown on Figure 4-14. The water year 1996 was chosen as the calibration year because it provided the most SWE field measurements. Unlike the Upper Rio Grande Watershed, which had daily SWE data, or even the Reynolds Creek Watershed, which had approximately bimonthly SWE data, SWE data for the Emerald Lake Watershed consists of approximately four measurements taken during the water year. The trade-off from the earlier mentioned watersheds, is that SWE data exists in more of the HRUs for the Emerald Lake Watershed than in the two previous watersheds. As a result, greater assurance on how the model is functioning throughout the entire watershed for Emerald Lake can be ascertained than for either of the previous watersheds. The results of the initial model run for these HRUs are presented graphically in Figures 7-1 through 7-5.

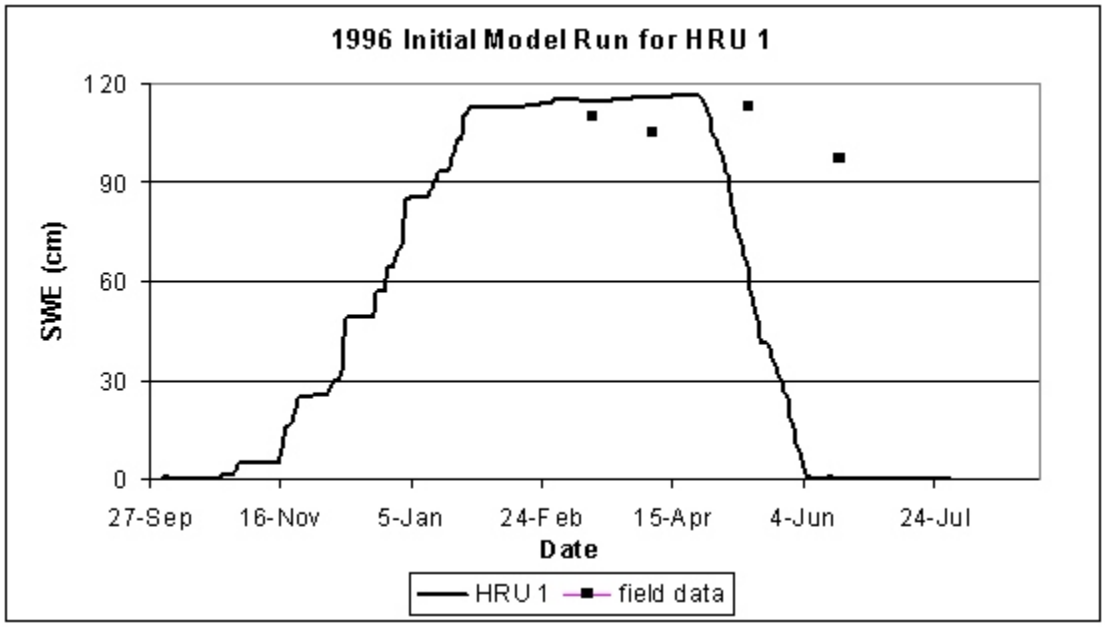

Figure 7-1. Initial model results for HRU 1 for 1996

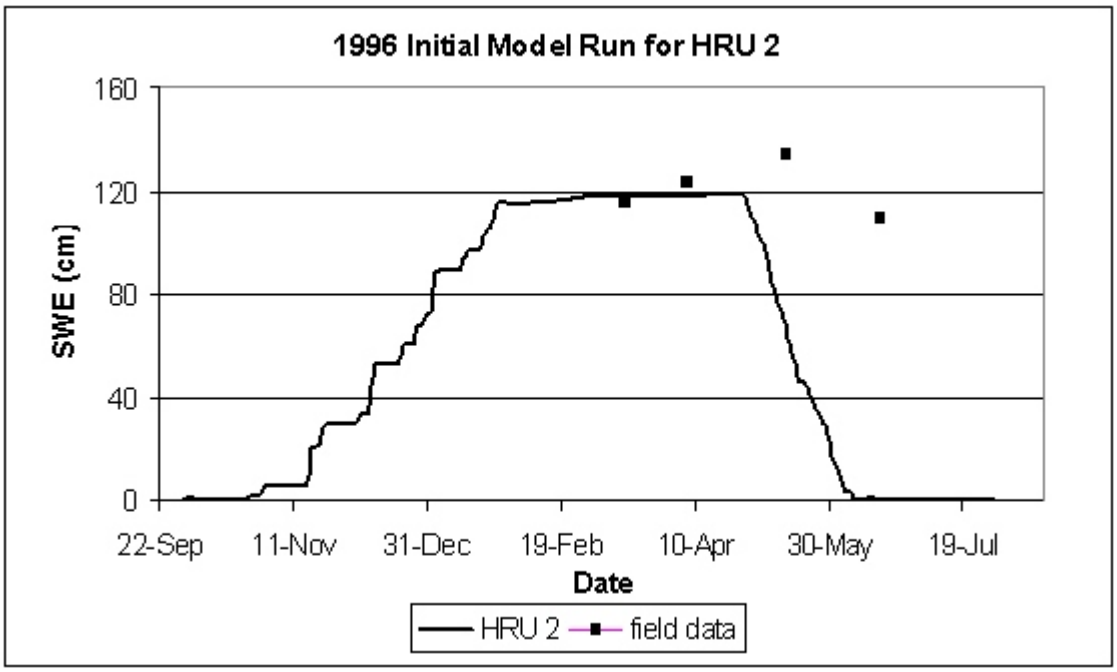

Figure 7-2. Initial model results for HRU 2 for 1996

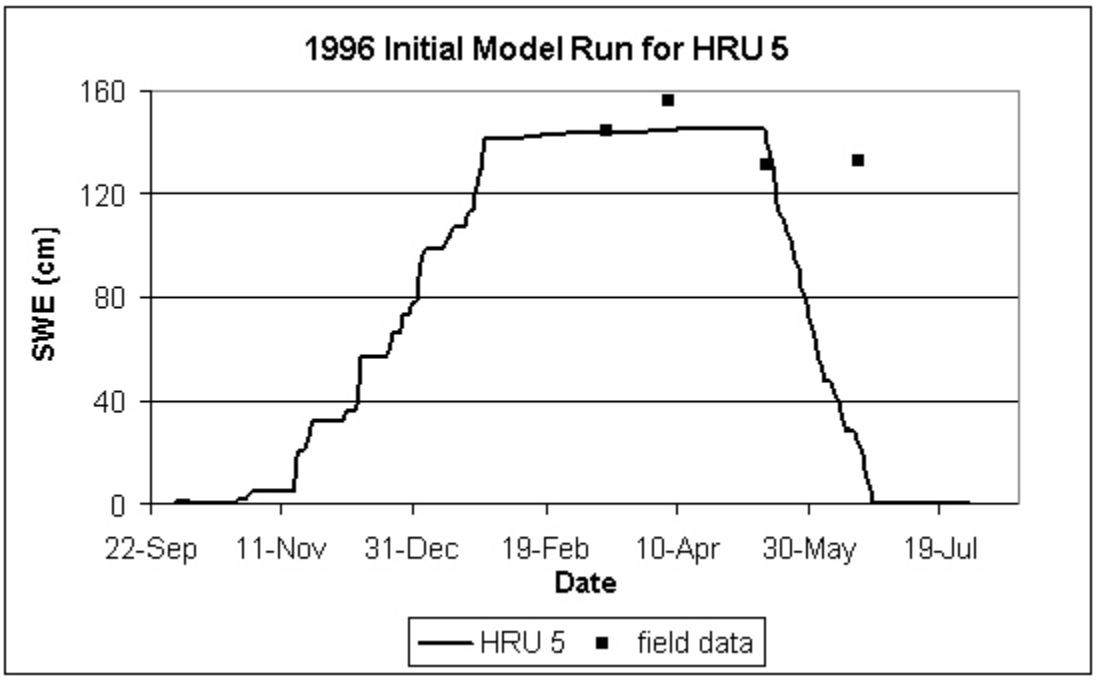

Figure 7-3. Initial model results for HRU 5 for 1996

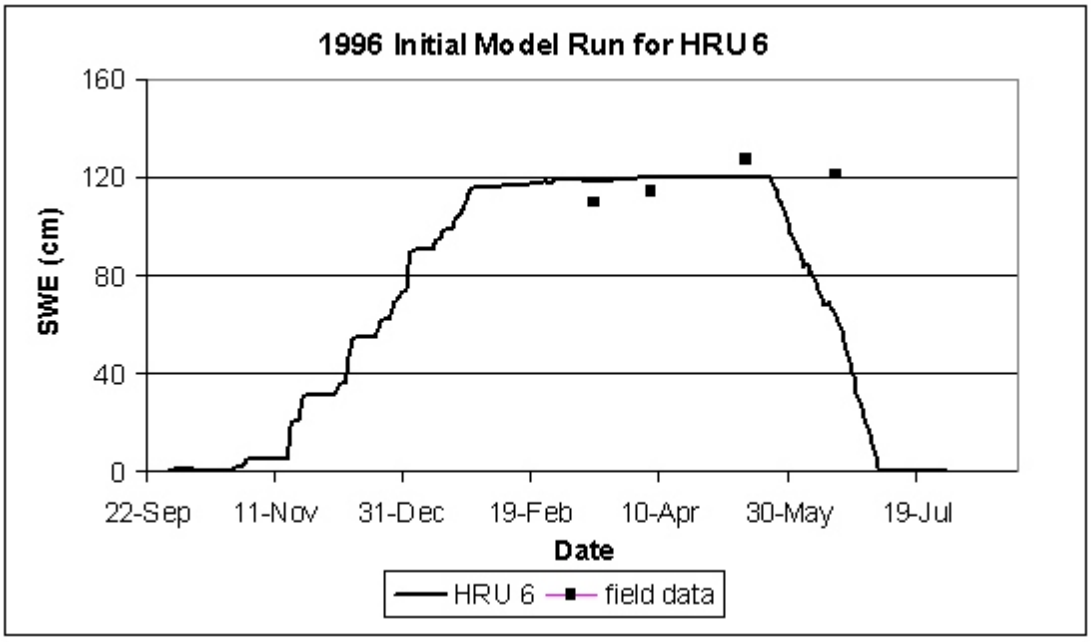

Figure 7-4. Initial model results for HRU 6 for 1996

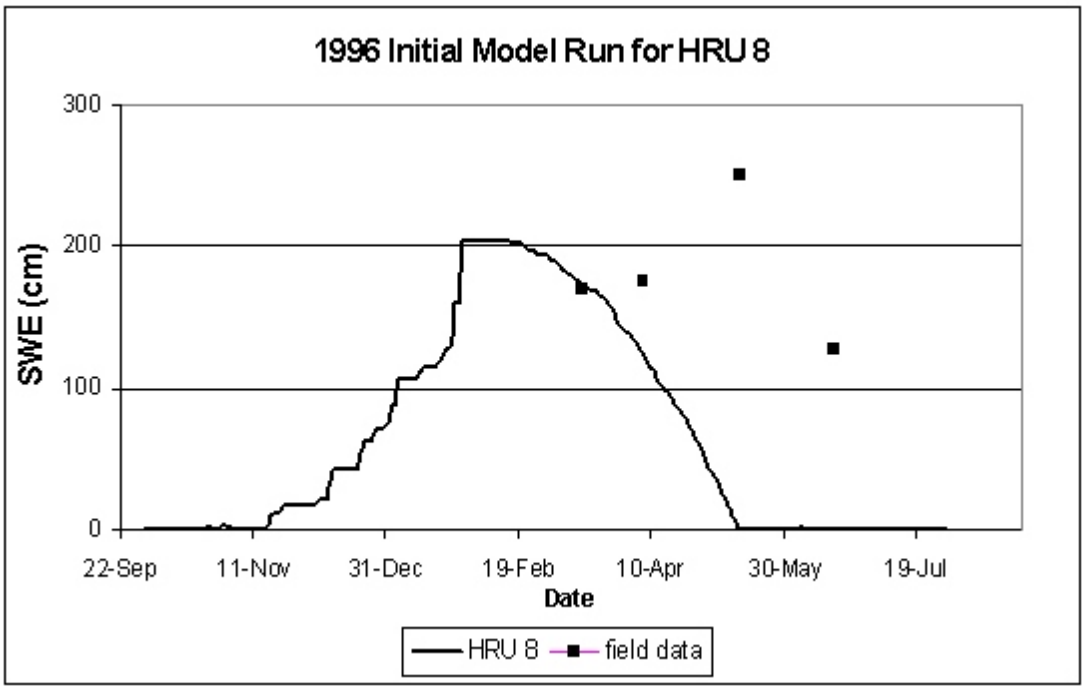

Figure 7-5. Initial model results for HRU 8 for 1996

A review of Figures 7-1 through 7-5 demonstrates that the pre-calibration model does not accurately match the field measured SWE data for this watershed. These figures show that for all HRUs, the ablation period is occurring too early in the water year. This fact suggests that the model is over predicting the net energy received at these HRUs, causing the premature occurrence of the date of snowpack ripening. As a result, the beginning of the melt season occurs too early. During the calibration period, free parameters affecting the net energy received for these HRUs were altered to address the identified problem.

As was the case for the previous watersheds, statistical analyses were performed on these initial runs to help determine how well the proposed model fit the measured

data. Unlike the previous watersheds, the analysis was only performed for the entire water year, and not the accumulation season and the ablation season. The reason for this is that the sample size is already very small (n = 4). To further subdivide these few data points would be fruitless. The same goodness-of-fit statistics that were used for the Upper Rio Grande and Reynolds Creek watersheds were also calculated for the Emerald Lake Watershed. However, the physically-based statistics previously calculated could not be used for this watershed due to a lack of measured SWE data. With only four data point, predicting peak measured SWE, estimating when the snowpack has ripened, or determining the length of the ablation period is not possible. Table 7-1 contains a summary of the goodness-of-fit statistics discussed above for the entire water year 1996, for the HRUs 1, 2, 5, 6 and 8.

Table 7-1. Summary of the goodness-of-fit statistics for the water year 1996, for the HRUs 1, 2, 5, 6 and 8.

--------	$\overline{e}$ (cm)	$\overline{e} / \overline{Y}$	S_e (cm)	S_e / S_y
HRU 1	-33.4	-0.32	26.5	3.79
HRU 2	-44.8	-0.37	33.9	3.13
HRU 5	-28.0	-0.20	55.4	4.81
HRU 6	-12.7	-0.11	29.2	3.87
HRU 8	-106.4	-0.59	142.8	2.81

A review of Table 7-1 indicates that the proposed model does not accurately match the field SWE data for any of the HRUs. This fact can best be seen by the very high values of S_e / S_y for each HRU. These values are all greater than 1.0, indicating

that the interannual mean SWE value provides a more accurate prediction for SWE than the model results. This fact can also be seen by the high values for the sample mean error, the mean relative error, and the standard error of the estimate. Attempts to use this model to make any predictions regarding SWE for this watershed will result in significant errors. Substantial improvement in all of these parameters is required before the proposed model can be considered accurate.

Autocorrelation between the time series of measured SWE values was not tested due to the small sample size. The small sample size dictated that it was not feasible to perform a hypothesis test using the "t" statistic to test for model bias.

7.3 SUBJECTIVE OPTIMIZATION PROCESS

As was the case with the previous two watersheds, the same subjective optimization process was performed for the Emerald Lake Watershed. The same input parameters, as identified earlier, were chosen to be modified, and the same criterion was used for the subjective optimization procedure. As mentioned earlier, attempts were made to decrease net energy received at these HRUs by altering the input parameters accordingly, to allow for later seasonal snow ablation. Table 7-2 contains a summary of the pre-calibration and post-calibration values for the identified input parameters.

Figures 7-6 through 7-10 show the post-calibration results for the water year 1996, for the HRUs 1,2, 5, 6 and 8. A review of Figures 7-6 and 7-10 indicate that visually, the proposed model matches the field data for 1996 for these sites more accurately than for the original model runs, although the model fit for HRU 8 remains

poor. Except for Figure 7-10, these figures show a marked improvement in more accurately matching the measured SWE data at the onset of the ablation period than did Figures 7-1 through 7-5. To verify model improvement, all statistics were recalculated for the post-calibration model runs. The results of these calculations can be found in Table 7-3.

Table 7-2. Summary of pre-calibration and post-calibration values for the identified input parameters.

Parameter	Physically realistic range of values	Pre-calibration value	Post-calibration value
S_h	0 to 1.0	0.90	0.78
F_d	0 to 1.0	0.90	0.80
f3(F)	-3.6 to -1.6	-2.6	-2.0
T_f	0 to -5	-2.5	-1.2

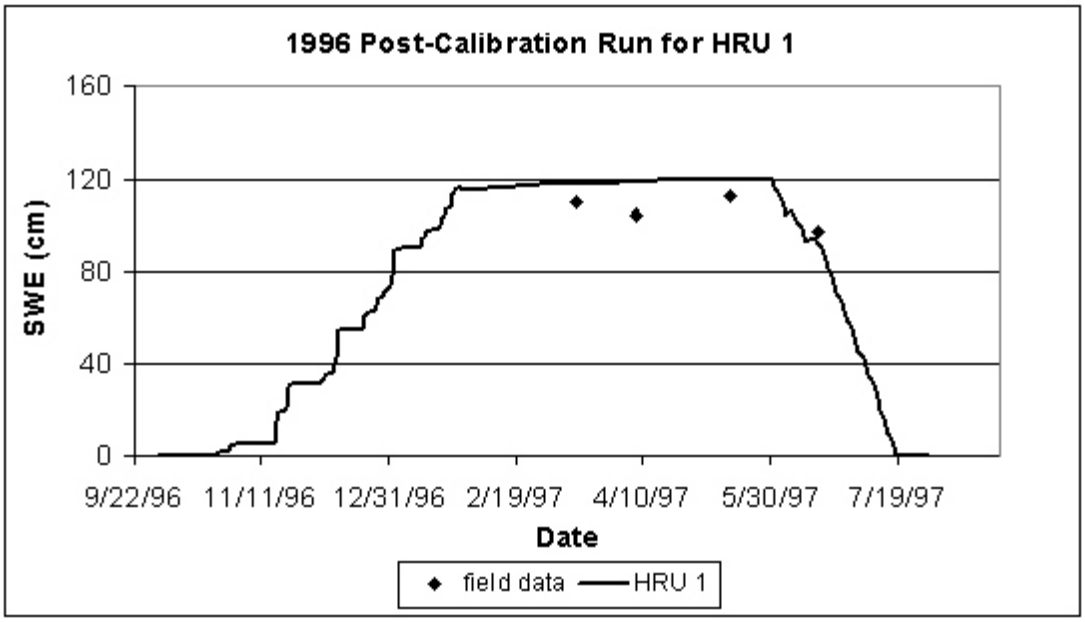

Figure 7-6. Post-calibration results for HRU 1 for 1996

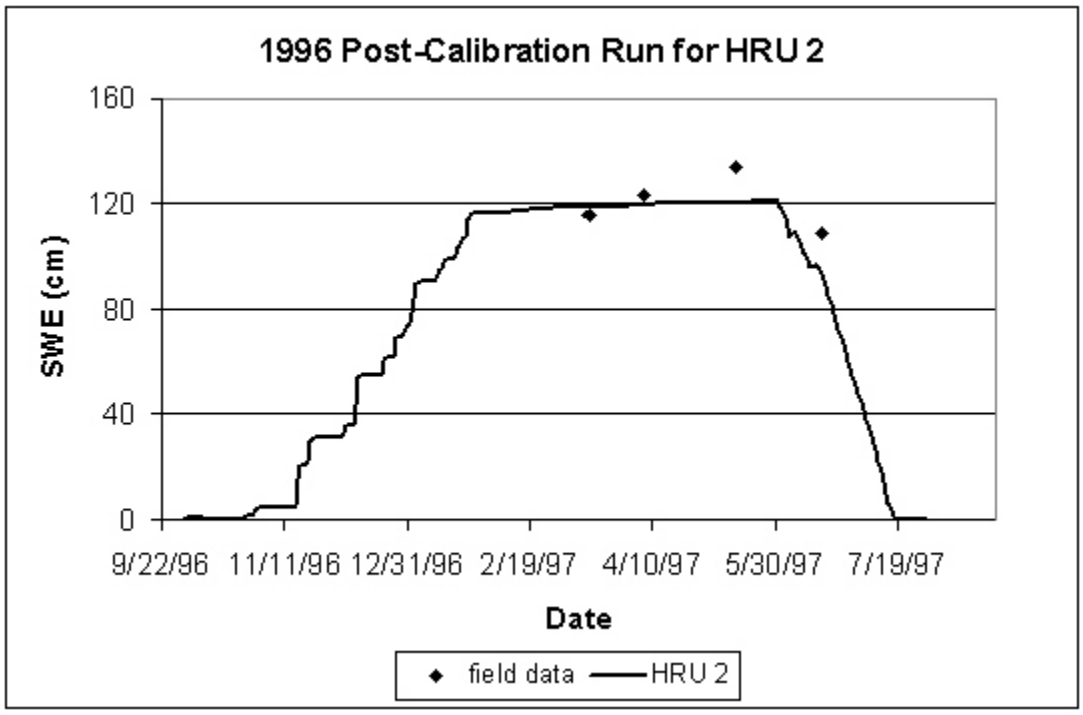

Figure 7-7. Post-calibration results for HRU 2 for 1996

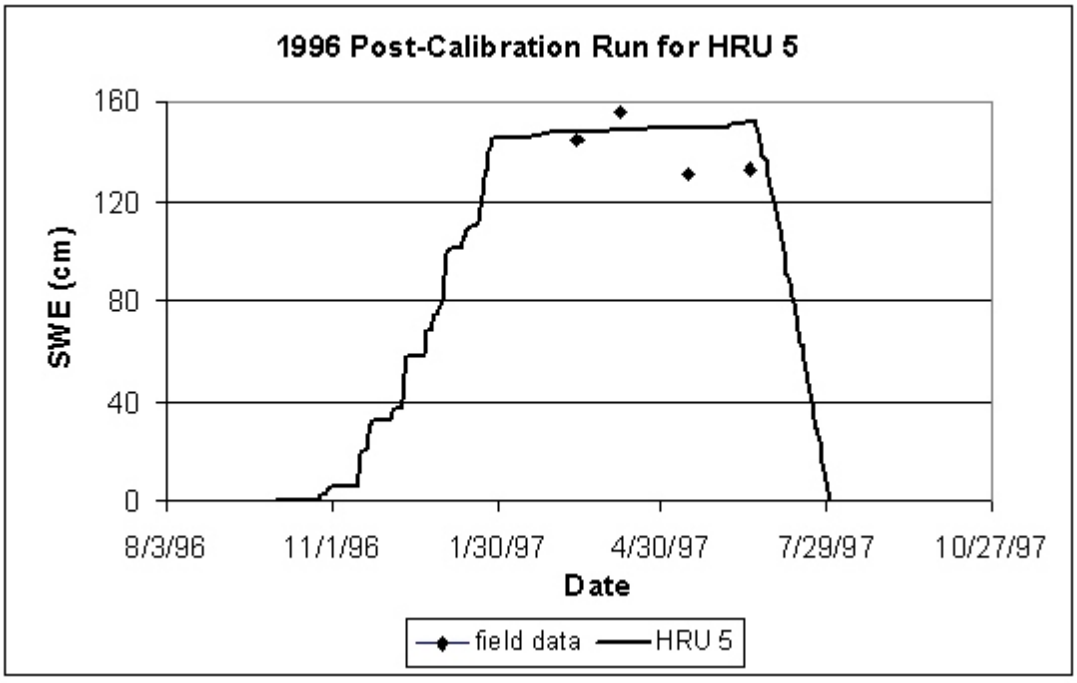

Figure 7-8. Post-calibration results for HRU 5 for 1996

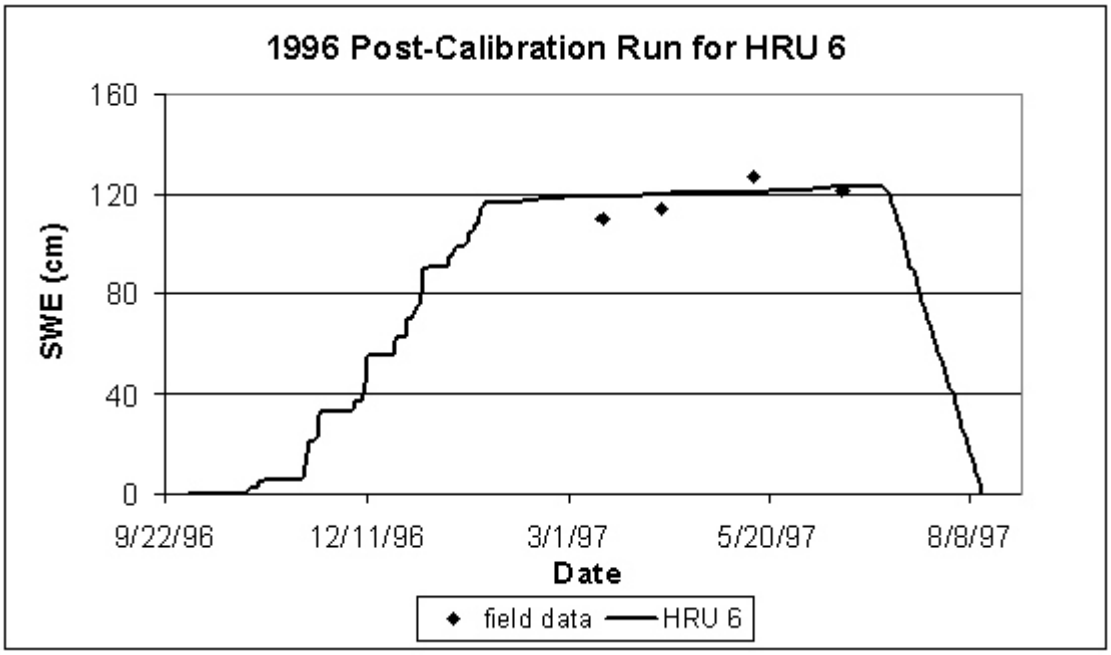

Figure 7-9. Post-calibration results for HRU 6 for 1996

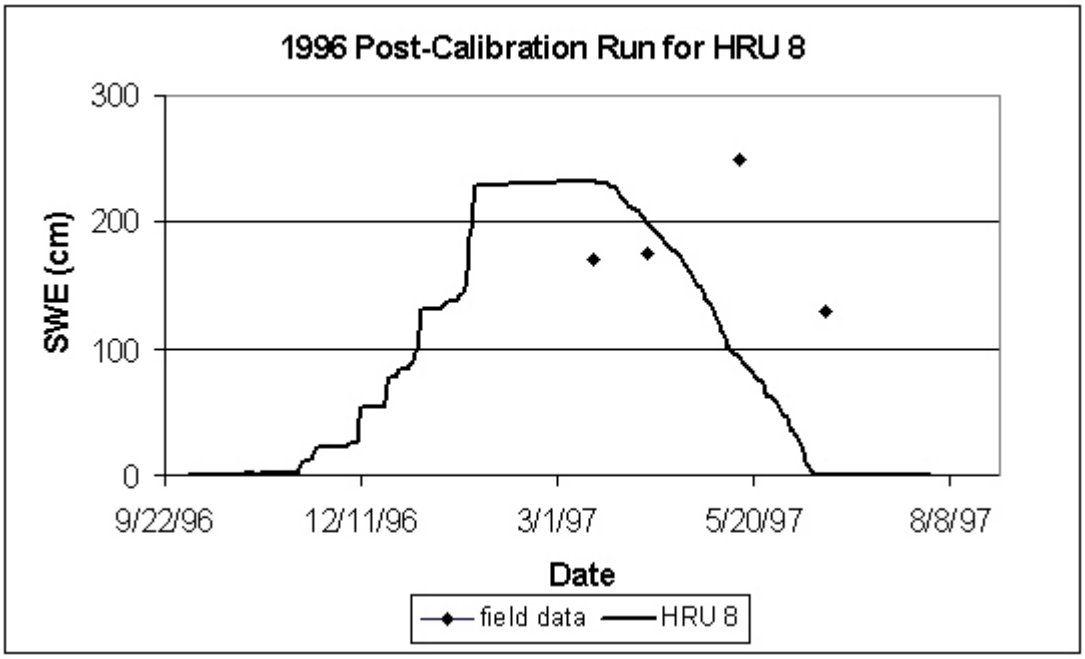

Figure 7-10. Post-calibration results for HRU 8 for 1996

Table 7-3. Comparison of the pre and post-calibration goodness-of-fit statistics for the water year 1996 for the HRUs 1, 2, 5, 6 and 8.

--------	$\overline{e}$ (cm)		$\overline{e}$ / $\overline{Y}$		S_e (cm)		S_e / S_y	
	Pre	Post	Pre	Post	Pre	Post	Pre	Post
HRU 1	-33.4	6.0	-0.32	0.08	26.5	9.1	3.79	0.97
HRU 2	-44.8	-7.4	-0.37	-0.06	33.9	10.6	3.13	0.93
HRU 5	-28.0	4.4	-0.20	0.05	55.4	9.9	4.81	0.86
HRU 6	-12.7	2.5	-0.11	0.04	29.2	6.3	3.87	0.83
HRU 8	-106.4	-50.2	-0.59	-0.28	142.8	61.6	2.81	1.21

A review of Table 7-3 indicates that the post-calibration model fits the measured SWE data for this watershed more accurately than for the pre-calibration model. All goodness-of-fit statistics are significantly better for the post-calibration model runs. Seventeen trials were necessary to fit the model. The statistical values in Table 7-3 represent the best of the 17 runs.

A review of Table 7-3 shows mixed results, in terms of model accuracy. The sample mean error, and mean relative error values for these HRUs are low (all but HRU 8), indicating that the model predictions match the field measured SWE values well. However, the S_e values are moderately high, and the S_e / S_y values are very high, all close to, or greater than 1.0, indicating that the predicted SWE value does not provide a significant improvement in accuracy over using the interannual mean SWE value.

Due to such a small sample size (n = 4), a great deal of confidence cannot be placed in the goodness-of-fit statistics. With this in mind, it is difficult to directly analyze the accuracy of the proposed model based solely upon the results found in Table

7-3. Although the results found in Table 7-3 indicate mixed results in terms of model accuracy, Figures 7-6 through 7-10 at least visually indicate that the model does match the measured SWE values relatively well, except for HRU 8.

A hypothesis for why the model accuracy is not as good for this watershed as it was for the other two watersheds is that the model predicts that significant avalanching occurs during the water year 1996. A review of Table 7-3 shows that the model accuracy is lowest for HRU 8. This HRU is in the low-lying section of the watershed, and the model predicts 75 cm of SWE being transported into HRU 8, from the surrounding HRUs, due to avalanching. Figure 7-11 shows a time series of SWE received at HRU 8 due to avalanching during the water year 1996. According to Sulakvelidze and Dolov (1973), the developed equation for avalanching transport generally yields SWE values that are within $\pm$ 15% of the actual SWE value. Additionally, the model predicts avalanching based upon the daily meteorological conditions, and these events may or may not occur in nature as predicted by the model. These facts are most likely the greatest source of error in estimating the SWE value for all the HRUs and especially HRU 8.

7.4 MODEL VALIDATION

Unlike the previous watersheds, only one additional year of remaining data was available to validate the model results. The remaining three years of existing data contain only two SWE measurements during the water year, so goodness-of-fit statistics were not calculated for these three years. The goodness-of-fit statistics were determined

for 1997, the additional year with four measured SWE values. Table 7-4 contains the statistical values for the HRUs for the water years 1996 and 1997.

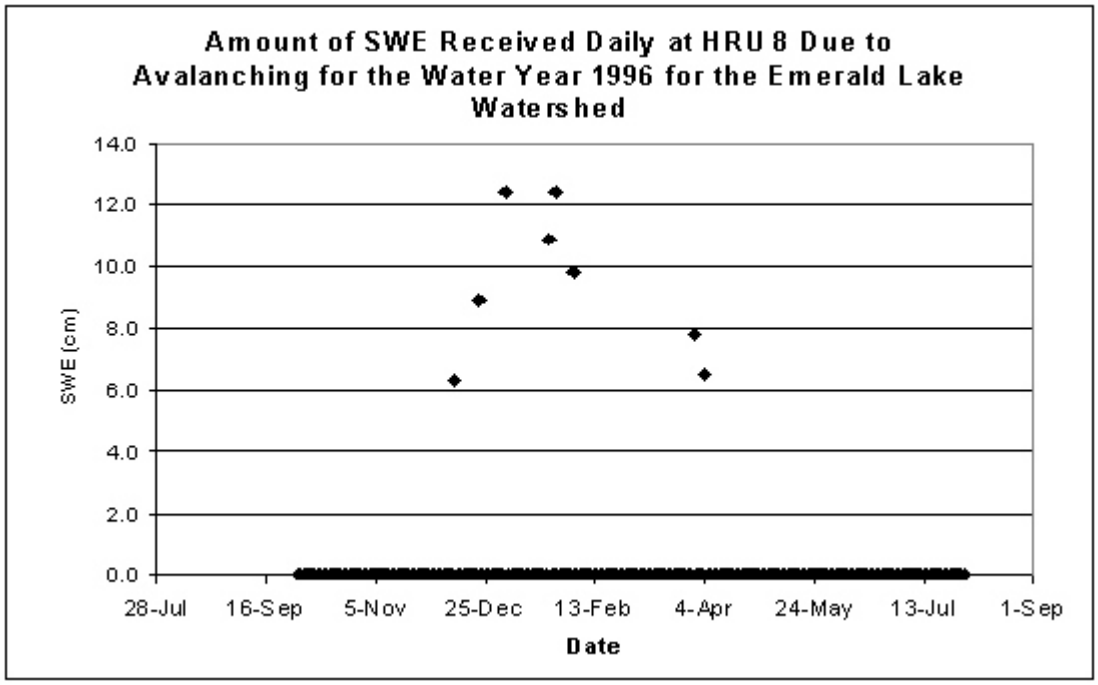

Figure 7-11. SWE received at HRU 8 due to avalanching for 1996

Table 7-4. Summary of the post-calibration goodness-of-fit statistics for the water years 1996 and 1997 for the HRUs 1, 2, 5, 6 and 8 (1996 is the calibration year and 1997 is the validation year).

--------	$\overline{e}$ (cm)		$\overline{e}$ / $\overline{Y}$		S_e (cm)		S_e / S_y	
	1996	1997	1996	1997	1996	1997	1996	1997
HRU 1	6.0	4.8	0.08	0.11	9.1	7.9	0.97	0.72
HRU 2	-7.4	8.1	-0.06	0.14	10.6	10.9	0.93	0.76
HRU 5	4.4	6.4	0.05	0.09	9.9	10.3	0.86	0.73
HRU 6	2.5	3.5	0.04	0.09	6.3	6.6	0.83	0.67
HRU 8	-50.2	-20.3	-0.28	-0.14	61.6	18.6	1.21	0.89

A review of Table 7-4 indicates that the model accuracy has modestly improved for the HRUs 1, 2, 5, and 6 for the water year 1997, as compared to 1996. The sample mean error, relative mean error, and S_e values are nearly the same for these HRUs for 1996 and 1997. These values are low, again indicating that the model predictions match the field measured SWE values well for the water year 1997. The improvement in model accuracy for these HRUs can be found in the modest improvement in the S_e / S_y values. Although improved, these S_e / S_y values still do not indicate a significant improvement in predictive accuracy over the interannual mean value of measured SWE.

The goodness-of-fit statistics for HRU 8, found in Table 7-4 show significant improvement in model accuracy for the water year 1997 when compared to 1996. The sample mean error, relative mean error, and S_e values are significantly better for this HRU. Additionally, the S_e / S_y value is modestly improved for HRU 8 for the water year 1997. Although improved, the goodness-of-fit statistics for HRU 8 still indicate low model accuracy.

The improvement in goodness-of-fit statistics for the water year 1997, especially for HRU 8, most likely coincides with the fact that the model predicts much less avalanching for the water year 1997 than for the water year 1996. HRU 8 received only 5 cm of SWE via avalanching from the other HRUs during the water year 1997, as opposed to the 75 cm of SWE received by HRU 8 during the water year 1996. The prediction of less avalanching for the water year 1997, leads to less model uncertainty in SWE transport between HRUs, and would account for an increase in model accuracy, as depicted for 1997.

7.5 SUMMARY OF RESULTS

The goodness-of-fit statistics indicate mixed results in model accuracy for the Emerald Lake Watershed. However, with only four field SWE measurements for two water years, the information learned from the statistical analyses is limited.

The model results for this watershed do demonstrate the difficulties in accurately predicting avalanching. These difficulties include determining if an avalanche occurs, and if it does, what volume of SWE is transported because of it. Not surprising, the goodness-of-fit statistics were better for the water year 1996, a year of little predicted avalanching, than for 1997, a year of significant predicted avalanching. The consequence of this difficulty would not affect crudely estimating the potential volume of runoff from this watershed. The total SWE within the watershed has been calculated by the model, and the difficult in avalanche predicting will only mean errors in the distribution of SWE to the various HRUs but not the total volume of SWE within the watershed. Significant errors could occur if the model is used to predict events associated with the ablation period, such as extreme discharge events, because the timing of the melt process will be influenced by errors in the spatial distribution of SWE throughout the watershed.

CHAPTER 8

SENSITIVITY ANALYSIS

8.1 INTRODUCTION

Two objectives of the research are: (1) to demonstrate the effects of the physical variables and parameters on the SWE distribution within a watershed, and (2) to show the benefit of additional data on model accuracy and when and where to collect the data. These objectives can be accomplished by means of performing post-calibration sensitivity analyses. A sensitivity analysis performed on the model input parameters can assess the relative importance of the input parameters and examine the effect of error in the input parameters on error in the model output. Additionally, a sensitivity analysis can be performed on the available SWE data for the watersheds to determine if the availability of daily, bimonthly, or sporadic SWE measurements plays a role in model accuracy.

A sensitivity analysis can also be performed on the procedure of subdividing the watershed into HRUs, to determine the sensitivity of the model output to the subdivision process. As previously mentioned in Chapter 4, the process of subdividing the watershed into HRUs is subjective; therefore, a watershed can be subdivided many different ways. The proposed model can be implemented for several variations, and the model output compared and analyzed for these different variations.

8.2 ANALYSIS OF OPTIMIZATION PARAMETERS

8.2.1 Introduction

As discussed in Chapters 5 through 7, several input parameters were optimized primarily due to difficulty in collecting the measured data required to estimate them. These parameters were: S_h, F_d, $f_3(F)$, and T_f. Sensitivity analyses was used to establish the relative importance of these uncertain input parameters. Sensitivity analyses was also used to determine the consequences, in terms of error in the model output, of the uncertainty in these input parameters. Relative sensitivity ($\$_r$) is defined as the percentage change in one factor due to a 1% change in another factor, and was used to evaluate the relative importance of these uncertain input parameters. The equation for relative sensitivity is as follows:

$$\$_r = \frac{\partial Y}{\partial X}\frac{X}{Y} \qquad (8\text{-}1)$$

Relative sensitivity values are dimensionless. Additionally, deviation sensitivity ($\$_d$) is defined as a change in a factor due to a change in a second factor, and will be used to examine the effect of errors in the identified input parameters on error in the model output. The equation for deviation sensitivity is as follows:

$$\$_d = \frac{\partial Y}{\partial X}\Delta X \qquad (8\text{-}2)$$

Deviation sensitivity values have units of the output variable Y, or in this case, SWE. Performing these analyses will provide information to the model user in terms of the

importance of data collection for the four identified input parameters. If these analyses show that these four parameters have little impact on model output, then this would justify setting these parameters as constants as opposed to spending the time and money required to field collect these data. This would also indicate that model accuracy is not significantly dependent upon the values chosen for these parameters. If these analyses show the opposite results, this would indicate to the modeler that proper data collection for these input parameters are essential for model accuracy.

The sensitivity analysis was performed by changing the value for one of the four identified input parameters in the model programming. The next step was to rerun the model for each of the three watersheds, for all of the previously examined water years. Next, the resulting model output was compared to the initial model output for each day of the water year. From this comparison, the following values were calculated: 1) the mean difference in daily SWE, 2) the range of differences in daily SWE, and 3) the difference in peak SWE value. These calculated difference were then used along with Equations 8-1 and 8-2 to calculate the relative sensitivity and deviation sensitivity for these four parameters, for an average SWE value during the entire water year, a range of SWE values during the water year, and for the peak SWE value. Finally, the mean value of relative and deviation sensitivity for all of the alternate runs were determined, for the mean difference in SWE for the entire water year, the range in SWE over the entire water year, and for the difference in peak SWE values.

The analysis was subdivided into three categories: HRUs that are completely forested, HRUs that are partially forested, and HRUs that lack a forest cover. This

subdivision was deemed necessary because the model sensitivity to these four input parameters was expected to vary depending upon canopy cover. Two of the four input parameters, F_d and $f_3(F)$, are only prevalent for forested HRUs, and a third parameter, S_h, is most likely significantly dependent upon HRU forest cover. To further explain, to simplify calculating net solar radiation, the model has a greater sensitivity to the terrain shading factor, S_h, for a nonforested HRU than for a forested HRU. This is due to the fact that the model algorithm used to calculate incoming solar radiation has been set up so that canopy cover greatly diminishes the amount of received incoming solar radiation to an HRU and thus changes in the terrain shading factor will result in smaller changes in received incoming solar radiation for a forested HRU compared to a nonforested HRU.

8.2.2 Sensitivity Analyses for Completely Forested HRUs

Table 8-1. Summary of the mean relative sensitivity values for the four input parameters for a completely forested HRU.

Rank	Parameter	Range of $\$_r$ for daily SWE values for entire water year	$\$_r$ for mean SWE value for entire water year	$\$_r$ for peak SWE value
1	F_d	0 to -3.68	-2.33	-1.98
2	$f_3(F)$	0 to -2.45	-1.61	-1.08
3	T_f	0 to -2.07	-1.19	-0.85
4	S_h	0 to -0.11	-0.01	-0.008

Table 8-1 contains a summary of the mean relative sensitivity values for the four

input parameters for a completely forested HRU. A review of this table shows two generalizations. First, all values found in these tables are negative. This fact indicates that as the parameters increase in magnitude, the predicted SWE values decrease in magnitude. Based upon the equations that contain these parameters, this finding is rational and lends credence to the sensitivity analysis being performed correctly. Second, the relative sensitivity values for all four of the parameters are greater in absolute magnitude when analyzing the sensitivity of the mean SWE value for the entire water year than for analyzing the sensitivity of the peak SWE value. The reason for this is that changes in these input parameters significantly affect net energy received at an HRU, and as previously discussed, thus greatly affect SWE values during the ablation period. This causes greater SWE differences late in the ablation period than at the time of snowpack ripening, corresponding to peak SWE values.

This second generalization can further be substantiated by realizing that the largest values for the relative sensitivity of daily SWE occur at the end of the melt season for all four parameters. Changes in these four parameters result in changes in net energy received during the water year. In turn, changes in net energy result in changes in the date in which the snowpack ripens and melt begins, and changes in the date in which the snowpack has completely ablated. When the input parameters are increased, the snowpack disappears on an earlier date. Consequently, the largest relative sensitivity values for all four parameters occur on days when the predicted snowpack has been completely ablated (using the increased parameters), and these values are compared to days when the snowpack exists under controlled modeled conditions. The

opposite of this is true when the input parameters are decreased.

A review of Table 8-1 shows that the relative sensitivity values are significant (an absolute value greater that 1.0) for F_d, $f_3(F)$, and T_f in terms of the mean SWE value for the entire water year. These values indicate that the model is very sensitive to changes in these three input parameters for completely forested HRUs. In terms of model sensitivity to the mean SWE value, F_d is twice as important a parameter as is T_f, and F_d is one and one-half times more important a parameter than $f_3(F)$. Consequently, these facts indicate that in order to achieve credible modeling results for forested HRUs, accurate input data for these parameters are important, and if resources are limited, data should be collected first for F_d, then for $f_3(F)$, and finally for T_f. Not surprisingly, Table 8-1 demonstrates that for forested HRUs, S_h is insignificant. As mentioned earlier, the model has been set up so that incoming solar radiation is greatly reduced for a completely forested HRU, and changes in the terrain shading parameter have little effect on total net energy received at a point, and thus SWE.

A review of Table 8-1 also shows that the relative sensitivity values are significant for F_d, $f_3(F)$, and T_f in terms of the peak SWE value. These values indicate that peak SWE is very sensitive to changes in these three input parameters for completely forested HRUs. In terms of model sensitivity of the peak SWE value, F_d is twice as important a parameter as is $f_3(F)$, and F_d is two and one-half times more important a parameter than T_f. Consequently, these facts indicate that in order to achieve credible modeling predictions of peak SWE for forested HRUs, accurate input data for these parameters are important, and if resources are limited, data should be

collected first for F_d, then for $f_3(F)$, and finally for T_f. Again, as expected, Table 8-1 demonstrates that for forested HRUs, S_h is insignificant in controlling peak SWE.

Table 8-2. Summary of the mean deviation sensitivity values for the four input parameters for a completely forested HRU.

Parameter	Physically realistic value range	Change in parameter value	$\$_d$ for mean SWE value for entire water year (cm)	$\$_d$ for peak SWE value (cm)
$f_3(F)$	-3.6 to -1.6	+/- 10%	+/- 0.43	+/- 0.32
T_f	0 to -5	+/- 10%	+/- 0.73	+/- 0.71
F_d	0 to 1.0	+/- 10%	+/- 0.59	+/- 0.48
S_h	0 to 1.0	+/- 10%	+/- 0.03	+/- 0.01

Table 8-2 contains a summary of the mean deviation sensitivity values for the four input parameters for a completely forested HRU. Typically, a deviation analysis involves determining the expected error in the criterion variable due to inaccuracies of the input data. The assumption made for this table is that the inaccuracies associated with these input parameters are +/- 10%. Extensive on-site data collection would be required at all three watersheds to better determine the actual inaccuracies of these input parameters, but this was not feasible for this study. The deviation sensitivity values found in this table are based upon this assumption of +/- 10% input parameter inaccuracy. Consequently, 10% was added to and subtracted from the actual parameter value to determine the deviation sensitivity values.

As was the case for the relative sensitivity values found in Table 8-1, all of the deviation sensitivity values associated with errors in the mean SWE values are greater

than the deviation sensitivity values associated with errors in the peak SWE values. Again this generalization is due to greater SWE errors being realized late in the ablation period due to the uncertainty of modeling net energy at a point.

Table 8-2 shows that significant errors could occur in estimating SWE for completely forested HRUs when errors exist in the parameters F_d, $f_3(F)$, and T_f. Potential for greater errors in SWE exist with inaccuracies in $f_3(F)$ and T_f, than for F_d. The reason for this is that $f_3(F)$ and T_f have a greater physical range in value than does F_d. This is especially true for T_f, which could be in error by several degrees Celsius.

Table 8-2 also indicates that inaccuracies in S_h have almost no effect on SWE output. As discussed earlier, inaccuracies in the shading factor are inconsequential for HRUs that are completely forested.

8.2.3 Sensitivity Analyses for Partially Forested HRUs

Table 8-3 contains a summary of the mean relative sensitivity values for the four input parameters for a partially forested HRU. A review of this table shows the same two generalizations that were noted, and discussed, in Table 8-1. The highest values found for the daily relative sensitivity values again coincide with the end of the ablation period, the explanation for which has been discussed in Section 8.2.2.

Table 8-3. Summary of the mean relative sensitivity values for the four input parameters for a partially forested HRU.

Rank	Parameter	Range of $\$_r$ for daily SWE values for entire water year	$\$_r$ for mean SWE value for entire water year	$\$_r$ for peak SWE value
1	S_h	0 to -2.32	-1.24	-0.19
2	$f_3(F)$	0 to -1.87	-1.05	-0.15
3	F_d	0 to -1.01	-0.35	-0.06
4	T_f	0 to -0.87	-0.33	-0.02

Table 8-3 shows that the relative sensitivity values are significant for S_h, and $f_3(F)$ for the mean value for the entire water year. These values indicate that the model results for partially forested HRUs are very sensitive to changes in these two input parameters. Table 8-2 also shows that the model has little sensitivity to changes in F_d and T_f for partially forested HRUs. In terms of model sensitivity to the mean SWE value, S_h and $f_3(F)$ are approximately the same and are three times as important as are T_f and F_d. This table suggests that modeling results, in terms of mean SWE values for partially forested HRUs, will greatly depend upon accurate input data for S_h and $f_3(F)$.

This table also shows that the model is not sensitive to changes in these four input parameters in terms of changes to peak SWE values. In terms of model sensitivity of the peak SWE value, S_h and $f_3(F)$ are again approximately the same and are three times as important as is $F_{d,}$ and are approximately twelve times more important than T_f.

Ultimately, this table indicates that in order to achieve credible modeling results for partially forested HRUs, accurate input data for the parameters S_h and $f_3(F)$ are

important, and if resources are limited, data should be collected first for S_h, then for $f_3(F)$, and finally for the less important parameters F_d and T_f.

Table 8-4 contains a summary of the mean deviation sensitivity values for the four input parameters for a partially forested HRU. An assumption again is made for this table that the inaccuracies associated with these input parameters are +/- 10%. As was the case for the relative sensitivity values found in Table 8-3, all of the deviation sensitivity values associated with errors in the mean SWE values are greater than the deviation sensitivity values associated with errors in the peak SWE values. Again this generalization is due to greater SWE errors being realized late in the ablation period due to the uncertainty of modeling net energy at a point.

Table 8-4. Summary of the mean deviation sensitivity values for the four input parameters for a partially forested HRU.

Parameter	Physically realistic value range	Change in parameter value	$\$_d$ for mean SWE value for entire water year (cm)	$\$_d$ for peak SWE value (cm)
$f_3(F)$	-3.6 to -1.6	+/- 10%	+/- 0.23	+/- 0.13
T_f	0 to -5	+/- 10%	+/- 0.39	+/- 0.22
F_d	0 to 1.0	+/- 10%	+/- 0.21	+/- 0.12
S_h	0 to 1.0	+/- 10%	+/- 0.73	+/- 0.23

Table 8-4 shows that moderate errors occur in estimating the mean SWE value for partially forested HRUs when inaccuracies exist in all four parameters. This is especially true for T_f. This parameter could contain an error of several degrees Celsius, and if this is the case, the resulting error in the mean SWE value would become

significant. This table suggests the importance of accurately collecting data for these input parameters so as to minimize the error in the mean SWE value for partially forested HRUs.

Table 8-4 also shows that significant errors do not occur in estimating the peak SWE value for partially forested HRUs even when the maximum errors exist in the parameters F_d, $f_3(F)$, and S_h. This fact indicates that estimating these input parameters for a partially forested HRU will not significantly affect the peak SWE model prediction. This is not the case, however, for T_f. If this parameter is off by several degrees Celsius, the resulting error in the peak SWE value would become significant.

8.2.4 Sensitivity Analyses for Nonforested HRUs

Table 8-5 contains a summary of the mean relative sensitivity values for the four input parameters for a nonforested HRU. A review of this table shows the same two generalizations that were noted, and discussed, in Table 8-1. The highest values found for the daily relative sensitivity values again coincide with the end of the ablation period, the explanation for which has been discussed in Section 8.2.2.

In terms of the mean SWE value, this table indicates that the only significant value is for the terrain shading factor, S_h, indicating that the model is sensitive to changes in S_h, for nonforested HRUs. As a result, modeling results for nonforested HRUs will greatly depend upon accurate input data for S_h. In terms of model sensitivity of the mean SWE value, S_h is six times as important a parameter as is T_f.

Table 8-5. Summary of the mean relative sensitivity values for the four input parameters for a nonforested HRU.

Rank	Parameter	Range of $\$_r$ for daily SWE values for entire water year	$\$_r$ for mean SWE value for entire water year	$\$_r$ for peak SWE value
1	S_h	0 to -3.06	-1.92	-0.32
2	T_f	0 to -0.78	-0.30	-0.02
3	$f_3(F)$	NA	NA	NA
4	F_d	NA	NA	NA

In terms of the peak SWE value, this table indicates that the modeled SWE output is not sensitive to the changes in any of the four input parameters for nonforested HRUs. In terms of relative importance, S_h is three times as important as is T_f.

This table suggests that modeling results in terms of mean SWE values for nonforested HRUs will greatly depend upon accurate input data for S_h. Also, this table indicates that in order to achieve credible modeling results for nonforested HRUs, accurate input data for the parameter S_h are important, and if resources are limited, data should be collected first for S_h, and then for the less important parameter T_f. Table 8-5 contains no sensitivity values for $f_3(F)$ and F_d because these parameters are only used for HRUs that have some degree of forest cover.

Table 8-6. Summary of the mean deviation sensitivity values for the four input parameters for a nonforested HRU.

Parameter	Physically realistic value range	Change in parameter value	$\$_d$ for mean SWE value for entire water year (cm)	$\$_d$ for peak SWE value (cm)
$f_3(F)$	-3.6 to -1.6	+/- 10%	NA	NA
T_f	0 to -5	+/- 10%	+/- 0.33	+/- 0.15
F_d	0 to 1.0	+/- 10%	NA	NA
S_h	0 to 1.0	+/- 10%	+/- 1.03	+/- 0.67

Table 8-6 contains a summary of the mean deviation sensitivity values for the four input parameters for a nonforested HRU. An assumption again is made for this table that the inaccuracies associated with these input parameters are +/- 10%. As was the case for the relative sensitivity values found in Table 8-5, all of the deviation sensitivity values associated with errors in the mean SWE values are greater than the deviation sensitivity values associated with errors in the peak SWE values. Again this generalization is due to greater SWE errors being realized late in the ablation period due to the uncertainty of modeling net energy at a point.

Table 8-6 shows that significant errors could occur in estimating SWE for nonforested HRUs when errors exist in the parameter S_h. This could also be the case for T_f, if this parameter is off by several degrees Celsius. If small inaccuracies exist in this parameter, the resulting error in SWE output would be insignificant.

8.2.5 Conclusions Regarding the Input parameters

Tables 8-1 through 8-3 indicate that as the HRU becomes more forested, the

model becomes more sensitive to changes in F_d, $f_3(F)$, and T_f, while the model becomes less sensitive to changes in S_h. These tables also shows that for different degrees of forest cover, all four of the optimized parameters are significant in terms of model sensitivity, indicating the need for accurate input data. Consequently, for a watershed that contains HRUs having varying forest cover, rigorous data collection of all four of these input parameters is essential to ensure model accuracy.

Tables 8-4 through 8-6 show that significant errors in SWE prediction can occur if appreciable errors exist in these four input parameters. The calibration process for the three watersheds studied involved calibrating these four input parameters for only a small number of HRUs within each watershed. For the Upper Rio Grande Watershed and the Reynolds Creek Watershed, the number of calibrated HRUs represented a small percentage of the total watershed. This last fact strongly suggests that accurate data collection of these input parameters is essential. To clarify this point, during the calibration process for the Upper Rio Grande Watershed, the final value for $f_3(F)$ was determined to be -1.6, based upon the results from HRUs 40 and 50. This value for $f_3(F)$ indicates that the canopy within these HRUs are jack pine (Dingman, 1994). As discussed in Chapter 4, several different tree species exist within this watershed. Each tree species will have a different $f_3(F)$ value associated with it. Yet, the calibration process assumes a value of -1.6 for $f_3(F)$ for all of the forested HRUs. If an HRU actually has balsam fir, which would have a corresponding $f_3(F)$ value of -3.6 (Dingman, 1994), a significant error in both input parameter and SWE value would occur. To prevent this from happening, accurate data should be collected for these four input

parameters for each HRU within the watershed. This would ensure that each HRU had spatially accurate data, as opposed to calibrating a single value for the entire watershed. These values could then be included in the input file created for each HRU, as described in Chapter 4, as opposed to being a generalized input parameter utilized by the model for all HRUs.

The terrain shading factor, $S_{h,}$ was determined to be a significant parameter for nonforested and partially forested HRUs. Several sources suggest a more realistic approach to estimating this parameter. Dubayah (1994) and Tarboton and Luce (1996) note that a terrain shading factor should vary with location and time, as the sun's incidence angle changes through the season.

8.3 ANALYSIS OF METEOROLOGICAL INPUT VARIABLES

8.3.1 Introduction

Tarboton and Luce (1996) quoted a previous study performed by Charbonneau (1981) in which Charbonneau tested different snowmelt runoff models, and "concluded that the choice of interpolation procedures for input data such as air temperature and precipitation is much more crucial than the level of sophistication of individual snowmelt models." This quote underscores the importance of assessing the impact of meteorological input data upon the accuracy of the developed model. Post-calibration determination of model sensitivity to meteorological data will provide the model user with significant information about the amount and type of required meteorological data, and may help to show the benefit of additional data on model accuracy.

Both relative sensitivity and deviation sensitivity analyses was performed on the meteorological data. Relative sensitivity analysis can provide information to the model user as to which of the meteorological input data are most important. Collecting and processing data can be difficult and expensive, and the results of the relative sensitivity analysis can help the model user determine what type of and how much meteorological data need to be collected. Deviation sensitivity analysis can provide useful information to the model user by estimating the expected error in SWE output based upon the precision of the data collection network.

The basic procedure performed to carry out these analyses is the same as described in Section 8.2, with one exception. The exception involves the fact that for the four optimized input parameters described in Section 8.2, the values of the parameters were changed within the program and the model was rerun. For the meteorological parameters, however, new input files had to be created for the entire water year, and these new input files were utilized by the model to calculate daily SWE. As a result, new meteorological input files were created by altering the input variable by a constant (systematic) one percent for the entire water year. These new, altered input files where then called by the model during the model run. After this task, the procedure for the analyses was the same as for the four optimized parameters. These analyses were performed for all three watersheds for all of the water years. As was the case for the earlier analyses, the results were divided into three categories: HRUs that are completely forested, HRUs that are partially forested, and HRUs that lack a forest cover. This categorization was deemed necessary because the model sensitivity to the

meteorological input variables was expected to vary depending upon canopy cover.

8.3.2 Sensitivity Analyses for Completely Forested HRUs

Table 8-7 contains a summary of the mean relative sensitivity values of modeled SWE to the meteorological input variables for a completely forested HRU. A review of this table shows the same two generalizations that were found for the optimized parameters. The first is that all values found in these tables are negative, except for total precipitation, P_T. This fact indicates that as input data increase in magnitude, the predicted SWE values decrease in magnitude, regardless of HRU canopy cover. Conversely, as total precipitation increases, the predicted SWE values increase in magnitude, regardless of HRU canopy cover. Based upon the equations that these meteorological parameters are contained in, these facts are rational and lends credence to the sensitivity analysis being performed correctly. The second generalization found in these tables is that the relative sensitivity values to all of the input variables are greater in absolute magnitude when analyzing the sensitivity of the mean SWE value for the entire water year than for analyzing the sensitivity of the peak SWE value, again regardless of HRU canopy cover. The reason for this is that, except for P_T, changes in these input parameters significantly affect net energy received at an HRU, and as previously discussed, thus greatly affecting SWE values during the ablation period. This causes greater SWE differences late in the ablation period than at the time of snowpack ripening, corresponding to peak SWE values. This second generalization can

further be substantiated by looking at the range of values for the relative sensitivity of daily SWE values. The largest values for all of the meteorological parameters occur at the end of the melt season. The reason for this was discussed in Section 8.2.2. In the case of P_T, the relative sensitivity values are approximately the same for the mean SWE value and for the peak SWE value, indicating that the model sensitivity to changes in total precipitation is relatively uniform throughout the entire year. Unlike the other meteorological data, P_T has units of mass and is not affected by the cyclical accumulation and ablation seasons. This point can be further illustrated by the fact that the largest daily relative sensitivity value (2.01) is approximately the same as the mean value throughout the entire water year (1.87).

Table 8-7. Summary of the mean relative sensitivity values for the meteorological input variables for a completely forested HRU.

Rank	Parameter	Range of $\$_r$ for daily SWE values for entire water year	$\$_r$ for mean SWE value for entire water year	$\$_r$ for peak SWE value
1	P_T	0 to 2.01	1.87	1.82
2	T_{Max}	0 to -2.21	-1.11	-0.89
3	T_{Min}	0 to -2.03	-1.09	-0.87
4	W_S	0 to -0.41	-0.19	-0.08
5	C_C	0 to -0.16	-0.08	-0.05
6	R_H	NA	NA	NA
7	S_R	NA	NA	NA

Note: relative humidity and incoming solar radiation data were only available for the Reynolds Creek Watershed which contained no completely forested HRUs.

A review of Table 8-7 shows that the relative sensitivity values are significant for P_T, T_{Max}, and $T_{Min,}$ in terms of the both the water year mean SWE and the peak SWE value. These values indicate that the model is very sensitive to changes in these three meteorological parameters for completely forested HRUs. Additionally, P_T is nearly twice as important a parameter as is T_{Max} and T_{Min}. Table 8-7 also shows that the relative sensitivity values for W_S and C_C are insignificant in terms of the mean or peak SWE value for the entire water year. These values indicate that the model is not sensitive to changes in these two meteorological parameters for completely forested HRUs.

Consequently, these facts indicate that in order to achieve credible modeling results for forested HRUs, accurate input data for P_T, $T_{Max,}$ and T_{Min} are important, and if resources are limited, data should be collected first for P_T, and then for T_{Max} and $T_{Min,}$ before data is collected for W_S and C_C. Table 8-7 contains no relative sensitivity values for both R_H and S_R. The reason for this is that data for relative humidity and solar radiation were only available for the Reynolds Creek Watershed. This watershed did not contain any HRUs that were completely forested (see Table 4-5), therefore these sensitivity values could not be determined. For the Upper Rio Grande Watershed, which contained many completely forested HRUs, R_H was estimated by means of Eq. (3-4), and S_R was estimated by means of Eq. (3-5).

Table 8-8 contains a summary of the mean deviation sensitivity values for the meteorological input parameters for a completely forested HRU. This table contain a column with the heading "Change in parameter value". When deviation sensitivity analyses were performed for the input parameters in the previous section, an assumption

was made that the inaccuracies associated with these input parameters were +/- 10% of the nominal variable value. Similarly, assumptions were made regarding the accuracy of the meteorological data, and the values found in the "Change in parameter value"column reflect these assumptions.

Table 8-8. Summary of the mean deviation sensitivity values for the meteorological input variables for a completely forested HRU.

Parameter	Change in parameter value	$\$_d$ for mean SWE value for entire water year (cm)	$\$_d$ for peak SWE value (cm)
P_T	+/- 0.1 (cm)	+/- 2.8	+/-7.3
T_{Max}	+/- 1.0 (^{0}C)	+/- 0.8	+/- 0.8
T_{Min}	+/- 1.0 (^{0}C)	+/- 0.8	+/- 0.7
W_S	+/- 1.0 (m/s)	+/- 0.3	+/- 0.2
C_C	+/- 0.1	+/- 0.2	+/- 0.2
R_H	+/- 0.1	NA	NA
S_R	+/- 1.0 (cal/cm^2 day)	NA	NA

The usefulness of the values found in this tables is to provide the model user information in terms of the expected errors in modeled SWE output based upon the accuracy of the recording instruments, and more importantly, the accuracy of the method for distributing gauge measurements to ungauged HRUs. As an example, if the accuracy of the precipitation gage within one of the studied watersheds is known to be +/- 0.1 cm, then the maximum expected error in SWE could be found in the above tables. By knowing instrument accuracy, the model user can produce a range of SWE output, similar to a confidence interval, that would incorporate the data recording errors.

Table 8-8 contains maximum SWE errors because the meteorological input files were systematically altered so that each daily value was increased or decreased uniformly throughout the water year. In reality, however, if a precipitation gage's accuracy was known to be +/- 0.1 cm, the daily precipitation totals would most likely be over predicted for some of the days, and would be under predicted for some of the days. This would result in smaller errors in modeled SWE output in terms of both mean SWE value throughout the water year, and for peak SWE value than if the daily precipitation totals were over or under predicted uniformly throughout the entire water year. Again, Table 8-8 contains no deviation sensitivity values for both R_H and S_R. The reason for this was explained above.

Table 8-8 indicates that significant errors could occur in SWE output even if the accuracy of the precipitation gauge is within +/- 0.1 cm. Significant errors could also occur in SWE output if the accuracy of the recording thermometers are within several degrees Celsius. This indicates to the model user or field technician the importance of knowing equipment accuracy, and operating and maintaining equipment to ensure the greatest degree of accuracy possible. Table 8-8 also suggest that low accuracy in the recording of wind speed and cloud cover data will cause minimal error in SWE output for completely forested HRUs.

8.3.3 Sensitivity Analyses for Partially Forested HRUs

Table 8-9 contains a summary of the mean relative sensitivity values for the meteorological input parameters for a partially forested HRU. A review of this table

shows the same generalizations that were found, and discussed, in Table 8-7.

Table 8-9. Summary of the mean relative sensitivity values for the meteorological input variables for a partially forested HRU.

Rank	Parameter	Range of $\$_r$ for daily SWE values for entire water year	$\$_r$ for mean SWE value for entire water year	$\$_r$ for peak SWE value
1	P_T	0 to 2.18	2.02	1.91
2	S_R	0 to -2.37	-1.41	–0.51
3	R_H	0 to -2.23	-1.12	-0.45
4	T_{Min}	0 to -1.91	-1.03	-0.32
5	T_{Max}	0 to -1.86	-1.00	-0.29
6	W_S	0 to -1.84	-0.82	-0.29
7	C_C	0 to -0.23	-0.11	-0.08

A review of Table 8-9 shows that the relative sensitivity values are significant for P_T, S_R, R_H, T_{Max}, $T_{Min,}$ and W_S in terms of the mean SWE value for the entire water year. These values indicate that the model is sensitive to changes in these meteorological parameters for partially forested HRUs. In terms of model sensitivity to the mean SWE value, P_T is nearly one and one-half times as important a parameter as is S_R, and is approximately twice as important a parameter as is R_H, $T_{Max,}$ T_{Min}, and W_S. The value for C_C is insignificant in terms of the mean SWE value for the entire water year, and this value indicates that the modeled mean SWE value is not sensitive to changes in C_C for partially forested HRUs.

This table also shows that the relative sensitivity values are significant for P_T, and moderately significant for S_R and R_H in terms of the peak SWE value. These values

indicate that the peak modeled SWE value is sensitive to changes in these meteorological parameters for partially forested HRUs. In terms of model sensitivity to the peak SWE value, P_T is approximately four times as important a parameter as S_R or R_H. Table 8-9 also shows that the relative sensitivity values for $T_{Max,}$ T_{Min}, $W_{S,}$ and C_C are insignificant in terms of the peak SWE value. These values indicate that the peak modeled SWE value is not sensitive to changes in these four meteorological parameters for partially forested HRUs.

Ultimately, this table indicates that in order to achieve credible modeling results for partially forested HRUs, accurate input data for P_T, S_R, R_H, T_{Max}, $T_{Min,}$ and W_S are important. Additionally, if resources are limited, data should be collected first for P_T, and then for S_R, R_H, T_{Max}, $T_{Min,}$ and W_S, in that order.

Table 8-10. Summary of the mean deviation sensitivity values for the meteorological input variables for a partially forested HRU.

Parameter	Change in parameter value	$\$_d$ for mean SWE value for entire water year (cm)	$\$_d$ for peak SWE value (cm)
P_T	+/- 0.1 (cm)	+/- 3.0	+/-7.5
T_{Max}	+/- 1.0 (^{0}C)	+/- 0.5	+/- 0.6
T_{Min}	+/- 1.0 (^{0}C)	+/- 0.6	+/- 0.5
W_S	+/- 1.0 (m/s)	+/- 0.7	+/- 0.6
C_C	+/- 0.1	+/- 0.2	+/- 0.2
R_H	+/- 0.1	+/- 0.8	+/- 0.8
S_R	+/- 1.0 (cal/cm^2 day)	+/- 0.7	+/- 0.6

Table 8-10 contains a summary of the mean deviation sensitivity values for the

meteorological input parameters for a partially forested HRU. The values found in the "Change in parameter value"column reflect the same assumptions regarding the accuracy of the meteorological data as were made for completely forested HRUs found in Table 8-8.

Table 8-10 indicates that significant errors could occur in SWE output even if the accuracy of the precipitation gauge or the interpolation method is within +/- 0.1 cm. Significant errors could also occur in SWE output if the accuracy of the recording devices are only within several units for air temperature, wind speed, relative humidity, and solar radiation. Table 8-10 also suggest that low accuracy in the recording of cloud cover data will cause minimal error in SWE output for partially forested HRUs.

8.3.4 Sensitivity Analyses for Nonforested HRUs

Table 8-11. Summary of the mean relative sensitivity values for the meteorological input variables for a nonforested HRU.

Rank	Parameter	Range of $\$_r$ for daily SWE values for entire water year	$\$_r$ for mean SWE value for entire water year	$\$_r$ for peak SWE value
1	P_T	0 to 2.37	2.21	2.20
2	S_R	0 to -2.62	-1.75	-0.66
3	W_S	0 to -2.12	-1.07	-0.57
4	T_{Max}	0 to -1.84	-0.91	-0.51
5	T_{Min}	0 to -1.80	-0.88	-0.52
6	R_H	0 to -1.44	-0.63	-0.49
7	C_C	0 to -0.25	-0.19	-0.11

Table 8-11 contains a summary of the mean relative sensitivity values for the meteorological input parameters for a nonforested HRU. A review of this table shows the same generalizations that were found, and discussed, in Tables 8-7 and 8-9.

A review of Table 8-11 shows that the relative sensitivity values are significant for P_T, S_R, W_S, T_{Max}, and T_{Min}, and moderately significant for R_H in terms of the mean SWE value for the entire water year. These values indicate that the modeled mean SWE value is sensitive to changes in these meteorological parameters for nonforested HRUs. In terms of model sensitivity to the mean SWE value, P_T is nearly twenty percent more important a parameter than S_R, is approximately twice as important a parameter as is T_{Max}, T_{Min}, and W_S, and is approximately three and one-half times as important a parameter as is R_H. Table 8-9 also shows that the relative sensitivity value for C_C is insignificant in terms of the mean SWE value for the entire water year. This value indicates that the modeled mean SWE is not sensitive to changes in this meteorological parameters for nonforested HRUs.

This table also shows that the relative sensitivity values are significant for P_T, and moderately significant for S_R, W_S, T_{Max}, T_{Min}, and R_H in terms of the peak SWE value. These values indicate that the modeled peak SWE value is sensitive to changes in these meteorological parameters for nonforested HRUs. In terms of model sensitivity to the peak SWE value, P_T is approximately four times as important a parameter as is S_R, W_S, T_{Max}, T_{Min}, and R_H. Table 8-9 also shows that the relative sensitivity value for C_C is insignificant in terms of the peak SWE value. This values indicate that peak SWE is not sensitive to changes in this meteorological parameters for nonforested HRUs.

This table indicates that in order to achieve credible modeling results for nonforested HRUs, accurate input data for P_T, S_R, $W_{S,}$ T_{Max}, $T_{Min,}$ and R_H are important, and if resources are limited, data should be collected first for P_T, and then for S_R, $W_{S,}$ T_{Max}, $T_{Min,}$ and R_H, in that order. C_C data is unimportant and this parameter could be set equal to a constant.

Table 8-12 contains a summary of the mean deviation sensitivity values for the meteorological input parameters for a nonforested HRU. The values found in the "Change in parameter value"column reflect the same assumptions regarding the accuracy of the meteorological data as were made for completely forested and partially forested HRUs found in Table 8-8 and 8-10.

Table 8-12 indicates that significant errors could occur in SWE output even if the accuracy of the precipitation gauge or interpolation method is within +/- 0.1 cm. Significant errors could also occur in SWE output if the accuracy of the recording devices, interpolation, or estimation methods are only within several units for wind speed, and solar radiation. Moderate errors could also occur in SWE output if the accuracy of the recording devices are only within several units for air temperature, and relative humidity. Table 8-12 also suggest that low accuracy in the recording of cloud cover data will cause minimal error in SWE output for nonforested HRUs.

Table 8-12. Summary of the mean deviation sensitivity values for the meteorological input variables for a nonforested HRU.

Parameter	Change in parameter value	$\$_d$ for mean SWE value for entire water year (cm)	$\$_d$ for peak SWE value (cm)
P_T	+/- 0.1 (cm)	+/- 3.3	+/-7.7
T_{Max}	+/- 1.0 (^{0}C)	+/- 0.4	+/- 0.4
T_{Min}	+/- 1.0 (^{0}C)	+/- 0.3	+/- 0.5
W_S	+/- 1.0 (m/s)	+/- 1.2	+/- 1.1
C_C	+/- 0.1	+/- 0.2	+/- 0.2
R_H	+/- 0.1	+/- 0.4	+/- 0.3
S_R	+/- 1.0 (cal/cm^2 day)	+/- 1.4	+/- 1.3

8.3.5 Conclusions Regarding the Meteorological Parameters

An overview of Tables 8-7, 8-9, and 8-11 indicate that total precipitation is the most important meteorological parameter, regardless of canopy cover. This result is logical and not surprising. Additionally, the relative sensitivity value of P_T increases as the canopy cover diminishes. This is also logical. As the canopy diminishes over an HRU, less precipitation is intercepted and ultimately lost, thus yielding a relative sensitivity value for SWE that is larger in magnitude. These tables also show that the model becomes more sensitive to solar radiation as the canopy cover decreases. Canopy cover reduces incoming solar radiation, and as canopy cover decreases, incoming solar radiation increases, thus the model becomes more sensitive to S_R as the canopy cover declines.

Tables 8-9 and 8-11 indicate that as canopy cover is reduced, the model becomes less sensitive to relative humidity. Modeled results indicate that for completely forested HRUs, longwave radiation is the dominant term in the energy equation. Incoming solar radiation is greatly reduced by the canopy. Additionally, sensible and latent heat exchanges are significantly reduced because of their dependence upon the wind speed, which is significantly reduced by canopy cover. Therefore, longwave radiation becomes the dominant energy term under canopy cover. R_H is an important component of calculating longwave radiation (see Eqs. (3-15) through (3-17)). As canopy cover is reduced, longwave radiation ceases to be the dominant term in the energy equation, and thus reduces the importance of R_H. This explains why the model becomes less sensitive to relative humidity as the canopy cover diminishes.

Tables 8-7, 8-9, and 8-11 indicate that the model becomes slightly less sensitive to changes in air temperature as the canopy cover decreases. Two factors affect this outcome. The first factor is as described above for R_H. T_{Max} and T_{Min} are used to calculate longwave radiation (see Eq. (3-3) and Eqs. (3- 15) through (3-17)). As the canopy cover decreases, longwave radiation becomes less dominant, and thus the model becomes less sensitive to changes in T_{Max} and T_{Min}. However, as the canopy cover decreases, wind speed increases, which ultimately increases the sensible heat exchange between the snowpack and the surrounding atmosphere. Air temperature is a component of sensible heat (see Eqs. (3-3) and (3-21)). As the canopy cover decreases, sensible heat exchange becomes more important, indicating that the model would become more sensitive to changes in T_{Max} and T_{Min}. The net result of these two

phenomena is that the change in longwave radiation is greater in magnitude than the change in sensible heat exchange, which explains why overall, the model becomes slightly less sensitive to T_{Max} and T_{Min} as the canopy cover diminishes.

Tables 8-7, 8-9, and 8-11 indicate that the model becomes more sensitive to changes in wind speed as the canopy cover is reduced. As previously discussed, canopy significantly reduces wind speed, and thus wind speed increases as canopy cover is diminished. Wind speed is also a component of both sensible and latent heat exchange (see Eqs. (3-21) and (3-24)). As canopy cover decreases, sensible and latent heat exchange become more important, indicating that the model becomes more sensitive to W_S.

Tables 8-7, 8-9, and 8-11 indicate that the model is not sensitive to changes in cloud cover regardless of the canopy cover. Cloud cover affects both solar and longwave radiation. When the HRU is heavily forested, both solar and longwave radiation are dependent upon the canopy cover, indicating that the model will not be sensitive to changes in C_C. When the HRU has little or no forest cover, both solar and longwave radiation become dependent upon cloud cover. For these HRUs, however, a change in cloud cover causes approximately the same change in magnitude of both solar and longwave radiation, but the changes are of opposite sign, thus resulting in a net change in radiation of nearly zero. So, even for HRUs with little to no forest cover, the model is not sensitive to changes in C_C. The lumped treatment of clouds in the model is simplistic. It makes sense that enhanced longwave radiation would partially balance lost shortwave radiation. A more realistic treatment, accounting for cloud height, type,

thickness, and air temperature, would probably yield different results..

Several inferences can be made regarding data collection based upon this analysis. This first of which is that despite the fact that the cloud cover data for the watersheds studied was gathered at significant distances from the watersheds, the model accuracy did not suffer. This indicates one of two possibilities. First, spending a great deal of time or money collecting this data to run the model is unnecessary. This turns out to be fortuitous since only sparse cloud cover data exist. Cloud cover could actually be set as a constant in the program. The other possibility is that the model not being sensitive to changes in C_C may point out a weakness in the algorithms used by the model to calculate incoming solar and longwave radiation.

Secondly, for heavily forested HRUs and/or watersheds, accurate air temperature and relative humidity data are essential; whereas accurate solar radiation and wind speed data are less important. Thirdly, for HRUs or watersheds with little or no canopy cover, accurate solar radiation, air temperature, wind speed, and relative humidity data are essential. The final inference is that regardless of canopy cover, total precipitation data are the most essential to ensure model accuracy. In an ideal situation, an analysis similar to one presented by Dingman (1994) could be performed to determine the optimal number of precipitation gages required for sufficient collection of precipitation data. This finding also underscores the need for research to improve both interpolation methods and techniques for distributed precipitation measurements using remote sensing.

8.4 ANALYSIS OF AVAILABLE SWE DATA FOR CALIBRATION

8.4.1 Introduction

As previously discussed in Chapters 5 through 7, daily measured SWE data were available for the Upper Rio Grande Watershed, whereas only bimonthly measured SWE data were available for the Reynolds Creek Watershed. Measured SWE data were even more sparse for the Emerald Lake Watershed, with only a few measured SWE data available for the entire season. These SWE data were used to calibrate/validate the model. How does the availability of this data affect the calibration process? To what extent does additional SWE data for a water year improve the calibration process? Is daily measured SWE data required to properly calibrate the model? These questions will be analyzed using SWE data collected for the Upper Rio Grande Watershed along with modeled SWE output. Calibrated results for HRUs 1, 40, and 50, corresponding to the Beartown, Middle Creek, and Wolf Creek Summit SNOTEL site, respectively, for the water year 1993 shall be used as a baseline to compare results obtained using less frequent SWE data. The results utilizing daily SNOTEL SWE data were originally presented in Chapter 5 (see Table 5-5).

8.4.2 Simulating the Availability of Bi-monthly SWE Data

The measured SWE data for the Reynolds Creek Watershed were collected at approximately a two-week interval, with the first measurement occurring in early December. For this particular analysis, it was assumed that the SNOTEL SWE data at the three sites (Beartown, Middle Creek, and Wolf Creek Summit) within the Upper Rio

Grande Watershed were also only available at a two-week interval. As part of this analysis, fourteen trials were examined with the first trial consisting of SNOTEL SWE data available on December 1, December 15, December 29, etc. . . The second trial consisted of SNOTEL SWE data available on December 2, December 16, December 30, etc. . . The last of the trials consisted of SNOTEL SWE data available on December 14, December 28, January 11, etc. . . The analysis was stopped after fourteen trials because the fifteenth trial would have begun on December 15, and would have mirrored the first trial, except for the first and last SNOTEL SWE points. For each of the fourteen trials, the model was run, and then calibrated using the bi-monthly SNOTEL SWE data along with the same methodology described in Chapter 5.

Table 8-13. Summary of the basin-wide post-calibration values for the calibrated input parameters for the Upper Rio Grande Watershed using bimonthly SWE data.

Parameter	Daily SWE data available	Simulating bimonthly SWE - average value	Simulating bimonthly SWE - range of values
S_h	0.83	0.86	0.82 : 0.89
F_d	0.80	0.77	0.74 : 0.82
$f_3(F)$	-1.6	-1.4	-1.6 : -1.3
T_f	-1.2	-1.4	-1.7 : -1.2

Table 8-13 contains a comparison of the final values determined by the calibration process for the previously identified input parameters. The values found in column two represent the calibrated values utilizing daily SWE values (see Table 5-4). The values found in column three represent the average calibrated values of the input parameters for all of the fourteen trials. The values in column four represent the range

of calibrated values of the input parameters determined from the fourteen trials. A review of this table indicates that the calibrated values determined by utilizing bi-monthly SNOTEL SWE data do not significantly differ from the calibrated values found using daily SNOTEL SWE data. In fact, the range of calibrated values found using bimonthly data encompass the calibrated value found using daily SWE data.

Tables 8-14 through 8-16 contain the results of the calibration analysis. These tables show the previously displayed results for the three HRUs of the Upper Rio Grande Watershed (see Table 5-5) for the water year 1993. These original results utilized daily available SNOTEL SWE data, and all goodness-of-fit and physically based statistics were calculated using daily SWE data. Also shown in this table, contained in column three, are the mean values determined for the fourteen trials which simulate having only bimonthly SNOTEL SWE data available. The final column in these tables show the range of results for each statistic to help indicate the maximum and minimum differences that occurred in the statistics due to the limitation of the bimonthly SNOTEL SWE data. All goodness-of-fit and physically based statistics found in columns three and four were calculated utilizing SWE data available only on a bi-monthly basis.

Table 8-14. Comparison of the goodness-of-fit statistics for the water year 1993, for HRU 1 of the Upper Rio Grande Watershed using bimonthly SWE data.

Parameter	Daily SWE data available	Simulating bimonthly SWE - average value	Simulating bimonthly SWE - range of values
$\overline{e}$ (cm)	-5.0	-5.9	-7.1 : -5.1
$\overline{e} / \overline{Y}$	-0.27	-0.36	-0.43 : -0.27
S_e (cm)	13.2	14.3	13.4 : 14.6
S_e / S_y	0.79	0.84	0.82 : 0.91
Peak SWE modeled (cm)	46.7	47.8	46.7 : 49.2
Peak SWE measured (cm)	52.3	50.6	49.3 : 52.3
Δ Peak SWE (cm)	-5.6	-2.8	-5.6 : -0.1
Δ Peak SWE / Peak SWE measured	-10.7%	-5.9%	-10.7% : -0.2%
Modeled date of snowpack ripening	April 10	April 13	April 8 : April 17
Estimated date of snowpack ripening from SNOTEL SWE measurements	May 4	April 22	April 10 : May 7
Δ Date of snowpack ripening (days)	-24	-10	-31 : 7
Modeled length of snowpack ablation period (days)	33	36	31 : 40
Measured length of snowpack ablation period (days)	29	24	17: 33
Δ length of snowpack ablation (days)	4	9	-2 : 24

Table 8-15. Comparison of the goodness-of-fit statistics for the water year 1993, for HRU 40 of the Upper Rio Grande Watershed using bimonthly SWE data.

Parameter	Daily SWE data available	Simulating bimonthly SWE - average value	Simulating bimonthly SWE - range of values
$\overline{e}$ (cm)	2.9	2.2	0.9 : 3.1
$\overline{e} / \overline{Y}$	0.19	0.17	0.12 : 0.24
S_e (cm)	7.1	7.2	3.5 : 8.2
S_e / S_y	0.60	0.62	0.44 : 0.74
Peak SWE modeled (cm)	41.2	42.4	40.9 : 44.3
Peak SWE measured (cm)	42.9	41.2	39.4: 42.9
Δ Peak SWE (cm)	-1.7	1.2	-2.0 : 4.9
Δ Peak SWE / Peak SWE measured	-4.0%	2.9%	-4.6% : 12.4%
Modeled date of snowpack ripening	April 29	April 26	April 23 : May 1
Estimated date of snowpack ripening from SNOTEL SWE measurements	May 5	May 10	May 4: May 14
Δ Date of snowpack ripening (days)	-6	-14	-21 : -4
Modeled length of snowpack ablation period (days)	56	58	55 : 60
Measured length of snowpack ablation period (days)	30	28	26 : 35
Δ length of snowpack ablation (days)	26	30	20 : 34

Table 8-16. Comparison of the goodness-of-fit statistics for the water year 1993, for HRU 50 of the Upper Rio Grande Watershed using bimonthly SWE data.

Parameter	Daily SWE data available	Simulating bimonthly SWE - average value	Simulating bimonthly SWE - range of values
$\overline{e}$ (cm)	0.5	-1.2	-1.9 : 0.4
$\overline{e} / \overline{Y}$	0.01	-0.10	-0.14 : 0.05
S_e (cm)	9.9	9.6	6.8 : 11.2
S_e / S_y	0.40	0.44	0.26 : 0.63
Peak SWE modeled (cm)	81.3	80.5	80.0 : 82.2
Peak SWE measured (cm)	89.2	87.8	86.6 : 89.2
Δ Peak SWE (cm)	-7.9	-7.3	-9.2 : -4.4
Δ Peak SWE / Peak SWE measured	-8.9%	-8.3%	-10.3% :-5.1%
Modeled date of snowpack ripening	May 11	May 14	May 9 : May 21
Estimated date of snowpack ripening from SNOTEL SWE measurements	May 4	May 9	May 4: May 14
Δ Date of snowpack ripening (days)	8	6	-6 : 18
Modeled length of snowpack ablation period (days)	70	67	62 : 73
Measured length of snowpack ablation period (days)	53	56	51 : 63
Δ length of snowpack ablation (days)	17	12	-1 : 23

The results found in Tables 8-14 through 8-16 indicate that the availability of only bimonthly data significantly affects the goodness-of-fit and physically significant

statistics that were calculated for these HRUs during the calibration process. This impact could lead to erroneous conclusions regarding model accuracy. It could also lead to erroneous predictions using the model output.

The values found in the three tables for the sample mean error, the mean relative error, and the standard error of the estimate show a relatively small range for all of the trials using only bimonthly SNOTEL SWE data. All of these bimonthly values are relatively close in value to the originally calculated values for the three HRUs, found in column two. The same conclusions initially drawn from these statistics concerning model accuracy would not differ using the bimonthly data. However, a significant difference exists for the S_e / S_y statistic. Whereas a relatively small range in these values exist in Table 8-14, the range is larger in the other two tables, especially Table 8-16. The range for S_e / S_y values in this table is 0.26 to 0.63. A value of 0.26 indicates that the model has greatly improved the reliability of prediction, and would be interpreted as a high level of model accuracy. A value of 0.63, however, indicates that the model has not significantly improved the reliability of prediction, and would be interpreted as a lack of model accuracy.

For the physically significant statistics, the values found in these tables also have mixed results. In determining the difference in measured and modeled peak SWE, only having bimonthly SWE data does not appear to create a significant difference. All of these values are close in magnitude to the values calculated during the calibration process using daily SNOTEL SWE data. However, a much larger range exists when estimating the difference in the date of snowpack ripening when using only the

bimonthly data. Table 8-14 contains the largest range with the estimated length varying from -31 days to +7 days. This large range could lead to significant consequences. If the model is calibrated using only bimonthly data, the model user may believe that the model output matches the measured data well in terms of estimating the date of snowpack ripening, when in fact, it could be off by several weeks. This would cause a delay in predicted snowmelt runoff, which could lead to problems with downstream crop planting. Additionally, a large range exists when estimating the difference in length of the ablation period. The largest range again exists in Table 8-14 where the difference in the length of the ablation period is -2 to +24 days. This significant uncertainty could again lead to errors in calibration and again could have significant downstream consequences. The model user may anticipate that the length of the ablation period can be closely estimated based upon an erroneous calibration process. This could lead to problems identifying possible extreme stream runoff events based upon the length of the ablation period.

The results of these three tables show that bimonthly SWE data is insufficient to adequately calibrate the model. Using only bimonthly data, the modeler may believe that the model is significantly more accurate, or significantly less accurate than what it actually is, and could be properly determined if daily SWE data exist. This could cause serious consequences if the model is then used to make predictions. This also indicates that the results presented in Chapter 6, regarding the calibration/validation of the Reynolds Creek Watershed based upon bimonthly measured SWE data, are less reliable than the results presented in Chapter 5 for the Upper Rio Grande Watershed.

8.4.3 Simulating the Availability of Weekly SWE Data

Collecting SWE data requires significant time and resources and can also be dangerous. It has been demonstrated that bimonthly SWE data is insufficient to properly calibrate the model. However, if it can be shown that data collected less frequently than daily is adequate for model calibration/validation, time, resources, and perhaps lives, can be saved. For this next analysis, it was assumed that SNOTEL SWE data at the three sites were available at a one-week interval. Seven trials were examined with the first trial consisting of SWE data available on December 1, December 8, December 15, etc. . . The second trial consisted of SWE data available on December 2, December 9, December 16, etc. . . The last of the trials consisted of SNOTEL SWE data available on December 7, December 14, December 21, etc. . . The analysis was stopped after seven trials because the eighth trial would have begun on December 8, which would have mirrored the first trial, except for the first and last SNOTEL SWE points. For each of the seven trials, the model was run, and then subjectively calibrated using weekly SNOTEL SWE data along with the methodology described in Chapter 5.

Table 8-17. Summary of the basin-wide post-calibration values for the calibrated input parameters for the Upper Rio Grande Watershed using weekly SWE data.

Parameter	Daily SWE data available	Simulating weekly SWE - average value	Simulating weekly SWE - range of values
S_h	0.83	0.85	0.83 : 0.87
F_d	0.80	0.79	0.76 : 0.81
$f_3(F)$	-1.6	-1.5	-1.6 : -1.4
T_f	-1.2	-1.3	-1.5 : -1.2

Table 8-17 contains a comparison of the final values determined by the calibration process for the previously identified input parameters. The values found in columns two, three, and four are similar to the values found in the corresponding columns in Table 8-13. A review of this table indicates that the calibrated values determined by utilizing weekly SNOTEL SWE data do not significantly differ from the calibrated values found using daily SNOTEL SWE data. In fact, the range of calibrated values found using weekly data encompass the calibrated value found using daily SWE data. Additionally, the values contained in columns three and four are closer to the values determined for these input parameters utilizing daily SNOTEL SWE data.

Tables 8-18 through 8-20 contain the results for the calibration analysis. These tables show the previously displayed results for the three HRUs of the Upper Rio Grande Watershed (see Table 5-5) for the water year 1993 in column two. Also shown in this table, contained in column three, are the mean values determined for the seven trials which simulates having only weekly SNOTEL SWE data available. The final column in these tables show the range of results for each statistic to help indicate the maximum and minimum differences that occurred in the statistics due to the limitation of the weekly SNOTEL SWE data.

Table 8-18. Comparison of the goodness-of-fit statistics for the water year 1993, for HRU 1 of the Upper Rio Grande Watershed using weekly SWE data.

Parameter	Daily SWE data available	Simulating weekly SWE - average value	Simulating weekly SWE - range of values
$\overline{e}$ (cm)	-5.0	-5.5	-5.9 : -5.1
$\overline{e} / \overline{Y}$	-0.27	-0.31	-0.37 : -0.27
S_e (cm)	13.2	13.7	13.4 : 14.1
S_e / S_y	0.79	0.82	0.79 : 0.87
Peak SWE modeled (cm)	46.7	47.2	46.3 : 48.3
Peak SWE measured (cm)	52.3	51.7	50.8 : 52.3
Δ Peak SWE (cm)	-5.6	-4.5	-6.0 : -2.4
Δ Peak SWE / Peak SWE measured	-10.7%	-8.7%	-11.4% : –4.7%
Modeled date of snowpack ripening	April 10	April 12	April 9 : April 15
Estimated date of snowpack ripening from SNOTEL SWE measurements	May 4	May 2	April 30: May 6
Δ Date of snowpack ripening (days)	-24	-28	-27 : -16
Modeled length of snowpack ablation period (days)	33	32	30 : 35
Measured length of snowpack ablation period (days)	29	25	23 : 30
Δ length of snowpack ablation (days)	4	7	0 : 12

Table 8-19. Comparison of the goodness-of-fit statistics for the water year 1993, for HRU 40 of the Upper Rio Grande Watershed using weekly SWE data.

Parameter	Daily SWE data available	Simulating weekly SWE - average value	Simulating weekly SWE - range of values
$\overline{e}$ (cm)	2.9	2.5	1.7 : 2.9
$\overline{e} / \overline{Y}$	0.19	0.18	0.16 : 0.21
S_e (cm)	7.1	7.2	6.2 : 7.6
S_e / S_y	0.60	0.63	0.58 : 0.71
Peak SWE modeled (cm)	41.2	41.7	41.0 : 42.2
Peak SWE measured (cm)	42.9	41.8	40.6: 42.9
Δ Peak SWE (cm)	-1.7	-0.1	-1.9 : 1.6
Δ Peak SWE / Peak SWE measured	-4.0%	-0.2%	-4.4% : 3.9%
Modeled date of snowpack ripening	April 29	April 26	April 24 : April 30
Estimated date of snowpack ripening from SNOTEL SWE measurements	May 5	May 8	May 6 : May 11
Δ Date of snowpack ripening (days)	-6	-12	-17 : -6
Modeled length of snowpack ablation period (days)	56	58	56 : 60
Measured length of snowpack ablation period (days)	30	28	26 : 31
Δ length of snowpack ablation (days)	26	30	25 : 34

Table 8-20. Comparison of the goodness-of-fit statistics for the water year 1993, for HRU 50 of the Upper Rio Grande Watershed using weekly SWE data.

Parameter	Daily SWE data available	Simulating weekly SWE - average value	Simulating weekly SWE - range of values
$\overline{e}$ (cm)	0.5	0.7	-0.3 : 1.3
$\overline{e} / \overline{Y}$	0.01	0.05	-0.02 : 0.09
S_e (cm)	9.9	9.7	7.9 : 10.5
S_e / S_y	0.40	0.42	0.36 : 0.50
Peak SWE modeled (cm)	81.3	82.1	80.3 : 84.5
Peak SWE measured (cm)	89.2	88.5	87.9 : 89.2
Δ Peak SWE (cm)	-7.9	-6.4	-8.9 : -3.4
Δ Peak SWE / Peak SWE measured	-8.9%	-7.2%	-9.9% : -3.9%
Modeled date of snowpack ripening	May 11	May 9	May 7 : May 13
Estimated date of snowpack ripening from SNOTEL SWE measurements	May 4	May 6	May 4: May 10
Δ Date of snowpack ripening (days)	7	3	-3 : 9
Modeled length of snowpack ablation period (days)	70	72	68 : 75
Measured length of snowpack ablation period (days)	53	55	52 : 59
Δ length of snowpack ablation (days)	17	17	11 : 23

The results found in Tables 8-18 through 8-20 using weekly SWE data matches the goodness-of-fit and physically significant statistics that were calculated for these HRUs better than when only bimonthly SWE data was available. This improvement

could help mitigate any erroneous conclusions that may be made regarding model accuracy. It could also help to buffer any erroneous predictions made using the model output.

The goodness-of-fit statistics found in these three tables show an average value closer to the value obtained using daily SNOTEL SWE data, than when compared to the results for the bimonthly SWE data. More importantly, the range of values for these statistics are much smaller than for the bimonthly SNOTEL SWE data. This can best be seen by examining the range of S_e / S_y values found in Table 8-20. These values range from 0.35 to 0.52. The difference in this range is not significant enough to draw varying conclusions concerning model accuracy. This was not the case, however, when looking at these same values corresponding to bimonthly SWE data. The range for S_e / S_y values found in Table 8-16 was 0.26 to 0.63. As previously discussed, a value of 0.26 would be interpreted as a high level of model accuracy, whereas a value of 0.63 would be interpreted as a lack of model accuracy. This is a significant difference between the two analyses utilizing different SWE data sets.

For the physically significant statistics, the values found in Tables 8-18 through 8-20 also are closer in value to the calibration result for daily SNOTEL SWE data than are the bimonthly results. Again, more importantly, the range of values for these statistics are much smaller than for the bimonthly SNOTEL SWE data. As an example, the range of the difference in the dates for estimating snowpack ripening found in Table 8-18 is -3 to +9 days. This range coincides well with 7 days established using daily SNOTEL SWE data. However, the corresponding values in Table 8-14 estimated the

range of the difference in the dates of snowpack ripening from -6 to +18 days. As mentioned earlier, using this range for snowpack ripening, established from the bimonthly SWE data, could lead to significant consequences. This however, would not be the case for the range in snowpack ripening determined from weekly SWE data. Additionally, the range for estimating the length of the ablation period found in Table 8-18 is much smaller and closer to the value calibrated with daily SWE data than is the corresponding range found in Table 8-14. This smaller range would decrease the likelihood of problems arising from using the model output for predicting purposes, such as identifying possible extreme stream runoff events based upon the length of the ablation period.

The results of Tables 8-18 through 8-20 show that weekly SWE data appear to be sufficient to adequately calibrate the model. The results of these three tables indicate that the goodness-of-fit and physically based statistics are close in value, when comparing modeled results, for daily SWE data and weekly SWE data. Using weekly SWE data should not lead the modeler to erroneous conclusions regarding model accuracy. If SWE data is field measured and collected for a watershed, knowing this fact could lead to significant savings in time and resources, and may limit the risk faced by the data collectors.

8.5 ANALYSIS OF THE HRU SUBDIVISION PROCESS

8.5.1 Introduction

As discussed in Chapter 4, the first step of the process of subdividing the

watershed into HRUs was to utilize the "Blockstats" command in ArcView to automatically combine single pixels into larger groupings. For the Upper Rio Grande and Reynolds Creek watersheds, single pixels were combined into groupings of 1050 pixels, whereas for the much smaller Emerald Lake Watershed, pixels were combined into groupings of sixteen pixels. After this was accomplished, ArcView was then used to determine the required physical parameters for each grouping. From this point, groupings were then subjectively combined again, based upon their physical characteristics, to form HRUs. The question that arises from this procedure is: how different would the spatial and temporal distributions of SWE be if the pixels were combined differently to form different subdivisions of HRUs with different physical characteristics?

This point will be examined for the Emerald Lake Watershed. This watershed was selected from the three studied because of its small size. The watershed's small size will result in fewer HRUs created during the alternative subdivision processes, which will also result in fewer required HRU and meteorological input files.

For this analysis, three different variations of HRU subdivisions were examined. These three variations were created by defining different pixel groupings using the "Blockstats" command. This command originally combined sixteen pixels into groupings. For these variations, the number of pixels combined using this command were: four, nine, and twenty. Once these groupings were created, the same procedure as originally used for further combining pixel groupings into HRUs was utilized.

8.5.2 Analysis of Alternative Pixel Groupings

Table 8-21. Summary of the physical parameters of the HRUs created for the Emerald Lake Watershed for the alternative pixel grouping of four.

HRU ID	Elevation (m)	Slope (degrees)	% Forest Cover*	Aspect (degrees)	Latitude (degrees)	Area (hectares)
1	2820	12	0	180	36.6	11
2	2845	22	0	270	36.6	9
3	3073	42	90 - Con	45	36.6	10
4	3096	34	0	15	36.6	9
5	3003	18	0	270	36.6	11
6	2947	37	0	45	36.6	15
7	3149	29	0	270	36.6	15
8	3062	24	0	0	36.6	13
9	3266	34	0	15	36.6	18

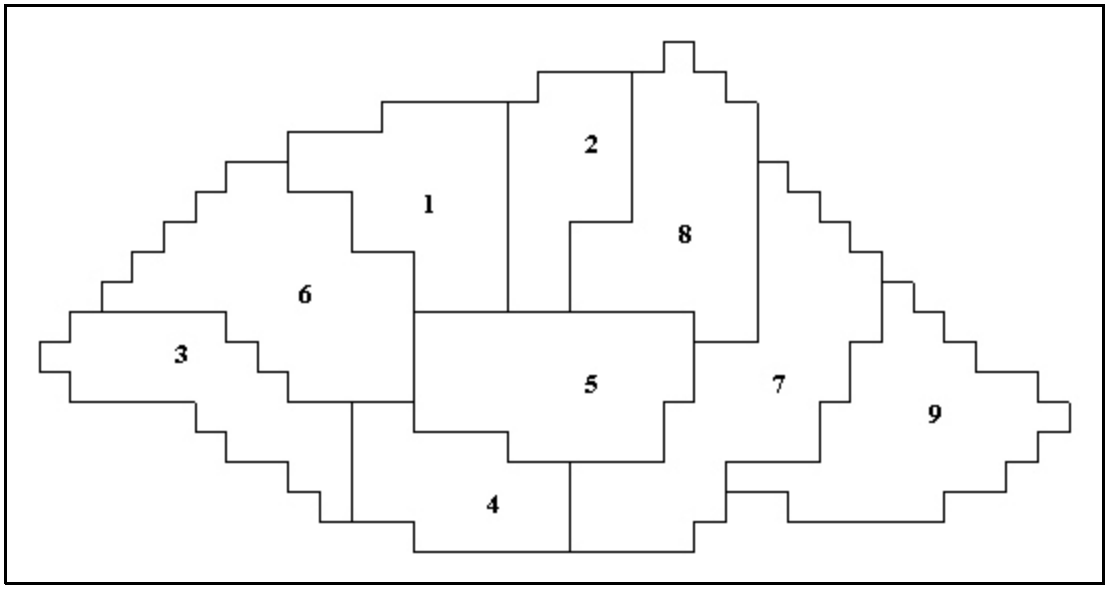

Figure 8-1. Delineation of HRUs for the Emerald Lake Watershed for the alternative pixel grouping of four.

Table 8-22. Summary of the physical parameters of the HRUs created for the Emerald Lake Watershed for the alternative pixel grouping of nine.

HRU ID	Elevation (m)	Slope (degrees)	% Forest Cover*	Aspect (degrees)	Latitude (degrees)	Area (hectares)
1	2820	11	0	200	36.6	12
2	3065	28	0	225	36.6	13
3	3091	36	85 - Con	45	36.6	9
4	3103	31	0	0	36.6	13
5	3030	20	0	300	36.6	12
6	3023	27	0	45	36.6	11
7	3129	26	0	270	36.6	12
8	2855	18	0	270	36.6	10
9	3268	33	0	300	36.6	19

* Con - coniferous forest

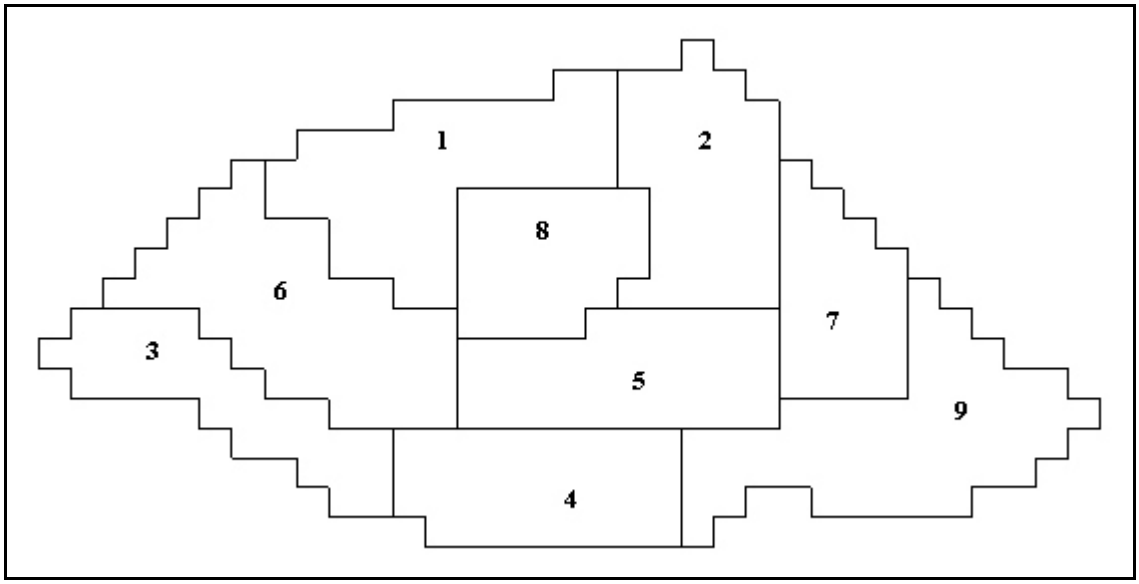

Figure 8-2. Delineation of HRUs for the Emerald Lake Watershed for the alternative pixel grouping of nine.

Table 8-23. Summary of the physical parameters of the HRUs created for the Emerald Lake Watershed for the alternative pixel grouping of twenty.

HRU ID	Elevation (m)	Slope (degrees)	% Forest Cover*	Aspect (degrees)	Latitude (degrees)	Area (hectares)
1	2830	21	0	180	36.6	12
2	3025	23	0	225	36.6	11
3	3091	21	0	270	36.6	8
4	3071	30	70 - Con	45	36.6	10
5	2955	33	0	270	36.6	11
6	2969	35	0	45	36.6	14
7	3051	32	0	0	36.6	15
8	2880	15	0	0	36.6	10
9	3227	36	0	300	36.6	20

* Con - coniferous forest

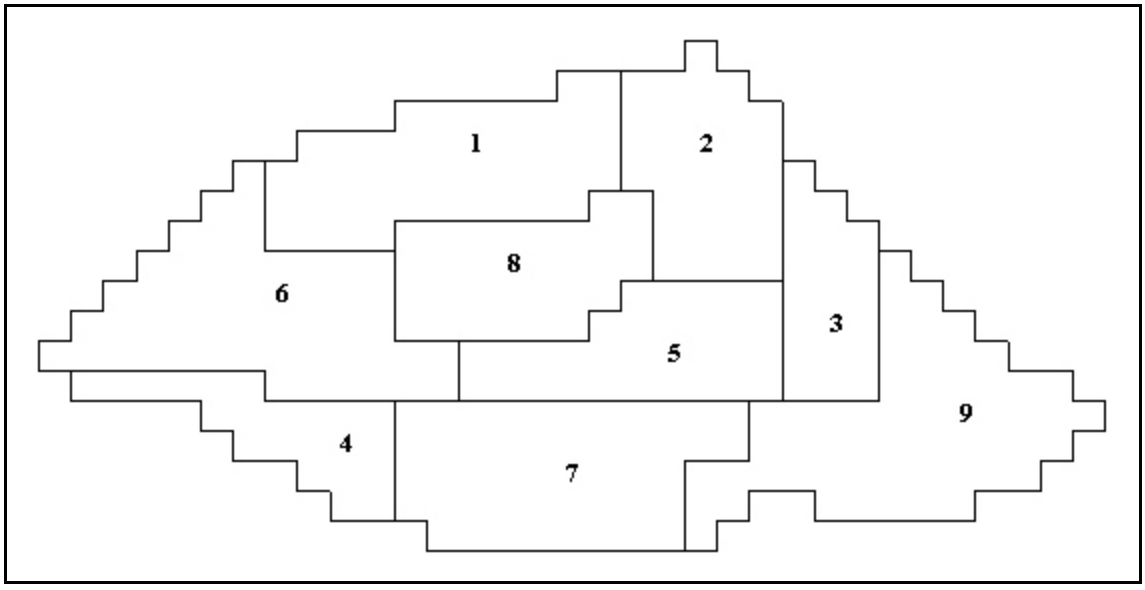

Figure 8-3. Delineation of HRUs for the Emerald Lake Watershed for the alternative pixel grouping of twenty.

Tables 8-21 through 8-23 and Figures 8-1 through 8-3 show the three alternative HRU configurations, along with the physical characteristics of the created HRUs for the three different pixel configurations. These figures and corresponding tables can be compared to the original HRU configuration (see Figure 4-12), and the HRU physical characteristics (see Table 4-8) for the Emerald Lake Watershed. The number of HRUs for the four configurations are similar, as is the range of values of the physical characteristics of the HRUs for the four configurations. Analyses of model runs will determine how different the spatial and temporal distribution of SWE is for the various configurations.

Once the HRUs had been created for the alternate pixel groupings, all corresponding HRU and meteorological input files were created in the same manner as for the initial configuration for the Emerald Lake Watershed. The model was then run for these three alternatives, and calibrated based upon the methodology described in Chapter 5. Table 8-24 contains a summary of the post-calibration values for the input parameters for the initial model run and for the three alternatives. Results of the alternatives were plotted along with the original SWE output and the measured SWE values for each of the five SWE measurement locations (see Figure 4-14), and can be found in Figures 8-4 through 8-8.

Tables were also created from these plots to compare peak SWE values, mean SWE values, date of snowpack ripening, and length of ablation period between the original model run, and the alternate HRU subdivisions. The information in these tables

will give an indication of how sensitive the model is to the HRU subdivision process.

Table 8-24. Summary of post-calibration values for the input parameters for the initial model run and for the three alternatives.

Parameter	Initial Value	4 Pixel Grouping Value	9 Pixel Grouping Value	20 Pixel Grouping Value
S_h	0.78	0.76	0.79	0.78
F_d	0.80	0.78	0.82	0.81
f3(F)	-2.0	-1.9	-2.2	-2.0
T_f	-1.2	-1.2	-1.1	-1.1

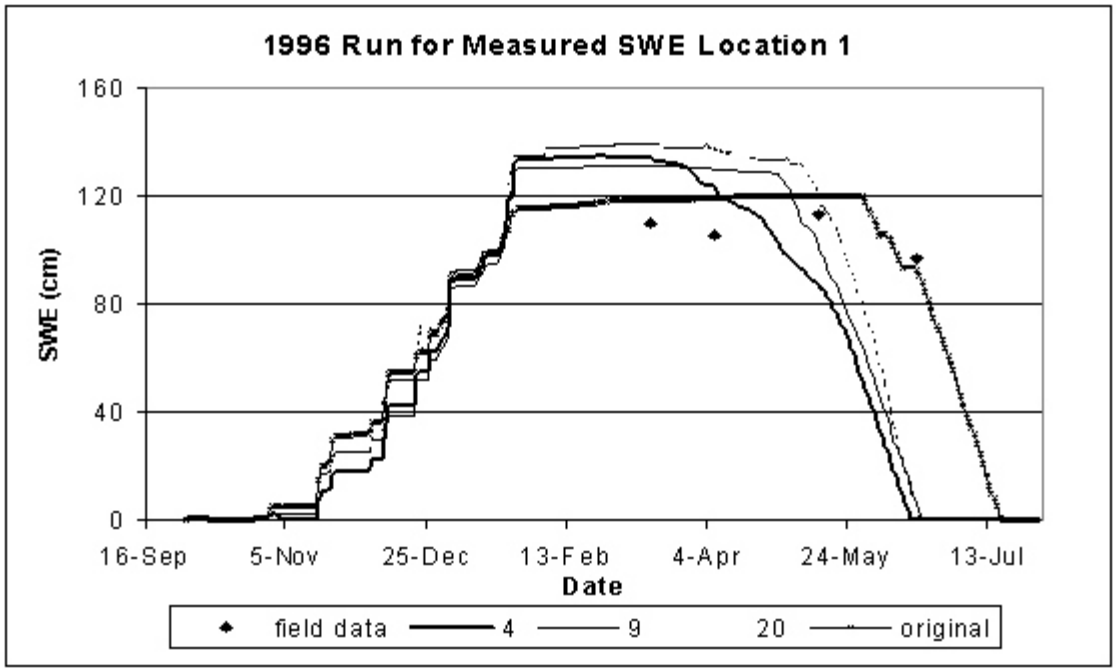

Figure 8-4. Comparison of Results for the different HRU subdivisions for the Emerald Lake Watershed for the SWE measurement at location 1.

Table 8-25. Summary of the SWE results for the four HRU configurations for the SWE measurement at location 1.

Parameter	Original Grouping	4 Pixel Grouping	9 Pixel Grouping	20 Pixel Grouping
Mean SWE (cm)	74.3	63.2	64.4	70.1
D Mean SWE (cm)	-	11.1	9.9	4.2
% Difference Mean SWE	-	14.9 %	13.3 %	5.6 %
Peak SWE (cm)	120.2	133.3	130.2	137.2
D Peak SWE (cm)	-	-13.1	-10.0	-17.0
% Difference Peak SWE	-	-10.9 %	-8.3 %	-14.1 %
Date of Snowpack Ripening	May 30	March 21	May 3	May 13
D Date of Ripening	-	70	27	17
Length of Ablation Period (days)	51	87	49	41
D Length of Ablation Period (days)	-	-36	2	10

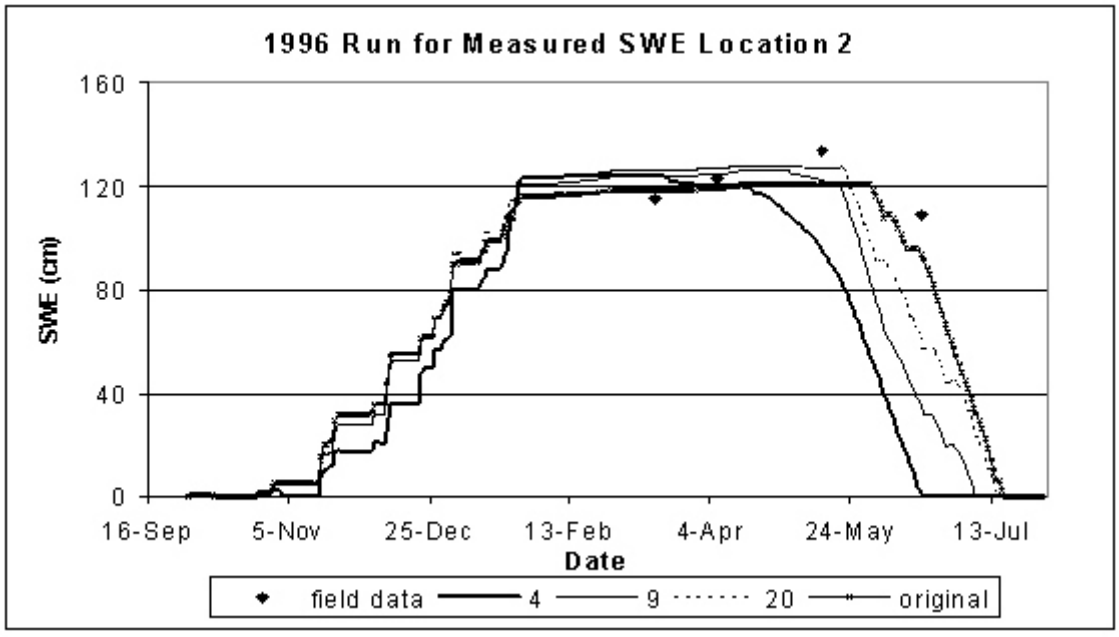

Figure 8-5. Comparison of Results for the different HRU subdivisions for the Emerald Lake Watershed for the SWE measurement at location 2.

Table 8-26. Summary of the SWE results for the four HRU configurations for the SWE measurement at location 2.

Parameter	Original Grouping	4 Pixel Grouping	9 Pixel Grouping	20 Pixel Grouping
Mean SWE (cm)	74.6	61.5	70.7	74.8
D Mean SWE (cm)	-	13.1	3.9	-0.2
% Difference Mean SWE	-	17.5 %	5.2 %	-0.3 %
Peak SWE (cm)	120.6	122.9	125.6	126.3
D Peak SWE (cm)	-	-2.3	-5.0	-5.7
% Difference Peak SWE	-	-1.9 %	-4.1 %	-4.7 %
Date of Snowpack Ripening	May 31	April 23	May 18	May 24
D Date of Ripening	-	38	14	8
Length of Ablation Period (days)	50	57	51	54
D Length of Ablation Period (days)	-	-7	-1	-4

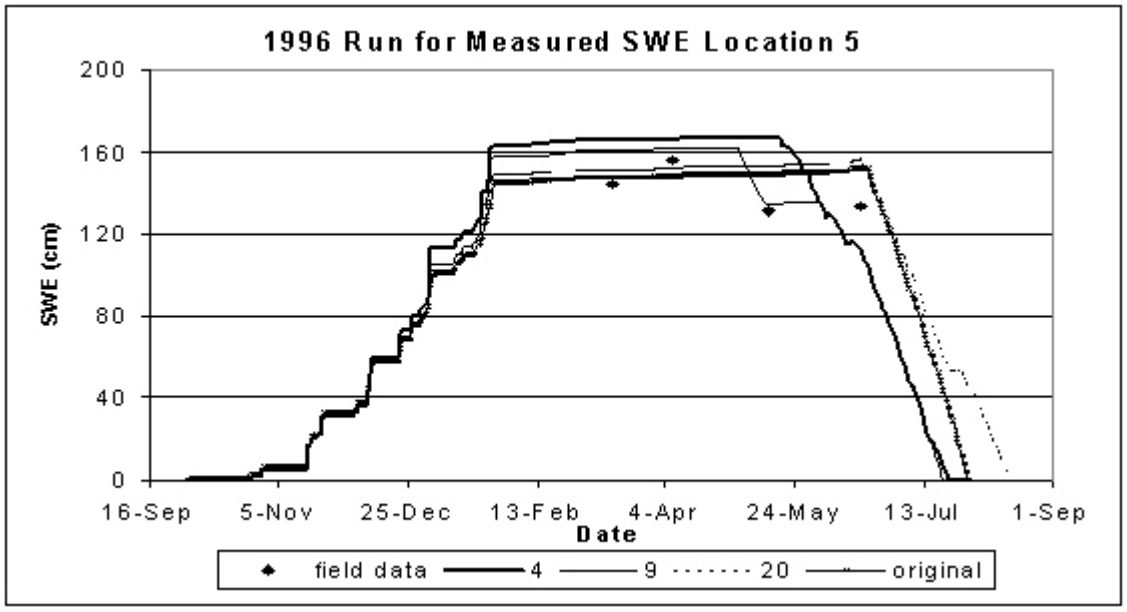

Figure 8-6. Comparison of results for the different HRU subdivisions for the Emerald Lake Watershed for the SWE measurement at location 5.

Table 8-27. Summary of the SWE results for the four HRU configurations for the SWE measurement at location 5.

Parameter	Original Grouping	4 Pixel Grouping	9 Pixel Grouping	20 Pixel Grouping
Mean SWE (cm)	97.5	99.2	94.4	98.1
D Mean SWE (cm)	-	-1.7	3.1	-0.6
% Difference Mean SWE	-	-1.7 %	3.2 %	-0.6 %
Peak SWE (cm)	151.6	165.4	161.5	154.7
D Peak SWE (cm)	-	-13.8	-9.9	-3.1
% Difference Peak SWE	-	-9.1 %	-6.5 %	-2.0 %
Date of Snowpack Ripening	June 21	May 21	June 8	June 18
D Date of Ripening	-	31	14	2
Length of Ablation Period (days)	41	60	43	49
D Length of Ablation Period (days)	-	-19	-2	-8

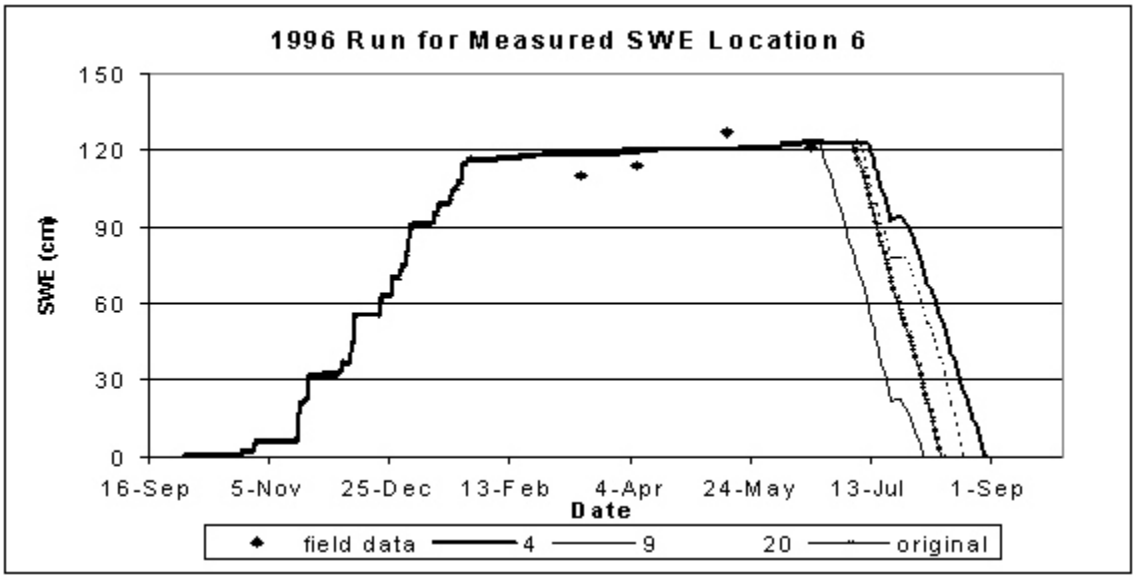

Figure 8-7. Comparison of Results for the different HRU subdivisions for the Emerald Lake Watershed for the SWE measurement at location 6.

Table 8-28. Summary of the SWE results for the four HRU configurations for the SWE measurement at location 6.

Parameter	Original Grouping	4 Pixel Grouping	9 Pixel Grouping	20 Pixel Grouping
Mean SWE (cm)	82.8	83.3	79.4	82.9
D Mean SWE (cm)	-	-0.5	3.4	-0.1
% Difference Mean SWE	-	-0.6 %	4.1 %	-0.1 %
Peak SWE (cm)	123.1	123.3	122.7	123.9
D Peak SWE (cm)	-	-0.2	0.4	-0.8
% Difference Peak SWE	-	-0.2 %	0.3 %	-0.6 %
Date of Snowpack Ripening	July 5	July 10	June 21	July 6
D Date of Ripening	-	-5	15	-1
Length of Ablation Period (days)	39	49	45	46
D Length of Ablation Period (days)	-	-10	-6	-7

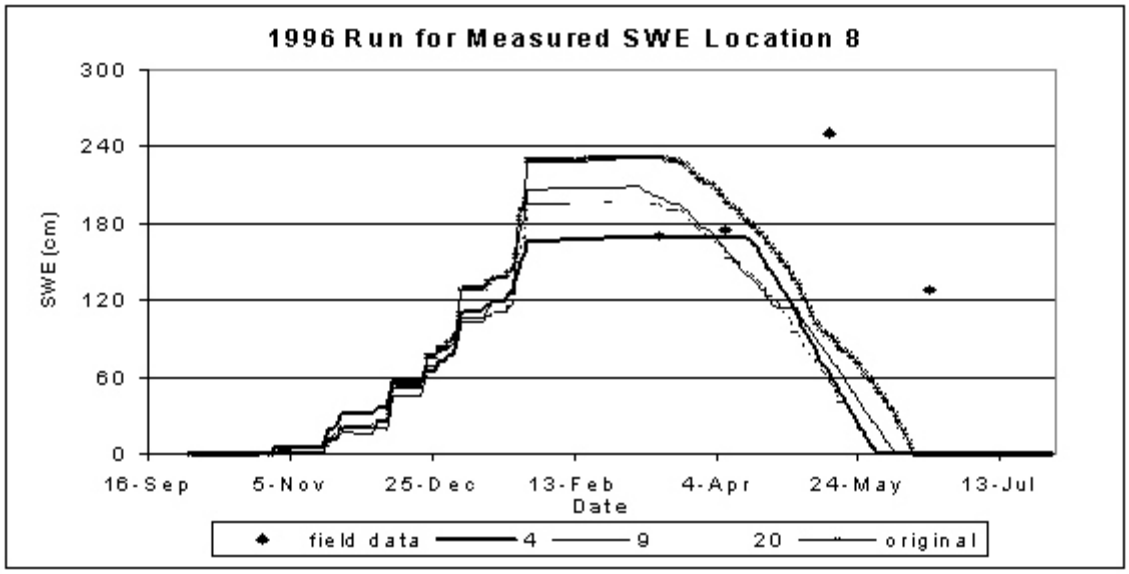

Figure 8-8. Comparison of Results for the different HRU subdivisions for the Emerald Lake Watershed for the SWE measurement at location 8.

Table 8-29. Summary of the SWE results for the four HRU configurations for the SWE measurement at location 8.

Parameter	Original Grouping	4 Pixel Grouping	9 Pixel Grouping	20 Pixel Grouping
Mean SWE (cm)	94.1	74.6	80.3	76.1
D Mean SWE (cm)	-	19.5	13.8	18.0
% Difference Mean SWE	-	20.7 %	14.7 %	19.1 %
Peak SWE (cm)	231.4	169.9	210.6	197.2
D Peak SWE (cm)	-	61.5	20.8	34.2
% Difference Peak SWE	-	26.6 %	9.0 %	14.8 %
Date of Snowpack Ripening	March 16	April 18	March 4	March 6
D Date of Ripening	-	-28	12	10
Length of Ablation Period (days)	90	46	91	85
D Length of Ablation Period (days)	-	44	-1	-5

Figure 8-4 shows a plot of the SWE time series for HRU 1 for the four different HRU configurations along with the field SWE data measured at location 1 (see Figure 4-14 for locations of SWE measurements). This figure shows that the SWE distribution for the initial pixel grouping of 16 has a smaller peak SWE value associated with it, and also begins its ablation period later in the year than do the SWE time series for the three alternate pixel groupings. Table 8-25 substantiates these claims. This table shows that the peak SWE values for the three alternate pixel groupings are greater than the peak SWE value for the initial pixel grouping by a range of 8.3% to 14.1%. Also, the date of snowpack ripening for the three alternate pixel groupings occurs earlier in the year than

the date of snowpack ripening for the initial pixel grouping by a range of 17 to 70 days. Significant differences also exist between the initial pixel grouping and the alternate groupings of 4 and 9 pixels in terms of mean SWE values. The mean SWE values for these alternate groupings are 14.9% and 13.3% smaller than the mean SWE value for the initial pixel grouping. In terms of length of ablation period, the alternate pixel groupings of 9 and 20 match closely to the initial grouping, but the alternate 4 pixel grouping has an ablation period that is 36 days longer than the ablation period for the initial pixel grouping.

A review of the HRU physical characteristics for the four different configurations help to explain the variations in the SWE time series. For the initial HRU configuration, HRU 1 has a mean slope of 30 degrees. This slope is steep enough to induce avalanching, and in fact, SWE is lost from HRU 1 during the initial run for the water year 1996 because of avalanching. Additionally, no other adjacent HRU contributes SWE to HRU 1 due to avalanching because of the slope and orientation of the adjacent HRUs. HRU 1, for the three alternate HRU configurations, all have slopes too mild for avalanches to occur. As a result, no SWE is lost from HRU 1 for any of the alternate configurations due to avalanching. Additionally, HRU 1, for the three alternate configurations, can receive SWE due to avalanching from adjacent HRUs. This explains the increase in peak SWE experienced by the alternate configurations.

For the initial configuration, HRU 1 is approximately 100 m higher in elevation than the for HRU 1 for the three alternate configuration. This fact means that temperatures throughout the year are colder for the initial configuration, ultimately

meaning less sensible heat exchange occurring during the ablation period. Also, HRU 1 for the initial configuration faces west, whereas for the alternate configurations, HRU 1 faces more south. This fact indicates that less incoming solar radiation is being received at HRU 1 for the initial configuration. Thus, significantly less net energy is being received at HRU 1 for the initial configuration, which leads to the snowpack ripening later in the year.

Figure 8-5 shows a plot of the SWE time series for HRU 2 for the four different HRU configurations along with the field SWE data measured at location 2 (see Figure 4-14 for locations of SWE measurements). This figure shows that the peak SWE values for the various configurations are approximately the same, and also that HRU 2 for the initial configuration begins its ablation period later in the year than do the SWE time series for the three alternate pixel groupings. Table 8-26 substantiates these claims. This table shows that the peak SWE values for the three alternate pixel groupings vary from the peak SWE value for the initial pixel grouping by a range of only 2.3% to 5.7%. The mean SWE values are also close in proximity for the initial HRU configuration and for the configuration utilizing the 9 and 20 pixel groupings. The mean SWE value, however, differs significantly between the initial configuration and the 4 pixel grouping configuration. This difference is 17.5% and is due not to the difference in peak SWE but rather to the much earlier onset of melt for the 4 pixel grouping alternate. As previously mentioned, the date of snowpack ripening for the three alternate pixel groupings occur earlier in the year than the date of snowpack ripening for the initial pixel grouping. The 9 and 20 pixel grouping alternates are

relatively close to the initial configuration, differing by 14 and 8 days, respectively. In terms of length of ablation period, the alternate pixel groupings match closely to the initial grouping, with a range in length of ablation period that is from 1 to 7 days longer than the ablation period for the initial pixel grouping.

A review of Table 4-8 and Tables 8-21 through 8-23 show that the physical characteristics for HRU 2 for the four different configurations are similar. The only notable exception is that the mean elevation for HRU 2 for the 4 pixel grouping configuration is approximately 200 m less than HRU 2 for the other configurations. This fact means that temperatures throughout the year are warmer for the 4 pixel grouping configuration, ultimately meaning greater sensible heat exchange occurring during the ablation period. This results in a significant increase in net energy being received at HRU 2 for this configuration, which leads to the snowpack ripening significantly earlier in the year.

Figure 8-6 shows a plot of the SWE time series for HRU 5 for the four different HRU configurations along with the field SWE data measured at location 5 (see Figure 4-14 for locations of SWE measurements). This figure shows that the SWE distribution for the initial configuration and for the 20 pixel grouping configuration are very similar, whereas the SWE time series for the 4 and 9 pixel grouping configurations are very similar. Table 8-27 substantiates these claims. This table shows that the mean SWE values, peak SWE values, date of snowpack ripening, and length of ablation period are very similar for the initial configuration and for the 20 pixel grouping configuration. The same can be said for the 4 and 9 pixel grouping alternates, although these values are

not as quite as close.

A review of the HRU physical characteristics for the four different configurations show that the mean slope for the initial configuration and for the 20 pixel grouping configuration are both great enough for avalanching to occur. This is not the case for the 4 and 9 pixel grouping configurations. These configurations do not transport SWE from HRU 5 because of avalanching, and this helps to explain why these two configurations have greater peak SWE values. These smaller slopes also help these HRUs to receive more incoming solar radiation, which results in an increase in net energy being received at HRU 5 for these two configurations. This explains why the snowpack ripens earlier in the year for the 4 and 9 pixel grouping configurations.

Figure 8-7 shows a plot of the SWE time series for HRU 6 for the four different HRU configurations along with the field SWE data measured at location 6 (see Figure 4-14 for locations of SWE measurements). This figure shows that the four SWE time series are nearly indistinguishable except for some differences that exist during the ablation period. Table 8-28 substantiates this claim. This table shows that the mean SWE values and the peak SWE values for the three alternate pixel groupings differ from the mean SWE and peak SWE values for the initial pixel grouping by less than 5.0%, with nearly all values differing by less than 1.0%. As previously mentioned, the date of snowpack ripening for the three alternate pixel groupings differ from the date of snowpack ripening for the initial pixel grouping. The 4 and 20 pixel grouping alternates have a snowpack that ripens later in the year as compared to the initial configuration, but the dates are relatively close to the initial configuration, differing by 5 and 1 days,

respectively. The 9 pixel grouping alternate has a snowpack that ripens earlier in the year as compared to the initial configuration, and differs in ripening date by 15 days. In terms of length of ablation period, the alternate pixel groupings match fairly closely to the initial grouping. All are longer in length with a range of 6 to 10 days longer than the ablation period for the initial pixel grouping.

A review of Table 4-8 and Tables 8-21 through 8-23 show that the physical characteristics for HRU 6 for the four different configurations are very similar. The mean elevations are all within 50 m of one another, indicating that temperatures throughout the year are approximately equal for the various configurations. The aspect for HRU 6 for the various configurations are the same, and the mean slopes are also similar in value. The differences in slope results in small differences in received solar radiation, which results in the minor difference in date of snowpack ripening and length of ablation period.

Figure 8-8 shows a plot of the SWE time series for HRU 8 for the four different HRU configurations along with the field SWE data measured at location 8 (see Figure 4-14 for locations of SWE measurements). This figure shows that the SWE distribution for the initial configuration has a larger mean SWE and peak SWE value associated with it than do the SWE time series for the three alternate pixel groupings. This figure also shows that the length of the ablation period for the initial configuration appears to be similar in length to the ablation period for the 9 and 20 pixel grouping configurations. Table 8-29 substantiates these claims. This table shows that the peak SWE values for the three alternate pixel groupings are smaller than the peak SWE value

for the initial pixel grouping by a range of 9.0% to 26.6%. The mean SWE values for the three alternate pixel groupings are smaller than the mean SWE value for the initial pixel grouping by a range of 14.7% to 20.7%. Also, the date of snowpack ripening for the 9 and 20 pixel groupings occur earlier in the year than the date of snowpack ripening for the initial pixel grouping, but the difference is relatively small (9 and 5 days, respectively) for these configurations. These two configurations are also close to the initial configuration in terms of length of ablation period, but the alternate 4 pixel grouping has an ablation period that is 44 days shorter than the ablation period for the initial pixel grouping, due to a peak SWE value that is 62.7 cm less than for the initial configuration.

A review of the HRU physical characteristics for the four different configurations help to explain the variations in the SWE time series. For the 4 pixel grouping configuration, HRU 8 has a mean slope large enough to cause avalanching. During the model run, this HRU lost a significant amount of SWE during the 1996 water year because of avalanching. Thus, this HRU has a significantly smaller peak SWE value than for the other configurations.

For the 4 pixel grouping configuration, HRU 8 is approximately 200 m higher in elevation than the for HRU 8 for the other three configurations. This fact means that temperatures throughout the year are colder for the 4 pixel configuration, ultimately meaning significantly less sensible heat exchange occurring during the ablation period. This fact indicates that less net energy is being received at HRU 8 for the 4 pixel configuration, which leads to the snowpack ripening later in the year.

8.5.3 Conclusions Regarding the HRU Subdivision Process

In summary, these findings indicate that the model is sensitive to different HRU subdivisions because of the resulting changes to the HRU physical characteristics. Peak SWE values appear only to be sensitive to changes in mean slope. This is the case because slope indicates whether or not avalanching can occur, and as was the case for HRU 8 for the different configurations, peak SWE values differed significantly between HRUs that did and did not have a sufficient slope for avalanching to occur. When avalanching is not a significant consideration for a watershed, peak SWE values for HRUs within the watershed, appear not to be sensitive to different HRU configurations.

Snowpack ripening, length of ablation period, and resulting mean SWE values are sensitive to significant changes in elevation, mean slope, or aspect. Significant changes in these parameters greatly affect net energy received at an HRU, thus affecting the melt season. The results of this analysis could help to explain some of the uncertainties regarding model output during the melt season. It has been demonstrated that modeling net energy at a point is difficult, and if the modeling of net energy is sensitive to changes in HRU configuration, this will lead to greater uncertainties in modeled SWE output during the ablation period.

Ultimately, the results of the analysis regarding the HRU Subdivision Process suggest that smaller HRUs provide more accurate SWE predictions. The analysis showed that joining adjacent pixel groupings may produce mean values for the physical characteristics, such as elevation and slope, that have a large variance associated with them. By decreasing the number of pixel groupings combined, and thus the size of the

HRUs, the variance in the mean values of the physical characteristics can be reduced. Reducing the size of the HRUs does have its drawbacks. More HRUs means requiring more interpolation of input variables, such as precipitation and air temperature, which could lead to greater input error. Further research is required to determine an optimal sizing of HRUs. This sizing should balance minimizing the variance of mean physical characteristic values, and thus improving SWE prediction ability, with the cost of the additional time required to produce an increased number of required input files and calibrate the model.

CHAPTER NINE

DETECTING PATTERNS IN SNOW WATER EQUIVALENCE

9.1 INTRODUCTION

Many snowmelt runoff models rely on snow depletion curves, which describe the seasonal decline of snow-covered fraction as a function of time or accumulated melt. A consequence of using these curves in forecasting is that an assumption is made regarding some uniformity in snowmelt basin response from year to year. Up until this point, the validity of this assumption regarding snowmelt basin uniformity has not been adequately addressed in the literature.

Verifying this assumption would demonstrate the value of depletion curve theory for short-term and extended hydrologic forecasting, and would contribute to creating generalized methods for estimating SWE in data-sparse regions. As discussed in Chapter 1, minor improvements in hydrologic forecasting, based upon enhanced SWE estimates, could result in significant economic impact in downstream communities.

The existence of similar, interannual spatial and temporal SWE patterns within a watershed could be identified by several methods. The first method would be to compute the first two statistical moments (mean and variance) of the SWE distributions within a watershed at various intervals throughout the water year, and analyze these values for any similarities or trends. The second method would be to determine if the spatial distribution of SWE at various times throughout the year was similar from year to year. This determination would be made using the Kolmogorov-Smirnov two-sample

nonparametric test. The final method would involve ranking the SWE for each HRU within the watershed at various intervals within the water year. These rankings would then be compared for specific dates from year to year to determine if any similarities or trends exists.

The SWE model has been developed and tested. It shall now be used in the analysis and investigation of the proposed question concerning similar, interannual spatial and temporal SWE patterns. Previous chapters (5 through 7) have shown that the model is not perfect, but the level of accuracy is sufficient to aid in this analysis.

9.2 DETERMINING SWE PATTERNS BY MEANS OF ANALYZING THE FIRST TWO MOMENTS OF THE SWE DISTRIBUTION

9.2.1 Distribution Comparison Using Statistical Moments for the Upper Rio Grande Watershed

Examining the mean SWE value throughout the watershed during a water year provides insight into the evolution of the probability density function of the SWE distribution in time. Realizing that the mean SWE value throughout the watershed may vary significantly from year to year does not mean that the SWE distribution throughout the watershed does not exhibit similarities from year to year. If the peak mean SWE value throughout the watershed occurs at approximately the same time from year to year, this would indicate that the shape of the probability density function of the SWE distribution shows similarities from year to year. Examining the variance of SWE throughout the watershed during a water year provides insight into the melt process of the watershed. If the peak mean SWE value and the variance of SWE are both

decreasing during the melt season, this would indicate that melt is occurring throughout the watershed and the difference in SWE between the HRUs that comprise the watershed is decreasing. If the peak mean SWE value is decreasing, but the variance of SWE is increasing during the melt season, this would indicate that (a) snow is melting at different rates, or (b) melt is occurring in part of the watershed, while accumulation is occurring in other parts of the watershed; in either case, the difference in SWE between the HRUs that comprise the watershed is increasing. If the values of the variance of SWE follow similar patterns from year to year, this would imply that similar melt patterns are occurring throughout the watershed from year to year.

Based upon the modeled SWE output for the entire Upper Rio Grande Watershed, the first two statistical moments (mean and variance) of the SWE distribution were computed and the mean and standard deviation were plotted at the beginning and middle of each month for each of the water years (Appendix L). Again, due to the high level of autocorrelation between daily SWE values, it was decided that computing the statistical moments on a bimonthly interval was sufficient.

Upon inspection of the plotted moments, two significant trends emerge. The first trend is that the greatest mean value of SWE, throughout the watershed, occurs at the beginning of May for seven of the eight years studied. The exception is 1999, where the greatest mean value occurs near the beginning of April. This trend indicates that melt begins for a significant portion of the watershed approximately at the beginning of May, thus causing a decrease in SWE after this date. Melt may occur before this time for part of the watershed, but the percent of area experiencing melt must be small as

offset by the increasing mean value of SWE throughout the watershed. Recognition of this trend could provide valuable information to downstream communities regarding the time frame as to when snow melt may begin to significantly affect stream discharge.

The second trend involves the variance, or dispersion, of the modeled SWE output. The greatest variance of the SWE output occurs in a period from the beginning of May to the beginning of June. This trend indicates that by the beginning of June, the snowpack throughout the watershed is ripe and that melt has ensued. SWE is increasing in portions of the watershed while decreasing in other areas. A review of the SWE maps created for the Upper Rio Grande Watershed (Appendix K) show that for each of the water years studied, some HRUs continue to accumulate SWE after other HRUs are decreasing in SWE due to melt. Recognition of this trend could provide valuable information to downstream communities by identifying the approximate date at which the entire watershed is contributing melt. This date would then help determine the length of the overall ablation period of the watershed and the length of time that snow melt may significantly affect stream discharge.

9.2.2 Distribution Comparison Using Statistical Moments for the Reynolds Creek Watershed

The first two statistical moments of the SWE distribution were computed and the mean and standard deviation were plotted at the beginning and middle of each month for each of the water years (Appendix M) based upon the modeled SWE output for the entire Reynolds Creek Watershed. Upon inspection of the plotted moments,

several trends emerge. The first trend is that the greatest mean value of SWE throughout the watershed occurs between the beginning of March and the beginning of April for all eight years studied. This trend indicates that melt begins for a significant portion of the watershed approximately from the beginning of March to the beginning of April, thus causing a decrease in SWE after this time period. Melt may occur before this time for part of the watershed, but the percent of area experiencing melt must be small as offset by the increasing mean value of SWE throughout the watershed. Recognition of this trend could provide valuable information to downstream communities regarding the time frame as to when snow melt may significantly affect stream discharge.

The second trend involves the variance of the modeled SWE output. For years in which the snowpack is small (mean SWE < 10 cm), the greatest variance of the SWE output occurs approximately at the same time the greatest mean SWE value occurs. These water years include 1989, 1990, 1991, 1993, and 1994 This trend indicates that for years with small snowpacks, by the time the maximum mean SWE value occurs within the watershed, the snowpack throughout the watershed is ripe and that melt is imminent. Recognition of this trend could provide valuable information to downstream communities by approximating the length of the overall ablation period of the watershed and the length of time that snow melt may significantly affect stream discharge.

The third trend also involves the variance of the modeled SWE output. For years in which the snowpack is deep (mean SWE > 10 cm), the greatest variance of SWE occurs approximately at the beginning of May. These water years include 1988,

1992, and 1995. This trend indicates that by the beginning of May, the snowpack throughout the watershed is ripe and that melt has ensued. This indication again shows that during the period from the beginning of May to the beginning of July, SWE is increasing in portions of the watershed (an unripe snowpack), while decreasing in other areas.

9.2.3 Distribution Comparison Using Statistical Moments for the Emerald Lake Watershed

Two statistical moments (mean and variance) were computed and the mean and standard deviation were plotted at the beginning and middle of each month for each of the water years (Appendix N) based upon the modeled SWE for the entire Emerald Lake Watershed. Upon inspection of the plotted moments, two significant trends emerge. The first trend is that the greatest mean value of SWE throughout the watershed occurs during the month of April for all five water years studied. This trend indicates that melt begins for a significant portion of the watershed during the month of April, thus causing a decrease in SWE after this time period. As previously discussed, melt may occur before this time for part of the watershed, but the percent of area experiencing melt must be small as offset by the increasing mean value of SWE throughout the watershed.

The second trend involves the variance of the modeled SWE output. The greatest variance of the SWE output occurs at a later date than the greatest mean SWE value for all of the water years. This trend indicates that after the date that the maximum mean SWE has occurred, the snowpack for most of the watershed is ripe and

melt has ensued. Additionally at this time, the remainder of the snowpack is not ripe, and this portion is still accumulating SWE.

9.3 DETERMINING PATTERNS BY COMPARING SWE DISTRIBUTIONS

9.3.1 Distribution Comparison Utilizing the Kolmogorov-Smirnov Two-Sample Nonparametric Test for the Upper Rio Grande Watershed

Histograms were created and plotted for each watershed to depict the SWE distribution on specific days throughout the water year. The histograms depict the total area of watershed that have a specific range of SWE for the first day of each month. Appendix O contains a series of histograms for an entire water year shown on one plot, for each of the water years studied. These series of histograms show how the SWE distribution increases during the accumulation period and then recedes during the ablation period. Again, due to the high level of autocorrelation between daily SWE values, it was decided that examining these histograms on the first day of each month was sufficient. From these histograms, the Kolmogorov-Smirnov two-sample test was used to determine if similar SWE distributions (patterns) exist interannually. As an example, does the modeled SWE distribution from January 1, 1994, match the modeled SWE distributions for January 1 of the other study years?

The K-S two-sample test was set up so that the null hypothesis was that the SWE distributions tested on various days from different years were similar. The acceptance of the null hypothesis would indicate similar SWE distributions, and would suggest similar interannual SWE patterns. Conversely, the alternate hypothesis was that

the SWE distributions tested on various days from different years were not similar. The acceptance of the alternate hypothesis would indicate dissimilar SWE distributions, and would suggest that similar interannual SWE patterns do not exist.

It was decided to utilize the K-S two-sample test only on dates in which the mean SWE values were similar. This decision was based upon the fact that the K-S two-sample test is sensitive to differences in the central tendency of the two sample distributions. If the mean SWE values of the two distributions varied significantly, the results of the K-S two-sample test would then indicate that the two SWE distributions are not similar. The results of the K-S two-sample tests were also divided into two subgroups: sample distributions tested during the accumulation period and sample distributions tested during the ablation period. This was done to determine if similar, interannual SWE patterns are more likely to exist during a specific time of the water year.

Appendix P contains the results of the K-S two-sample tests for both the accumulation and ablation periods for the Upper Rio Grande Watershed. The results of the nonparametric tests indicate that for the Upper Rio Grande Watershed, SWE distributions with similar mean values were not similar from year to year for any level of significance. These results apply to both the accumulation and ablation period. These results suggest that significant model input variability exists. Since the physical characteristics of a watershed remain fairly constant in time (aspect, slope, etc.), the input variability is most likely found in the meteorological input parameters. This variability is most likely caused by short term meteorological phenomena, such as

random storm patterns and wind patterns. This claim will be examined in more detail in section 9.4.

The results of the K-S two-sample nonparametric tests suggest that the SWE distribution for a particular day within the watershed is affected by meteorological variability, which produce random distributions from year to year. Consequently, meteorological variability within the watershed may hinder the formation of similar SWE patterns from year to year.

9.3.2 Distribution Comparison Utilizing the Kolmogorov-Smirnov Two-Sample Nonparametric Test for the Reynolds Creek Watershed

As was the case for the Upper Rio Grande Watershed, histograms were created and plotted for the Reynolds Creek Watershed to depict the SWE distribution on specific days throughout the water year. Again, the histograms depict the total area of watershed that have a specific range of SWE for the first day of each month. Appendix Q contains a series of histograms for an entire water year shown on one plot, for each of the water years studied. The K-S two-sample test was again utilized to determine if the modeled SWE distributions showed similar, interannual patterns during the accumulation and ablation periods.

Appendix R contains the results of the K-S two-sample tests for both the accumulation and ablation periods for the Reynolds Creek Watershed. The results of the nonparametric tests during the accumulation period are mixed for the Reynolds Creek Watershed. During the accumulation period, three of the tests (1, 4, and 9) indicate that

the tested SWE distributions were similar for any level of significance. Four of the tests (2, 5, 6, and 8) indicate that the tested SWE distributions were not similar for any level of significance. Two of the tests (3 and 7) indicate that the tested SWE distributions were not similar when the level of significance was high, but were similar for lower values of the level of significance. These results suggest that during the accumulation period, model input variability exists which is responsible for the variability in modeled SWE output. As discussed for the previous watershed, the input variability is most likely found in the meteorological input parameters. It appears that, unlike the previous watershed, the degree of variability is not large enough to prevent some similar, interannual SWE patterns from occurring.

The results of the nonparametric tests during the ablation period suggest that the SWE distributions with similar mean values were not similar from year to year for most values of the level of significance. Four of the tests (1, 3, 6, and 8) suggest that the SWE distributions were not similar from year to year for any level of significance. Four of the tests (2, 4, 5, and 7) indicate that the tested SWE distributions were not similar when the level of significance was high, but were similar for lower values of the level of significance.

These results suggest that greater input variability exists during the ablation period for the Reynolds Creek Watershed. This could be caused by one of two things. The first possibility could be, as discussed in chapters 5 through 7, that greater model error occurs during the ablation period. The second possibility is that greater meteorological variability occurs during the ablation period.

9.3.3 Distribution Comparison Utilizing the Kolmogorov-Smirnov Two-Sample Nonparametric Test for the Emerald Lake Watershed

As was the case for the previous two watersheds, histograms were created and plotted for the Emerald Lake Watershed to depict the SWE distribution on specific days throughout the water year. As previously discussed , the histograms depict the total area of watershed that have a specific range of SWE for the first day of each month. Appendix S contains a series of histograms for an entire water year shown on one plot, for each of the water years studied. The K-S two-sample test was again utilized to determine if the modeled SWE distributions showed similar, interannual patterns during the accumulation and ablation periods.

Appendix T contains the results of the K-S two-sample tests for both the accumulation and ablation periods for the Emerald Lake Watershed. The results of the nonparametric tests during the accumulation period are mixed for the Emerald Lake Watershed. During the accumulation period, test 2 indicates that the tested SWE distributions were similar for any level of significance. Four of the tests (1, 3, 4, and 6) indicate that the tested SWE distributions were not similar for any level of significance. Test 5 indicates that the tested SWE distributions were not similar when the level of significance was high, but were similar for lower values of the level of significance.

These results suggest that during the accumulation period, model input variability exists which is responsible for the variability in modeled SWE output. As discussed for the previous watersheds, the input variability is most likely found in the meteorological input parameters. The variability could also be the result of additional

SWE transport phenomena, most notably avalanching. It appears that, like the Reynolds Creek Watershed, the degree of variability is not large enough to prevent some similar, interannual SWE patterns from occurring.

The results of the nonparametric tests during the ablation period suggest that the SWE distributions with similar mean values were not similar from year to year for any level of significance. It should be noted that only two tests were run during the ablation period due to the widely varying mean SWE values. Consequently, conclusions are difficult to reach based upon such a limited sample size.

9.4 DETERMINING PATTERNS BY RANKING SWE AND METEOROLOGICAL INPUTS FOR HRUs CONTAINING METEOROLOGICAL STATIONS

9.4.1 Distribution Comparison by a Ranking Method for the Upper Rio Grande Watershed

As stated in Chapter 5, HRUs 1, 40, and 50 coincide with SNOTEL stations at Beartown, Middle Creek, and Wolf Creek Summit. For these three HRUs, SWE values and meteorological input data were ranked on the first day of each month for each of the water years studied. The purpose of this ranking was to determine, at least on a limited basis, if similar rankings exist in these HRUs in terms of SWE totals from year to year. Similar SWE rankings would suggest the existence of similar, interannual SWE patterns. If similar SWE patterns exist from year to year, the SWE ranking for an HRU should be approximately the same for that particular date from year to year. These HRUs were chosen for this analysis because actual field measured data were available at

the SNOTEL stations. If similar interannual SWE patterns exist for the Upper Rio Grande Watershed, a pattern should emerge in terms of SWE rankings, such as HRU 50 almost always has more SWE than HRU 1, which almost always has more SWE than HRU 40.

The Upper Rio Grande Watershed was chosen for this analysis because this watershed had the most meteorological stations (3) that had both SWE data and meteorological data available. The Reynolds Creek Watershed had only one such station and no such stations existed for the Emerald Lake Watershed.

As stated in Chapter 4, the meteorological input parameters for the Upper Rio Grande Watershed were: cloud cover, wind speed, total precipitation, and air temperature. Other required meteorological inputs, such as solar radiation and relative humidity, were not available at the SNOTEL stations and thus were estimated by equations developed for the model. As also mentioned in Chapter 4, cloud cover data were uniform throughout the watershed, meaning each HRU had the same cloud cover input data. Consequently, the cloud cover data were not ranked. As a result, SWE, daily wind speed, total precipitation, and average air temperature were ranked for HRUs 1, 40, and 50 within the Upper Rio Grande Watershed. Wind speed data were corrected for an HRU's canopy cover as per Eq. 3-8. Appendix U contains a summary table of these rankings.

The SWE ranking values contained in Appendix U for each date are based upon the actual SWE values in each HRU on that particular date. As an example, on November 1, 1993, the SWE rankings for HRUs 1, 40, and 50 show that HRU 50 has

the most SWE on that date, HRU 40 has the second most SWE on that date, and that HRU 1 has the lowest amount of SWE on that date. The meteorological ranking values contained in Appendix U for each date are based upon an average value determined from the previous month. As an example, on November 1, 1993, the precipitation rankings for HRUs 1, 40, and 50 show that HRU 50 had the highest average, daily precipitation value throughout the month of October, 1993, HRU 1 had the second highest average, daily precipitation value throughout October, 1993, and that HRU 40 had the lowest average, daily precipitation value throughout October, 1993. Average values from the previous month for meteorological inputs were chosen, as opposed to an actual daily value for a particular day, because a single daily value could produce an anomaly that an average monthly value would help to minimize.

A review of Appendix U shows an interesting development in the interannual SWE rankings for HRUs 1, 40, and 50. For the eight water years studied, a great deal of variability exists in the SWE rankings during the early accumulation period. Six different rankings of SWE occur on November 1. On December 1, the number of different SWE rankings drops to four. On January 1, the number of different SWE rankings drops to three. On this same date, four of the years have a ranking of 1, 3, 2, indicating that for these years, HRU 1 has the greatest amount of SWE, followed by HRU 50, and then HRU 40. Additionally, HRU 40 has the lowest SWE for seven of the eight years studied.

As the accumulation progresses, the SWE rankings continue to increase in uniformity. On February 1, the number of different SWE rankings drops to two. On

this date, five of the years have a ranking of 2, 3, 1, indicating that for these years, HRU 50 has the greatest amount of SWE, followed by HRU 1, and then HRU 40. Additionally, HRU 40 has the lowest SWE for all eight years studied. On March 1 and April 1, seven of the years have a ranking of 2, 3, 1, with the exception being 1999, which shows HRU 1 having the greatest amount of SWE, followed by HRU 50, and then HRU 40. Again, HRU 40 has the lowest SWE for all eight years studied, for both of these dates.

As the ablation period begins, greater variability can again be seen in the SWE rankings. On May 1, the number of different SWE rankings increases to three. On this date, five of the years still have a ranking of 2, 3, 1, and for seven of the years, HRU 40 still has the lowest SWE. On June 1, the number of different SWE rankings is still three. However, no single ranking is prevalent. For only five of the years does HRU 40 contain the least amount of SWE.

The question that arises is what causes the similarities and differences found in the SWE rankings for HRUs 1, 40, and 50 for the eight water years studied. The similarities in SWE ranking could be the result of the physical parameters of the watershed. The slope, elevation, aspect, etc. of an HRU remain constant from year to year and could be responsible, at least partially, for similar SWE rankings. The differences in SWE rankings suggest the existence of yearly variability associated with the meteorological input data. If the physical parameters of the watershed and the meteorological input data were consistent in ranking from year to year, the SWE rankings for each HRU would most likely also be consistent from year to year.

With this fact in mind, it would be logical to assume that there may exist a correlation between the ranking of meteorological input data and the corresponding ranking of SWE. A review of Appendix U indicates that the ranking of SWE for the three HRUs does not appear to be correlated to the ranking of average daily air temperature. The ranking of average daily air temperature is somewhat consistent from month to month and from year to year for the three HRUs. HRU 50 consistently has the highest (of the three HRUs) average daily air temperature. The average daily air temperature for HRUs 1 and 40 are very similar, and this fact is reflected in the rankings. These results are not surprising. A review of Table 4-2 shows that Wolf Creek Summit (HRU 50) is approximately 180 meters lower in ground elevation than Beartown (HRU 1) and Middle Creek (HRU 40). Consequently, it is expected that Wolf Creek Summit would have the highest average air temperature of the three HRUs. Beartown is close in ground elevation to Middle Creek, and thus these two HRUs typically have similar average daily air temperatures. If a strong correlation existed between the ranking of average air temperature and the ranking of SWE, it would then be expected that the SWE ranking of HRU 50 would typically be the lowest of the three due to the greatest average daily air temperature. This lowest ranking would be expected because a greater average daily air temperature would result in a greater percentage of total precipitation occurring as rain, and this would also increase the sensible heat exchange at this HRU throughout the water year. A review of Appendix U shows that HRU 50 rarely has the lowest SWE ranking suggesting that a strong correlation does not exist between average daily air temperature ranking and SWE

ranking for these three HRUs.

A similar analysis can be made regarding the average daily wind speed for the three HRUs. HRU 1 consistently has the highest average daily wind speed, while HRUs 40 and 50 consistently have approximately the same average daily wind speed, and thus the same lower ranking than HRU 1. Again, these results are not surprising. A review of Table 4-1 shows that HRU 1 has no canopy cover. However, HRUs 40 and 50 are completely forested with conifers. Thus, the wind speed through HRUs 40 and 50 are greatly reduced by the canopy cover. If a significant correlation existed between average daily wind speed ranking and SWE ranking, it would be anticipated that the SWE rankings for HRUs 40 and 50 would be similar since the rankings for average daily wind speed for these two HRUs are the same. A review of Appendix U shows that the SWE rankings for HRUs 40 and 50 frequently, especially from February to May, indicate that HRU 50 has the most SWE while HRU 40 has the least amount of SWE. Consequently, there does not appear to be a correlation between SWE ranking and average daily wind speed ranking for these three HRUs.

Relative sensitivity analysis discussed in Chapter 8 indicated that the most important meteorological input data were precipitation. With this fact in mind, it would be logical to assume that there would exist a strong correlation between the ranking of average daily precipitation and the ranking of SWE. However, the results found in Appendix U do not support this assumption. Only on one date (January 1) does the ranking of average daily precipitation match the ranking of SWE for a majority of the years (five). Additionally, on December 1 and on June 1, only one of the years has

similar ranking for both average daily precipitation and SWE.

The ranking of meteorological input data suggest that the variability found in the SWE rankings may be caused by a combination of the variability found in the different meteorological data. Additionally, the variability found in the SWE rankings appears to be greatest early in the accumulation period and late in the ablation period. This fact would lend credence to the claim that the variability in SWE rankings may be caused by a combination of the variability found in the different meteorological data. During the early accumulation and late ablation periods, fluctuations in the average daily air temperature can have a significant impact on SWE by affecting whether precipitation occurs as rain or snow. Fluctuations in the average daily air temperature during these periods can also have an impact on SWE by affecting the sensible heat exchange, total net energy received at an HRU, and thus the melt rate. Similarly, fluctuations in the average daily wind speed during these periods can also have an impact on SWE by affecting the turbulent heat exchanges, total net energy received at an HRU, and thus the melt rate.

9.5 CONCLUSIONS

The results of the tests performed to determine if similar SWE patterns exist interannually indicate that significant variability occurs within the SWE distribution from year to year, for all three watersheds. Based upon the plotted moments, some generalizations could be made regarding the SWE distributions for each watershed. Valuable knowledge regarding the total amount of SWE, and the length of the ablation

period, among other information, could be learned by downstream communities from these generalizations. These generalizations do not provide information concerning the spatial or temporal distribution of SWE within the watershed, and therefore do not provide information or evidence of similar or dissimilar SWE patterns from year to year.

The results from the Kolmogorov-Smirnov Two-Sample test were mixed for all three watersheds. Some interannual uniformity in the spatial SWE distributions were noted, but most test results indicated that the SWE distributions were not similar from year to year. As discussed earlier, these results could be caused by one of two things: model error, or meteorological variability.

The results of the HRU rankings for the Upper Rio Grande watershed suggest that significant meteorological input variability occurring early in the accumulation period and late in the ablation period causes significant variability in SWE rankings, and thus SWE patterns. This meteorological variability is minimized during the remainder of the water year which seems to help minimize the variability in SWE patterns during this period also.

How do the results presented in this chapter affect depletion curve theory? The results of the K-S two-sample tests suggest that meteorological variability may prevent the formation of similar, interannual SWE patterns within a watershed. The results of the HRU rankings for the Upper Rio Grande Watershed suggest that meteorological variability during the early accumulation period and late ablation period may also prevent the formation of similar, interannual SWE patterns within a watershed.

However, the results of the HRU rankings for the Upper Rio Grande Watershed also suggest that meteorological variability may be minimized during the remainder of the water year, thus allowing the formation of similar, interannual SWE patterns within the watershed. This fact indicates that the spatial probability density functions of SWE are most similar at the beginning of the melt season. These results seem to validate the depletion curve theory. Several key assumptions of depletion curve theory occur during the time period in which similar patterns occurred for the Upper Rio Grande Watershed. As an example, depletion curve theory applies when a snowpack becomes ripe and melt (depletion) occurs. The SWE rankings for the Upper Rio Grande Watershed during the months of March and April indicate uniformity in SWE rankings. Results presented in Chapter 5 also indicate that the snowpack of HRUs 1, 40, and 50 typically become ripe during this time period. Consequently, while using depletion curve theory, if assumptions are made concerning the ripening of the snowpack for the Upper Rio Grande Watershed, the results of the SWE rankings suggest that minimal error would be associated with these assumptions.

It should be noted that these conclusions are based upon data from three SNOTEL sites for eight water years. A more thorough investigation is necessary.

CHAPTER TEN

CONCLUSIONS AND RECOMMENDATIONS

10.1 INTRODUCTION

Studies, such as the one performed by Ferrris and Congalton (1989), have indicated that snowmelt accounts for a significant percentage of the annual stream flow in many areas of the world, including the Sierra Nevada, the Rockies, the Alps, the Andes, and the Himalayan Mountains. The western United States and other parts of the world rely heavily upon the annual economic value of snowmelt water. Additionally, studies such as the one done by Castruccio et al. (1980), indicated that a minor increase in river forecast accuracy would result in significant economic benefits to downstream communities.

To improve upon the quality of stream discharge forecasting, means of more accurately estimating the snow content during the accumulation season and through the melt season is needed. Thus one goal of the research was to provide more accurate input to river forecasting models by developing a spatial-temporal model to forecast the SWE within a watershed.

Most accumulation and ablation models, such as the National Weather Service River Forecast System SNOW-17 snow model, do not attempt to model the redistribution of snow by means of wind transport and avalanching. The developed SWE model improved upon existing snow models by incorporating all of the physical processes involving snow accumulation and ablation, including wind transport and

avalanching. Many models, such as the SNOW-17 snow model and the SRM, rely on snow depletion curves. The developed SWE model does not incorporate the depletion curve theory because the current literature does not adequately address its validity. Several models exist which estimate the redistribution of SWE by means of wind transport, such as the Snow-Transport Model for Complex Terrain created by Liston and Sturm (1998). However, these models, as well as the developed SWE model, typically rely upon daily average wind speed as opposed to hourly data. Unlike these other models, the developed SWE model utilized conditional probability to improve upon the wind transport estimates.

The conceptual model of spatially distributed SWE accumulation and depletion was calibrated and validated with spatially distributed observations from three watersheds. The effects of the physical variables and parameters on the SWE distribution within a watershed was demonstrated. How data were used in the calibration/validation of the model, including showing the benefit of additional data on model accuracy was also demonstrated.

10.2 MODEL PERFORMANCE

As presented in Chapters 5, 6, and 7, statistical analyses were performed for all three watersheds to determine model performance. The analyses performed were consistent for all three watersheds. Additionally, the results of the analyses were consistent in that it indicated that the model produced accurate results during the accumulation period for all three watersheds. Similarly, the same analyses indicated

that the model produced less accurate results during the ablation period for all three watersheds.

For the three watersheds during the accumulation period, goodness-of-fit statistics consistently indicated that the model accurately matched the field measured SWE data. The sample mean error, mean relative error, standard deviation of the measured data, standard error of the estimate, and the ratio of the standard error of the estimate to the standard deviation of the measured data consistently indicated that the model produced accurate results during this period for all three watersheds. Additionally, the peak modeled SWE matched closely to the measured peak SWE for the water years studied for all three watersheds.

These goodness-of-fit statistics and accurate prediction of the peak SWE indicate that the model can be useful in providing estimates of available snowmelt runoff to downstream communities. This information can ultimately result in significant economic benefit to these downstream communities. Optimizing crop planting strategy is just one example of the economic benefit that can be gained by having more accurate estimates of peak SWE.

For the three watersheds during the ablation period, goodness-of-fit statistics consistently indicated that the model did not accurately match the field measured SWE data. The sample mean error, mean relative error, standard deviation of the measured data, standard error of the estimate, and the ratio of the standard error of the estimate to the standard deviation of the measured data consistently indicated that the model did not improve the reliability of prediction as compared to the interannual mean SWE during

the ablation period for all three watersheds.

Additionally, it was determined that the model did not accurately match the physically significant values of the measured SWE data during the ablation period. Significant differences existed when comparing the measured and modeled date at which the snowpack became ripe, and the measured and modeled length of the ablation period.

These goodness-of-fit statistics and inaccurate predictions of the snowpack ripening date, and the length of the ablation period indicate that the model should not be used to make predictions during the ablation period. Inaccurate predictions, such as identifying an extreme discharge event, could have a deleterious impact on downstream communities, perhaps resulting in loss of property or life. Methods for improving model accuracy are discussed in the following section.

The developed SWE model utilized conditional probability to improve upon the accuracy of estimating sublimation rates, or wind transport rates. Conditional probability was used to estimate the portion of a day that the threshold wind speed was exceeded given the fact that the daily average wind speed was less than the threshold wind speed. This allowed for a more accurate representation of the sublimation and wind transport processes.

10.3 IMPROVING MODEL ACCURACY

To increase the usefulness of the model, ways of improving the model accuracy during the ablation period should be investigated. As previously discussed in Chapters

5 through 7, this task can best be accomplished by improving upon the methods of measuring and modeling net energy at a point. As shown in Eq. 3-14, the processes that constitute total net energy are: solar radiation, longwave radiation, sensible heat, latent heat, advective (rain) energy, and conductive heat exchange with the ground. As also previously discussed, advective (rain) energy and conductive heat exchange with the ground represent a very small portion of total net energy. As a result, efforts should be made to increase the accuracy of estimating solar radiation, longwave radiation, sensible heat, and latent heat.

As shown in Eq. 3-5 for solar radiation, the parameters that affect incoming solar radiation are: received clear sky radiation (K_{CS}), cloud cover (C_C), the snowpack albedo (A_{LB}), a shading factor (S_h), and a tree type factor ($f_3(F)$). Received clear sky radiation is dependent upon the day of year, and other constant watershed parameters, such as latitude and ground slope. As discussed in Chapter 3, many references exist for determining the albedo of a snowpack.

As demonstrated in Chapter 8, sensitivity analysis showed that cloud cover is an unimportant input for the overall net energy received at a point and that modeled output is insensitive to changes in cloud cover values. This was due to the effects that cloud cover had on longwave and incoming solar radiation. The unimportance of cloud cover is a result of the simplistic approach of modeling cloud cover. A more realistic approach of taking into account the height of the cloud cover as well as the air temperature would improve upon the accuracy of estimating both solar radiation and longwave radiation.

As previously mentioned, the algorithm for estimating net solar radiation is simplified. A more realistic distinction between modeling direct and diffuse solar radiation would improve the overall accuracy of estimating incoming solar radiation.

Additionally, improving the ability to estimate incoming solar radiation can be made by improving the ability to estimate S_h and $f_3(F)$. The shading factor for an HRU could be improved by a site investigation. An HRU could be examined to determine what percentage of the day the HRU is significantly shaded. This percentage could then be the value for the shading factor. The tree type factor for an HRU could also be improved by a site investigation, or by aerial photography. As discussed in Chapter 3, this tree type factor is dependent upon tree species, which again could be ascertained by either of these methods.

With improved estimates for both S_h and $f_3(F)$, each HRU should have a unique value for these inputs as opposed to a single value representing the entire watershed. These unique values could then be entered into the HRU physical characteristics input file, as opposed to setting these values as constants for all HRUs.

High resolution Lidar Swath mapping (e.g., NOVA Digital Systems, Incorporated, 2001. "LiDAR Mapping") can be used to improve the accuracy and precision of DEMs, and thus could contribute to better estimates of terrain slope and shading. To further improve estimates of incoming solar radiation, GIS could be used to create a time series of terrain shading factors for each HRU of the watershed. These time series could reflect the physical spatial variation of the watershed and account for the incidence angle of the sun as the seasons change.

As shown in Eq. 3-15 for longwave radiation, the parameters that affect longwave radiation are: the snowpack surface temperature (T_{SURF}), and the effective emissivity of the atmosphere and canopy ($_{at}$). In turn, as per Eqs. 3-16, 3-17, 3-4, and 3-25, the inputs affecting T_{SURF} and $_{at}$ are: average daily air temperature, minimum daily air temperature, cloud cover, forest cover, and a temperature factor defining the difference between the air temperature and the snow surface temperature (T_f). As previously mentioned, cloud cover is an unimportant input in the model as it presently treats net radiation. Values for forest cover are determined by means of land use data, and as long as these data are accurate, the corresponding forest cover values should also be accurate. Values for minimum and average daily air temperature should be accurate provided the field instruments are functioning properly.

Consequently, improvements in longwave radiation estimates could be made by monitoring or measuring snowpack surface temperatures on a regular basis. As demonstrated in Chapter 8, relative and deviation sensitivity analyses found that T_f is an important input for HRUs that are completely forested. Sensitivity analysis also showed that modeled output was sensitive to changes in T_f, especially for completely forested HRUs. Field measurements of T_{SURF} could significantly improve the accuracy of this variable, which in turn could increase the accuracy of longwave radiation estimates. For large watersheds, such as the Upper Rio Grande Watershed, T_{SURF} field measurements should be taken at several locations. Remote sensing may also prove useful in the estimation of T_{SURF} .

As shown in Eq. 3-21 for sensible heat exchange, the parameters that affect sensible heat are: average daily air temperature, snowpack surface temperature, wind speed through the canopy, if a canopy exists (W_{CAN}), and a stability correction factor (f_s). In turn, as per Eqs. 3-20 and 3-8, the inputs affecting W_{CAN} and f_s are: daily average air temperature, snowpack surface temperature, forest cover (F), forest density (F_d), and wind speed. Possible improvements in daily average air temperature, snowpack surface temperature, and forest cover have been discussed earlier in this chapter.

As previously discussed in Chapter 4, no current methods exist to extrapolate and distribute wind speeds from measurement sites to the watershed. Therefore improvements in wind speed estimates would involve recording more wind measurements on site, if feasible. Improvements in wind speed estimates could also be made by incorporating developing meteorological models designed to improve upon wind forecasting. Estimates for forest density could be improved upon by site inspection or by aerial photography. With improved estimates for F_d, each HRU should have a unique value for this input as opposed to a single value representing the entire watershed. This unique value could then be entered into the HRU physical characteristics input file, as was recommended for S_h and $f_3(F)$.

As shown in Eqs. 3-24 for latent heat exchange, the parameters that affect latent heat are: wind speed through the canopy, if a canopy exists, a stability correction factor , the vapor pressure at the snow surface (e_{ss}), and the near surface vapor pressure (e_a). Possible improvements in W_{CAN} and f_s have been discussed earlier in this chapter.

As per Eqs. 3-17, 3-4, and 3-23, the inputs affecting e_{ss} and e_a are: average daily

air temperature, minimum daily air temperature, and the snowpack surface temperature. Possible improvements in all of these inputs have been discussed earlier in this chapter.

Improvements in estimating the net energy received at a point will increase the accuracy of the model during the ablation period. This would result in better estimates of the date in which the snowpack ripens and the length of the ablation period. These improvements would ultimately allow the model user to utilize model output for predictive purposes such as identifying possible extreme stream discharge events or estimating the date at which stream discharge is affected by snowmelt. Ultimately, the developed SWE model should not be used for forecasting until model accuracy is increased during the ablation period.

As discussed in Chapter 4, conditional probability was utilized as an attempt to determine what percentage of a day the actual wind speed may have been greater than a threshold wind speed when the average wind speed for that particular day was less than the threshold wind speed. Figure 10-1 shows a plot of the conditional probability analysis performed on the wind data for the Upper Rio Grande Watershed. This figure suggests that for days in which the average wind speed was greater than the threshold wind speed (4.8 m/s), a fraction of these days still experienced wind speeds less than the threshold. This indicates that wind driven physical processes, such as wind transport of SWE, were over predicted on days that the average daily wind speed was greater than the threshold wind speed. Further work should incorporate a more thorough analysis of conditional probability.

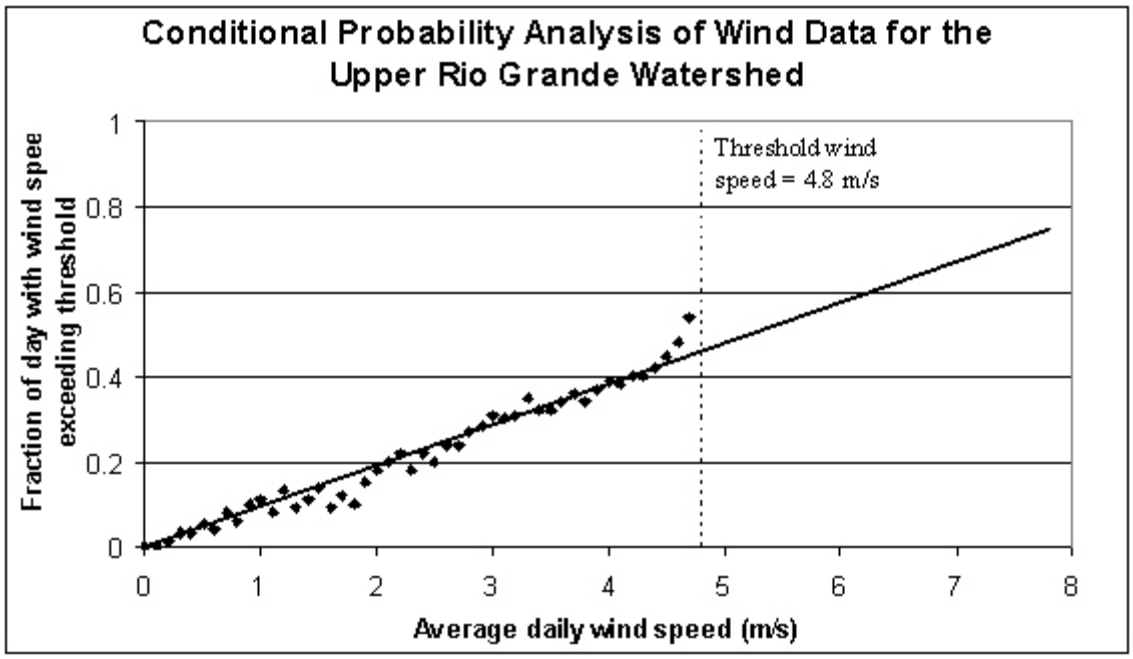

Figure 10-1. Plot of conditional probability analysis performed on the wind data for the Upper Rio Grande Watershed.

10.4 RESULTS OF THE SENSITIVITY ANALYSIS

The results of the sensitivity analyses presented in Chapter 8 regarding meteorological input data indicated that total precipitation is the most important meteorological parameter, regardless of canopy cover. Additionally, the relative sensitivity value of P_T increases as the canopy cover diminishes, corresponding to a decrease in interception. These results also indicated that model sensitivity to solar radiation, relative humidity, air temperature, and wind speed is dependent upon the canopy cover of an HRU. Additionally, these results indicated that the model was not sensitive to changes in cloud cover regardless of the canopy cover. These analyses ultimately aid the model user by identifying which input data are most important in

terms of data collection.

The results of the sensitivity analyses regarding the availability of SWE data suggest that weekly SWE data are sufficient to adequately calibrate the model. Knowing this fact could lead to significant savings in time and resources by requiring weekly, as opposed to daily, SWE field measurements, and thus may limit the risk faced by the data collectors. Additionally, if less than weekly SWE data are available, as was the case for the Reynolds Creek Watershed, greater uncertainty exists when attempting to calibrate/validate the model.

The results of the sensitivity analysis regarding the HRU subdivision process indicated that the model is sensitive to different HRU subdivisions because of the resulting changes to the HRU physical characteristics. Peak SWE values appeared to be sensitive primarily to changes in mean slope. Snowpack ripening, length of ablation period, and the resulting mean SWE values appeared to be sensitive to significant changes in elevation, mean slope, or aspect, resulting from the varying subdivision process. The results of the analysis regarding the HRU subdivision process ultimately suggest that smaller HRUs provide more accurate SWE predictions. However, smaller HRUs mean more HRUs and more parameters to estimate. A model user must use judgement to find the proper balance.

10.5 ASSESSING THE SIMILARITY OF SWE PATTERNS

As presented in Chapter 9, variability exists in the interannual SWE distributions for all three watersheds. The Kolmogorov-Smirnov two-sample nonparametric test was

used to test two different distributions. This test is sensitive to differences in any characteristics of a distribution, such as central tendency, dispersion, or skewness. As a result, the distributions tested were required to have similar means, or the results of the test would always indicate that the distributions were dissimilar. Results of the Kolmogorov-Smirnov two-sample nonparametric tests suggest that model input variability prevents similar interannual SWE distributions from consistently occurring for all three watersheds. Since the physical characteristics of a watershed remain essentially constant in time, the input variability must be contained in the meteorological data. This variability is most likely the result of short- term phenomena, such as storm and wind patterns. In addition to input variability, nonlinear transport processes, such as wind transport and avalanching, could also prevent similar interannual SWE distributions from consistently occurring.

The results of the SWE and meteorological rankings for the Upper Rio Grande Watershed support the claim that model input variability prevents similar interannual SWE distributions from consistently occurring during the early accumulation period and late ablation period. However, the results of the rankings also indicated that similar interannual SWE distributions occur consistently during the remainder of the water year despite meteorological variability during this same time period. These results suggest that meteorological variability has much less effect on SWE distributions during this time period, approximately January to May for the Upper Rio Grande Watershed.

The results of the rankings for the Upper Rio Grande Watershed seem to validate the depletion curve theory. Most of the assumptions regarding the depletion curve

theory apply at the time of snowpack ripening. One such example is estimating the date in which a snowpack becomes ripe and thus melt (depletion) begins. During this time, SWE rankings for the Upper Rio Grande Watershed were fairly consistent from year to year suggesting the existence of similar, interannual SWE patterns. These similar, interannual SWE patterns allow for the assumptions made regarding the depletion curve theory in the early part of the melt season.

10.6 RECOMMENDED FUTURE RESEARCH

Future research should be concentrated on three tasks. The first task has been previously discussed, and is the improvement of model accuracy. Improvements to the model accuracy must be made during the ablation period if the model is to be used for predicting or forecasting. As previously discussed, efforts should center upon increasing the accuracy of predicting net energy at a point.

The second task involves additional analyses of identifying similar, interannual SWE patterns. Many methods of stream forecasting utilize the depletion curve theory. The assumptions of this theory have not been adequately tested. The results from the Upper Rio Grande Watershed appear to support the theory early in the ablation period. However, these results are based on a few years in a single watershed. Additional watersheds need to be tested to determine the validity of the depletion curve theory. To test the depletion curve theory will require analytical tools to study the temporal evolution of the spatial probability density function of SWE, as well as accurate, finely resolved maps of SWE, whether from remote sensing or from improved distributed

models.

Part of the analyses of identifying interannual SWE patterns involved the creation of a time series of SWE maps for the Upper Rio Grande Watershed. To fully determine if these maps support the existence of interannual SWE patterns, additional analyses involving spatial statistics need to be performed.

The final task involves utilizing modeled SWE output as input for an existing hydrologic runoff model. If modeled SWE output can be used to improve upon stream discharge forecasting, downstream communities could reap significant benefits. Accurate melt predictions of SWE on a warm, windy day, accompanied by heavy rain, could help to identify a severe discharge event which could not only result in an economic benefit to downstream communities, but could also quite possibly help to save lives.

Appendix A

Summary of the Physical Characteristics of the HRUs Created for the Three Watersheds

Table 4-1. Summary of the physical parameters of the HRUs created for the Upper Rio Grande Watershed.

HRU ID	Elevation (m)	Slope (degrees)	% Forest Cover*	Aspect (degrees)	Latitude (degrees)	Area (km^2)
1	3716	4	0	135	37.7	27.6
2	3691	5.2	0	135	37.8	110.2
3	3472	2	10 - Con	135	37.6	12.4
4	3404	4.8	70 - Con	135	37.6	38
5	3675	6.7	10 - Con	45	37.6	21.9
6	3634	3.9	20 - Con	45	37.6	12.4
7	3560	7.6	80 - Con	90	37.6	58.9
8	3625	8.1	90 - Con	45	37.6	15.2
9	3178	4.7	90 - Con	60	37.6	64.6
10	3137	3.4	40 - Mix	60	37.6	87.4
11	3427	5.8	60 - Mix	90	37.7	39.9
12	3748	5.2	20 - Con	135	37.9	5.7
13	3286	3.5	70 - Con	135	37.8	88.4
14	3521	4.3	70 - Con	135	37.9	15.2
15	3460	7	90 - Con	45	37.5	26.6
16	3054	4.3	90 - Con	315	37.6	69.4
17	3381	6.5	90 - Con	0	37.6	62.7
18	3622	5.1	20 - Con	25	37.5	15.2
19	3517	6.2	60 - Con	90	37.5	43.7
20	3419	4	70 - Con	225	37.9	86.5
21	3143	3	20 - Con	90	37.8	12.4
22	3059	3	50 - Con	180	37.7	41.9
23	2905	2.4	20 - Con	225	37.6	51.3

Table 4-1. Summary of the physical parameters of the HRUs created for the Rio Grande Watershed, Continued.

HRU ID	Elevation (m)	Slope (degrees)	% Forest Cover*	Aspect (degrees)	Latitude (degrees)	Area (km^2)
24	2771	1.1	90 - Con	45	37.6	9.5
25	3285	9.7	100 - Con	0	37.4	22.8
26	3234	6.5	90 - Con	0	37.5	96.9
27	3563	3.4	20 - Con	135	37.8	57
28	3663	6.6	30 - Con	225	37.9	26.6
29	3370	6.3	80 - Mix	45	37.7	37.1
30	2952	5.2	80 - Mix	45	37.6	21.9
31	2754	1	0	315	37.6	30.4
32	2966	6.2	70 - Mix	90	37.6	37.1
33	3459	5.3	80 - Mix	180	37.8	57
34	3045	10.9	70 - Mix	180	37.7	58.9
35	2896	2	0	225	37.6	42.8
36	3483	6.5	90 - Con	0	37.4	96.9
37	2805	6.1	90 - Mix	45	37.6	37.1
38	3221	10.1	100 - Con	45	37.6	49.4
39	3279	6.4	90 - Con	315	37.5	74.1
40	3423	9	100 - Con	0	37.5	44.7
41	3259	5.8	70 - Mix	225	37.8	35.2
42	3591	2.3	30 - Con	180	37.8	10.5
43	3495	4.1	90 - Con	180	37.8	25.7
44	3300	5.2	100 - Con	180	37.7	63.7
45	2922	4.5	90 - Con	225	37.6	58
46	3456	4	10 - Con	180	37.7	20.9

Table 4-1. Summary of the physical parameters of the HRUs created for the Rio Grande Watershed, Continued.

HRU ID	Elevation (m)	Slope (degrees)	% Forest Cover*	Aspect (degrees)	Latitude (degrees)	Area (km^2)
47	3249	6.6	100 - Con	45	37.5	96.9
48	3130	5.7	100 - Con	45	37.6	59.9
49	2762	3.8	100 - Con	90	37.6	34.2
50	3391	6.2	100 - Con	60	37.3	26.6
51	3123	7.9	100 - Con	60	37.3	22.8
52	3265	7.3	100 - Con	0	37.3	105.5
53	3267	6.2	100 - Con	330	37.3	93.1
54	3163	7	100 - Con	90	37.4	20.9
55	3009	7.1	100 - Con	90	37.4	34.2
56	2749	5.8	100 - Con	90	37.6	83.6
57	2965	4.2	100 - Con	45	37.4	11.4
58	3324	3.1	100 - Con	45	37.3	20.9
59	2798	6	100 - Con	90	37.4	47.5
60	2592	4.2	90 - Con	90	37.5	14.3
61	3416	3.7	100 - Con	225	37.6	39
62	3530	3.8	90 - Con	90	37.7	17.1
63	3610	3.9	0	225	37.7	6.7
64	3194	5.8	100 - Con	180	37.6	80.8
65	3002	4.9	100 - Con	315	37.4	79.8
66	3244	5.2	100 - Con	225	37.7	12.4
67	3007	7.2	40 - Con	180	37.7	24.7
68	3062	10.8	100 - Con	180	37.6	13.3
69	2734	6.5	100 - Con	135	37.6	7.6

Table 4-1. Summary of the physical parameters of the HRUs created for the Rio Grande Watershed, Continued.

HRU ID	Elevation (m)	Slope (degrees)	% Forest Cover*	Aspect (degrees)	Latitude (degrees)	Area (km^2)
70	2822	5.6	0	180	37.6	53.2
71	3338	4.4	90 - Con	315	37.4	96
72	2644	3.4	0	225	37.6	19
73	2999	6.2	100 - Con	0	37.5	23.8
74	2772	4.9	90 - Con	0	37.5	26.6
75	2583	4	60 - Con	60	37.5	53.2
76	2967	7	90 - Con	45	37.6	14.3
77	2490	0.9	0	90	37.5	123.5
78	2657	4	0	135	37.6	87.4
79	3081	8.1	90 - Mix	45	37.4	31.4
80	2926	7.4	0	315	37.4	36.1
81	2907	8.9	0	60	37.5	23.8
82	2659	5.9	0	45	37.5	32.3
83	2920	6.5	70 - Mix	135	37.6	11.4

*Con - coniferous forest; Mix- mixture of coniferous and deciduous forest.

Table 4-5. Summary of the physical parameters of the HRUs created for the Reynolds Creek Watershed.

HRU ID	Elevation (m)	Slope (degrees)	% Forest Cover*	Aspect (degrees)	Latitude (degrees)	Area (km^2)
1	1622	18	50 - Dec	135	43.3	3.8
2	1487.5	17	0	135	43.3	3.8
3	1322.3	9.3	0	160	43.3	6.65
4	1612	19	50 - Mix	135	43.3	2.85
5	1522.4	15.8	30 - Mix	135	43.3	4.75
6	1355.8	12.5	0	90	43.3	6.65
7	1215	6.8	0	90	43.3	8.55
8	1169	4.2	0	60	43.2	11.4
9	1267.5	6.7	0	270	43.2	8.55
10	1577	13.9	50 - Mix	90	43.2	8.55
11	1396	12.6	50 - Mix	90	43.2	7.6
12	1208	5.3	0	45	43.2	11.4
13	1614.3	12.8	40 - Mix	45	43.2	7.6
14	1308	7.2	0	315	43.2	8.55
15	1210.5	2.3	0	0	43.2	5.7
16	1448	12.5	50 - Dec	45	43.2	8.55
17	1282	7	0	0	43.2	5.7
18	1408.5	9.3	0	315	43.2	5.7
19	1527	14	50 - Mix	45	43.1	8.55
20	1402.5	13.5	0	0	43.1	5.7
21	1565.5	12.3	0	315	43.1	5.7
22	1649	10.7	0	315	43.1	5.7
23	1801	15	50 - Mix	290	43.1	2.85

Table 4-5. Summary of the physical parameters of the HRUs created for the Reynolds Creek Watershed, continued.

HRU ID	Elevation (m)	Slope (degrees)	% Forest Cover*	Aspect (degrees)	Latitude (degrees)	Area (km^2)
24	1633	15.1	60 - Mix	135	43	9.5
25	1763	14.5	0	270	43	5.7
26	1830.4	13.3	50 - Mix	43	43	7.6
27	1837	12.7	60 - Mix	315	43	6.65
28	1978	12	70 - Mix	45	43	8.55

*Dec - deciduous forest; Mix- mixture of coniferous and deciduous forest.

Table 4-9. Summary of the physical parameters of the HRUs created for the Emerald Lake Watershed.

HRU ID	Elevation (m)	Slope (degrees)	% Forest Cover*	Aspect (degrees)	Latitude (degrees)	Area (hectares)
1	2935	30	0	260	36.6	11
2	3037	26	0	270	36.6	15
3	3237	30	0	315	36.6	16.5
4	3122	33	0	345	36.6	11
5	3032	27.5	0	0	36.6	19.5
6	2965	34	0	45	36.6	13.5
7	3087	40	80 - Con	60	36.6	6.5
8	2865	17	0	0	36.6	18

*Con - coniferous forest

Appendix B

Plots Depicting the Characteristics of the HRUs Created for the Upper Rio Grande Watershed.

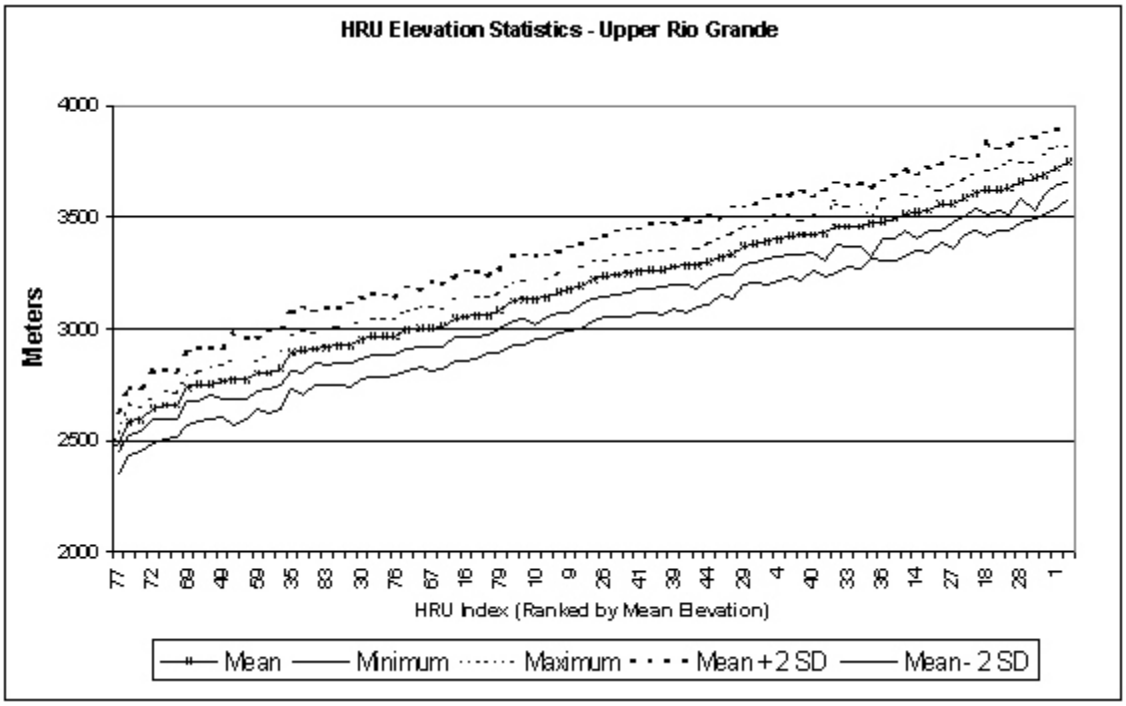
HRU Elevation Statistics - Upper Rio Grande
Meters
4000
3500
3000
2500
2000
77 72 69 49 89 85 83 80 76 67 16 79 10 9 26 41 38 44 29 4 40 33 36 14 27 18 28 1
HRU Index (Ranked by Mean Elevation)
Mean
Minimum
Maximum
Mean + 2 SD
Mean - 2 SD

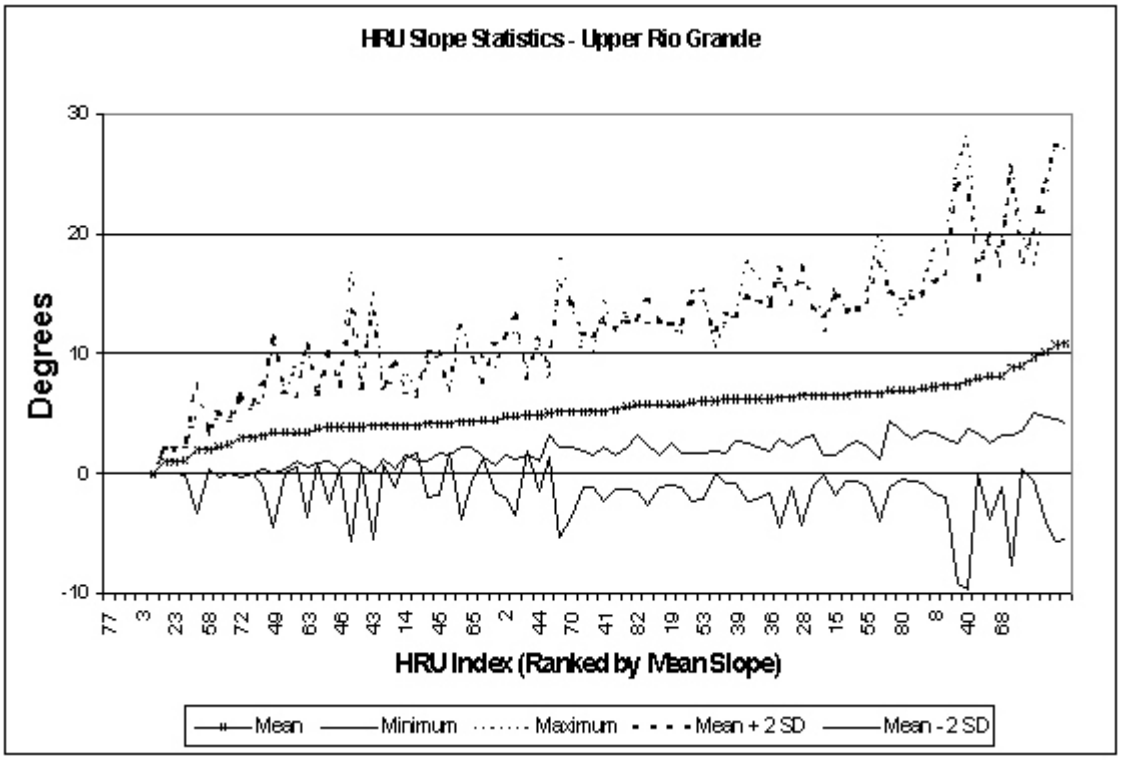
HRU Slope Statistics - Upper Rio Grande
Degrees
30
20
10
0
-10
77 3 23 58 72 49 63 46 43 14 45 65 2 44 70 41 82 19 53 39 36 28 15 55 80 8 40 68
HRU Index (Ranked by Mean Slope)
Mean
Minimum
Maximum
Mean + 2 SD
Mean - 2 SD

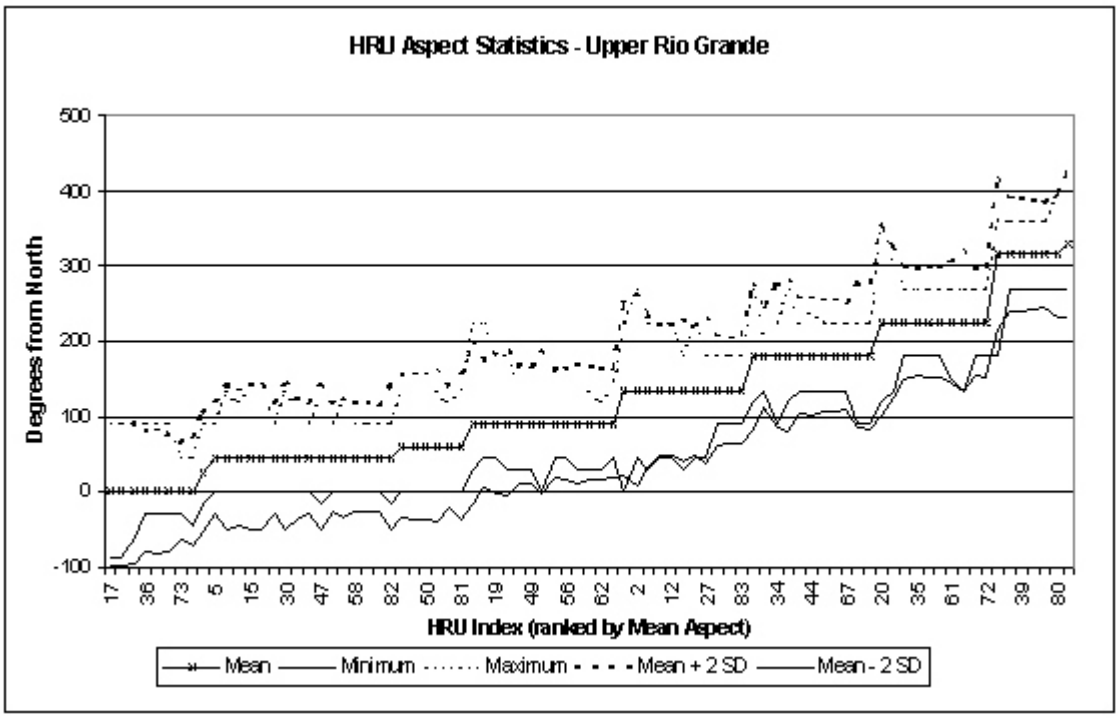
HRU Aspect Statistics - Upper Rio Grande
Degrees from North
500
400
300
200
100
0
-100
17 36 73 5 15 30 47 58 82 50 81 19 49 56 62 2 12 27 83 34 44 67 20 35 61 72 39 80
HRU Index (ranked by Mean Aspect)
Mean
Minimum
Maximum
Mean + 2 SD
Mean - 2 SD

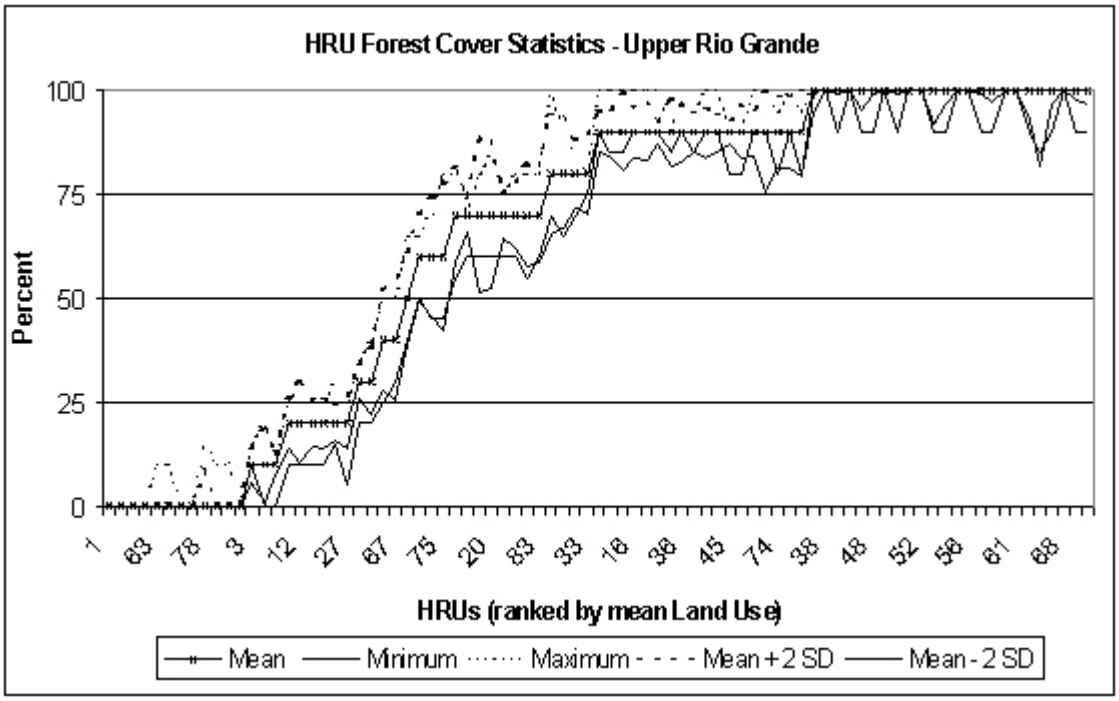
HRU Forest Cover Statistics - Upper Rio Grande
Percent
100
75
50
25
0
1 63 78 3 12 27 67 75 20 83 33 16 36 45 74 38 48 52 56 61 68
HRUs (ranked by mean Land Use)
Mean
Minimum
Maximum
Mean + 2 SD
Mean - 2 SD

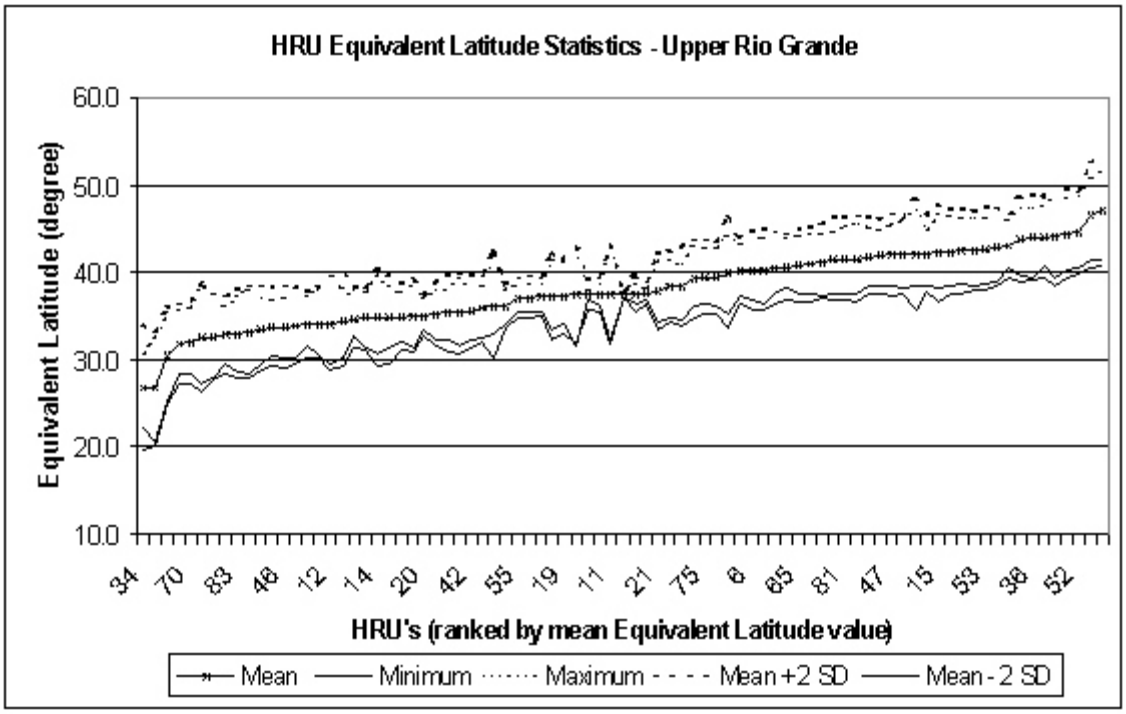

Note: See Eq. 4-1 on page 69 for determining equivalent latitude.

Appendix C

The Conditional Probability Analysis Performed on the Wind Data for the Upper Rio Grande Watershed.

Table 4-4. Results of the conditional probability analysis performed on the wind data for the Upper Rio Grande Watershed.

Daily average wind speed (m / s)	Sample Size (days)	Probability that the hourly data exceeded the threshold value (4.8 m / s)
0	10	0.00
0.1	12	0.00
0.2	17	0.01
0.3	17	0.03
0.4	15	0.03
0.5	25	0.05
0.6	15	0.04
0.7	17	0.08
0.8	17	0.06
0.9	21	0.10
1.0	18	0.11
1.1	20	0.08
1.2	27	0.13
1.3	24	0.09
1.4	21	0.11
1.5	23	0.14
1.6	35	0.09
1.7	26	0.12
1.8	34	0.10
1.9	27	0.15
2.0	31	0.18

Table 4-4. Results of the conditional probability analysis performed on the wind data for the Upper Rio Grande Watershed, Continued.

Daily average wind speed (m / s)	Sample Size (days)	Probability that the hourly data exceeded the threshold value (4.8 m / s)
2.1	26	0.20
2.2	31	0.22
2.3	27	0.18
2.4	30	0.22
2.5	34	0.20
2.6	35	0.24
2.7	26	0.24
2.8	40	0.27
2.9	32	0.28
3.0	38	0.31
3.1	41	0.30
3.2	37	0.31
3.3	24	0.35
3.4	41	0.32
3.5	45	0.32
3.6	28	0.34
3.7	39	0.36
3.8	31	0.34
3.9	38	0.37
4.0	22	0.39
4.1	42	0.38

Table 4-4. Results of the conditional probability analysis performed on the wind data for the Upper Rio Grande Watershed, Continued.

Daily average wind speed (m / s)	Sample Size (days)	Probability that the hourly data exceeded the threshold value (4.8 m / s)
4.2	28	0.40
4.3	28	0.40
4.4	24	0.42
4.5	19	0.45
4.6	27	0.48
4.7	22	0.54
TOTAL	1307	-

Appendix D

Plots Depicting the Characteristics of the HRUs Created for the Reynolds Creek Watershed.

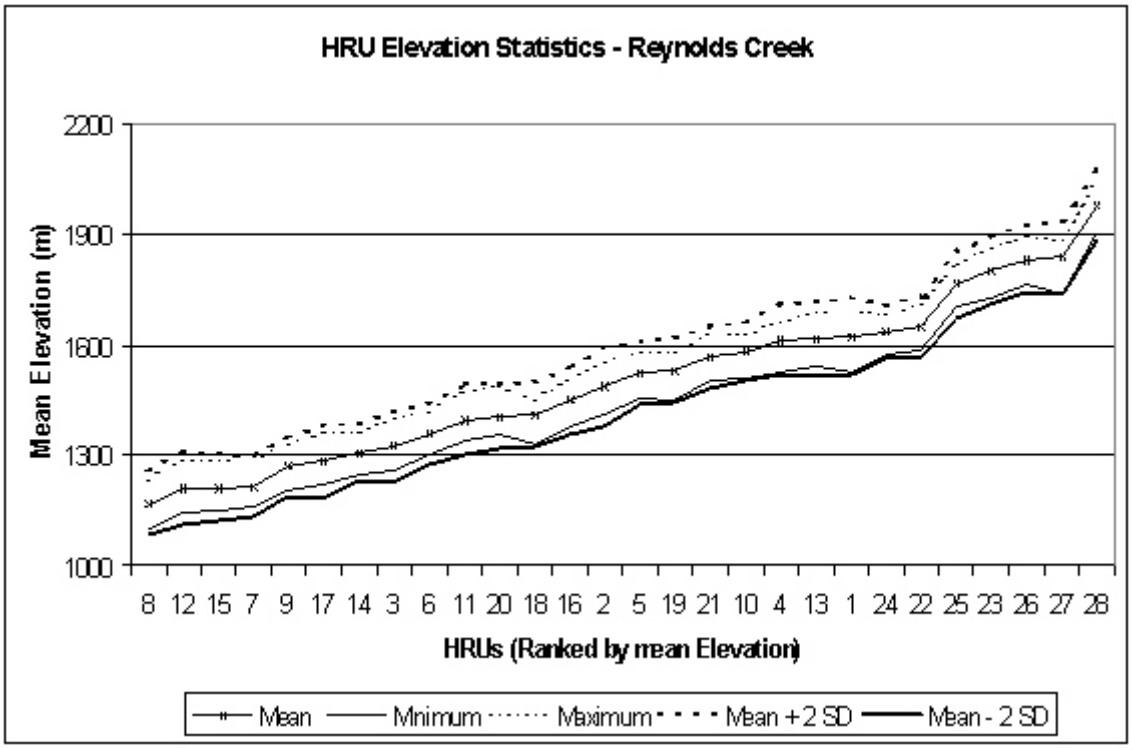
HRU Elevation Statistics - Reynolds Creek
Mean Elevation (m)
2200
1900
1600
1300
1000
8 12 15 7 9 17 14 3 6 11 20 18 16 2 5 19 21 10 4 13 1 24 22 25 23 26 27 28
HRUs (Ranked by mean Elevation)
Mean
Mnimum
Maximum
Mean +2 SD
Mean - 2 SD

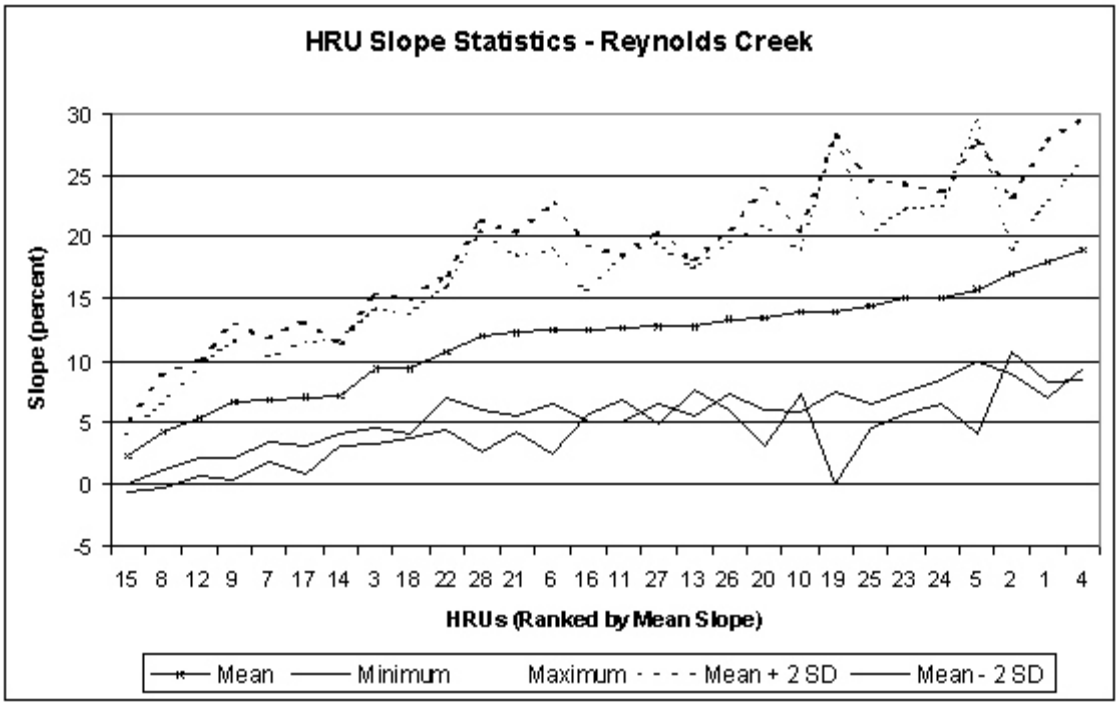
HRU Slope Statistics - Reynolds Creek
Slope (percent)
30
25
20
15
10
5
0
-5
15 8 12 9 7 17 14 3 18 22 28 21 6 16 11 27 13 26 20 10 19 25 23 24 5 2 1 4
HRUs (Ranked by Mean Slope)
Mean
Minimum
Maximum
Mean + 2 SD
Mean - 2 SD

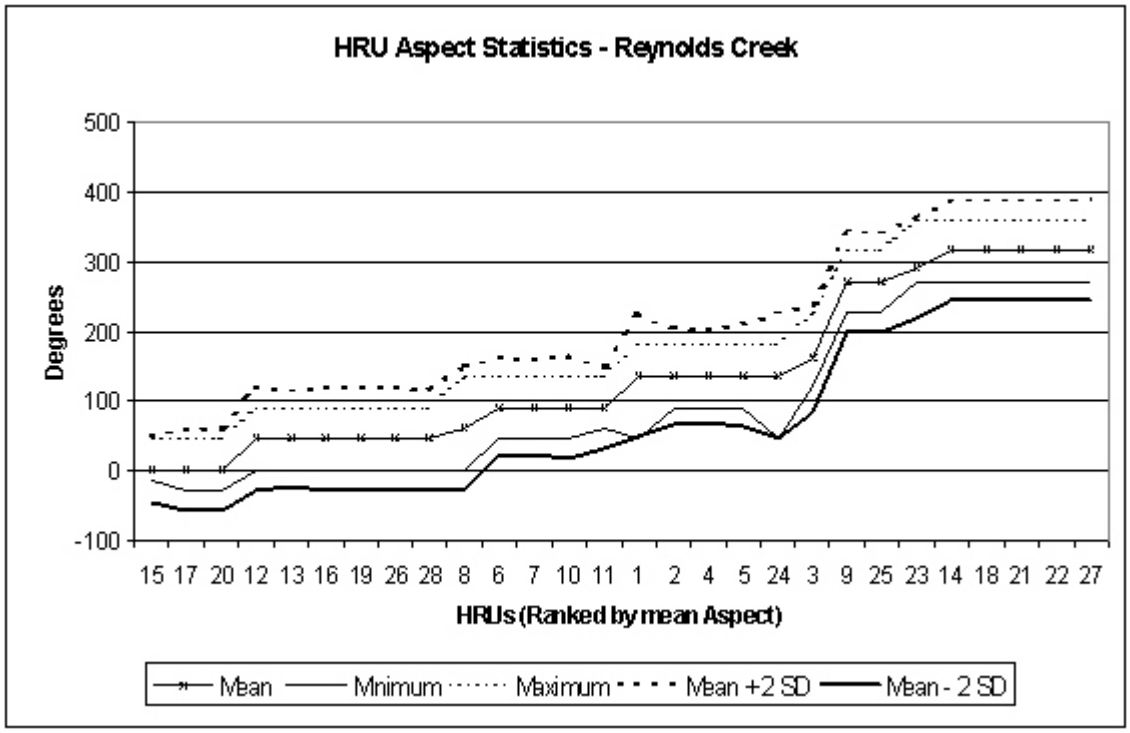
HRU Aspect Statistics - Reynolds Creek
Degrees
500
400
300
200
100
0
-100
15 17 20 12 13 16 19 26 28 8 6 7 10 11 1 2 4 5 24 3 9 25 23 14 18 21 22 27
HRUs (Ranked by mean Aspect)
Mean
Mnimum
Maximum
Mean +2 SD
Mean - 2 SD

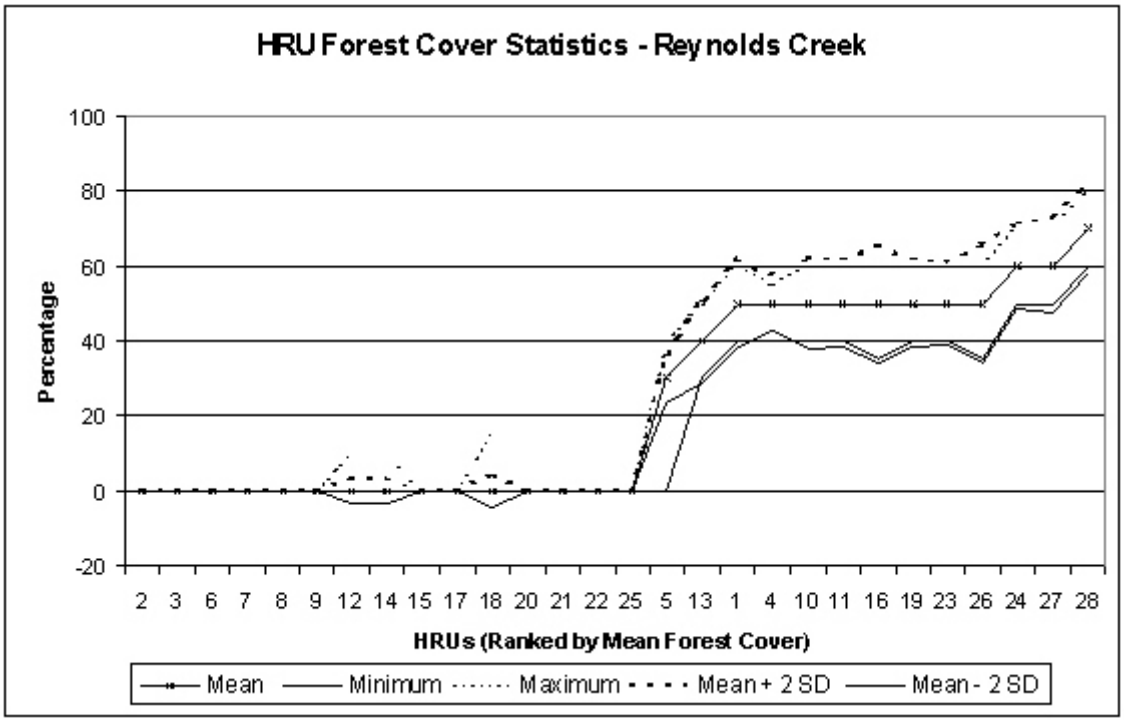
HRU Forest Cover Statistics - Reynolds Creek
Percentage
100
80
60
40
20
0
-20
2 3 6 7 8 9 12 14 15 17 18 20 21 22 25 5 13 1 4 10 11 16 19 23 26 24 27 28
HRUs (Ranked by Mean Forest Cover)
Mean
Minimum
Maximum
Mean + 2 SD
Mean - 2 SD

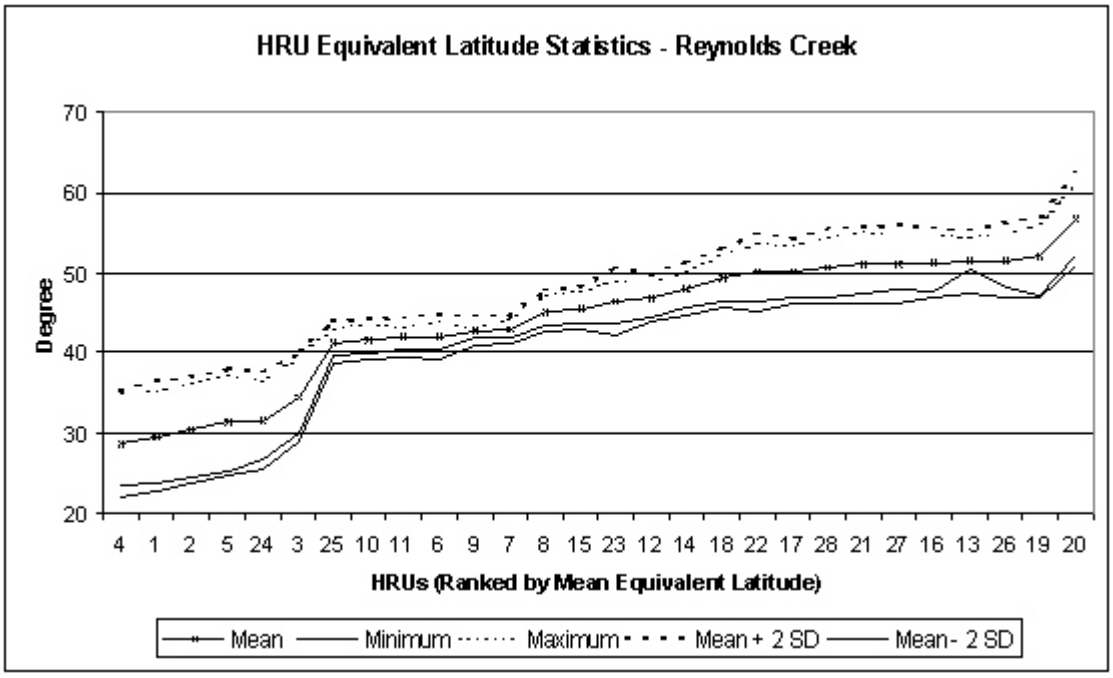

Note: See Eq. 4-1 on page 69 for determining equivalent latitude.

Appendix E

The Conditional Probability Analysis Performed on the Wind Data for the Reynolds Creek Watershed.

Table 4-7. Results of the conditional probability analysis performed on the wind data for the Reynolds Creek Watershed.

Daily average wind speed (m / s)	Sample Size (days)	Probability that the hourly data exceeded the threshold value (4.8 m / s)
0	7	0.00
0.1	14	0.00
0.2	11	0.01
0.3	13	0.00
0.4	12	0.02
0.5	12	0.02
0.6	15	0.03
0.7	17	0.08
0.8	17	0.05
0.9	23	0.06
1.0	21	0.10
1.1	16	0.08
1.2	27	0.08
1.3	21	0.10
1.4	20	0.12
1.5	28	0.11
1.6	31	0.07
1.7	24	0.12
1.8	29	0.18
1.9	24	0.17
2.0	26	0.18

Table 4-7. Results of the conditional probability analysis performed on the wind data for the Reynolds Creek Watershed, Continued.

Daily average wind speed (m / s)	Sample Size (days)	Probability that the hourly data exceeded the threshold value (4.8 m / s)
2.1	14	0.18
2.2	35	0.19
2.3	25	0.26
2.4	30	0.21
2.5	36	0.24
2.6	34	0.23
2.7	28	0.27
2.8	33	0.25
2.9	36	0.31
3.0	31	0.31
3.1	34	0.30
3.2	27	0.32
3.3	33	0.31
3.4	34	0.33
3.5	44	0.33
3.6	34	0.37
3.7	39	0.31
3.8	28	0.34
3.9	35	0.41
4.0	37	0.35
4.1	33	0.38

Table 4-7. Results of the conditional probability analysis performed on the wind data for the Reynolds Creek Watershed, Continued.

Daily average wind speed (m / s)	Sample Size (days)	Probability that the hourly data exceeded the threshold value (4.8 m / s)
4.2	36	0.36
4.3	28	0.45
4.4	25	0.38
4.5	21	0.48
4.6	23	0.53
4.7	22	0.52
TOTAL	1243	-

Appendix F

Plots Depicting the Characteristics of the HRUs Created for the Emerald Lake Watershed.

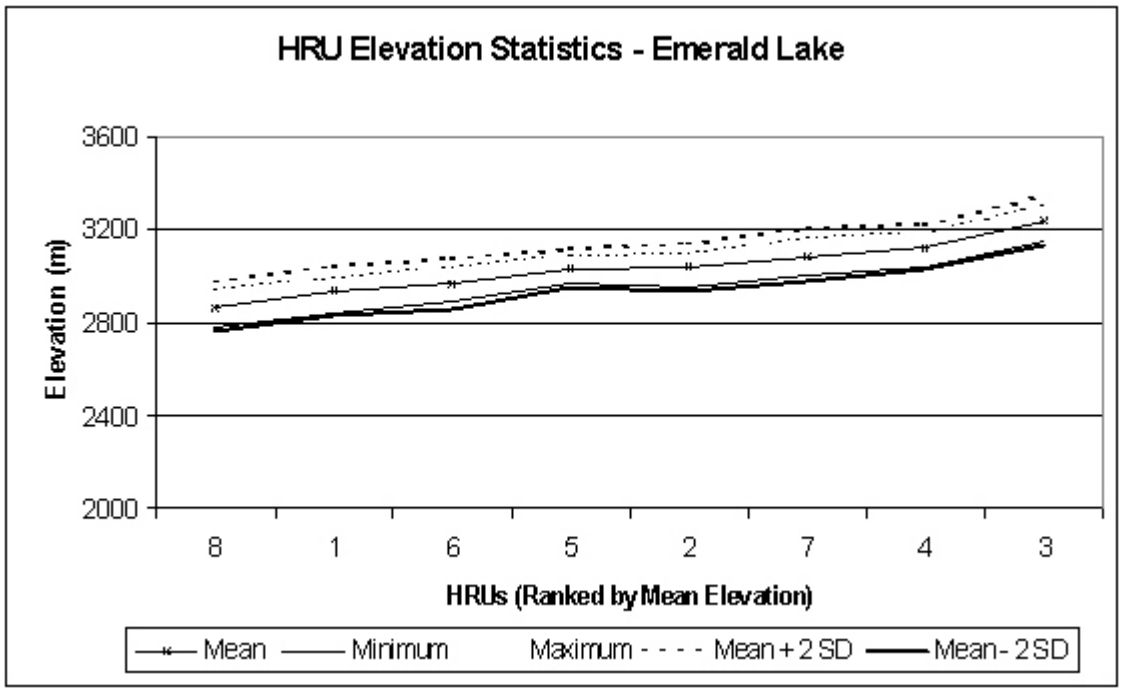
HRU Elevation Statistics - Emerald Lake
3600
3200
2800
2400
2000
Elevation (m)
8
1
6
5
2
7
4
3
HRUs (Ranked by Mean Elevation)
Mean
Minimum
Maximum
Mean + 2 SD
Mean - 2 SD

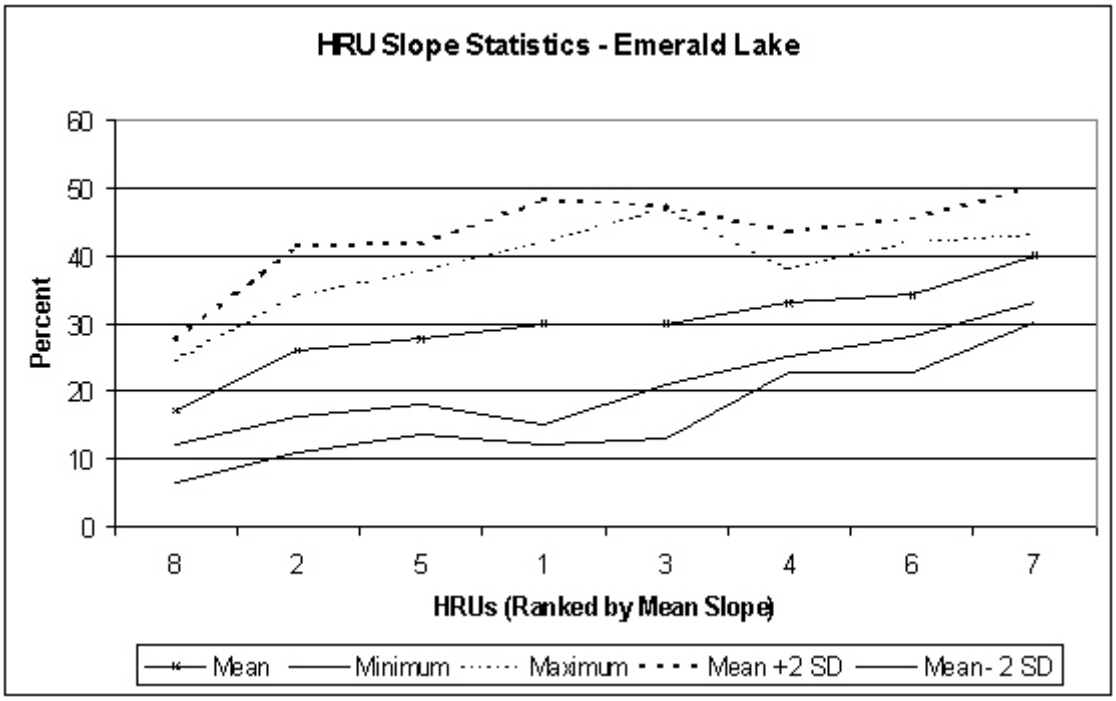
HRU Slope Statistics - Emerald Lake
60
50
40
30
20
10
0
Percent
8
2
5
1
3
4
6
7
HRUs (Ranked by Mean Slope)
Mean
Minimum
Maximum
Mean +2 SD
Mean - 2 SD

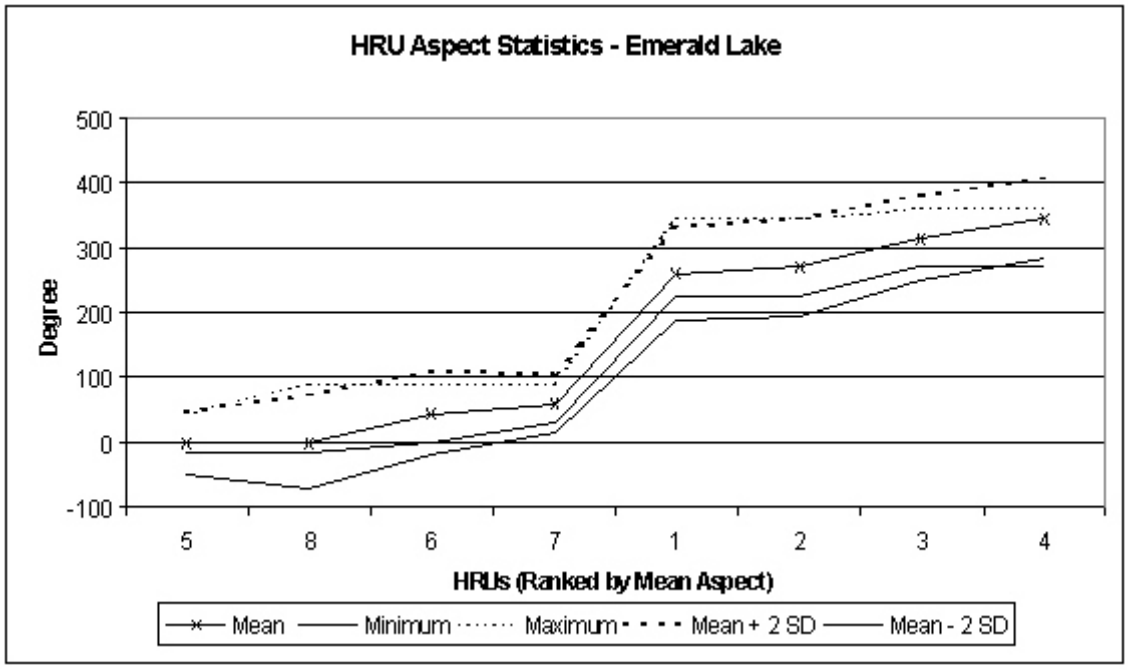
HRU Aspect Statistics - Emerald Lake
Degree
500
400
300
200
100
0
-100
5
8
6
7
1
2
3
4
HRUs (Ranked by Mean Aspect)
Mean
Minimum
Maximum
Mean + 2 SD
Mean - 2 SD

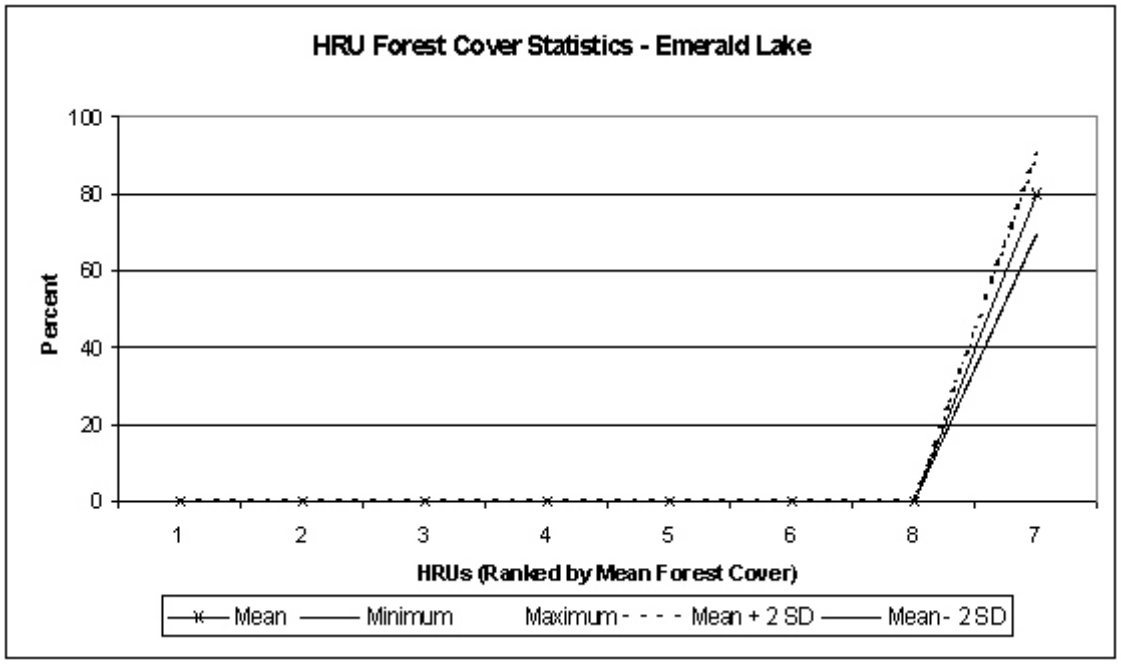
HRU Forest Cover Statistics - Emerald Lake
Percent
100
80
60
40
20
0
1
2
3
4
5
6
8
7
HRUs (Ranked by Mean Forest Cover)
Mean
Minimum
Maximum
Mean + 2 SD
Mean - 2 SD

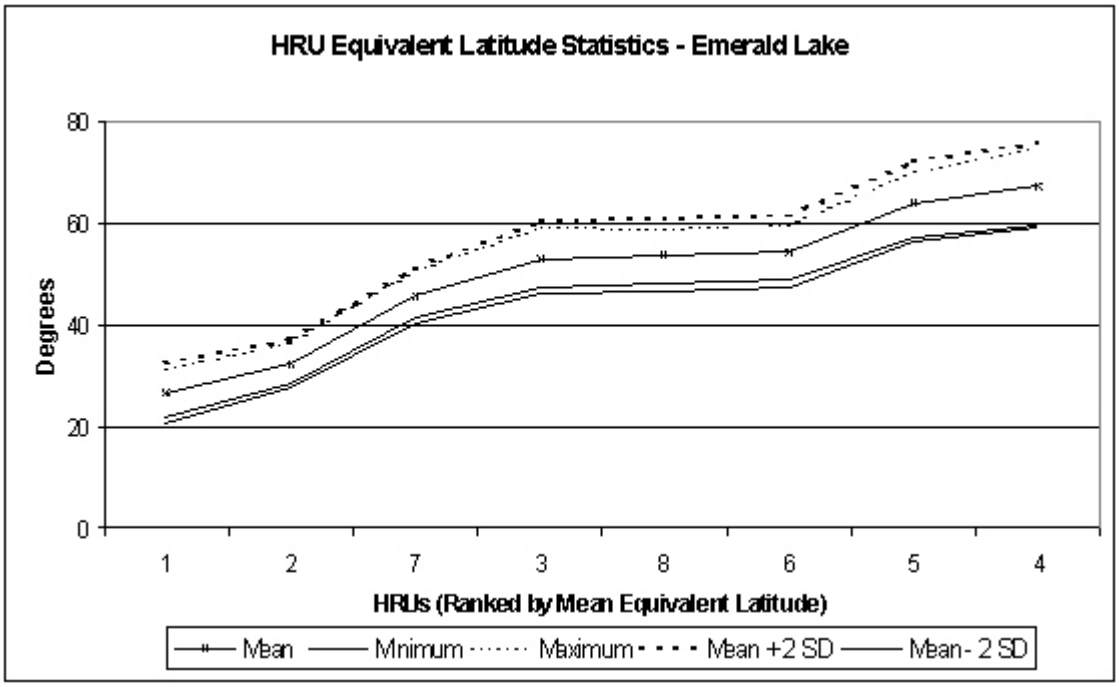

Note: See Eq. 4-1 on page 69 for determining equivalent latitude.

Appendix G

The Conditional Probability Analysis Performed on the Wind Data for the Emerald Lake Watershed

Table 4-11. Results of the conditional probability analysis performed on the wind data for the Emerald Lake Watershed concerning sublimation.

Daily average wind speed (m / s)	Sample Size (days)	Probability that the hourly data exceeded the threshold value (4.8 m / s)
0	13	0.00
0.1	11	0.00
0.2	13	0.00
0.3	12	0.02
0.4	14	0.05
0.5	16	0.04
0.6	17	0.05
0.7	18	0.05
0.8	19	0.09
0.9	24	0.08
1.0	17	0.08
1.1	18	0.11
1.2	19	0.09
1.3	24	0.07
1.4	24	0.09
1.5	22	0.10
1.6	24	0.11
1.7	28	0.15
1.8	23	0.13
1.9	21	0.14
2.0	23	0.18

Table 4-11. Results of the conditional probability analysis performed on the wind data for the Emerald Lake Watershed concerning sublimation, Continued.

Daily average wind speed (m / s)	Sample Size (days)	Probability that the hourly data exceeded the threshold value (4.8 m / s)
2.1	25	0.15
2.2	28	0.16
2.3	29	0.18
2.4	31	0.21
2.5	32	0.22
2.6	34	0.15
2.7	29	0.20
2.8	21	0.19
2.9	31	0.22
3.0	33	0.21
3.1	29	0.27
3.2	32	0.23
3.3	43	0.22
3.4	39	0.26
3.5	36	0.31
3.6	31	0.28
3.7	36	0.30
3.8	32	0.35
3.9	39	0.37
4.0	34	0.40
4.1	36	0.38

Table 4-11. Results of the conditional probability analysis performed on the wind data for the Emerald Lake Watershed concerning sublimation, Continued.

Daily average wind speed (m / s)	Sample Size (days)	Probability that the hourly data exceeded the threshold value (4.8 m / s)
4.2	29	0.42
4.3	21	0.47
4.4	23	0.45
4.5	26	0.51
4.6	19	0.50
4.7	21	0.52
TOTAL	1219	-

Appendix H

The Results of the Conditional Probability Analysis Performed on the Wind Data for the Emerald Lake Watershed for Wind Transport from an Alpine HRU

Table 4-12. Results of the conditional probability analysis performed on the wind data for the Emerald Lake Watershed for wind transport from an alpine HRU.

Daily average wind speed (m / s)	Sample Size (days)	Probability that the hourly data exceeded the threshold value (5.0 m / s)
0	13	0.00
0.1	11	0.00
0.2	13	0.00
0.3	12	0.01
0.4	14	0.04
0.5	16	0.03
0.6	17	0.04
0.7	18	0.04
0.8	19	0.07
0.9	24	0.08
1.0	17	0.08
1.1	18	0.10
1.2	19	0.08
1.3	24	0.06
1.4	24	0.08
1.5	22	0.10
1.6	24	0.11
1.7	28	0.15
1.8	23	0.13
1.9	21	0.14
2.0	23	0.18

Table 4-12. Results of the conditional probability analysis performed on the wind data for the Emerald Lake Watershed for wind transport from an alpine HRU, continued.

Daily average wind speed (m / s)	Sample Size (days)	Probability that the hourly data exceeded the threshold value (5.0 m / s)
2.1	25	0.14
2.2	28	0.15
2.3	29	0.17
2.4	31	0.20
2.5	32	0.21
2.6	34	0.14
2.7	29	0.20
2.8	21	0.19
2.9	31	0.22
3.0	33	0.21
3.1	29	0.27
3.2	32	0.23
3.3	43	0.21
3.4	39	0.25
3.5	36	0.30
3.6	31	0.27
3.7	36	0.29
3.8	32	0.35
3.9	39	0.37
4.0	34	0.39
4.1	36	0.36

Table 4-12. Results of the conditional probability analysis performed on the wind data for the Emerald Lake Watershed for wind transport from an alpine HRU, continued.

Daily average wind speed (m / s)	Sample Size (days)	Probability that the hourly data exceeded the threshold value (5.0 m / s)
4.2	29	0.41
4.3	21	0.47
4.4	23	0.44
4.5	26	0.50
4.6	19	0.49
4.7	21	0.49
4.8	18	0.51
4.9	16	0.54
TOTAL	1253	-

Appendix I

The Results of the Conditional Probability Analysis Performed on the Wind Data for the Emerald Lake Watershed for Wind Transport from a Valley or Prairie HRU

Table 4-13. Results of the conditional probability analysis performed on the wind data for the Emerald Lake Watershed for wind transport from a valley or prairie HRU.

Daily average wind speed (m / s)	Sample Size (days)	Probability that the hourly data exceeded the threshold value (6.5 m / s)
0	13	0.00
0.1	11	0.00
0.2	13	0.00
0.3	12	0.00
0.4	14	0.00
0.5	16	0.00
0.6	17	0.00
0.7	18	0.00
0.8	19	0.00
0.9	24	0.00
1.0	17	0.00
1.1	18	0.00
1.2	19	0.00
1.3	24	0.00
1.4	24	0.00
1.5	22	0.00
1.6	24	0.0
1.7	28	0.00
1.8	23	0.00
1.9	21	0.00
2.0	23	0.00
2.1	25	0.01

Table 4-13. Results of the conditional probability analysis performed on the wind data for the Emerald Lake Watershed for wind transport from a valley or prairie HRU, continued.

Daily average wind speed (m / s)	Sample Size (days)	Probability that the hourly data exceeded the threshold value (6.5 m / s)
2.2	28	0.00
2.3	29	0.00
2.4	31	0.01
2.5	32	0.02
2.6	34	0.02
2.7	29	0.04
2.8	21	0.04
2.9	31	0.02
3.0	33	0.05
3.1	29	0.07
3.2	32	0.08
3.3	43	0.11
3.4	39	0.15
3.5	36	0.10
3.6	31	0.15
3.7	36	0.19
3.8	32	0.17
3.9	39	0.17
4.0	34	0.19
4.1	36	0.18
4.2	29	0.21
4.3	21	0.25

Table 4-13. Results of the conditional probability analysis performed on the wind data for the Emerald Lake Watershed for wind transport from a valley or prairie HRU, continued.

Daily average wind speed (m / s)	Sample Size (days)	Probability that the hourly data exceeded the threshold value (6.5 m / s)
4.4	23	0.24
4.5	26	0.30
4.6	19	0.29
4.7	21	0.29
4.8	18	0.31
4.9	16	0.34
5.0	18	0.37
5.1	16	0.36
5.2	16	0.37
5.3	17	0.40
5.4	14	0.40
5.5	15	0.41
5.6	11	0.45
5.7	9	0.43
5.8	14	0.45
5.9	12	0.49
6.0	11	0.46
6.1	9	0.48
6.2	9	0.48
6.3	10	0.51
6.4	8	0.52
TOTAL	1442	-

Appendix J

A Comparison of Modeled Results With Satellite Imagery for the Upper Rio Grande Watershed

Note: The maps on the left side differ slightly than the maps on the right side due to small differences in delineation and projection.

A Comparison of Modeled Results With Satellite Imagery for the Water Year 1993

Day 75:

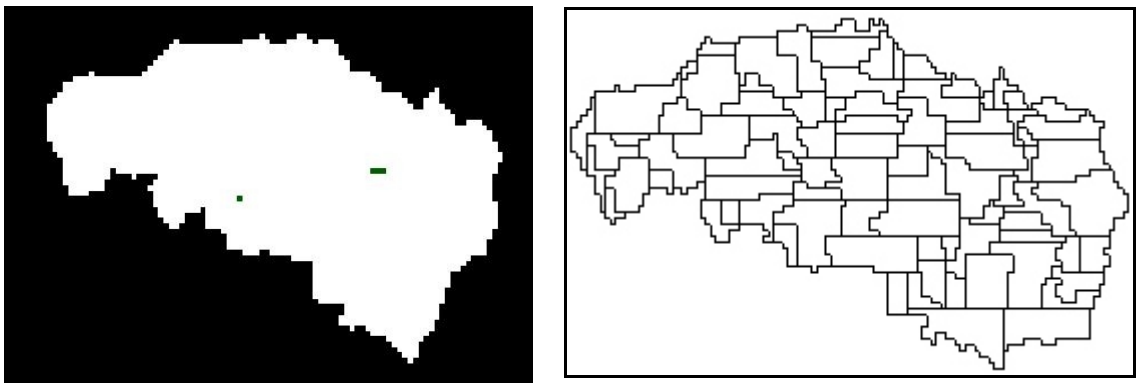

Day 91:

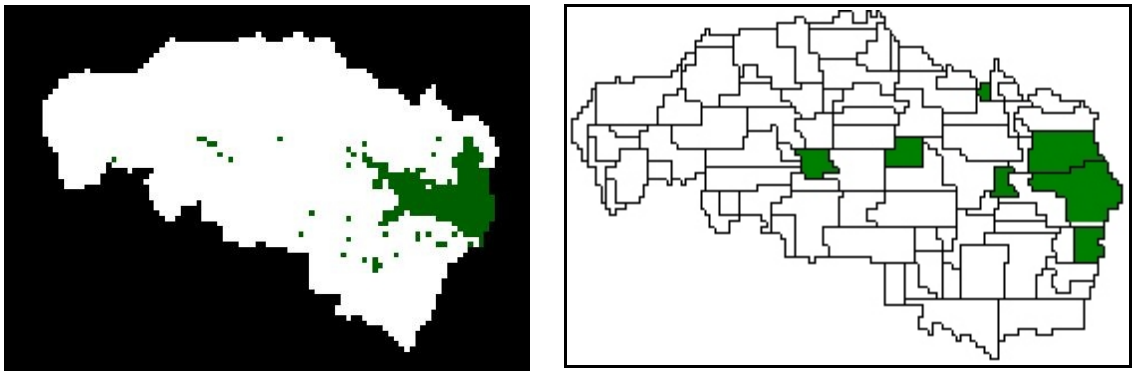

Day 98:

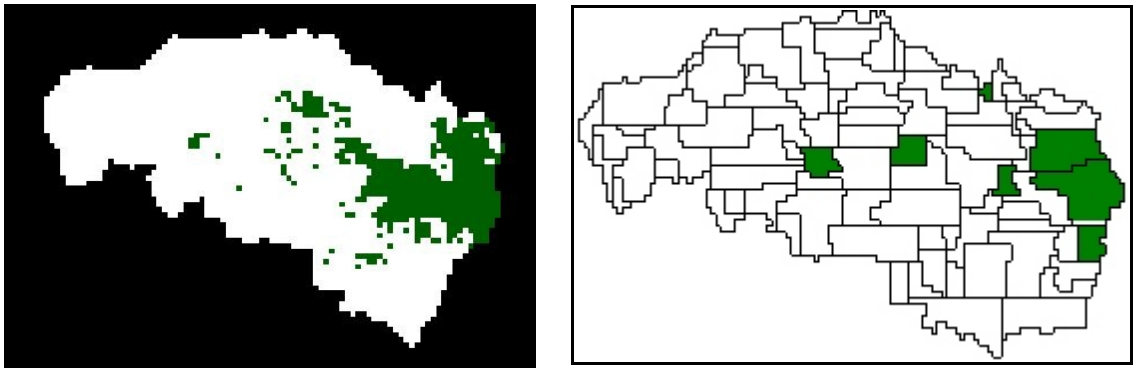

Day 115:

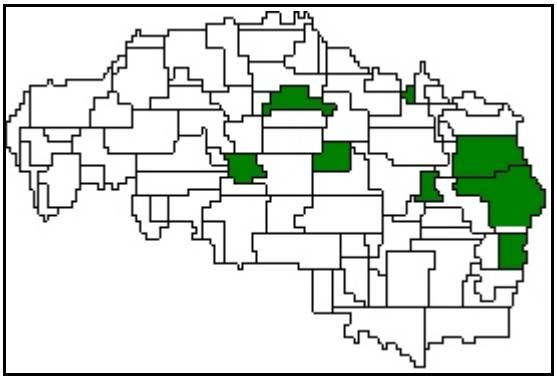

Day 130:

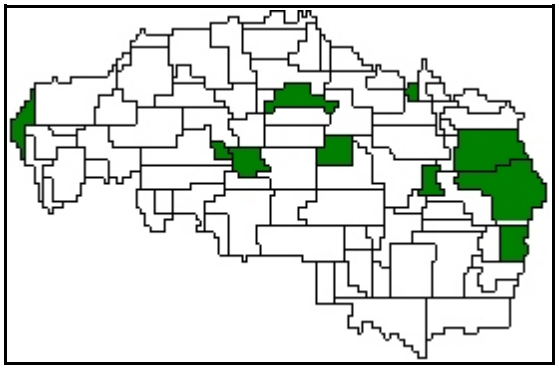

Day 150:

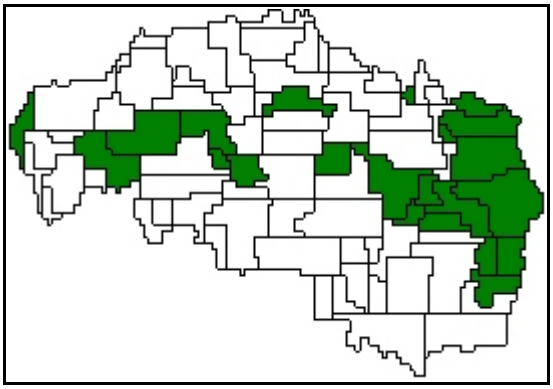

Day 171:

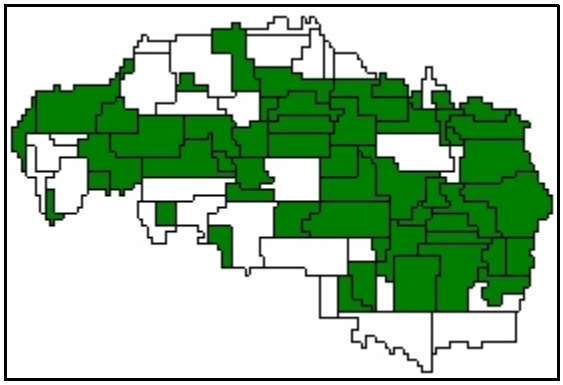

Day 181:

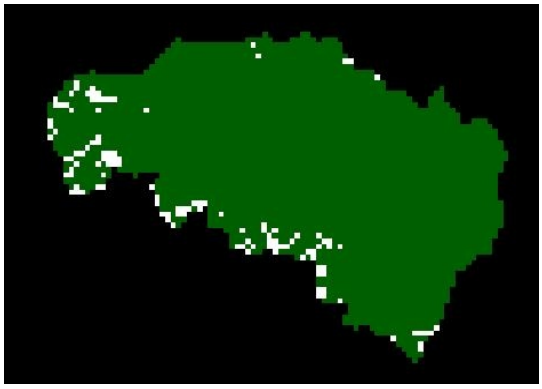

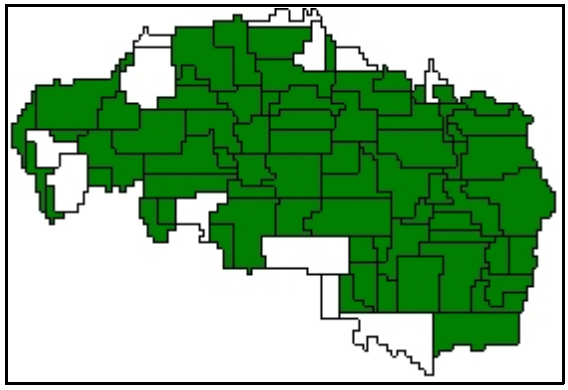

A Comparison of Modeled Results With Satellite Imagery for the Water Year 1994

Day 63:

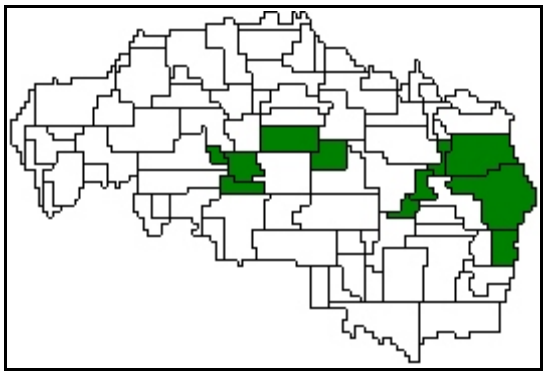

Day 72:

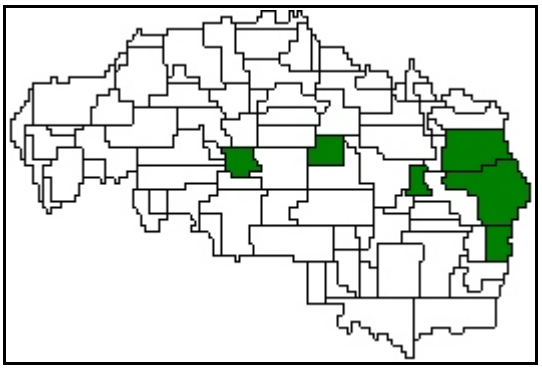

Day 90:

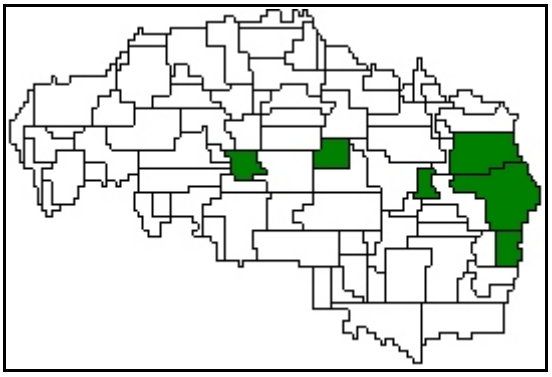

Day 102:

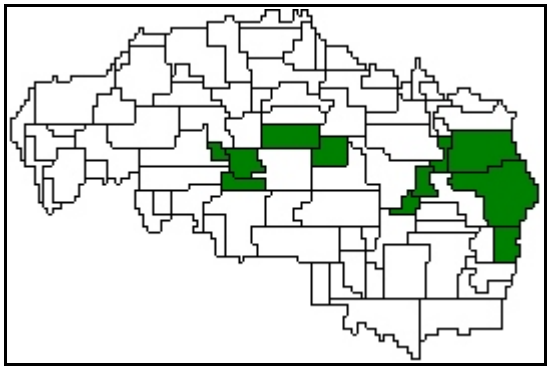

Day 128:

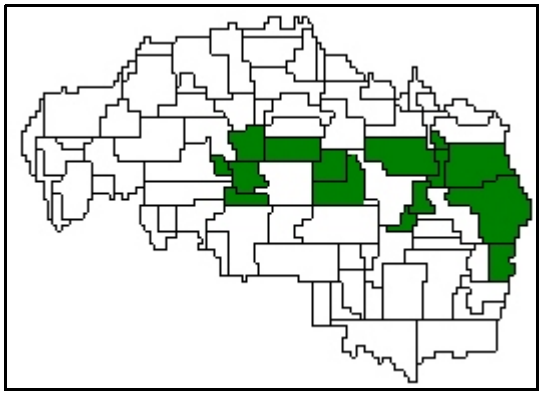

Day 140:

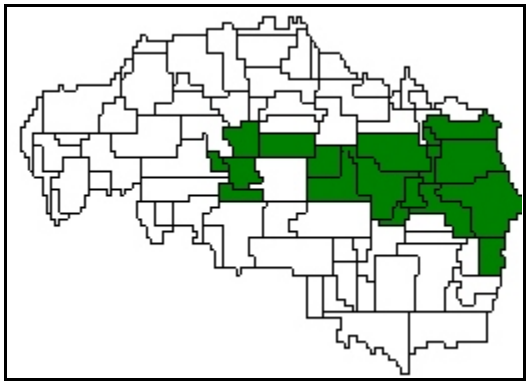

Day 149:

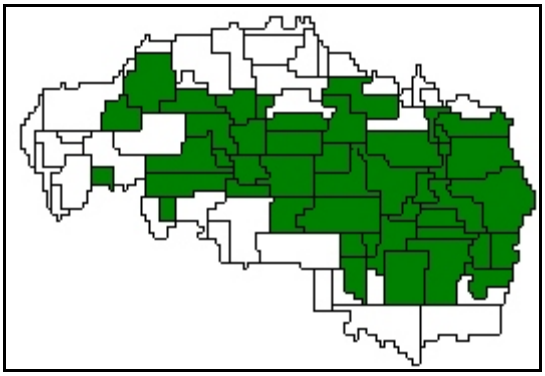

A Comparison of Modeled Results With Satellite Imagery for the Water Year 1995

Day 91:

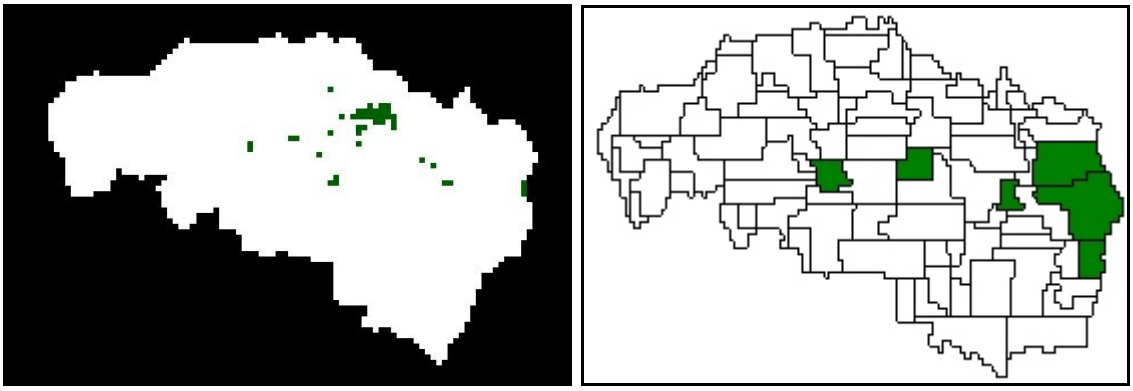

Day 101:

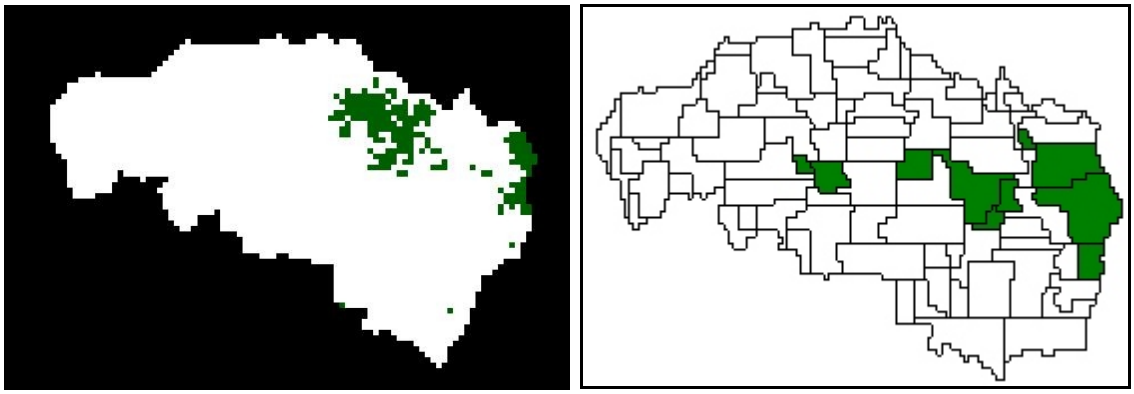

Day 156:

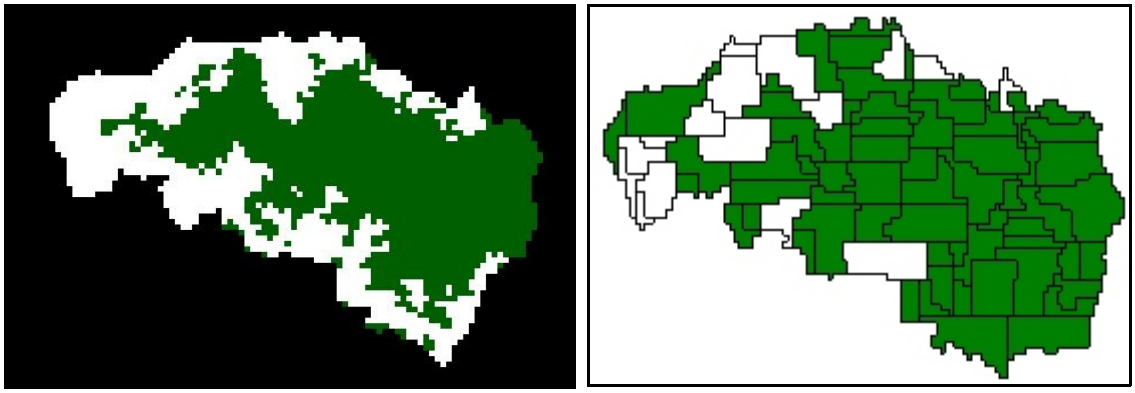

Day 169:

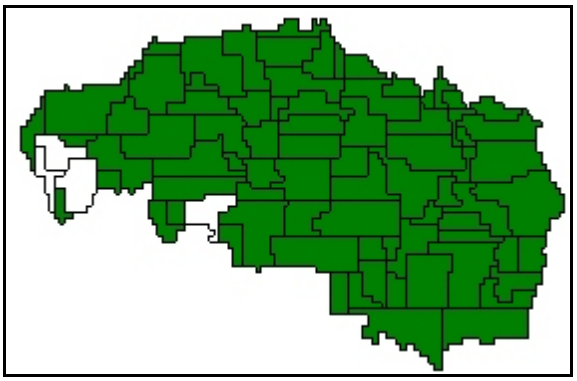

Day 177:

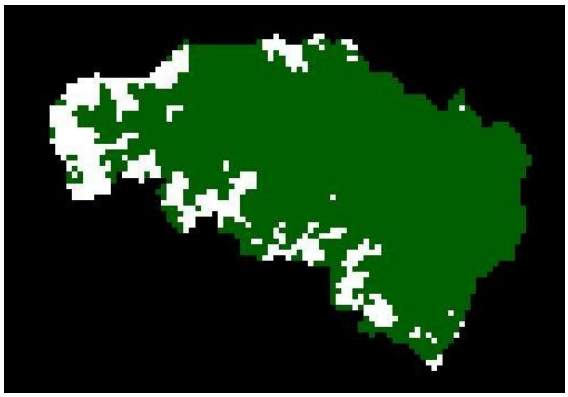

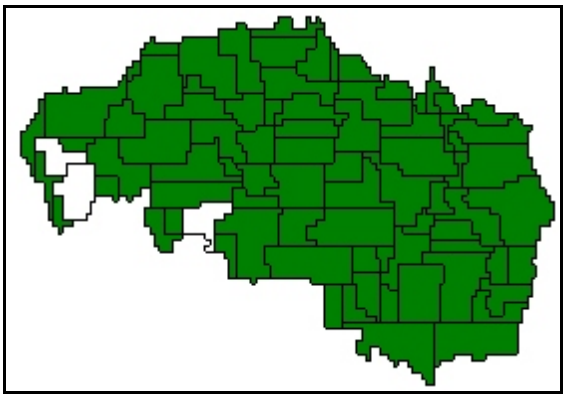

A Comparison of Modeled Results With Satellite Imagery for the Water Year 1996

Day 79:

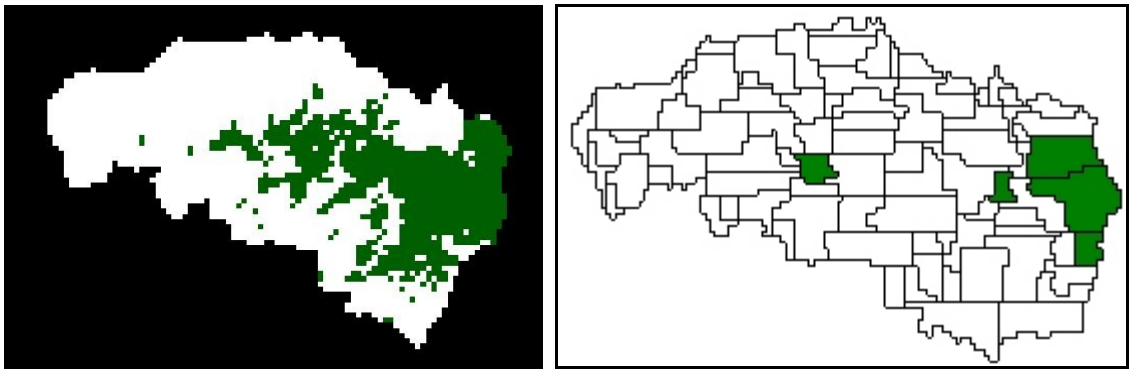

Day 93:

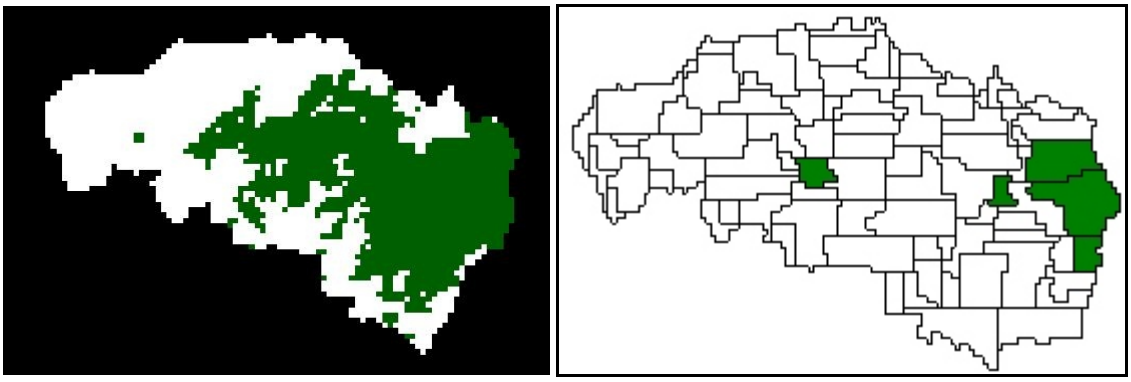

Day 107:

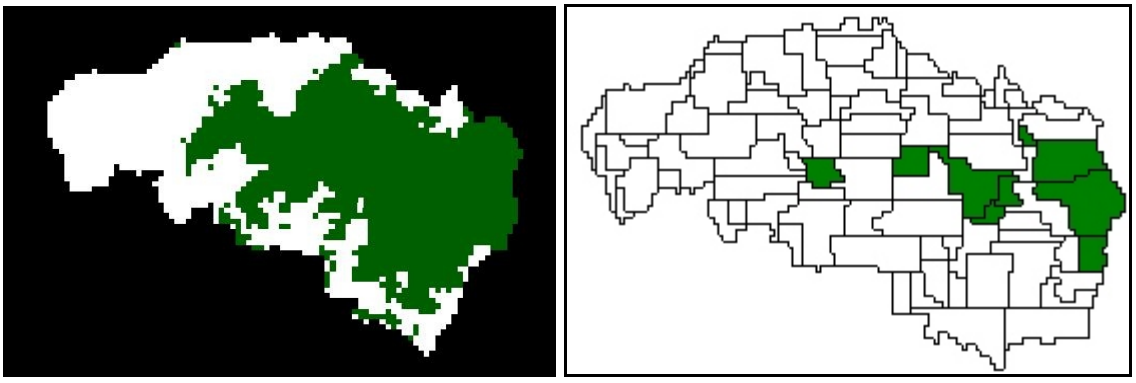

Day 128:

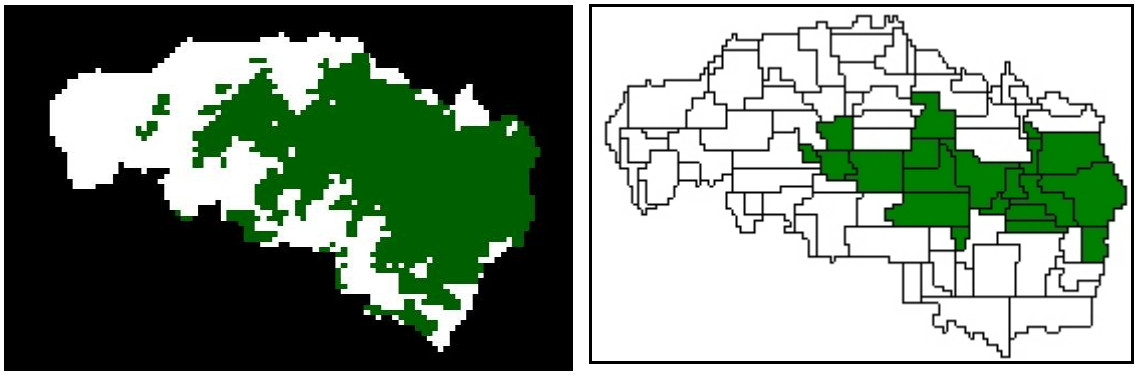

Day 144:

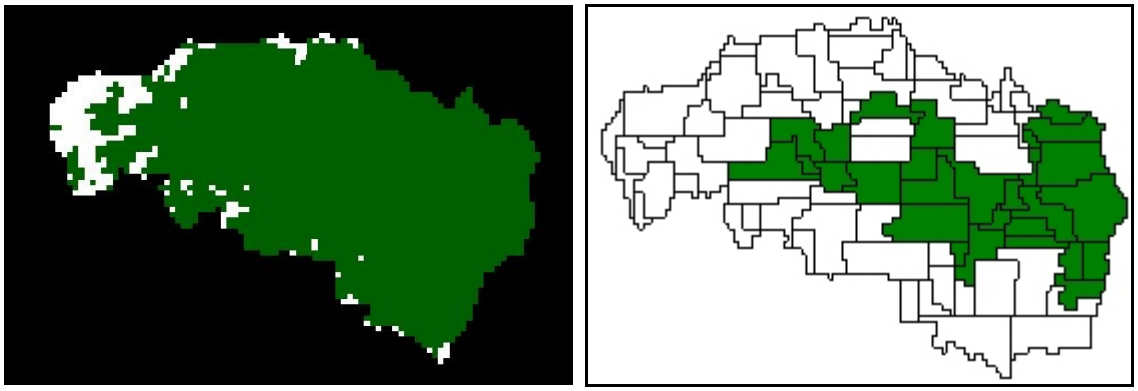

Day 171:

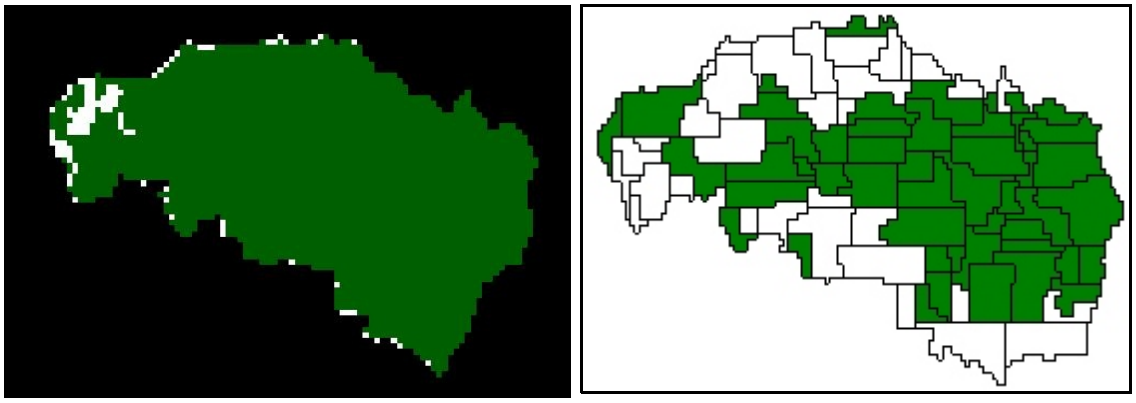

A Comparison of Modeled Results With Satellite Imagery for the Water Year 1997

Day 72:

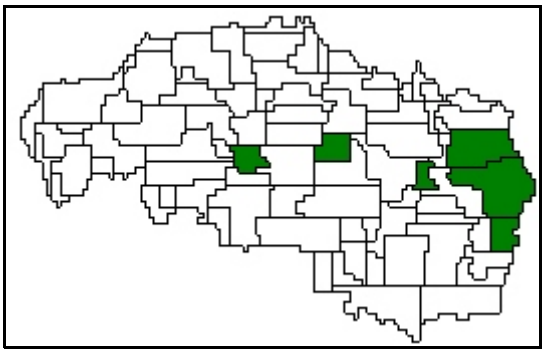

Day 84:

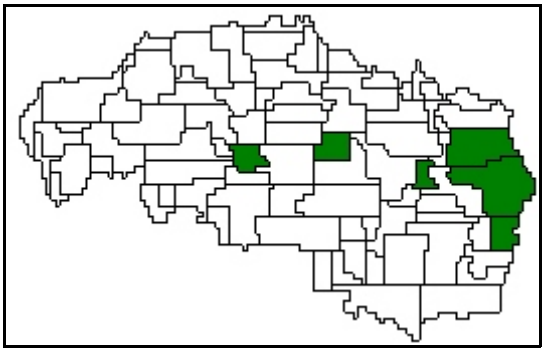

Day 126:

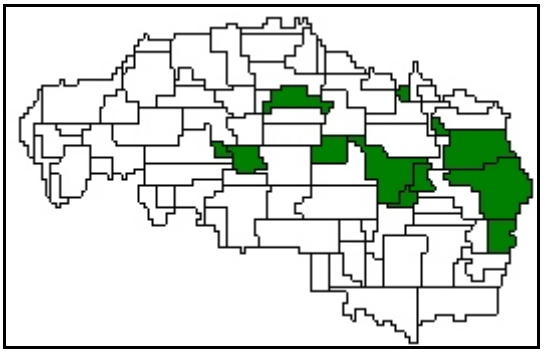

Day 147:

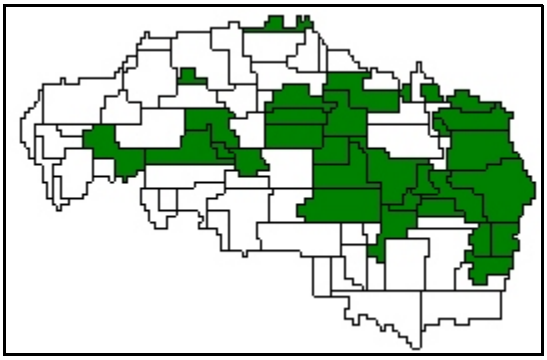

Day 165:

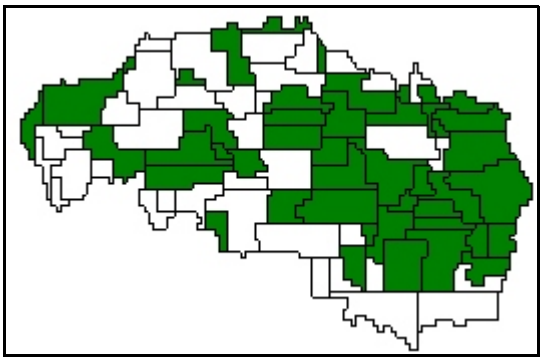

Day 182:

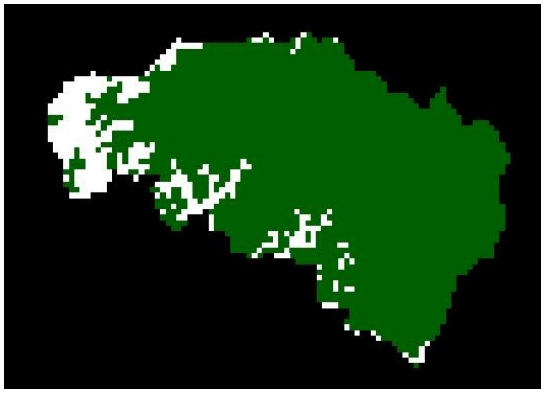

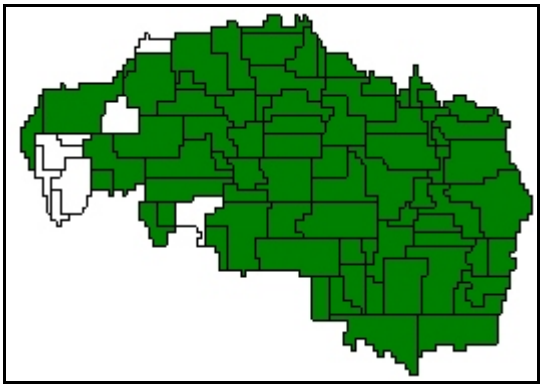

A Comparison of Modeled Results With Satellite Imagery for the Water Year 1998

Day 71:

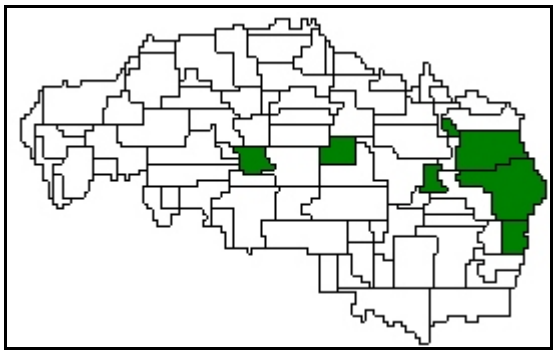

Day 85:

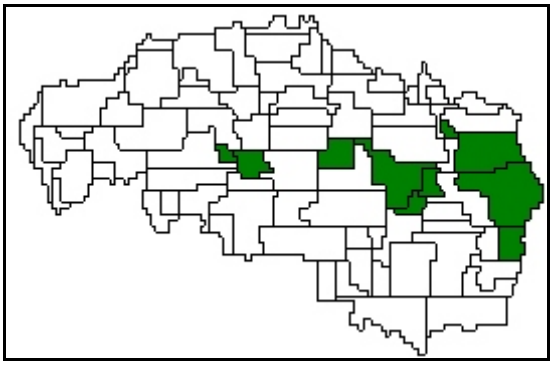

Day 97:

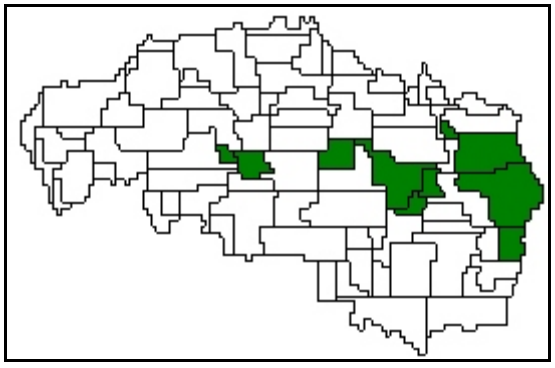

Day 118:

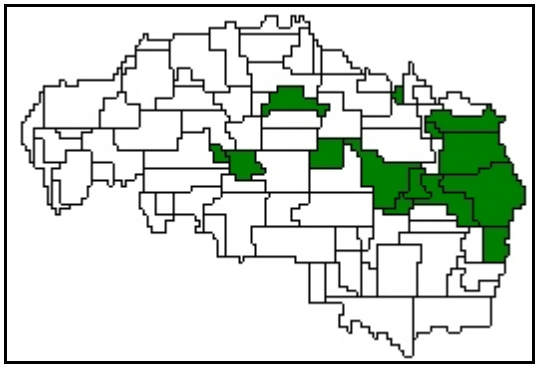

Day 132:

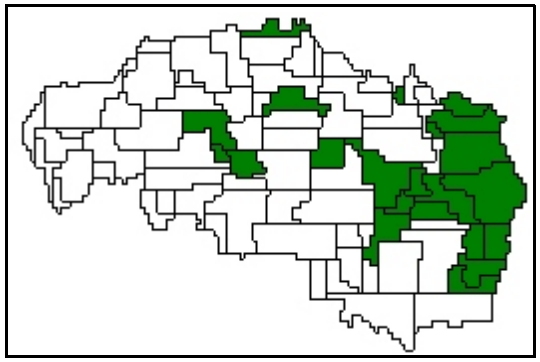

Day 146:

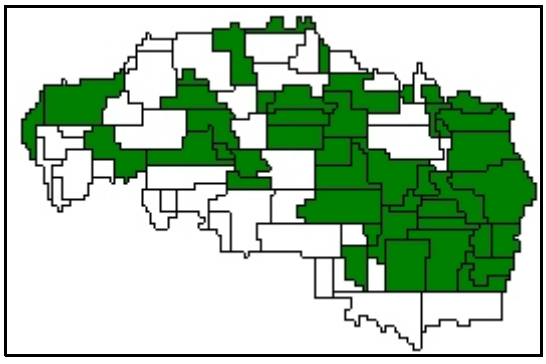

Day 167:

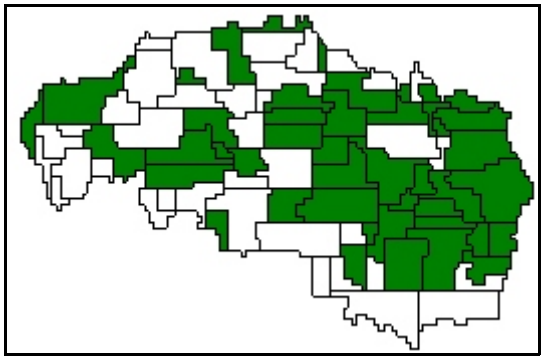

Day180:

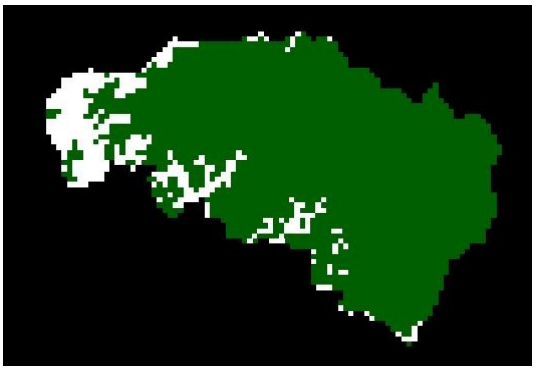

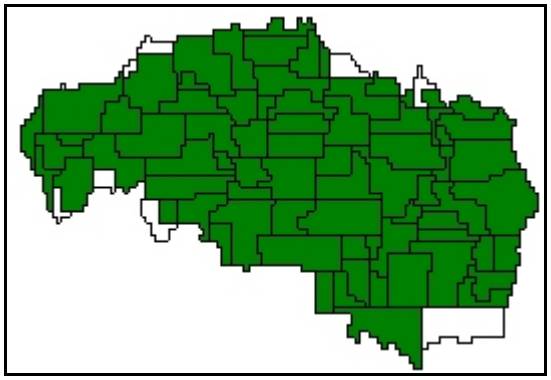

A Comparison of Modeled Results With Satellite Imagery for the Water Year 1999

Day 73:

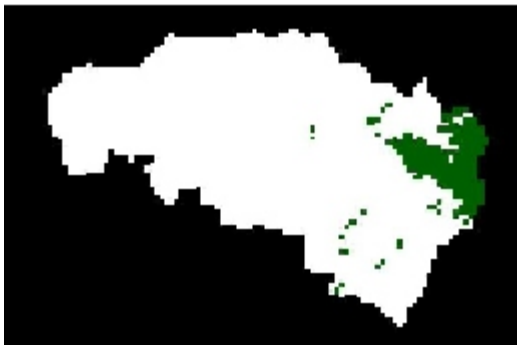

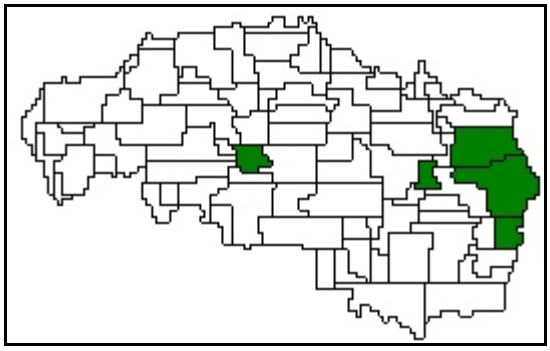

Day 82:

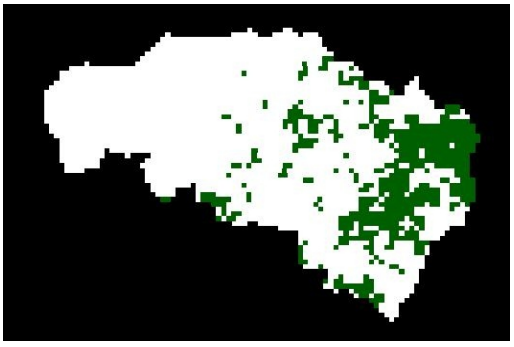

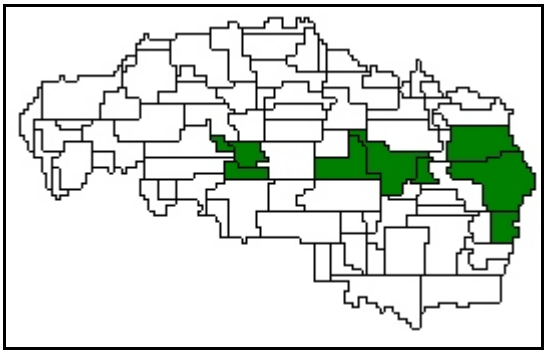

Day 98:

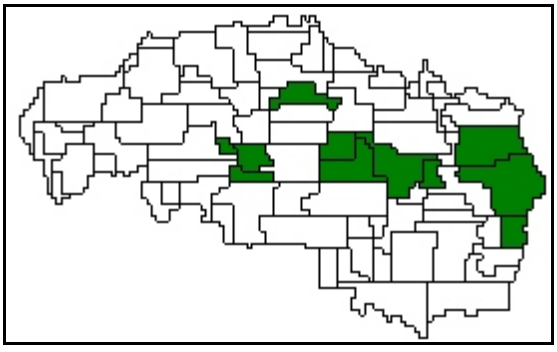

Day 133:

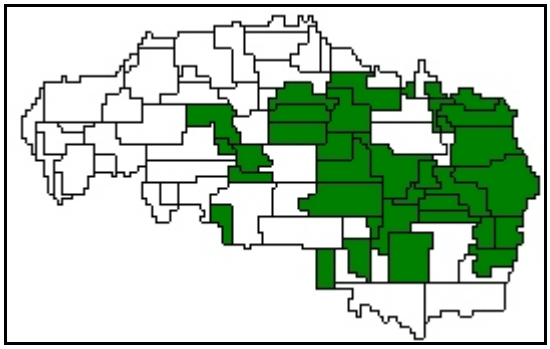

Day 140:

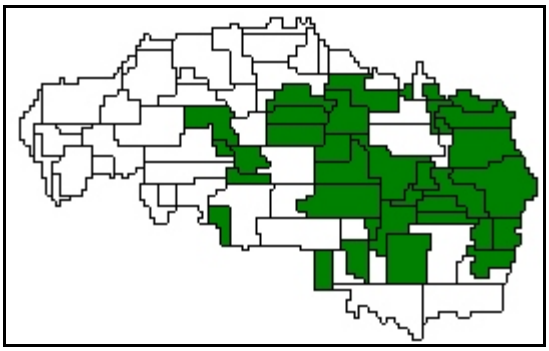

Appendix K

Model-Derived Snow Water Equivalent Maps for
the Upper Rio Grande Watershed

Legend Used for the SWE Mapping

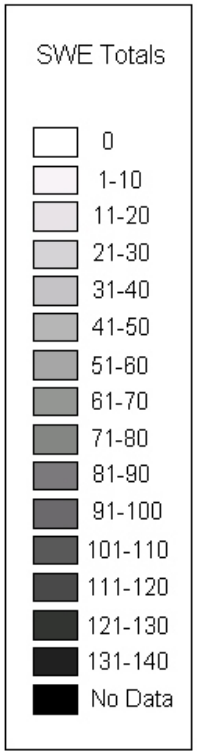

The units of SWE are in cm

Note: The model assumes uniform SWE over each HRU. See Figure 4-2 for diagram of HRUs.

SWE Maps for the Water Year 1993

November 1, 1992

November 8, 1992

November 15, 1992

November 22,1992

November 29, 1992

December 6, 1992

December 13, 1992

December 20, 1992

December 27, 1992

January 3, 1993

January 10, 1993

January 17, 1993

January 24, 1993

January 31, 1993

February 7, 1993

February 14, 1993

February 21, 1993

February 28, 1993

March 7, 1993

March 14, 1993

March 21, 1993

March 28, 1993

April 4, 1993

April11, 1993

April 18, 1993

April 25, 1993

May 2, 1993

May 7, 1993

May 12, 1993

May 17, 1993

May 22, 1993

May 27, 1993

June 1, 1993

June 6, 1993

June 11, 1993

June 16, 1993

June 21, 1993

June 26, 1993

July 1, 1993

July 6, 1993

July 11, 1993

July 16, 1993

July 21, 1993

July 26, 1993

SWE Maps for the Water Year 1994

November 1, 1993

November 8, 1993

November 15, 1993

November 22, 1993

November 29, 1993

December 6, 1993

December 13, 1993

December 20, 1993

December 27, 1993

January 3, 1994

January 10, 1994

January 17, 1994

January 24, 1994

January 31, 1994

February 7, 1994

February 14, 1994

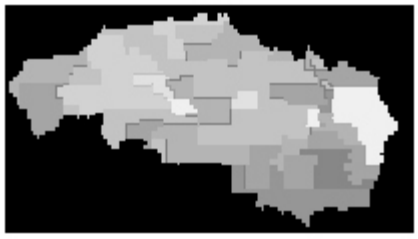

February 21, 1994

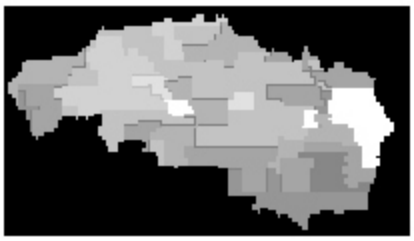

February 28, 1994

March 7, 1994

March 14, 1994

March 21, 1994

March 28, 1994

April 4, 1994

April 11, 1994

April 18, 1994

April 25, 1994

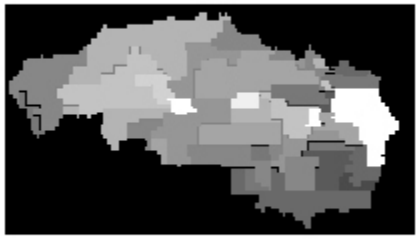

May 2, 1994

May 7, 1994

May 12, 1994

May 17, 1994

May 22, 1994

May 27, 1994

June 1, 1994

June 6, 1994

June 11, 1994

June 16, 1994

June 21, 1994

June 26, 1994

July 1, 1994

July 6, 1994

July 11, 1994

July 16, 1994

July 21, 1994

July 26, 1994

SWE Maps for the Water Year 1995

November 1, 1994

November 8, 1994

November 15, 1994

November 22, 1994

November 29, 1994

December 6, 1994

December 13, 1994

December 20, 1994

December 27, 1994

January 3, 1995

January 10, 1995

January 17, 1995

January 24, 1995

January 31, 1995

February 7, 1995

February 14, 1995

February 21, 1995

February 28, 1995

March 7, 1995

March 14, 1995

March 21, 1995

March 28, 1995

April 4, 1995

April 11, 1995

April 18, 1995

April 25, 1995

May 2, 1995

May 7, 1995

May 12, 1995

May 17, 1995

May 22, 1995

May 27, 1995

June 1, 1995

June 6, 1995

June 11, 1995

June 16, 1995

June 21, 1995

June 26, 1995

July 1, 1995

July 6, 1995

July 11, 1995

July 16, 1995

July 21, 1995

July 26, 1995

SWE Maps for the Water Year 1996

November 1, 1995

November 8, 1995

November 15, 1995

November 22, 1995

November 29, 1995

December 6, 1995

December 13, 1995

December 20, 1995

December 27, 1995

January 3, 1996

January 10, 1996

January 17, 1996

January 24, 1996

January 31, 1996

February 7, 1996

February 14, 1996

February 21, 1996

February 28, 1996

March 7, 1996

March 14, 1996

March 21, 1996

March 28, 1996

April 4, 1996

April 11, 1996

April 18, 1996

April 25, 1996

May 2, 1996

May 7, 1996

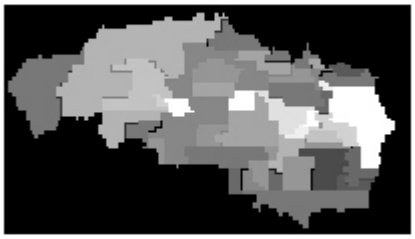

May 12, 1996

May 17, 1996

May 22, 1996

May 29, 1996

June 1, 1996

June 6, 1996

June 11, 1996

June 16, 1996

June 21, 1996

June 26, 1996

July 1, 1996

July 6, 1996

July 11, 1996

July 16, 1996

July 21, 1996

July 26, 1996

SWE Maps for the Water Year 1997

November 1, 1996

November 8, 1996

November 15, 1996

November 22, 1996

November 29, 1996

December 6, 1996

December 13, 1996

December 20, 1996

December 27, 1996

January 3, 1997

January 10, 1997

January 17, 1997

January 24, 1997

January 31, 1997

February 7, 1997

February 14, 1997

February 21, 1997

February 28, 1997

March 7, 1997

March 14, 1997

March 21, 1997

March 28, 1997

April 4, 1997

April 11, 1997

April 18, 1997

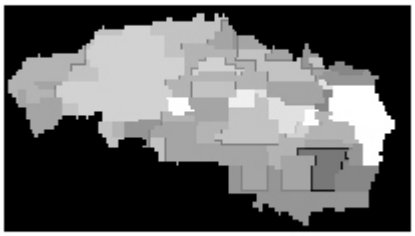

April 25, 1997

May 2, 1997

May 7, 1997

May 12, 1997

May 17, 1997

May 22, 1997

May 27, 1997

June 1, 1997

June 6, 1997

June 11, 1997

June 16, 1997

June 21, 1997

June 26, 1997

July 1, 1997

July 6, 1997

July 11, 1997

July 16, 1997

July 21, 1997

July 26, 1997

SWE Maps for the Water Year 1998

November 1, 1997

November 8, 1997

November 15, 1997

November 22, 1997

November 29, 1997

December 6, 1997

December 13, 1997

December 20, 1997

December 27, 1997

January 3, 1998

January 10, 1998

January 17, 1998

January 24, 1998

January 31, 1998

February 7, 1998

February 14, 1998

February 21, 1998

February 28, 1998

March 7, 1998

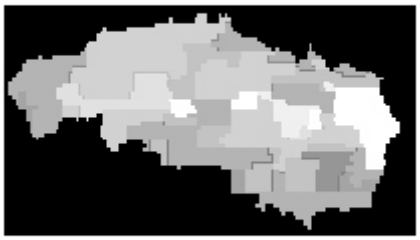

March 14, 1998

March 21, 1998

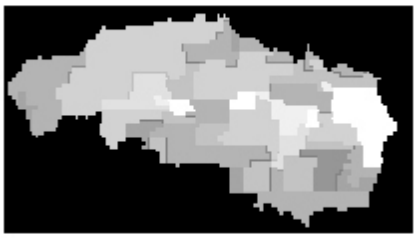

March 28, 1998

April 4, 1998

April 11, 1998

April 18, 1998

April 25, 1998

May 2, 1998

May 7, 1998

May 12, 1998

May 17, 1998

May 22, 1998

May 27, 1998

June 1, 1998

June 6, 1998

June 11, 1998

June 16, 1998

June 21, 1998

June 26, 1998

July 1, 1998

July 6, 1998

July 11, 1998

July 16, 1998

July 21, 1998

July 26, 1998

SWE Maps for the Water Year 1999

November 1, 1998

November 8, 1998

November 15, 1998

November 22, 1998

November 29, 1998

December 6, 1998

December 13, 1998

December 20, 1998

December 27, 1998

January 3, 1999

January 10, 1999

January 17, 1999

January 24, 1999

January 31, 1999

February 7, 1999

February 14, 1999

February 21, 1999

February 28, 1999

March 7, 1999

March 14, 1999

March 21, 1999

March 28, 1999

April 4, 1999

April11, 1999

April 18, 1999

April 25, 1999

May 2, 1999

May 7, 1999

May 12, 1999

May 17, 1999

May 22, 1999

May 27, 1999

June 1, 1999

June 6, 1999

June 11, 1999

June 16, 1999

June 21, 1999

June 26, 1999

July 1, 1999

July 6, 1999

July 11, 1999

July 16, 1999

July 21, 1999

July 26, 1999

SWE Maps for the Water Year 2000

November 1, 1999

November 8, 1999

November 15, 1999

November 22, 1999

November 29, 1999

December 6, 1999

December 13, 1999

December 20, 1999

December 27, 1999

January 3, 2000

January 10, 2000

January 17, 2000

January 24, 2000

January 31, 2000

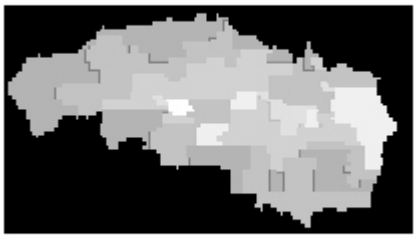

February 7, 2000

February 14, 2000

February 21, 2000

February 28, 2000

March 7, 2000

March 14, 2000

March 21, 2000

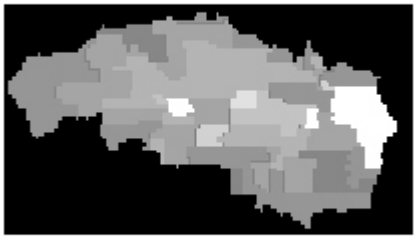

March 28, 2000

April 4, 2000

April 11, 2000

April18, 2000

April 25, 2000

May 2, 2000

May 7, 2000

May 12, 2000

May 17, 2000

May 22, 2000

May 27, 2000

June 1, 2000

June 6, 2000

June 11, 2000

June 16, 2000

June 21, 2000

June 26, 2000

July 1, 2000

July 6, 2000

July 11, 2000

July 16, 2000

July 21, 2000

July 26, 2000

Appendix L

Moment Plots for the Upper Rio Grande Watershed

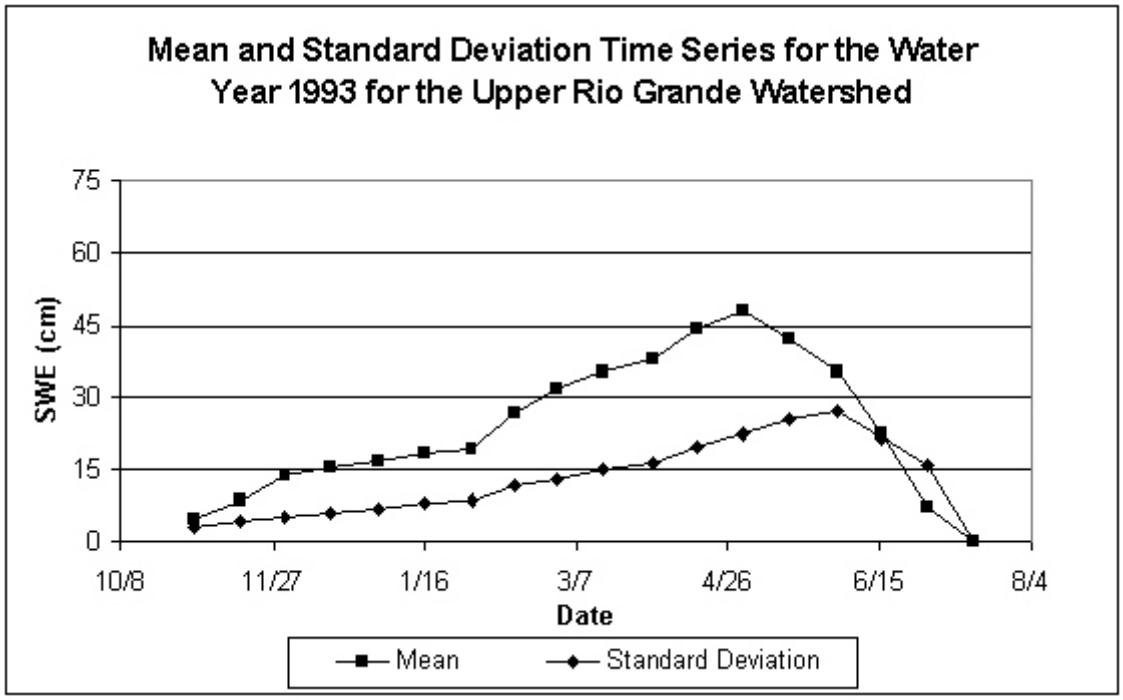
Mean and Standard Deviation Time Series for the Water Year 1993 for the Upper Rio Grande Watershed
75
60
45
30
15
0
SWE (cm)
10/8
11/27
1/16
3/7
4/26
6/15
8/4
Date
Mean
Standard Deviation

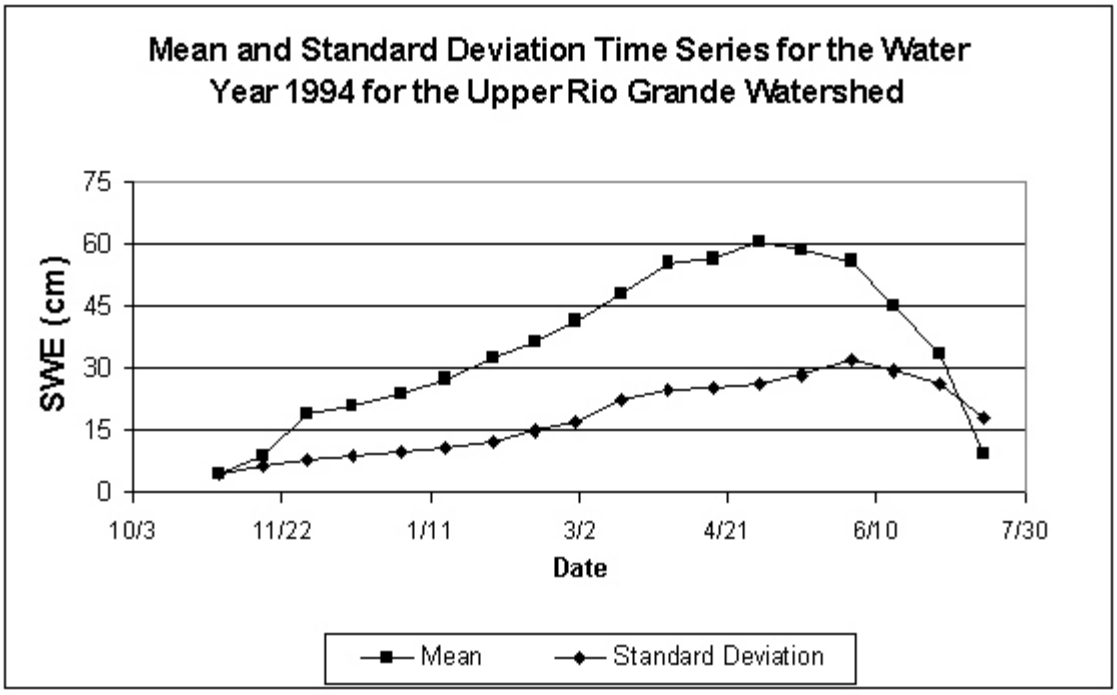
Mean and Standard Deviation Time Series for the Water Year 1994 for the Upper Rio Grande Watershed
75
60
45
30
15
0
SWE (cm)
10/3
11/22
1/11
3/2
4/21
6/10
7/30
Date
Mean
Standard Deviation

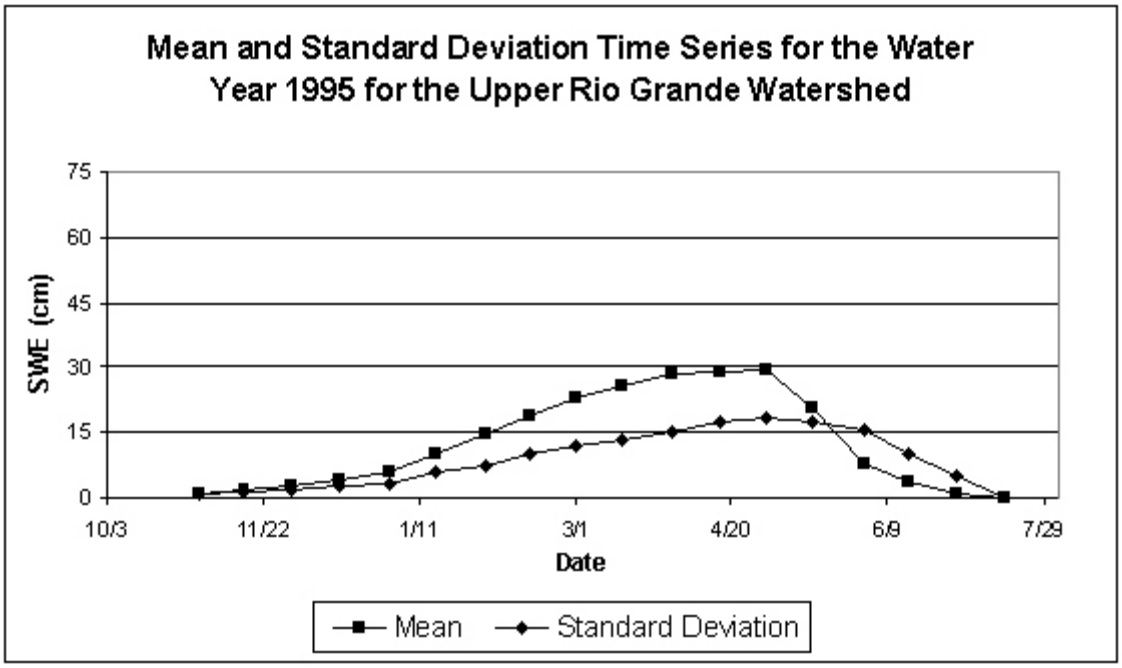
Mean and Standard Deviation Time Series for the Water Year 1995 for the Upper Rio Grande Watershed
SWE (cm)
75
60
45
30
15
0
10/3
11/22
1/11
3/1
4/20
6/9
7/29
Date
Mean
Standard Deviation

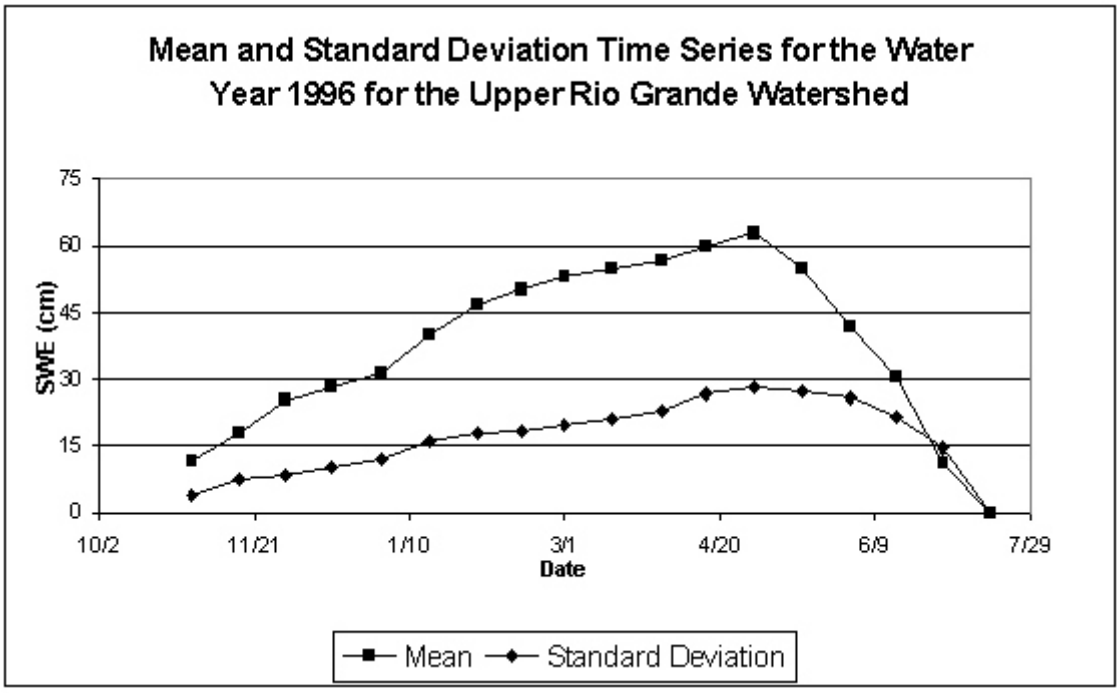
Mean and Standard Deviation Time Series for the Water Year 1996 for the Upper Rio Grande Watershed
SWE (cm)
75
60
45
30
15
0
10/2
11/21
1/10
3/1
4/20
6/9
7/29
Date
Mean
Standard Deviation

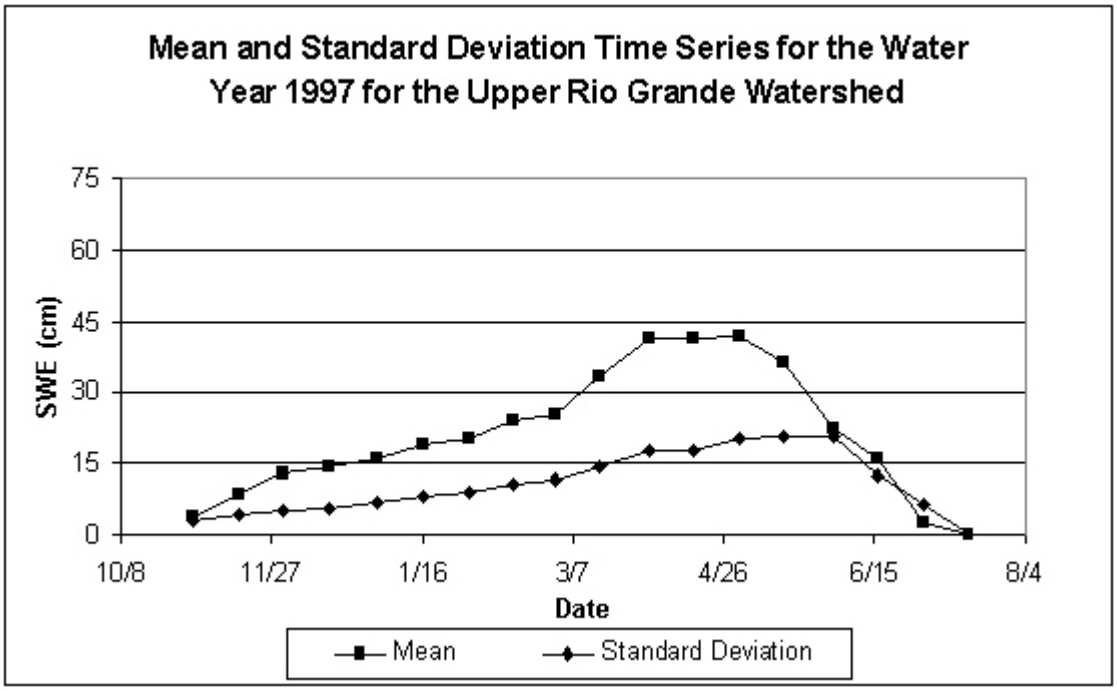
Mean and Standard Deviation Time Series for the Water Year 1997 for the Upper Rio Grande Watershed
SWE (cm)
75
60
45
30
15
0
10/8
11/27
1/16
3/7
4/26
6/15
8/4
Date
Mean
Standard Deviation

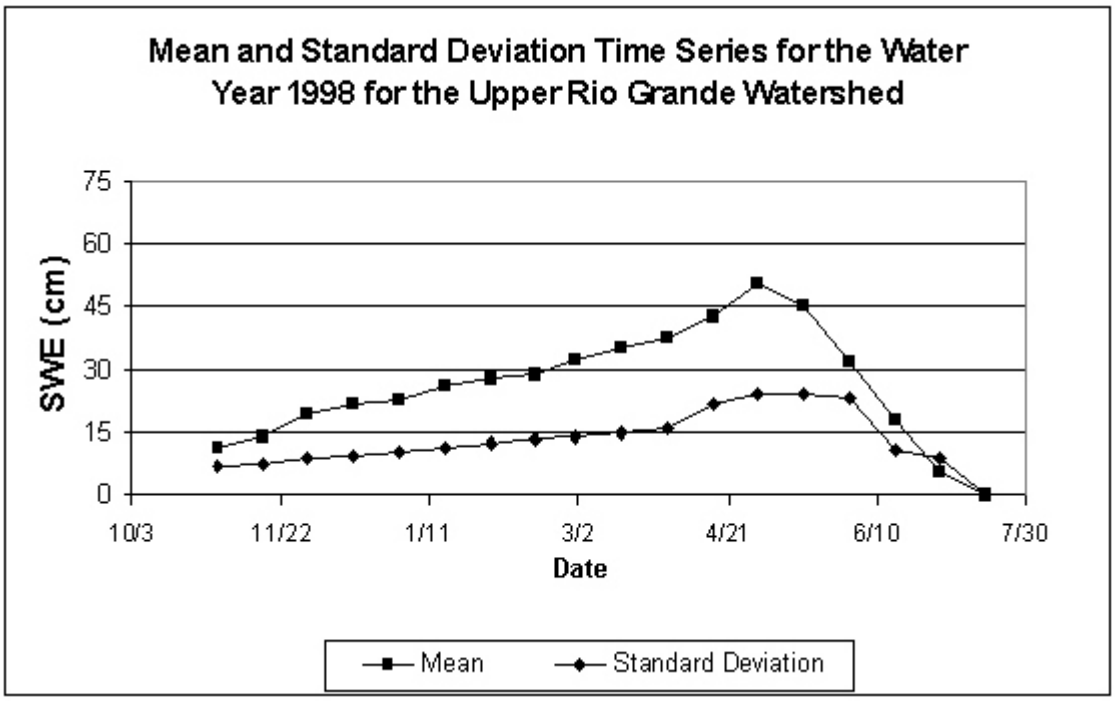
Mean and Standard Deviation Time Series for the Water Year 1998 for the Upper Rio Grande Watershed
SWE (cm)
75
60
45
30
15
0
10/3
11/22
1/11
3/2
4/21
6/10
7/30
Date
Mean
Standard Deviation

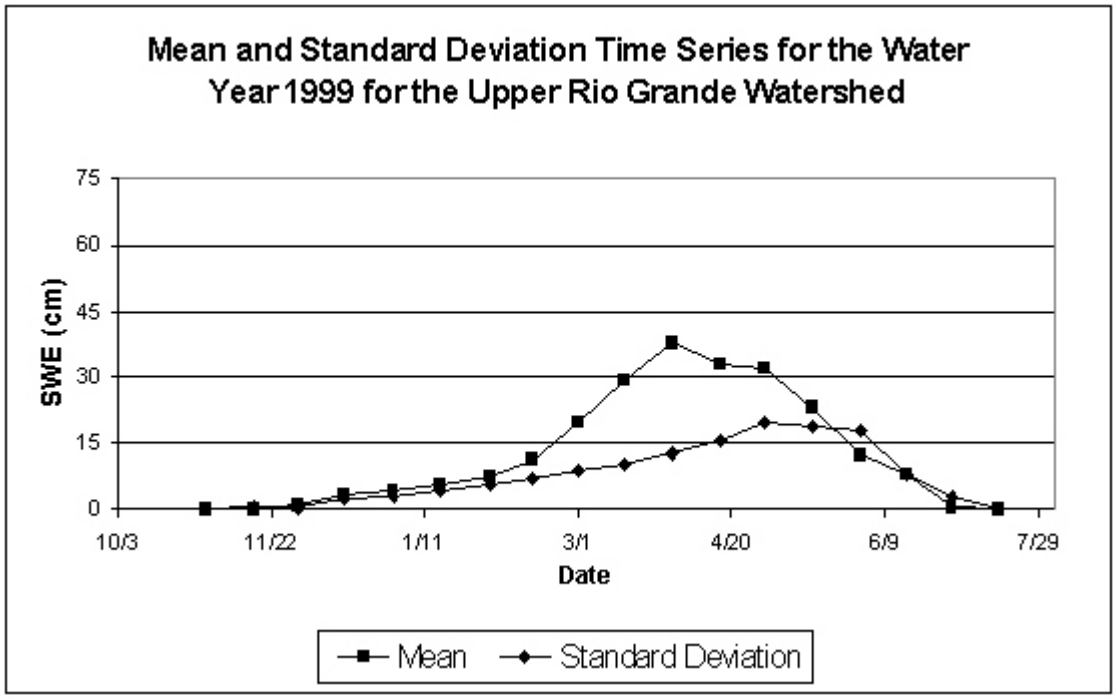
Mean and Standard Deviation Time Series for the Water Year 1999 for the Upper Rio Grande Watershed
SWE (cm)
75
60
45
30
15
0
10/3
11/22
1/11
3/1
4/20
6/9
7/29
Date
Mean
Standard Deviation

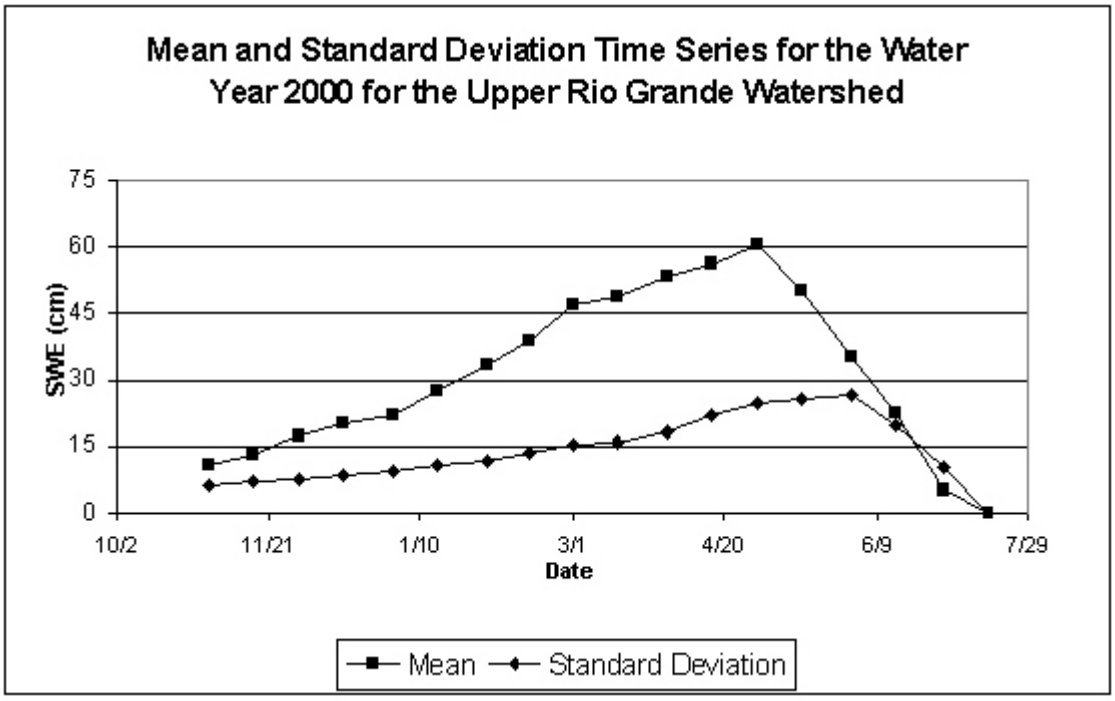
Mean and Standard Deviation Time Series for the Water Year 2000 for the Upper Rio Grande Watershed
SWE (cm)
75
60
45
30
15
0
10/2
11/21
1/10
3/1
4/20
6/9
7/29
Date
Mean
Standard Deviation

Appendix M

Moment Plots for the Reynolds Creek Watershed

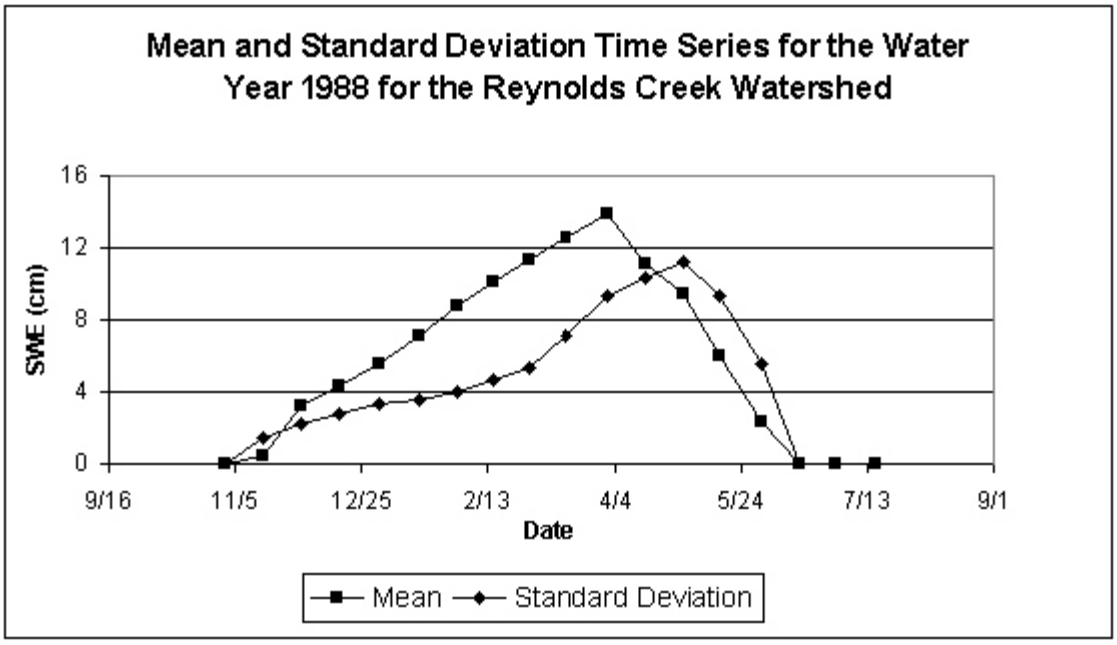
Mean and Standard Deviation Time Series for the Water Year 1988 for the Reynolds Creek Watershed
SWE (cm)
16
12
8
4
0
9/16
11/5
12/25
2/13
4/4
5/24
7/13
9/1
Date
Mean
Standard Deviation

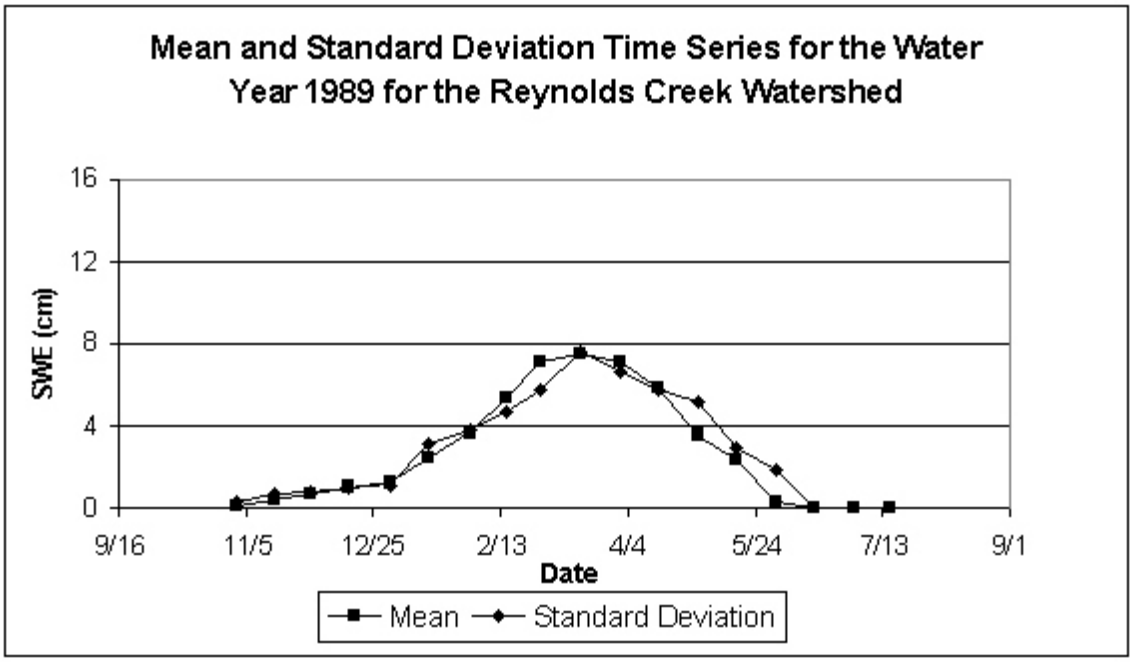
Mean and Standard Deviation Time Series for the Water Year 1989 for the Reynolds Creek Watershed
SWE (cm)
16
12
8
4
0
9/16
11/5
12/25
2/13
4/4
5/24
7/13
9/1
Date
Mean
Standard Deviation

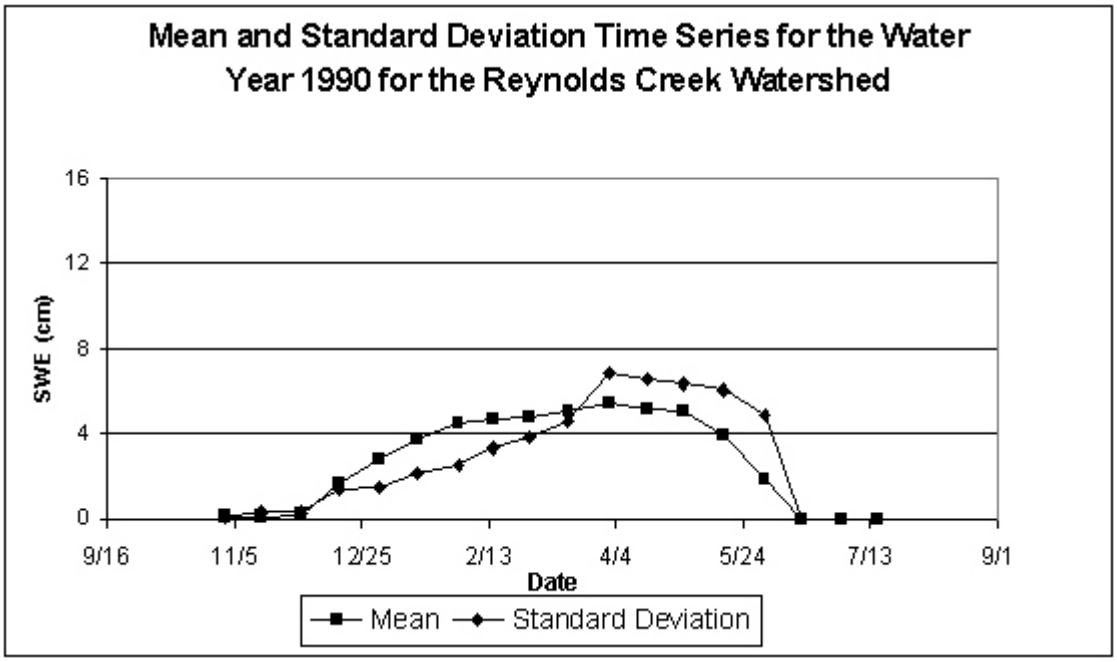
Mean and Standard Deviation Time Series for the Water Year 1990 for the Reynolds Creek Watershed
SWE (cm)
16
12
8
4
0
9/16
11/5
12/25
2/13
4/4
5/24
7/13
9/1
Date
Mean
Standard Deviation

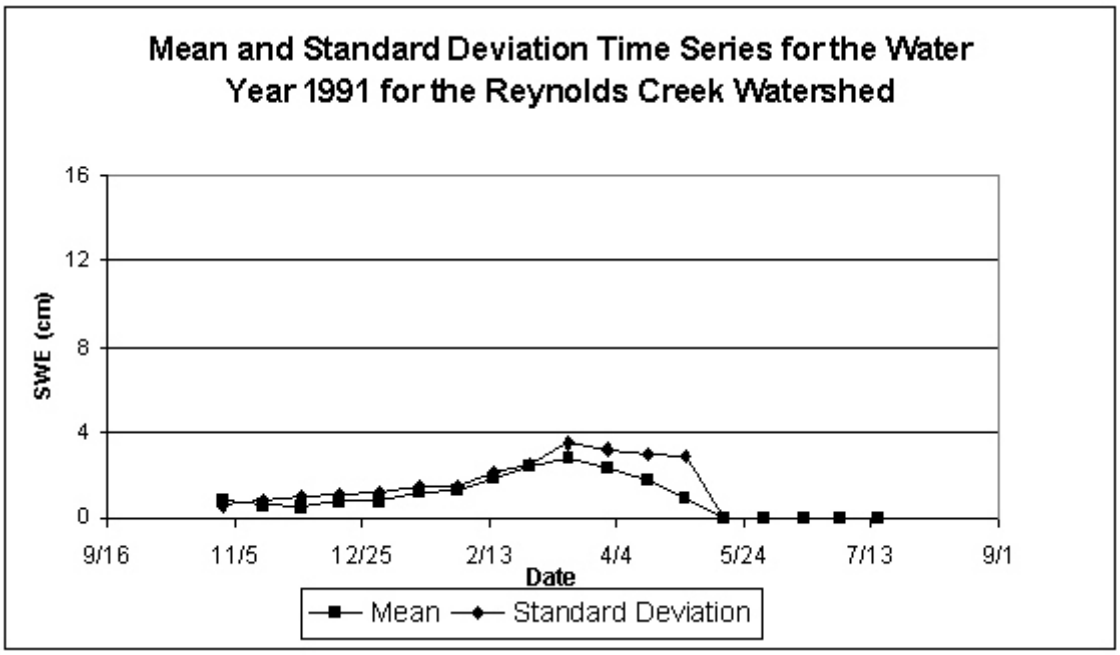
Mean and Standard Deviation Time Series for the Water Year 1991 for the Reynolds Creek Watershed
SWE (cm)
16
12
8
4
0
9/16
11/5
12/25
2/13
4/4
5/24
7/13
9/1
Date
Mean
Standard Deviation

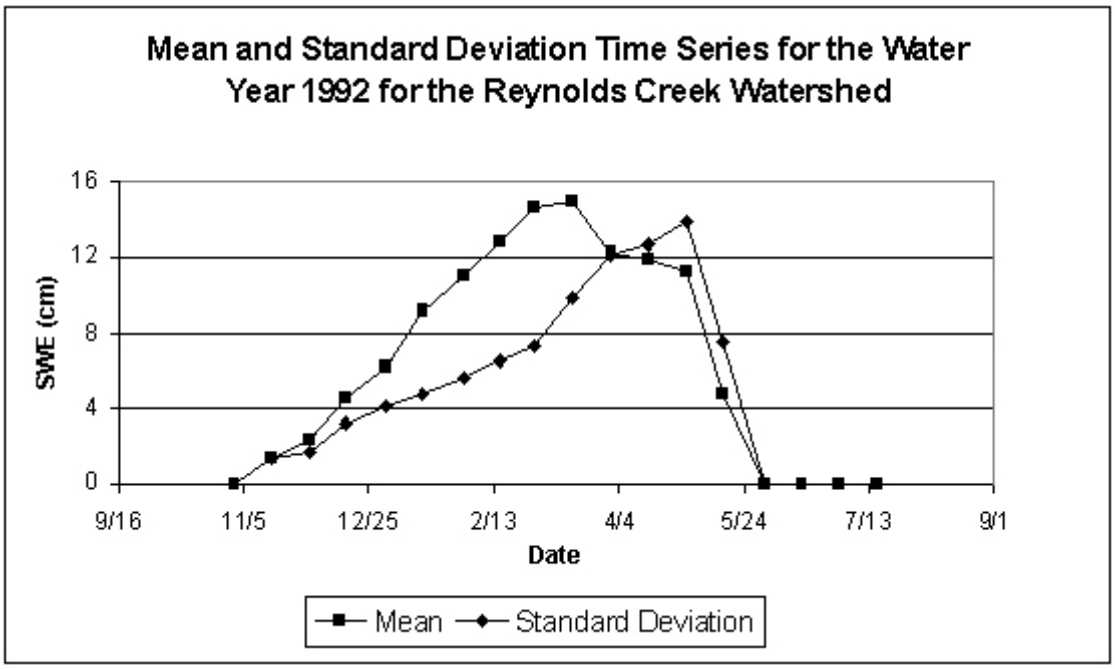
Mean and Standard Deviation Time Series for the Water Year 1992 for the Reynolds Creek Watershed
SWE (cm)
16
12
8
4
0
9/16
11/5
12/25
2/13
4/4
5/24
7/13
9/1
Date
Mean
Standard Deviation

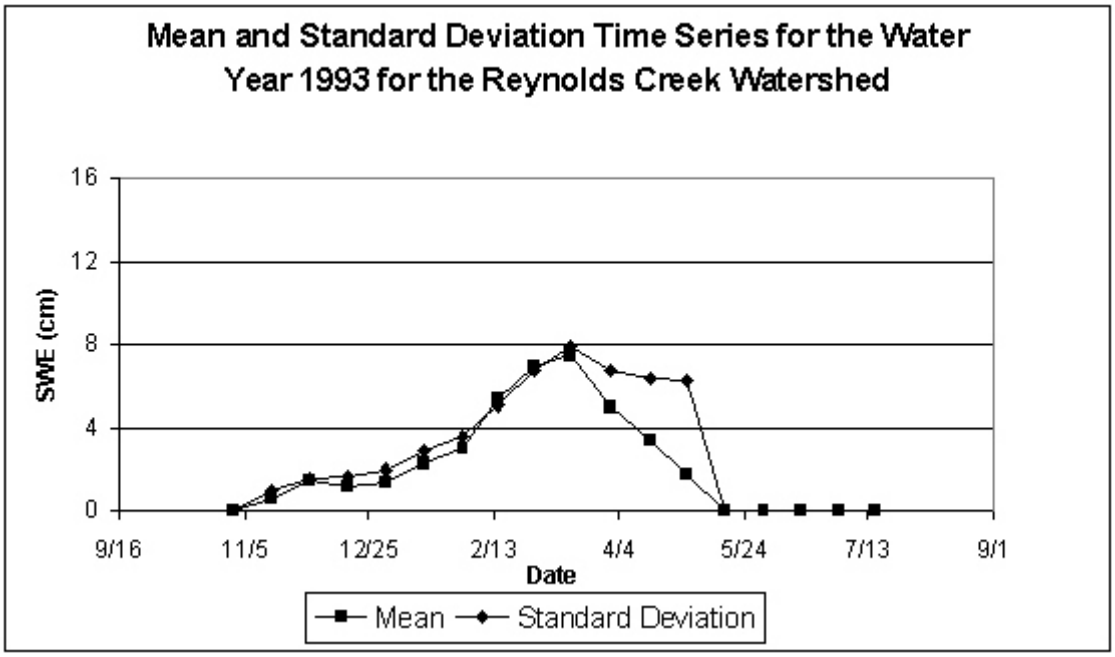
Mean and Standard Deviation Time Series for the Water Year 1993 for the Reynolds Creek Watershed
SWE (cm)
16
12
8
4
0
9/16
11/5
12/25
2/13
4/4
5/24
7/13
9/1
Date
Mean
Standard Deviation

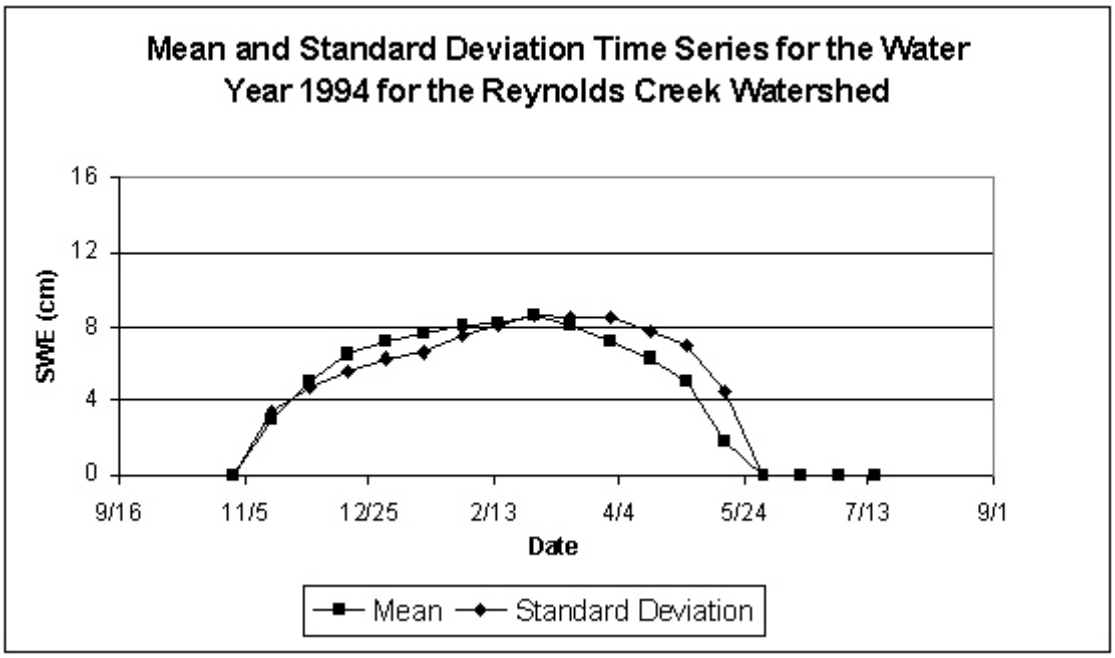
Mean and Standard Deviation Time Series for the Water Year 1994 for the Reynolds Creek Watershed
SWE (cm)
16
12
8
4
0
9/16
11/5
12/25
2/13
4/4
5/24
7/13
9/1
Date
Mean
Standard Deviation

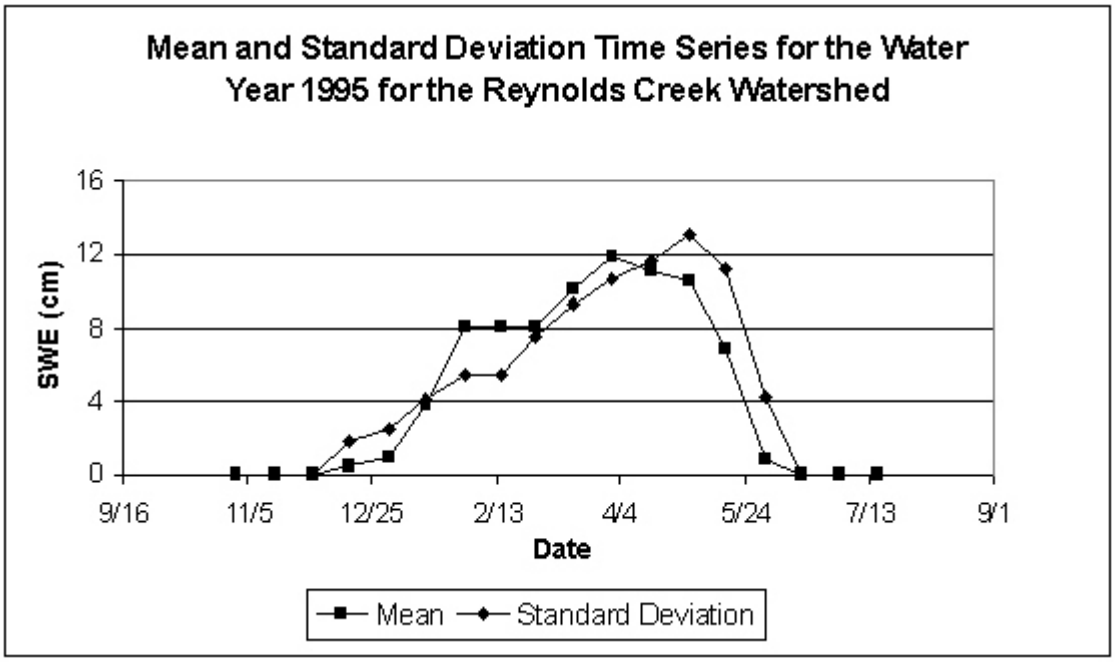
Mean and Standard Deviation Time Series for the Water Year 1995 for the Reynolds Creek Watershed
SWE (cm)
16
12
8
4
0
9/16
11/5
12/25
2/13
4/4
5/24
7/13
9/1
Date
Mean
Standard Deviation

Appendix N

Moment Plots for the Emerald Lake Watershed

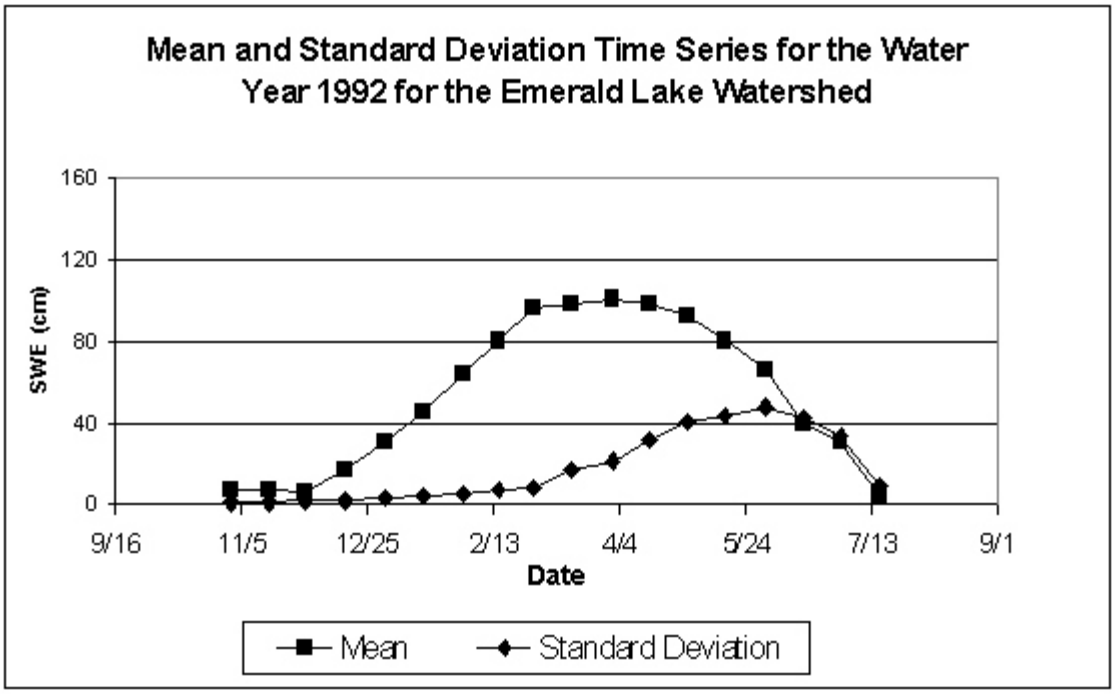
Mean and Standard Deviation Time Series for the Water Year 1992 for the Emerald Lake Watershed
160
120
80
40
0
SWE (cm)
9/16
11/5
12/25
2/13
4/4
5/24
7/13
9/1
Date
Mean
Standard Deviation

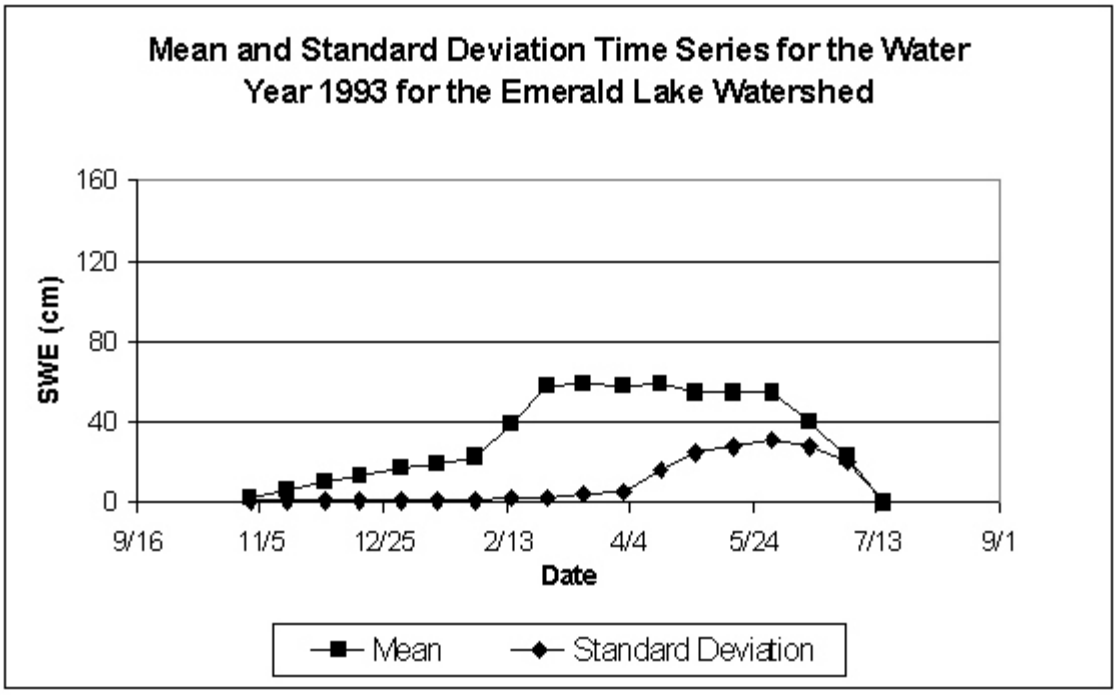
Mean and Standard Deviation Time Series for the Water Year 1993 for the Emerald Lake Watershed
160
120
80
40
0
SWE (cm)
9/16
11/5
12/25
2/13
4/4
5/24
7/13
9/1
Date
Mean
Standard Deviation

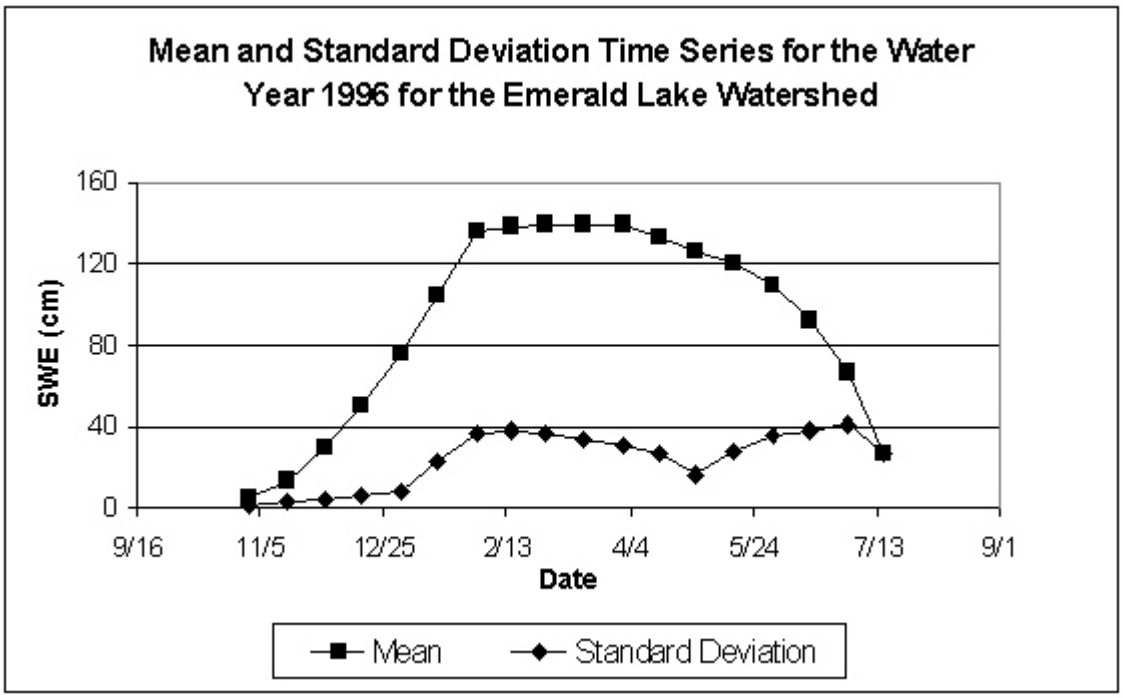
Mean and Standard Deviation Time Series for the Water Year 1996 for the Emerald Lake Watershed
SWE (cm)
160
120
80
40
0
9/16
11/5
12/25
2/13
4/4
5/24
7/13
9/1
Date
Mean
Standard Deviation

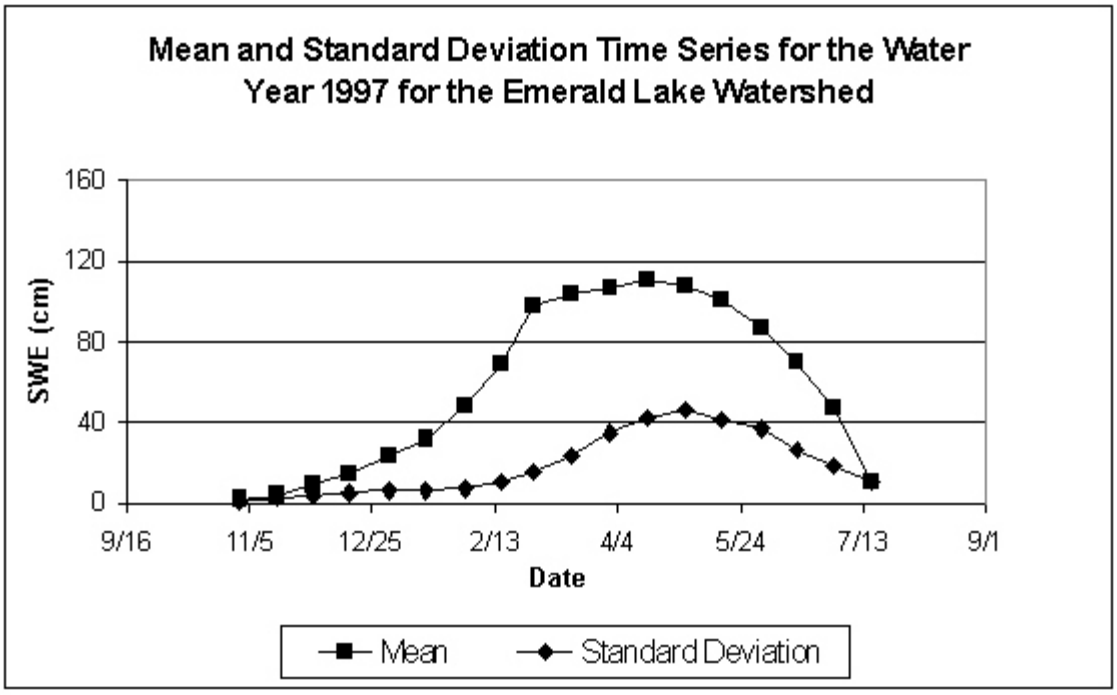
Mean and Standard Deviation Time Series for the Water Year 1997 for the Emerald Lake Watershed
SWE (cm)
160
120
80
40
0
9/16
11/5
12/25
2/13
4/4
5/24
7/13
9/1
Date
Mean
Standard Deviation

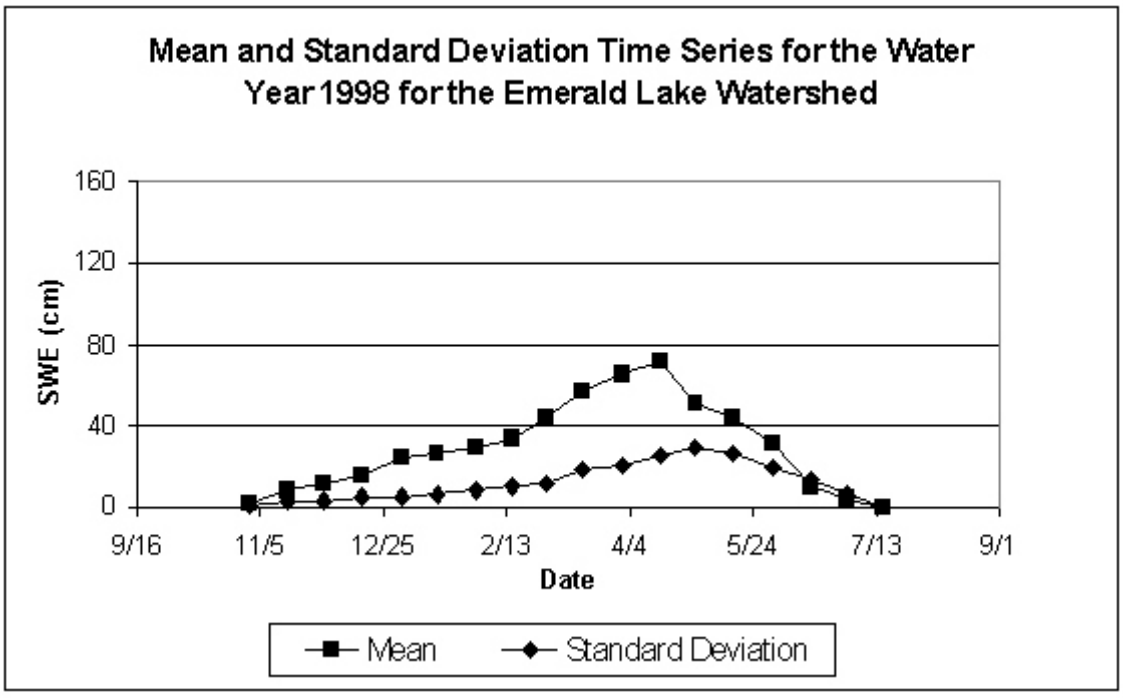
Mean and Standard Deviation Time Series for the Water Year 1998 for the Emerald Lake Watershed
160
120
80
40
0
SWE (cm)
9/16
11/5
12/25
2/13
4/4
5/24
7/13
9/1
Date
Mean
Standard Deviation

Appendix O

Time Series Plots of Modeled Snow Water Equivalent Distributions
for the Upper Rio Grande Watershed

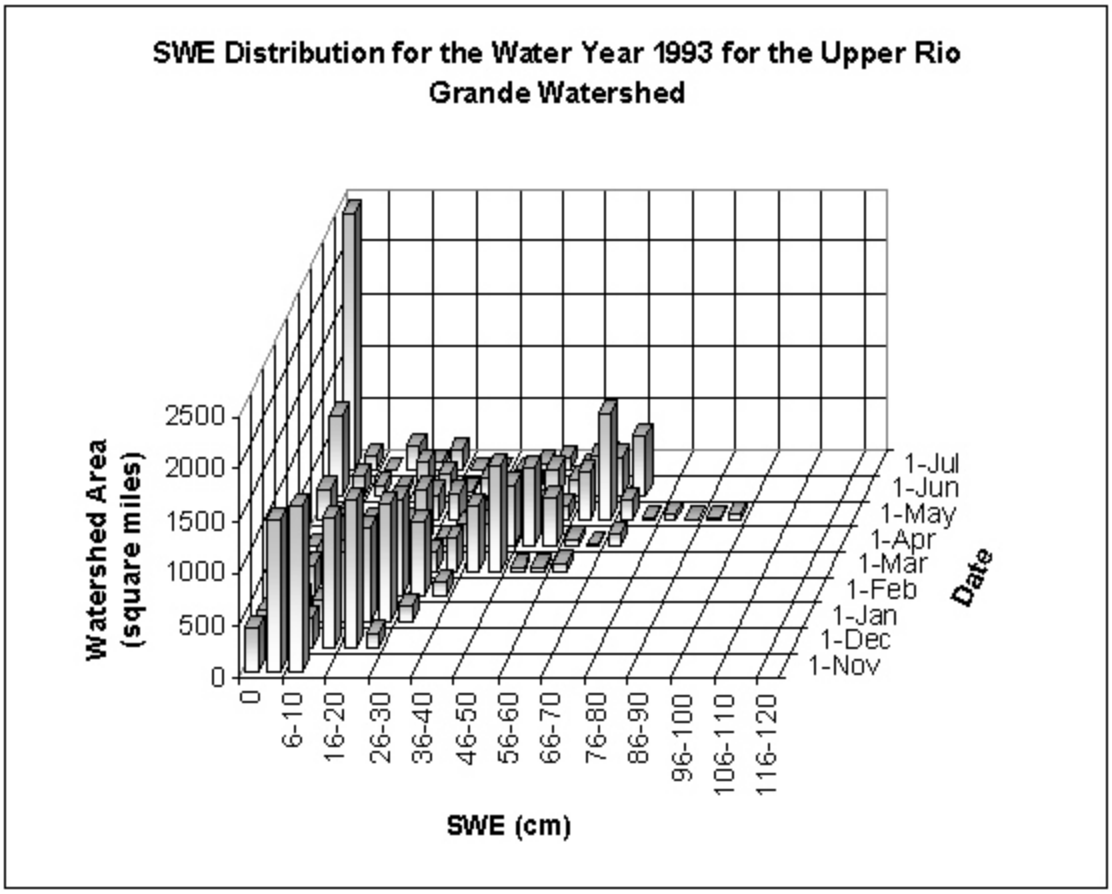
SWE Distribution for the Water Year 1993 for the Upper Rio Grande Watershed
Watershed Area (square miles)
2500
2000
1500
1000
500
0
0
6-10
16-20
26-30
36-40
46-50
56-60
66-70
76-80
86-90
96-100
106-110
116-120
SWE (cm)
1-Jul
1-Jun
1-May
1-Apr
1-Mar
1-Feb
1-Jan
1-Dec
1-Nov
Date

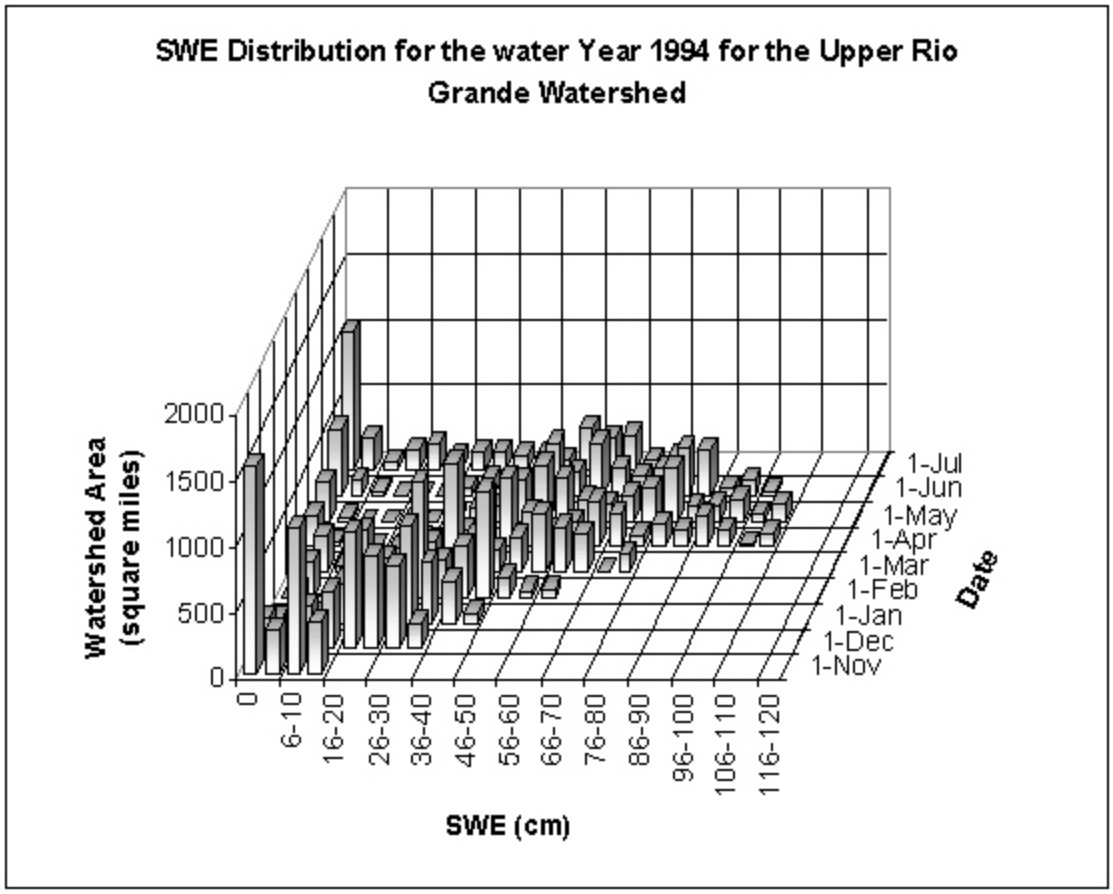
SWE Distribution for the water Year 1994 for the Upper Rio Grande Watershed
Watershed Area (square miles)
2000
1500
1000
500
0
0
6-10
16-20
26-30
36-40
46-50
56-60
66-70
76-80
86-90
96-100
106-110
116-120
SWE (cm)
1-Jul
1-Jun
1-May
1-Apr
1-Mar
1-Feb
1-Jan
1-Dec
1-Nov
Date

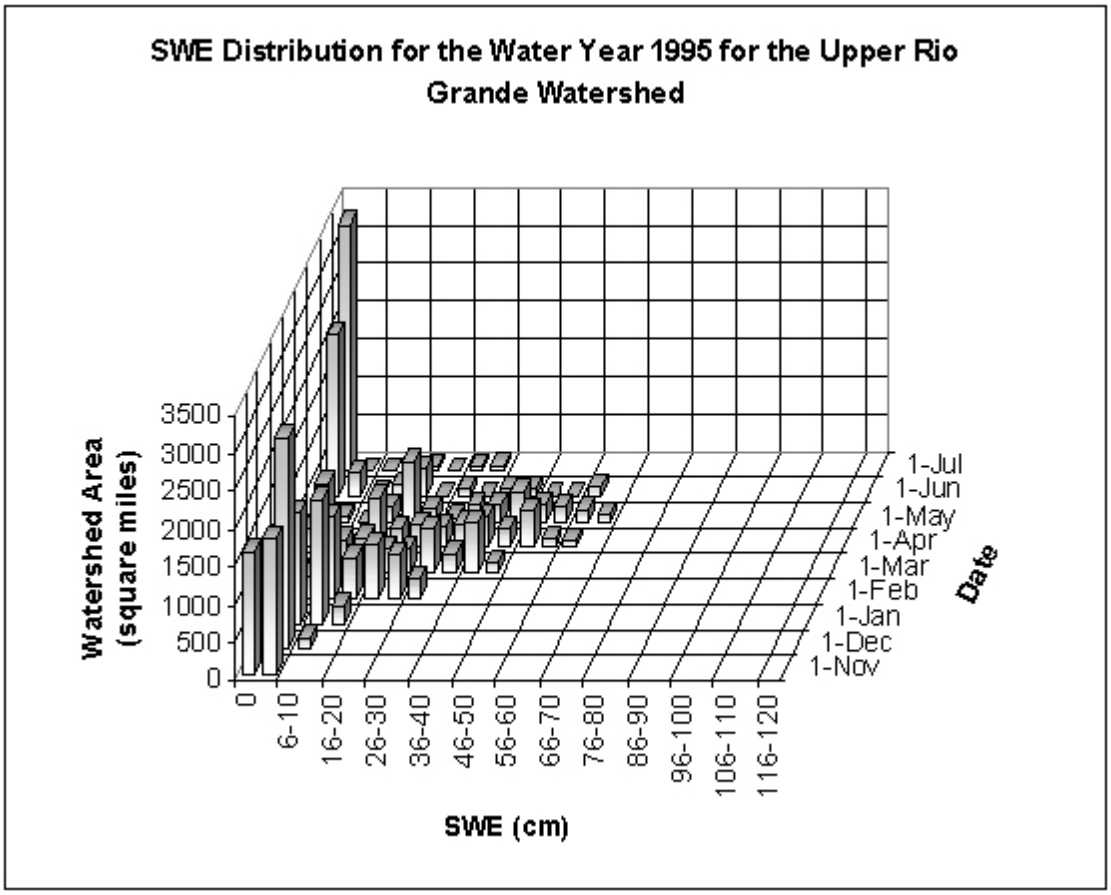
SWE Distribution for the Water Year 1995 for the Upper Rio Grande Watershed
Watershed Area (square miles)
3500
3000
2500
2000
1500
1000
500
0
0
6-10
16-20
26-30
36-40
46-50
56-60
66-70
76-80
86-90
96-100
106-110
116-120
SWE (cm)
1-Jul
1-Jun
1-May
1-Apr
1-Mar
1-Feb
1-Jan
1-Dec
1-Nov
Date

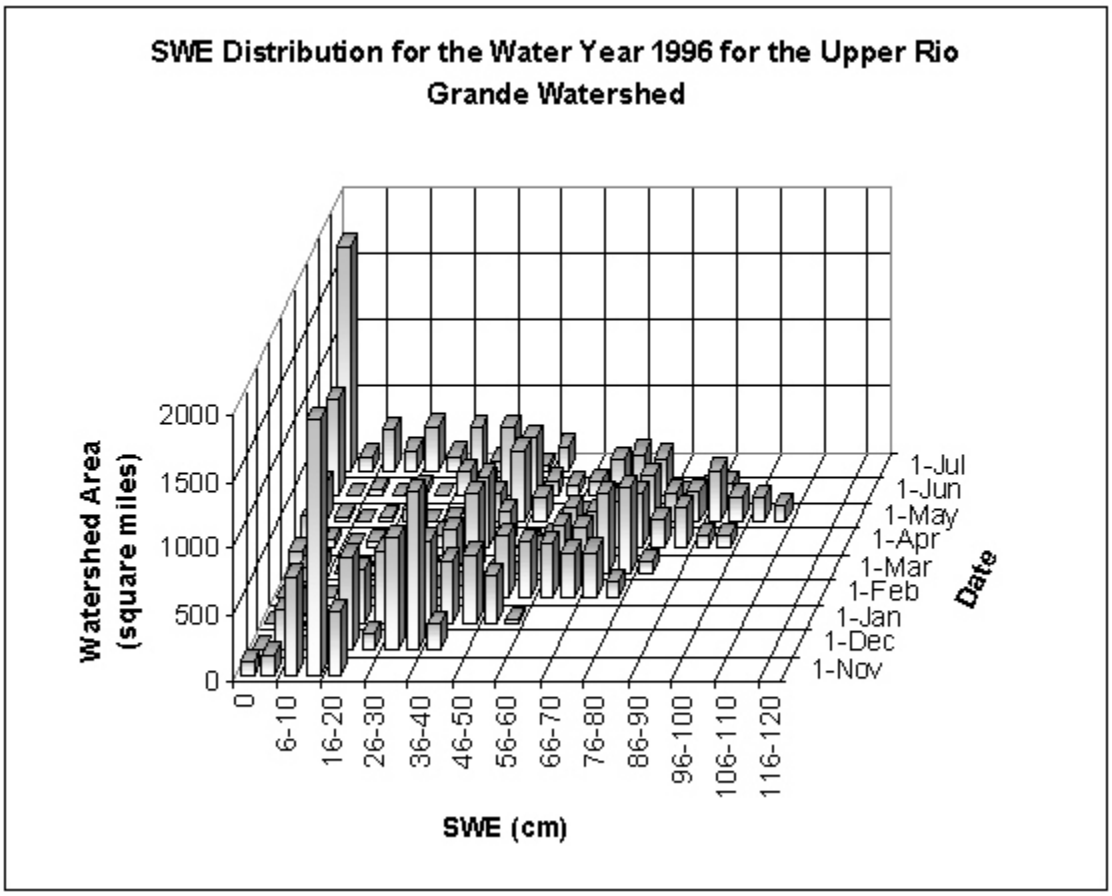
SWE Distribution for the Water Year 1996 for the Upper Rio Grande Watershed
Watershed Area (square miles)
2000
1500
1000
500
0
0
6-10
16-20
26-30
36-40
46-50
56-60
66-70
76-80
86-90
96-100
106-110
116-120
SWE (cm)
1-Jul
1-Jun
1-May
1-Apr
1-Mar
1-Feb
1-Jan
1-Dec
1-Nov
Date

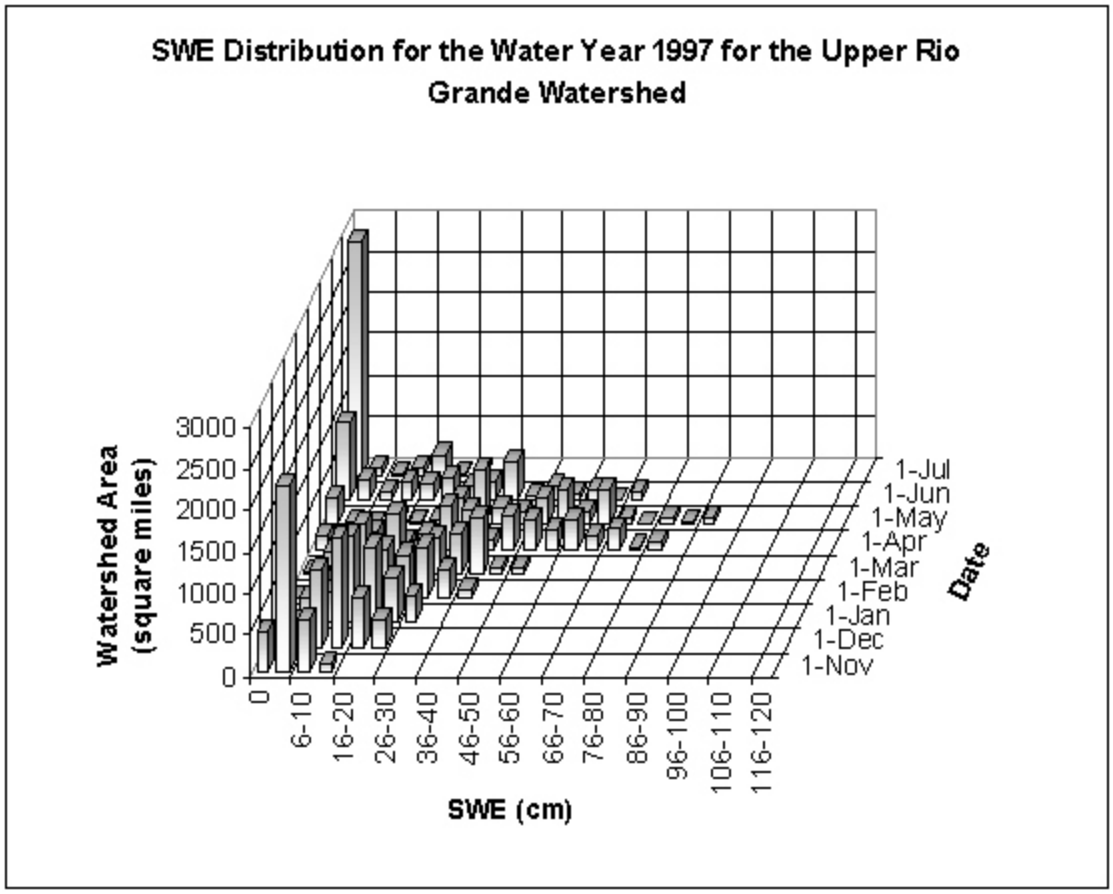
SWE Distribution for the Water Year 1997 for the Upper Rio Grande Watershed
Watershed Area (square miles)
3000
2500
2000
1500
1000
500
0
0
6-10
16-20
26-30
36-40
46-50
56-60
66-70
76-80
86-90
96-100
106-110
116-120
SWE (cm)
1-Jul
1-Jun
1-May
1-Apr
1-Mar
1-Feb
1-Jan
1-Dec
1-Nov
Date

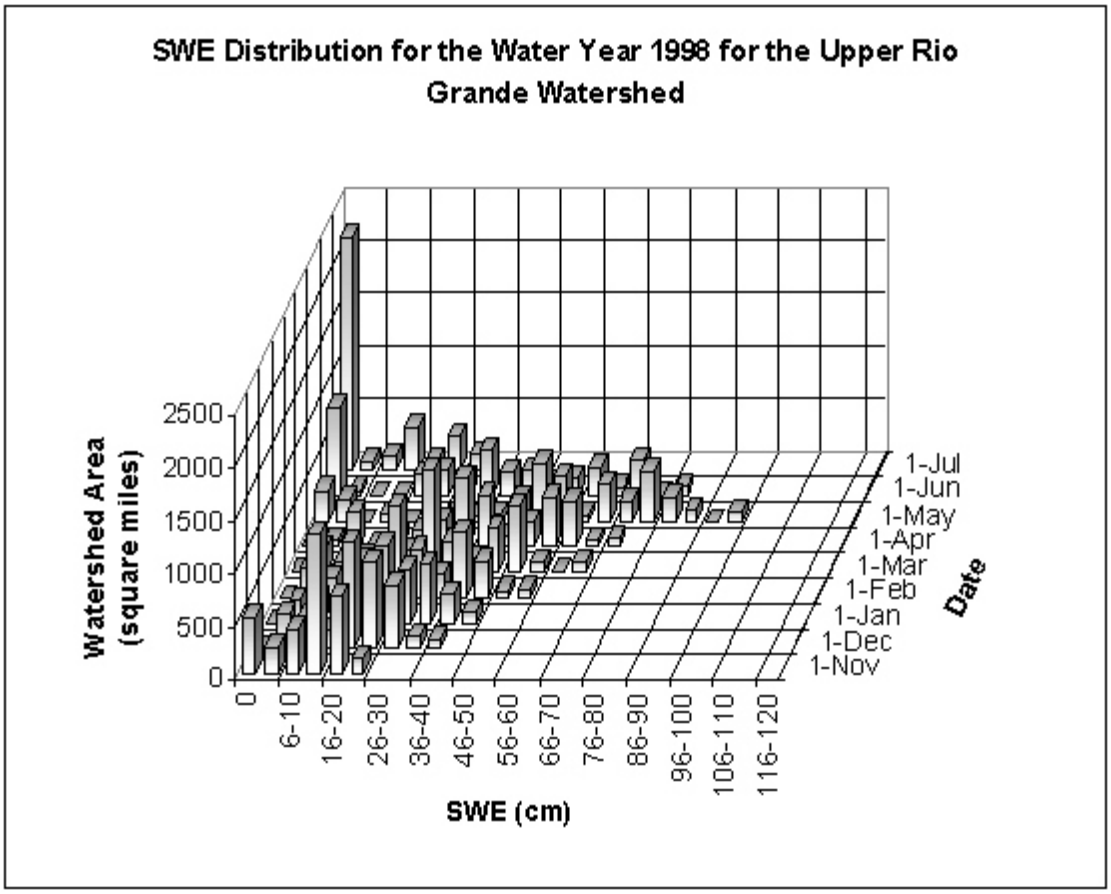
SWE Distribution for the Water Year 1998 for the Upper Rio Grande Watershed
Watershed Area (square miles)
2500
2000
1500
1000
500
0
0
6-10
16-20
26-30
36-40
46-50
56-60
66-70
76-80
86-90
96-100
106-110
116-120
SWE (cm)
1-Jul
1-Jun
1-May
1-Apr
1-Mar
1-Feb
1-Jan
1-Dec
1-Nov
Date

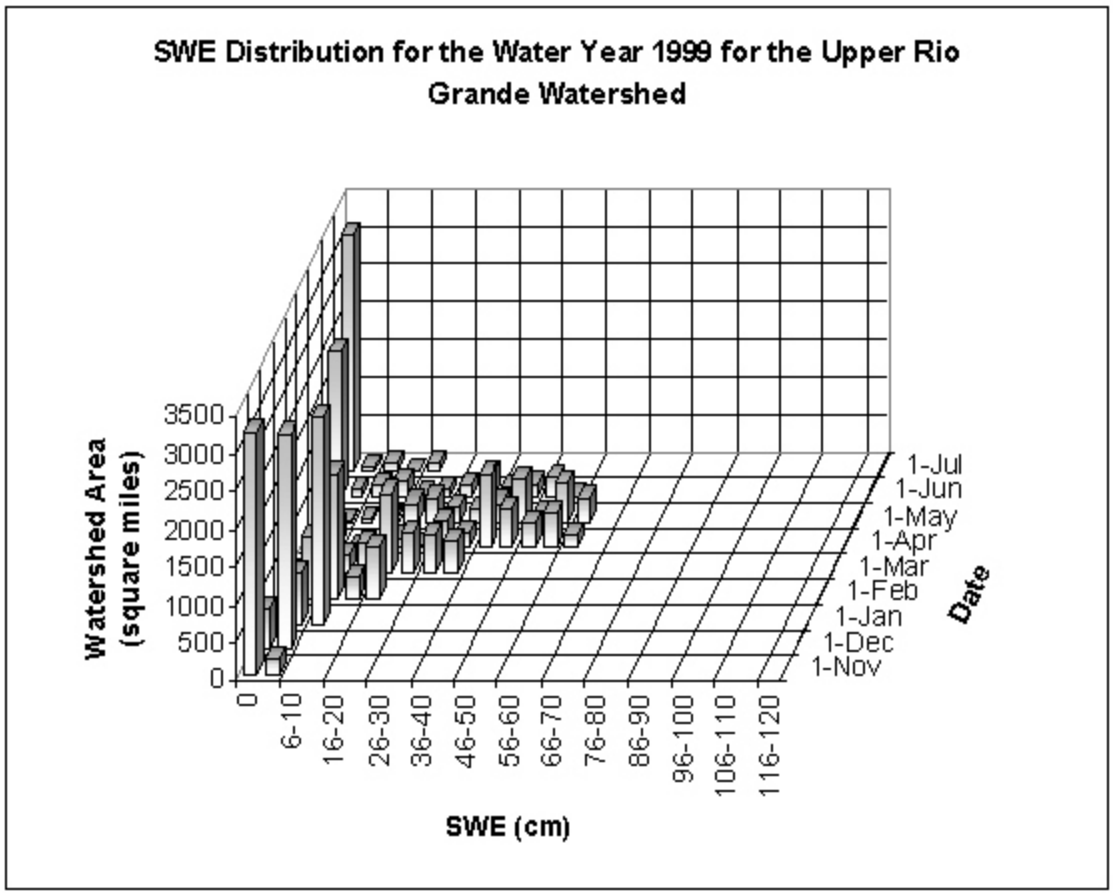
SWE Distribution for the Water Year 1999 for the Upper Rio Grande Watershed
Watershed Area (square miles)
3500
3000
2500
2000
1500
1000
500
0
0
6-10
16-20
26-30
36-40
46-50
56-60
66-70
76-80
86-90
96-100
106-110
116-120
SWE (cm)
1-Jul
1-Jun
1-May
1-Apr
1-Mar
1-Feb
1-Jan
1-Dec
1-Nov
Date

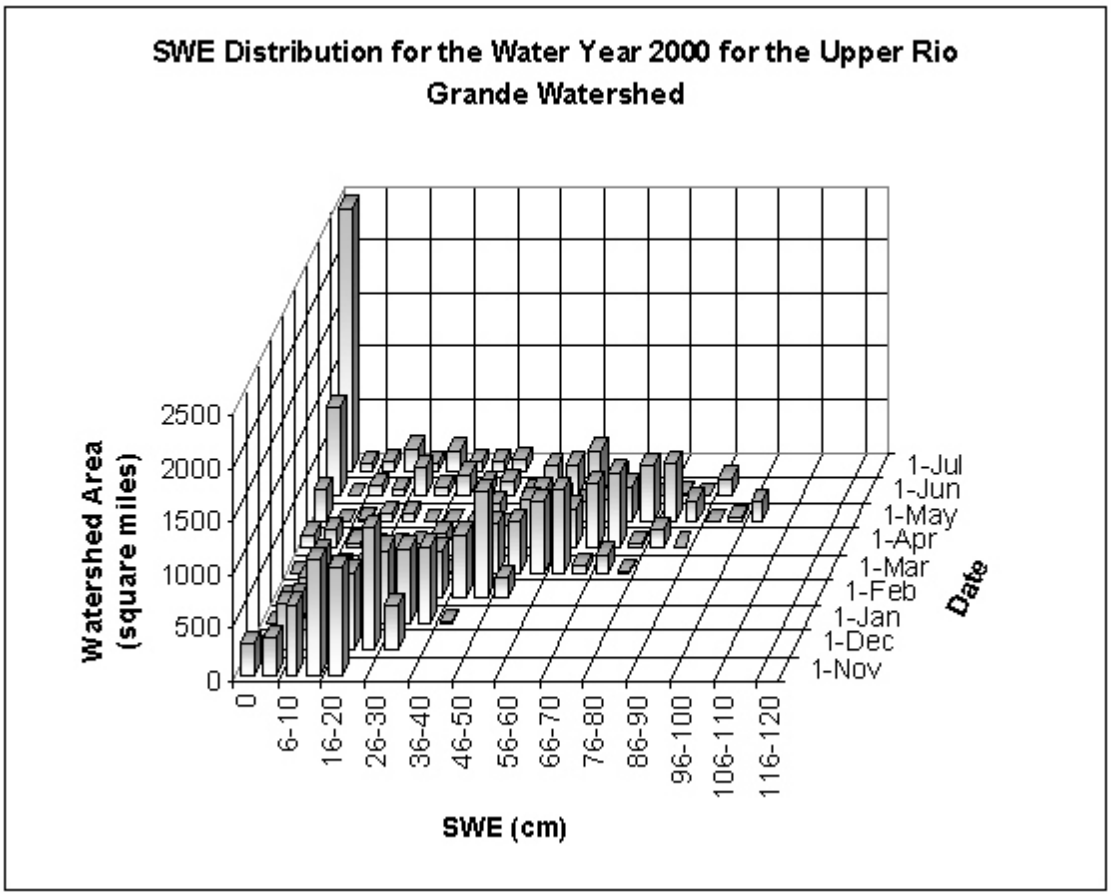
SWE Distribution for the Water Year 2000 for the Upper Rio Grande Watershed
Watershed Area (square miles)
2500
2000
1500
1000
500
0
0
6-10
16-20
26-30
36-40
46-50
56-60
66-70
76-80
86-90
96-100
106-110
116-120
SWE (cm)
1-Jul
1-Jun
1-May
1-Apr
1-Mar
1-Feb
1-Jan
1-Dec
1-Nov
Date

Appendix P

Results of the Kolmogorov-Smirnov Two-Sample Test for the Upper Rio Grande Watershed

Note: The null hypothesis associated with the Kolmogorov-Smirnov two-sample test is that the distributions of the two SWE samples are the same.

Table P-1. Results of the Kolmogorov-Smirnov Two-Sample Test during the accumulation period for the Upper Rio Grande Watershed (n = 304).

Test Number	Date	Mean SWE (cm)	Test Statistic (D)	Level of Significance ( )	Critical D Value (D)	Decision
1	1/1/94	16.98	0.0778	0.1	0.0292	**reject**
	12/1/00	17.37		0.05	0.0329	**reject**
				0.025	0.0358	**reject**
				0.01	0.0394	**reject**
				0.005	0.0419	**reject**
				0.001	0.0472	**reject**
2	12/1/94	18.99	0.0678	0.1	0.0292	**reject**
	12/1/98	19.40		0.05	0.0329	**reject**
				0.025	0.0358	**reject**
				0.01	0.0394	**reject**
				0.005	0.0419	**reject**
				0.001	0.0472	**reject**
3	3/1/94	31.89	0.1136	0.1	0.0292	**reject**
	2/1/95	32.43		0.05	0.0329	**reject**
				0.025	0.0358	**reject**
				0.01	0.0394	**reject**
				0.005	0.0419	**reject**
				0.001	0.0472	**reject**
4	2/1/95	32.43	0.2761	0.1	0.0292	**reject**
	3/1/98	32.33		0.05	0.0329	**reject**
				0.025	0.0358	**reject**
				0.01	0.0394	**reject**
				0.005	0.0419	**reject**
				0.001	0.0472	**reject**

Table P-1. Results of the Kolmogorov-Smirnov Two-Sample Test during the accumulation period for the Upper Rio Grande Watershed, continued.

Test Number	Date	Mean SWE (cm)	Test Statistic (D)	Level of Significance ( )	Critical D Value (D)	Decision
5	3/1/94	31.89	0.2944	0.1	0.0292	**reject**
	3/1/98	32.33		0.05	0.0329	**reject**
				0.025	0.0358	**reject**
				0.01	0.0394	**reject**
				0.005	0.0419	**reject**
				0.001	0.0472	**reject**
6	1/16/94	18.43	0.5983	0.1	0.0292	**reject**
	1/16/97	18.93		0.05	0.0329	**reject**
				0.025	0.0358	**reject**
				0.01	0.0394	**reject**
				0.005	0.0419	**reject**
				0.001	0.0472	**reject**
7	11/16/93	8.76	0.2500	0.1	0.0292	**reject**
	11/16/97	8.61		0.05	0.0329	**reject**
				0.025	0.0358	**reject**
				0.01	0.0394	**reject**
				0.005	0.0419	**reject**
				0.001	0.0472	**reject**
8	12/1/93	13.68	0.2119	0.1	0.0292	**reject**
	1/16/98	13.91		0.05	0.0329	**reject**
				0.025	0.0358	**reject**
				0.01	0.0394	**reject**
				0.005	0.0419	**reject**
				0.001	0.0472	**reject**

Table P-1. Results of the Kolmogorov-Smirnov Two-Sample Test during the accumulation period for the Upper Rio Grande Watershed, continued.

Test Number	Date	Mean SWE (cm)	Test Statistic (D)	Level of Significance ( )	Critical D Value (D)	Decision
9	5/1/94	48.05	0.3378	0.1	0.0292	**reject**
	3/16/01	48.66		0.05	0.0329	**reject**
				0.025	0.0358	**reject**
				0.01	0.0394	**reject**
				0.005	0.0419	**reject**
				0.001	0.0472	**reject**

Table P-2. Results of the Kolmogorov-Smirnov Two-Sample Test during the ablation period for the Upper Rio Grande Watershed (n = 304).

Test Number	Date	Mean SWE (cm)	Test Statistic (D)	Level of Significance ( )	Critical D Value (D)	Decision
1	6/1/94	35.22	0.1086	0.1	0.0292	**reject**
	6/1/01	35.10		0.05	0.0329	**reject**
				0.025	0.0358	**reject**
				0.01	0.0394	**reject**
				0.005	0.0419	**reject**
				0.001	0.0472	**reject**
2	7/1/94	7.47	0.0865	0.1	0.0292	**reject**
	6/1/96	7.95		0.05	0.0329	**reject**
				0.025	0.0358	**reject**
				0.01	0.0394	**reject**
				0.005	0.0419	**reject**
				0.001	0.0472	**reject**
3	6/1/96	7.95	0.1856	0.1	0.0292	**reject**
	6/16/00	8.11		0.05	0.0329	**reject**
				0.025	0.0358	**reject**
				0.01	0.0394	**reject**
				0.005	0.0419	**reject**
				0.001	0.0472	**reject**
4	6/16/94	22.44	0.3350	0.1	0.0292	**reject**
	6/1/98	22.26		0.05	0.0329	**reject**
				0.025	0.0358	**reject**
				0.01	0.0394	**reject**
				0.005	0.0419	**reject**
				0.001	0.0472	**reject**

Table P-2. Results of the Kolmogorov-Smirnov Two-Sample Test during the ablation period for the Upper Rio Grande Watershed, continued.

Test Number	Date	Mean SWE (cm)	Test Statistic (D)	Level of Significance ( )	Critical D Value (D)	Decision
5	5/16/00	23.18	0.3991	0.1	0.0292	**reject**
	6/16/01	22.69		0.05	0.0329	**reject**
				0.025	0.0358	**reject**
				0.01	0.0394	**reject**
				0.005	0.0419	**reject**
				0.001	0.0472	**reject**
6	6/1/98	22.26	0.2908	0.1	0.0292	**reject**
	5/16/00	23.18		0.05	0.0329	**reject**
				0.025	0.0358	**reject**
				0.01	0.0394	**reject**
				0.005	0.0419	**reject**
				0.001	0.0472	**reject**
7	6/16/94	22.44	0.3243	0.1	0.0292	**reject**
	6/16/01	22.69		0.05	0.0329	**reject**
				0.025	0.0358	**reject**
				0.01	0.0394	**reject**
				0.005	0.0419	**reject**
				0.001	0.0472	**reject**
8	6/16/94	22.44	0.1915	0.1	0.0292	**reject**
	5/16/00	23.18		0.05	0.0329	**reject**
				0.025	0.0358	**reject**
				0.01	0.0394	**reject**
				0.005	0.0419	**reject**
				0.001	0.0472	**reject**

Table P-2. Results of the Kolmogorov-Smirnov Two-Sample Test during the ablation period for the Upper Rio Grande Watershed, continued.

Test Number	Date	Mean SWE (cm)	Test Statistic (D)	Level of Significance ( )	Critical D Value (D)	Decision
9	6/1/94	35.22	0.2476	0.1	0.0292	**reject**
	5/16/98	36.11		0.05	0.0329	**reject**
				0.025	0.0358	**reject**
				0.01	0.0394	**reject**
				0.005	0.0419	**reject**
				0.001	0.0472	**reject**

Appendix Q

Time Series Plots of Modeled Snow Water Equivalent Distributions
for the Reynolds Creek Watershed

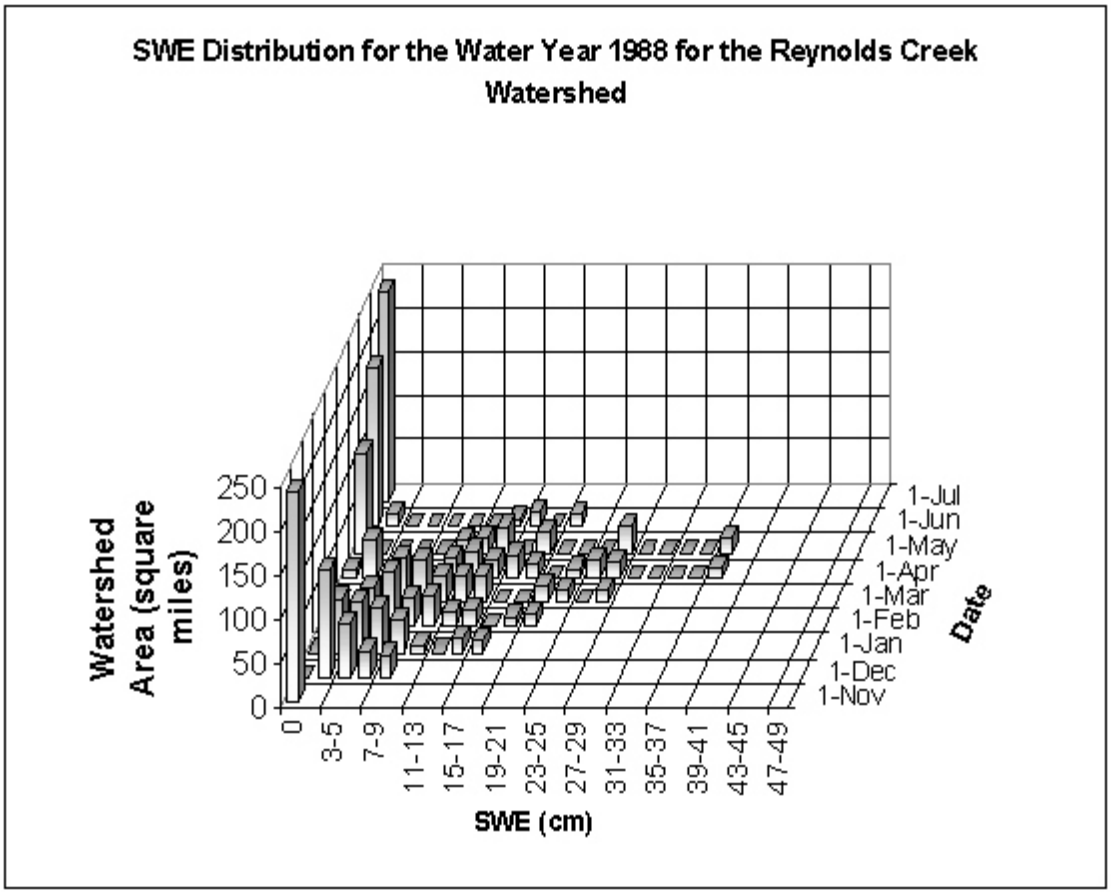
SWE Distribution for the Water Year 1988 for the Reynolds Creek Watershed
Watershed Area (square miles)
250
200
150
100
50
0
0
3-5
7-9
11-13
15-17
19-21
23-25
27-29
31-33
35-37
39-41
43-45
47-49
SWE (cm)
1-Jul
1-Jun
1-May
1-Apr
1-Mar
1-Feb
1-Jan
1-Dec
1-Nov
Date

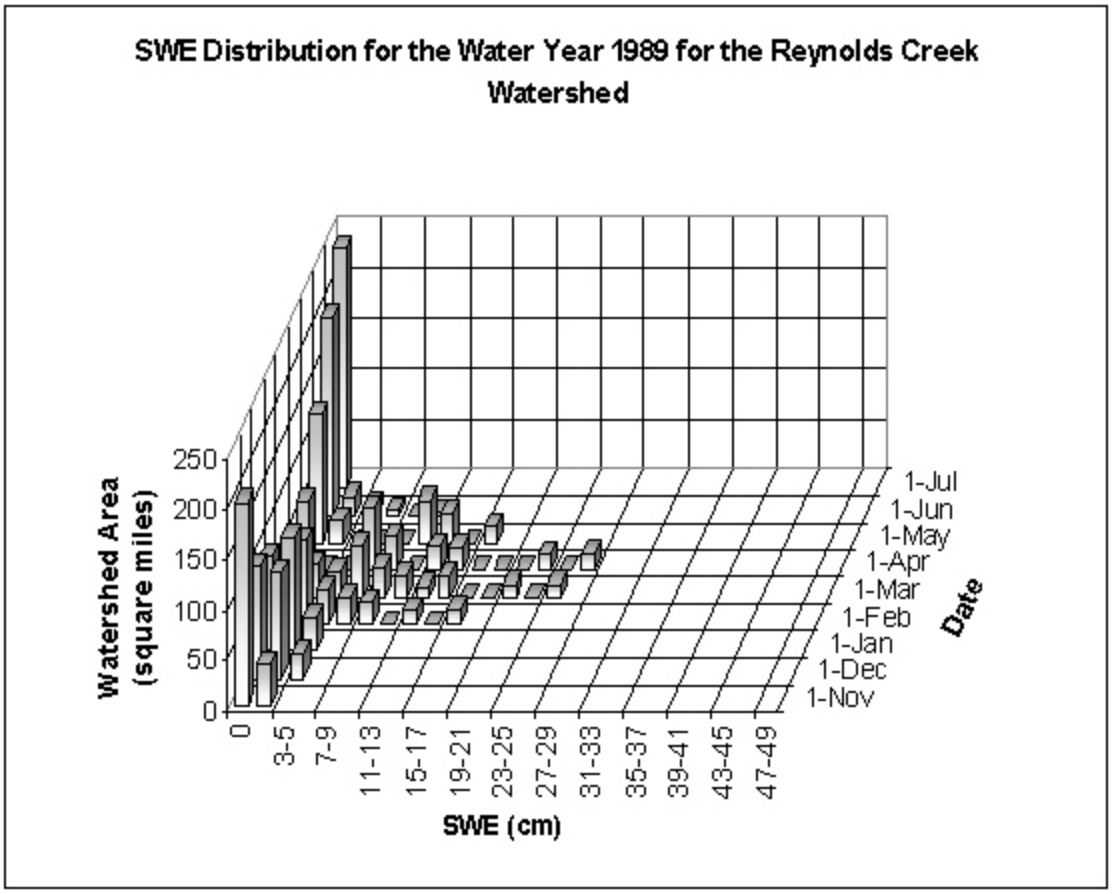
SWE Distribution for the Water Year 1989 for the Reynolds Creek Watershed
Watershed Area (square miles)
250
200
150
100
50
0
0
3-5
7-9
11-13
15-17
19-21
23-25
27-29
31-33
35-37
39-41
43-45
47-49
SWE (cm)
1-Jul
1-Jun
1-May
1-Apr
1-Mar
1-Feb
1-Jan
1-Dec
1-Nov
Date

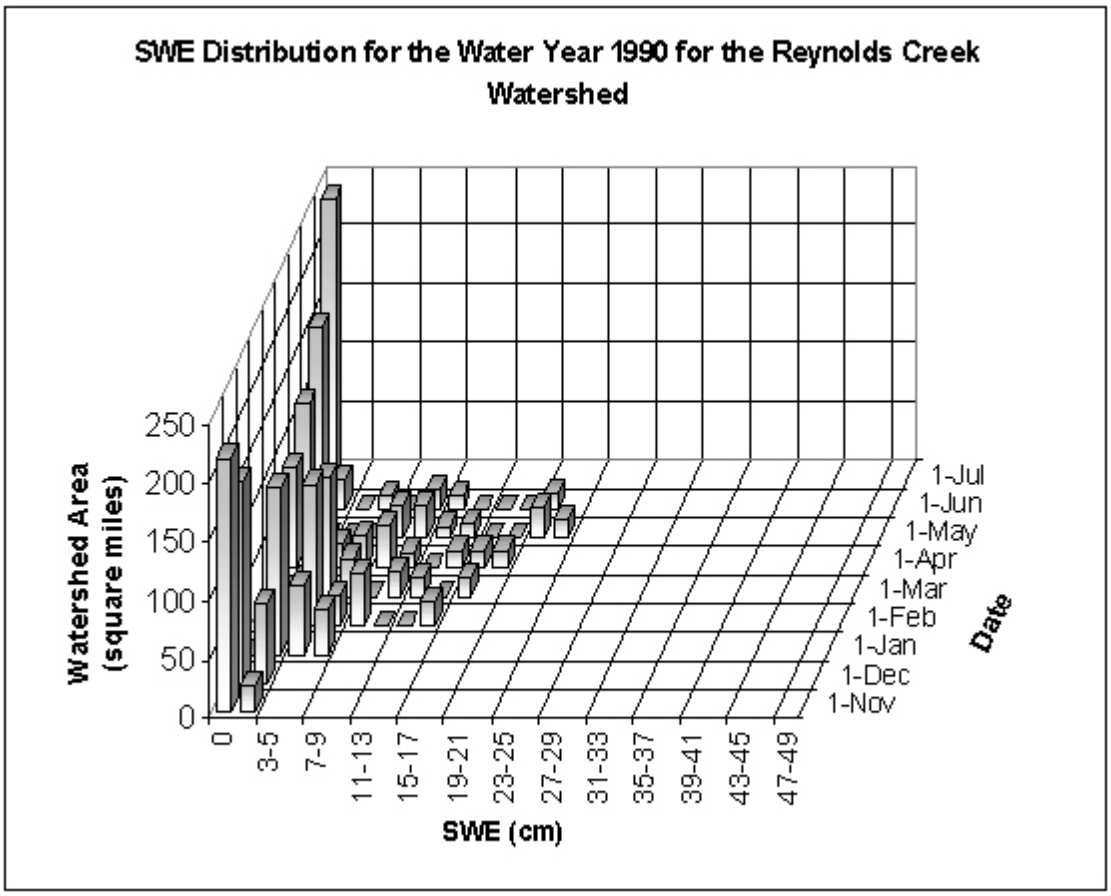
SWE Distribution for the Water Year 1990 for the Reynolds Creek Watershed
Watershed Area (square miles)
250
200
150
100
50
0
0
3-5
7-9
11-13
15-17
19-21
23-25
27-29
31-33
35-37
39-41
43-45
47-49
SWE (cm)
1-Jul
1-Jun
1-May
1-Apr
1-Mar
1-Feb
1-Jan
1-Dec
1-Nov
Date

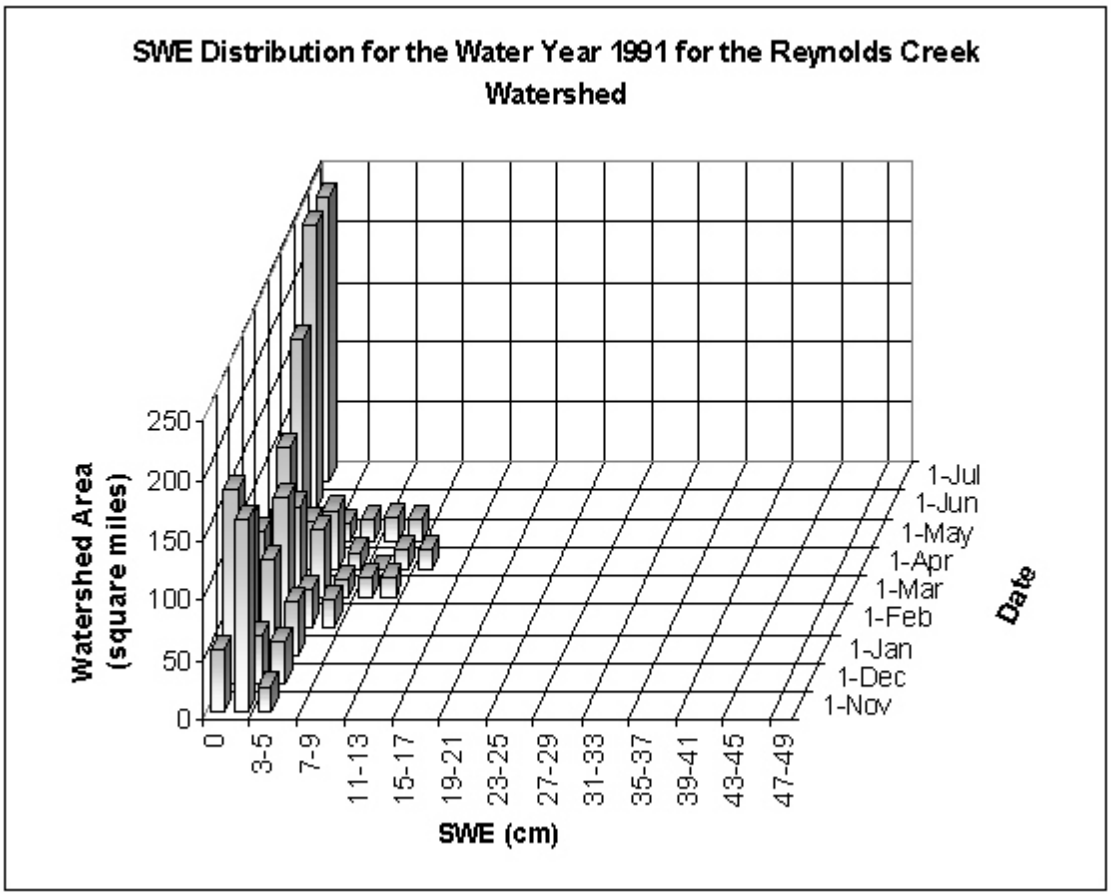
SWE Distribution for the Water Year 1991 for the Reynolds Creek Watershed
Watershed Area (square miles)
250
200
150
100
50
0
0
3-5
7-9
11-13
15-17
19-21
23-25
27-29
31-33
35-37
39-41
43-45
47-49
SWE (cm)
1-Jul
1-Jun
1-May
1-Apr
1-Mar
1-Feb
1-Jan
1-Dec
1-Nov
Date

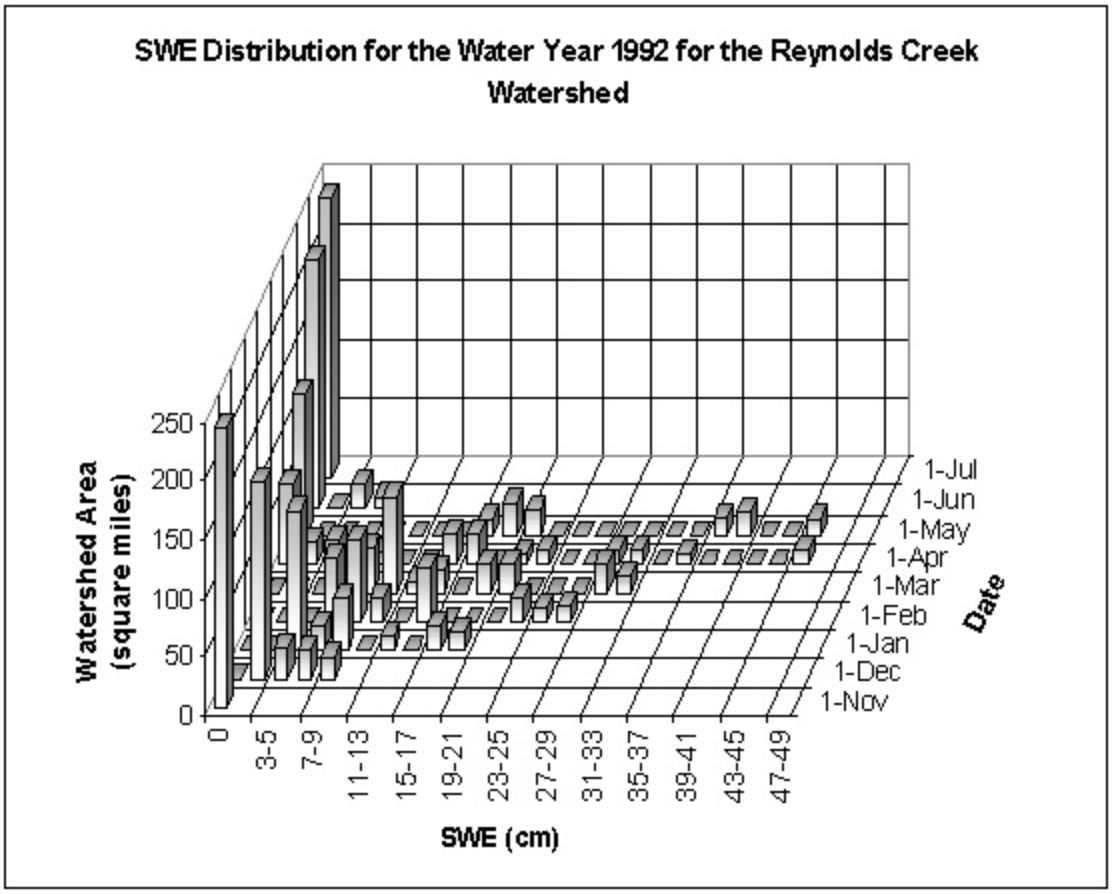
SWE Distribution for the Water Year 1992 for the Reynolds Creek Watershed
Watershed Area (square miles)
250
200
150
100
50
0
0
3-5
7-9
11-13
15-17
19-21
23-25
27-29
31-33
35-37
39-41
43-45
47-49
SWE (cm)
1-Jul
1-Jun
1-May
1-Apr
1-Mar
1-Feb
1-Jan
1-Dec
1-Nov
Date

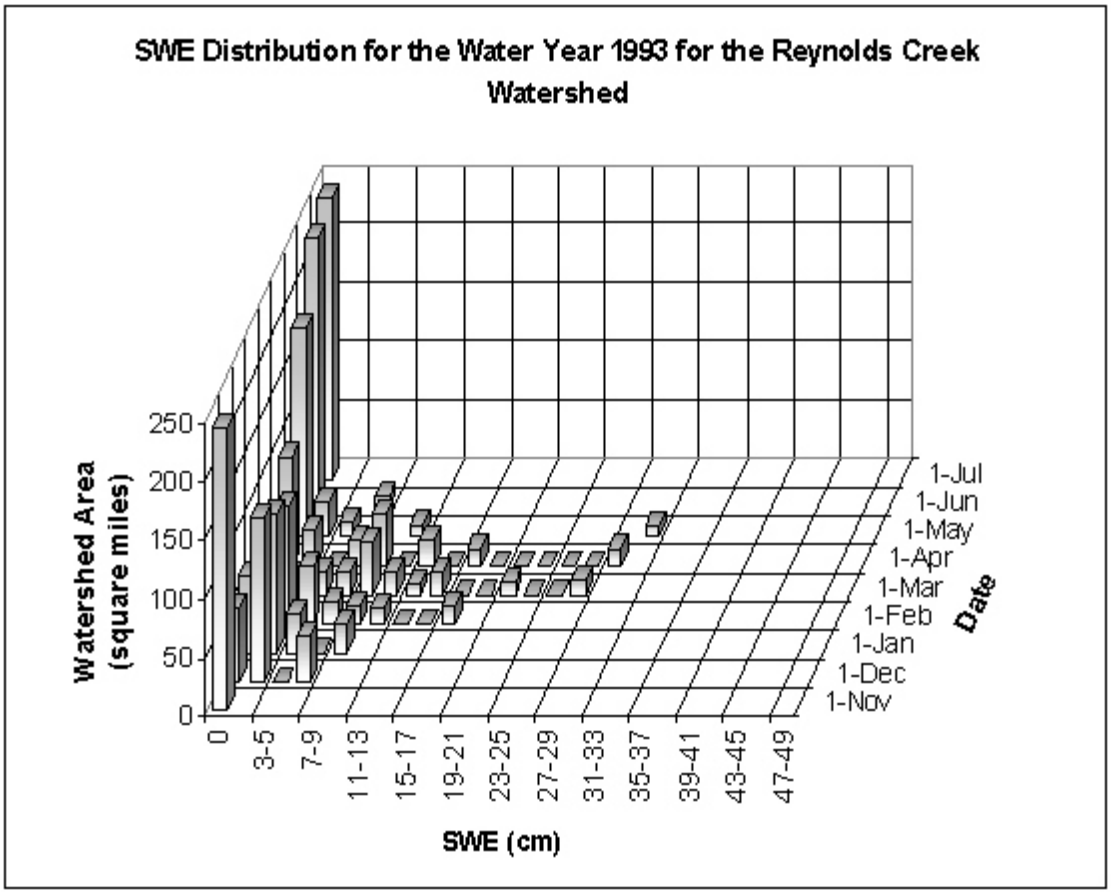
SWE Distribution for the Water Year 1993 for the Reynolds Creek Watershed
Watershed Area (square miles)
250
200
150
100
50
0
0
3-5
7-9
11-13
15-17
19-21
23-25
27-29
31-33
35-37
39-41
43-45
47-49
SWE (cm)
1-Jul
1-Jun
1-May
1-Apr
1-Mar
1-Feb
1-Jan
1-Dec
1-Nov
Date

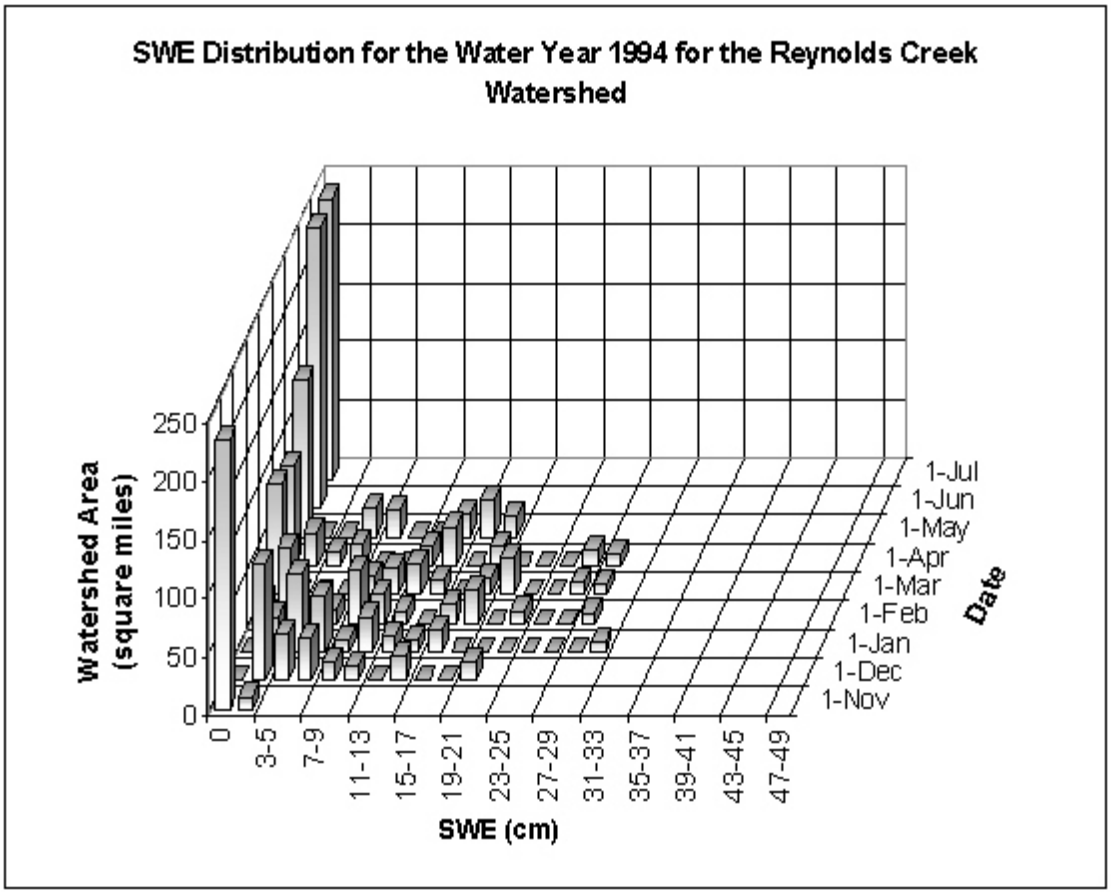
SWE Distribution for the Water Year 1994 for the Reynolds Creek Watershed
Watershed Area (square miles)
250
200
150
100
50
0
0
3-5
7-9
11-13
15-17
19-21
23-25
27-29
31-33
35-37
39-41
43-45
47-49
SWE (cm)
1-Jul
1-Jun
1-May
1-Apr
1-Mar
1-Feb
1-Jan
1-Dec
1-Nov
Date

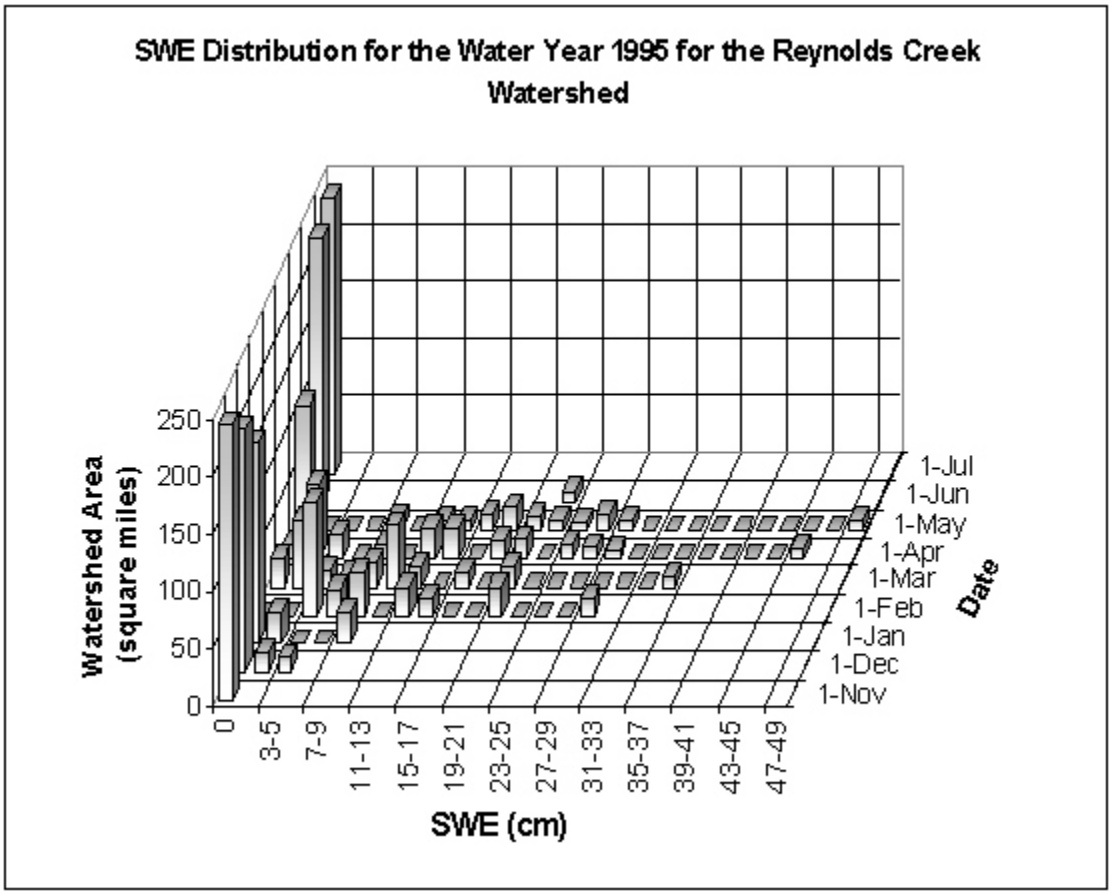
SWE Distribution for the Water Year 1995 for the Reynolds Creek Watershed
Watershed Area (square miles)
250
200
150
100
50
0
0
3-5
7-9
11-13
15-17
19-21
23-25
27-29
31-33
35-37
39-41
43-45
47-49
SWE (cm)
1-Jul
1-Jun
1-May
1-Apr
1-Mar
1-Feb
1-Jan
1-Dec
1-Nov
Date

Appendix R

Results of the Kolmogorov-Smirnov Two-Sample Test for the Reynolds Creek Watershed

Note: The null hypothesis associated with the Kolmogorov-Smirnov two-sample test is that the distributions of the two SWE samples are the same.

Table R-1. Results of the Kolmogorov-Smirnov Two-Sample Test during the accumulation period for the Reynolds Creek Watershed (n = 304).

Test Number	Date	Mean SWE (cm)	Test Statistic (D)	Level of Significance ( )	Critical D Value (D)	Decision
1	3/1/89	11.25	0.1078	0.1	0.1120	**accept**
	2/1/93	11.01		0.05	0.1248	**accept**
				0.025	0.1358	**accept**
				0.01	0.1496	**accept**
				0.005	0.1588	**accept**
				0.001	0.1790	**accept**
2	12/1/88	3.25	0.1841	0.1	0.1120	**reject**
	2/1/90	3.68		0.05	0.1248	**reject**
				0.025	0.1358	**reject**
				0.01	0.1496	**reject**
				0.005	0.1588	**reject**
				0.001	0.1790	**reject**
3	12/1/88	3.25	0.1213	0.1	0.1120	**reject**
	2/1/94	3.02		0.05	0.1248	**accept**
				0.025	0.1358	**accept**
				0.01	0.1496	**accept**
				0.005	0.1588	**accept**
				0.001	0.1790	**accept**
4	2/1/90	3.68	0.711	0.1	0.1120	**accept**
	2/1/94	3.02		0.05	0.1248	**accept**
				0.025	0.1358	**accept**
				0.01	0.1496	**accept**
				0.005	0.1588	**accept**
				0.001	0.1790	**accept**

Table R-1. Results of the Kolmogorov-Smirnov Two-Sample Test during the accumulation period for the Reynolds Creek Watershed, continued.

Test Number	Date	Mean SWE (cm)	Test Statistic (D)	Level of Significance ( )	Critical D Value (D)	Decision
5	2/1/90	3.68	0.1841	0.1	0.1120	**reject**
	1/16/91	3.69		0.05	0.1248	**reject**
				0.025	0.1358	**reject**
				0.01	0.1496	**reject**
				0.005	0.1588	**reject**
				0.001	0.1790	**reject**
6	1/16/96	3.79	0.2092	0.1	0.1120	**reject**
	1/16/91	3.69		0.05	0.1248	**reject**
				0.025	0.1358	**reject**
				0.01	0.1496	**reject**
				0.005	0.1588	**reject**
				0.001	0.1790	**reject**
7	12/16/88	4.41	0.1221	0.1	0.1120	**reject**
	2/1/91	4.44		0.05	0.1248	**accept**
				0.025	0.1358	**accept**
				0.01	0.1496	**accept**
				0.005	0.1588	**accept**
				0.001	0.1790	**accept**
8	12/16/88	4.41	0.2061	0.1	0.1120	**reject**
	12/16/92	4.57		0.05	0.1248	**reject**
				0.025	0.1358	**reject**
				0.01	0.1496	**reject**
				0.005	0.1588	**reject**
				0.001	0.1790	**reject**

Table R-1. Results of the Kolmogorov-Smirnov Two-Sample Test during the accumulation period for the Reynolds Creek Watershed, continued.

Test Number	Date	Mean SWE (cm)	Test Statistic (D)	Level of Significance ( )	Critical D Value (D)	Decision
9	2/1/91	4.44	0.1103	0.1	0.1120	**accept**
	12/16/92	4.57		0.05	0.1248	**accept**
				0.025	0.1358	**accept**
				0.01	0.1496	**accept**
				0.005	0.1588	**accept**
				0.001	0.1790	**accept**

Table R-2. Results of the Kolmogorov-Smirnov Two-Sample Test during the ablation period for the Reynolds Creek Watershed (n = 304).

Test Number	Date	Mean SWE (cm)	Test Statistic (D)	Level of Significance ( )	Critical D Value (D)	Decision
1	6/1/89	2.36	0.3412	0.1	0.1120	**reject**
	4/1/92	2.30		0.05	0.1248	**reject**
				0.025	0.1358	**reject**
				0.01	0.1496	**reject**
				0.005	0.1588	**reject**
				0.001	0.1790	**reject**
2	6/1/89	2.36	0.1688	0.1	0.1120	**reject**
	5/16/90	2.28		0.05	0.1248	**reject**
				0.025	0.1358	**reject**
				0.01	0.1496	**reject**
				0.005	0.1588	**reject**
				0.001	0.1790	**accept**
3	4/1/92	2.30	0.3975	0.1	0.1120	**reject**
	5/16/90	2.28		0.05	0.1248	**reject**
				0.025	0.1358	**reject**
				0.01	0.1496	**reject**
				0.005	0.1588	**reject**
				0.001	0.1790	**reject**
4	5/1/95	5.09	0.1444	0.1	0.1120	**reject**
	5/1/91	5.08		0.05	0.1248	**reject**
				0.025	0.1358	**reject**
				0.01	0.1496	**accept**
				0.005	0.1588	**accept**
				0.001	0.1790	**accept**

Table R-2. Results of the Kolmogorov-Smirnov Two-Sample Test during the ablation period for the Reynolds Creek Watershed, continued.

Test Number	Date	Mean SWE (cm)	Test Statistic (D)	Level of Significance ( )	Critical D Value (D)	Decision
5	5/1/95	5.09	0.1585	0.1	0.1120	**reject**
	4/1/94	4.96		0.05	0.1248	**reject**
				0.025	0.1358	**reject**
				0.01	0.1496	**reject**
				0.005	0.1588	**accept**
				0.001	0.1790	**accept**
6	4/16/95	6.31	0.2314	0.1	0.1120	**reject**
	4/16/90	5.85		0.05	0.1248	**reject**
				0.025	0.1358	**reject**
				0.01	0.1496	**reject**
				0.005	0.1588	**reject**
				0.001	0.1790	**reject**
7	4/16/95	6.31	0.1514	0.1	0.1120	**reject**
	5/16/96	6.67		0.05	0.1248	**reject**
				0.025	0.1358	**reject**
				0.01	0.1496	**reject**
				0.005	0.1588	**accept**
				0.001	0.1790	**accept**
8	5/16/89	6.07	0.1854	0.1	0.1120	**reject**
	4/16/90	5.85		0.05	0.1248	**reject**
				0.025	0.1358	**reject**
				0.01	0.1496	**reject**
				0.005	0.1588	**reject**
				0.001	0.1790	**reject**

Appendix S

Time Series Plots of Modeled Snow Water Equivalent Distributions
for the Emerald Lake Watershed

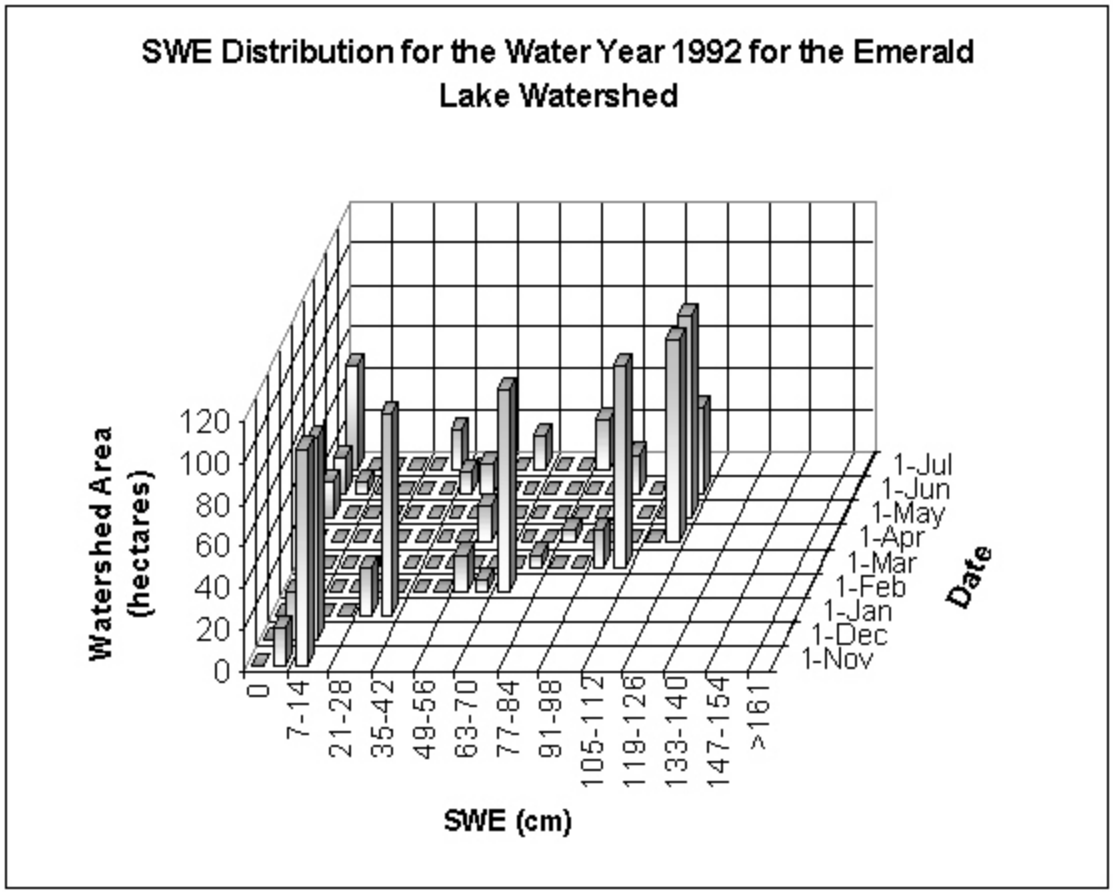
SWE Distribution for the Water Year 1992 for the Emerald Lake Watershed
Watershed Area (hectares)
120
100
80
60
40
20
0
0
7-14
21-28
35-42
49-56
63-70
77-84
91-98
105-112
119-126
133-140
147-154
>161
SWE (cm)
1-Jul
1-Jun
1-May
1-Apr
1-Mar
1-Feb
1-Jan
1-Dec
1-Nov
Date

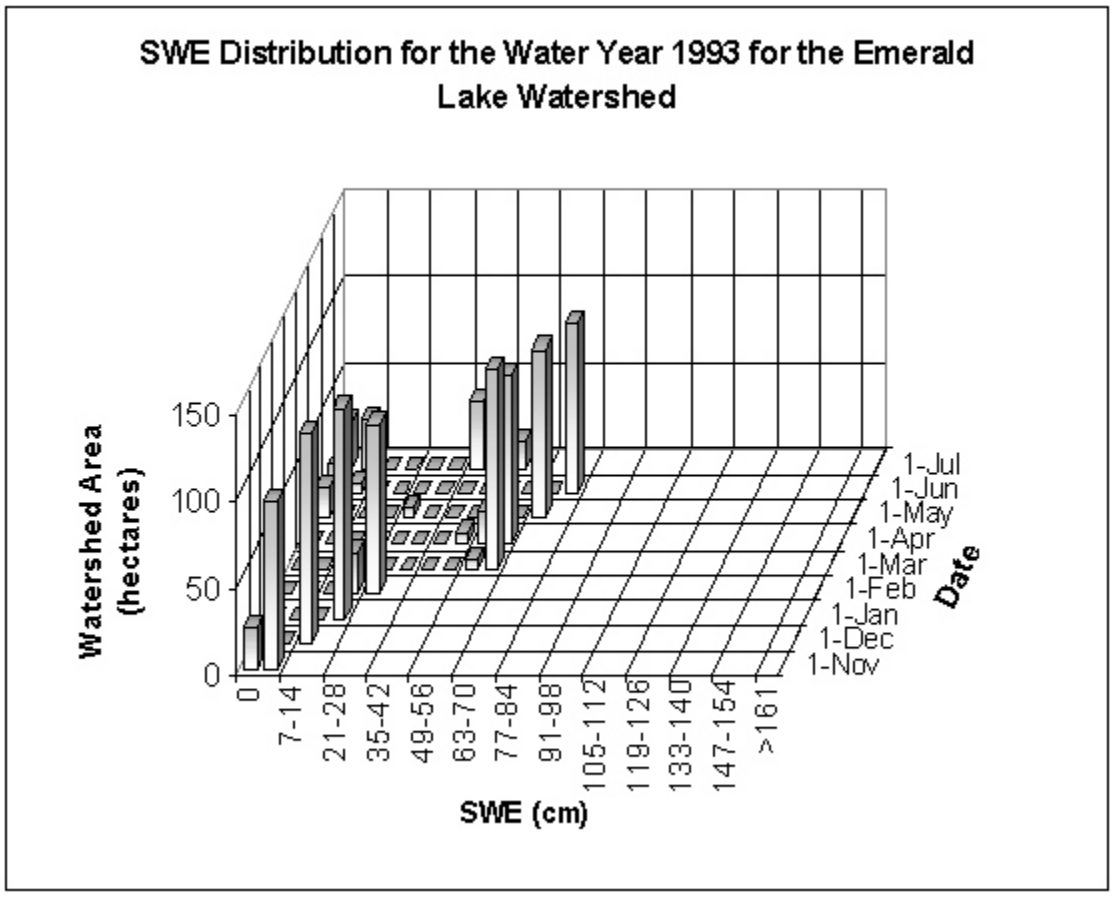
SWE Distribution for the Water Year 1993 for the Emerald Lake Watershed
Watershed Area (hectares)
150
100
50
0
0
7-14
21-28
35-42
49-56
63-70
77-84
91-98
105-112
119-126
133-140
147-154
>161
SWE (cm)
1-Jul
1-Jun
1-May
1-Apr
1-Mar
1-Feb
1-Jan
1-Dec
1-Nov
Date

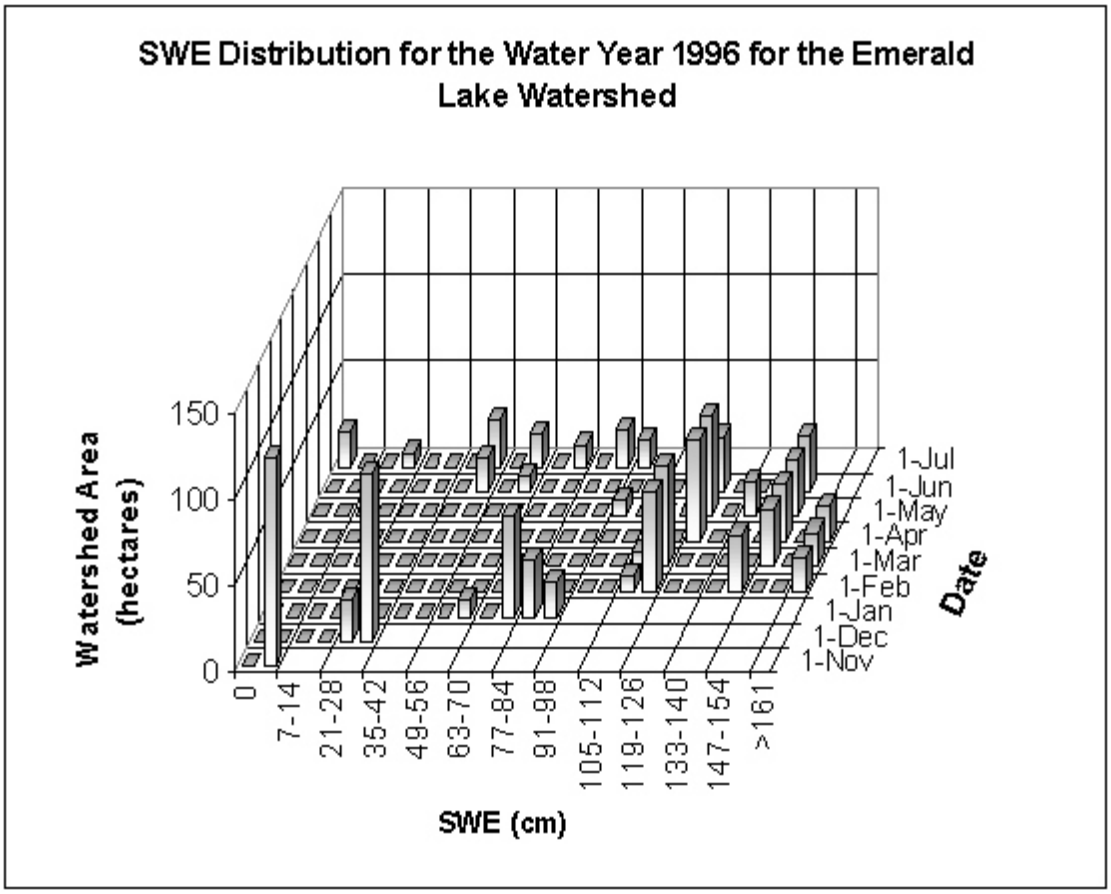
SWE Distribution for the Water Year 1996 for the Emerald Lake Watershed
Watershed Area (hectares)
150
100
50
0
0
7-14
21-28
35-42
49-56
63-70
77-84
91-98
105-112
119-126
133-140
147-154
>161
SWE (cm)
1-Jul
1-Jun
1-May
1-Apr
1-Mar
1-Feb
1-Jan
1-Dec
1-Nov
Date

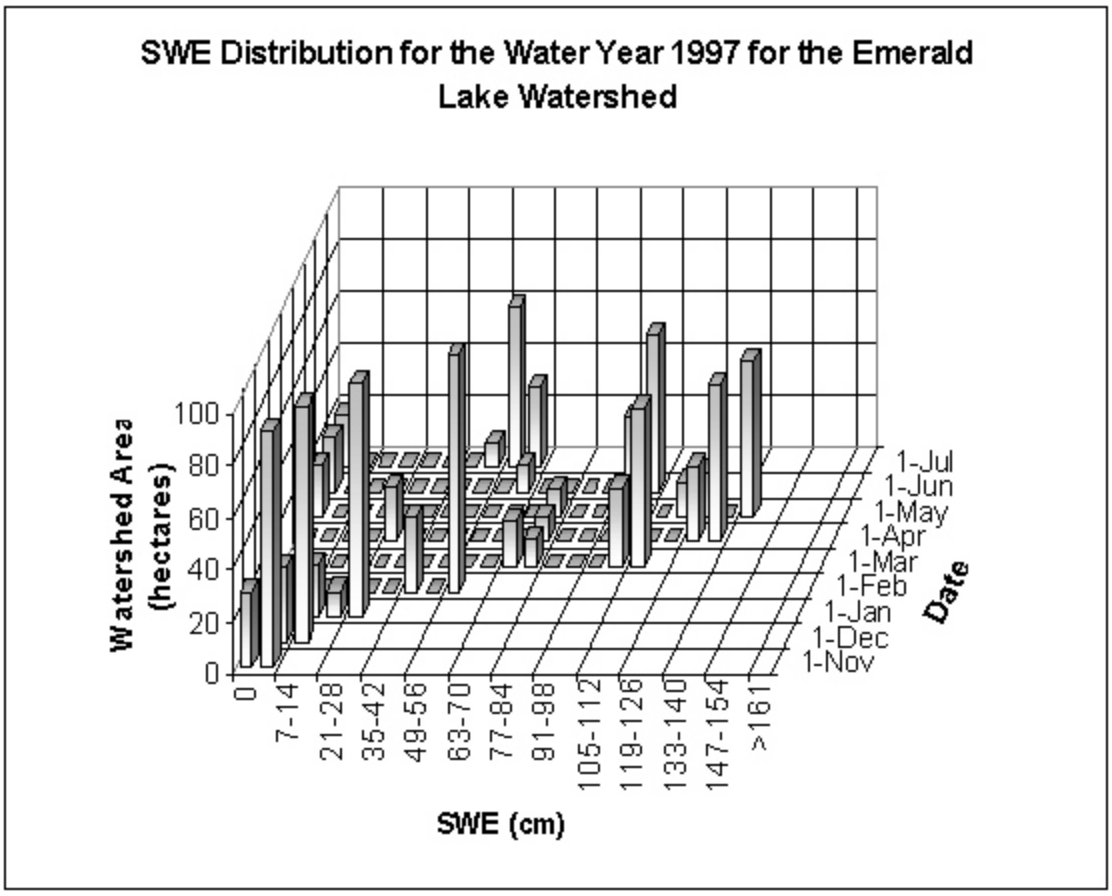
SWE Distribution for the Water Year 1997 for the Emerald Lake Watershed
Watershed Area (hectares)
100
80
60
40
20
0
0
7-14
21-28
35-42
49-56
63-70
77-84
91-98
105-112
119-126
133-140
147-154
>161
SWE (cm)
1-Jul
1-Jun
1-May
1-Apr
1-Mar
1-Feb
1-Jan
1-Dec
1-Nov
Date

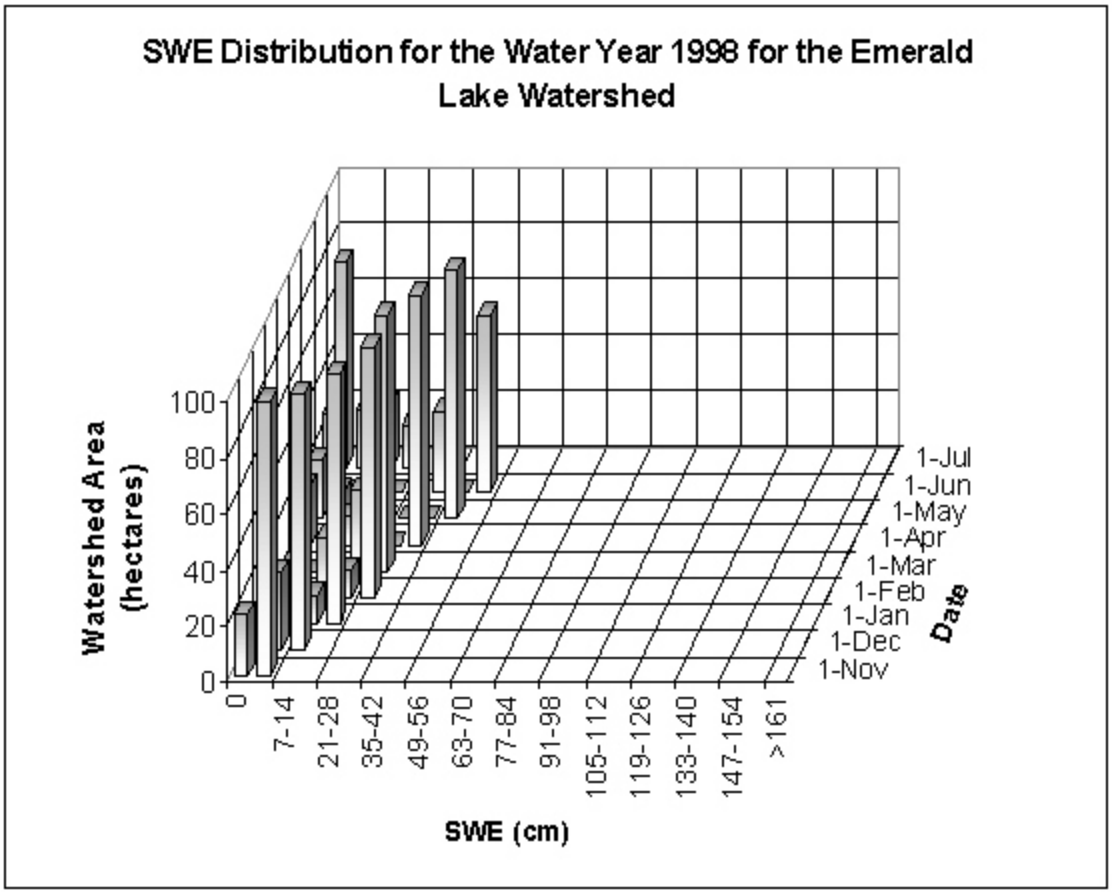
SWE Distribution for the Water Year 1998 for the Emerald Lake Watershed
Watershed Area (hectares)
0
20
40
60
80
100
0
7-14
21-28
35-42
49-56
63-70
77-84
91-98
105-112
119-126
133-140
147-154
>161
SWE (cm)
1-Jul
1-Jun
1-May
1-Apr
1-Mar
1-Feb
1-Jan
1-Dec
1-Nov
Date

Appendix T

Results of the Kolmogorov-Smirnov Two-Sample Test for the Emerald Lake Watershed

Note: The null hypothesis associated with the Kolmogorov-Smirnov two-sample test is that the distributions of the two SWE samples are the same.

Table T-1. Results of the Kolmogorov-Smirnov Two-Sample Test during the accumulation period for the Emerald Lake Watershed (n = 304).

Test Number	Date	Mean SWE (cm)	Test Statistic (D)	Level of Significance ( )	Critical D Value (D)	Decision
1	3/1/93	97.17	0.5083	0.1	0.1572	**reject**
	3/1/98	96.97		0.05	0.1752	**reject**
				0.025	0.1907	**reject**
				0.01	0.2100	**reject**
				0.005	0.2229	**reject**
				0.001	0.2512	**reject**
2	1/1/93	30.32	0.0083	0.1	0.1572	**accept**
	2/1/99	29.90		0.05	0.1752	**accept**
				0.025	0.1907	**accept**
				0.01	0.2100	**accept**
				0.005	0.2229	**accept**
				0.001	0.2512	**accept**
3	1/1/93	30.32	0.8017	0.1	0.1572	**reject**
	12/1/96	29.49		0.05	0.1752	**reject**
				0.025	0.1907	**reject**
				0.01	0.2100	**reject**
				0.005	0.2229	**reject**
				0.001	0.2512	**reject**
4	12/1/96	29.49	0.2583	0.1	0.1572	**reject**
	2/1/99	29.90		0.05	0.1752	**reject**
				0.025	0.1907	**reject**
				0.01	0.2100	**reject**
				0.005	0.2229	**reject**
				0.001	0.2512	**reject**

Table T-1. Results of the Kolmogorov-Smirnov Two-Sample Test during the accumulation period for the Emerald Lake Watershed, continued.

Test Number	Date	Mean SWE (cm)	Test Statistic (D)	Level of Significance ( )	Critical D Value (D)	Decision
5	2/1/94	22.41	0.1782	0.1	0.1572	**reject**
	1/1/99	23.97		0.05	0.1752	**reject**
				0.025	0.1907	**accept**
				0.01	0.2100	**accept**
				0.005	0.2229	**accept**
				0.001	0.2512	**accept**
6	1/1/93	30.32	0.4267	0.1	0.1572	**reject**
	1/16/98	31.83		0.05	0.1752	**reject**
				0.025	0.1907	**reject**
				0.01	0.2100	**reject**
				0.005	0.2229	**reject**
				0.001	0.2512	**reject**

Table T-2. Results of the Kolmogorov-Smirnov Two-Sample Test during the ablation period for the Emerald Lake Watershed (n = 304).

Test Number	Date	Mean SWE (cm)	Test Statistic (D)	Level of Significance ( )	Critical D Value (D)	Decision
1	7/1/93	30.69	0.3471	0.1	0.1572	**reject**
	6/1/99	31.48		0.05	0.1752	**reject**
				0.025	0.1907	**reject**
				0.01	0.2100	**reject**
				0.005	0.2229	**reject**
				0.001	0.2512	**reject**
2	6/16/93	39.66	0.5207	0.1	0.1572	**reject**
	6/16/94	39.97		0.05	0.1752	**reject**
				0.025	0.1907	**reject**
				0.01	0.2100	**reject**
				0.005	0.2229	**reject**
				0.001	0.2512	**reject**

Appendix U

Snow Water Equivalent and Meteorological Ranking for HRUs With SNOTEL Stations for the Upper Rio Grande Watershed

Date	HRU	SWE Rank	Precipitation Rank	Wind Speed Rank	Average Air Temperature Rank
11/1/93	1	3	3	1	3
	40	2	2	3	2
	50	1	1	3	1
12/1/93	1	3	2	1	2
	40	2	3	3	3
	50	1	1	3	1
1/1/94	1	2	2	1	2
	40	3	3	3	3
	50	1	1	3	1
2/1/94	1	2	1	1	3
	40	3	3	3	2
	50	1	2	3	1
3/1/94	1	2	2	1	2
	40	3	3	3	3
	50	1	1	3	1
4/1/94	1	2	3	1	3
	40	3	2	3	2
	50	1	1	3	1
5/1/94	1	3	3	1	3
	40	2	2	3	2
	50	1	1	3	1
6/1/94	1	3	2	1	2
	40	2	1	3	3
	50	1	3	3	1

Date	HRU	SWE Rank	Precipitation Rank	Wind Speed Rank	Air Temperature Rank
11/1/94	1	3	3	1	3
	40	2	2	3	2
	50	1	1	3	1
12/1/94	1	3	2	1	3
	40	2	3	3	2
	50	1	1	3	1
1/1/95	1	2	2	1	2
	40	3	3	3	3
	50	1	1	3	1
2/1/95	1	2	2	1	3
	40	3	3	3	2
	50	1	1	3	1
3/1/95	1	2	2	1	3
	40	3	3	3	2
	50	1	1	3	1
4/1/95	1	2	2	1	3
	40	3	3	3	2
	50	1	1	3	1
5/1/95	1	2	3	1	2
	40	3	1	3	3
	50	1	2	3	1
6/1/95	1	2	2	1	3
	40	3	3	3	2
	50	1	1	3	1

Date	HRU	SWE Rank	Precipitation Rank	Wind Speed Rank	Air Temperature Rank
11/1/95	1	2	3	1	2
	40	3	2	3	3
	50	1	1	3	1
12/1/95	1	3	1	1	3
	40	1	3	3	2
	50	2	2	3	1
1/1/96	1	1	1	1	3
	40	3	3	3	2
	50	2	2	3	1
2/1/96	1	1	2	1	2
	40	3	3	3	3
	50	2	1	3	1
3/1/96	1	2	3	1	3
	40	3	2	3	2
	50	1	1	3	1
4/1/96	1	2	2	1	3
	40	3	3	3	2
	50	1	1	3	1
5/1/96	1	1	2	1	3
	40	3	3	3	2
	50	2	1	3	1
6/1/96	1	3	1	1	2
	40	3	3	3	3
	50	1	2	3	1

Date	HRU	SWE Rank	Precipitation Rank	Wind Speed Rank	Air Temperature Rank
11/1/96	1	1	1	1	3
	40	2	2	3	2
	50	3	3	3	1
12/1/96	1	2	3	1	2
	40	3	2	3	3
	50	1	1	3	1
1/1/97	1	1	2	1	2
	40	3	3	3	3
	50	2	1	3	1
2/1/97	1	2	2	1	3
	40	3	3	3	2
	50	1	1	3	1
3/1/97	1	2	2	1	3
	40	3	3	3	2
	50	1	1	3	1
4/1/97	1	2	3	1	2
	40	3	2	3	3
	50	1	1	3	1
5/1/97	1	2	2	1	3
	40	3	3	3	2
	50	1	1	3	1
6/1/97	1	3	1	1	3
	40	2	3	3	2
	50	1	2	3	1

Date	HRU	SWE Rank	Precipitation Rank	Wind Speed Rank	Air Temperature Rank
11/1/97	1	3	3	1	3
	40	1	2	3	2
	50	2	1	3	1
12/1/97	1	3	2	1	2
	40	2	3	3	3
	50	1	1	3	1
1/1/98	1	3	2	1	3
	40	2	3	3	2
	50	1	1	3	1
2/1/98	1	2	1	1	2
	40	3	3	3	3
	50	1	2	3	1
3/1/98	1	2	3	1	3
	40	3	2	3	2
	50	1	1	3	1
4/1/98	1	2	3	1	3
	40	3	2	3	2
	50	1	1	3	1
5/1/98	1	2	3	1	2
	40	3	1	3	3
	50	1	2	3	1
6/1/98	1	2	1	1	2
	40	3	3	3	3
	50	1	2	3	1

Date	HRU	SWE Rank	Precipitation Rank	Wind Speed Rank	Air Temperature Rank
11/1/98	1	3	3	1	2
	40	2	2	3	3
	50	1	1	3	1
12/1/98	1	2	2	1	2
	40	3	3	3	3
	50	1	1	3	1
1/1/99	1	2	2	1	3
	40	3	3	3	2
	50	1	1	3	1
2/1/99	1	2	1	1	3
	40	3	3	3	2
	50	1	2	3	1
3/1/99	1	2	3	1	3
	40	3	2	3	2
	50	1	1	3	1
4/1/99	1	2	3	1	2
	40	3	2	3	3
	50	1	1	3	1
5/1/99	1	2	3	1	3
	40	3	1	3	2
	50	1	2	3	1
6/1/99	1	3	1	1	3
	40	2	3	3	2
	50	1	2	3	1

Date	HRU	SWE Rank	Precipitation Rank	Wind Speed Rank	Air Temperature Rank
11/1/99	1	1	1	1	3
	40	1	2	3	2
	50	1	3	3	1
12/1/99	1	1	2	1	2
	40	3	1	3	3
	50	2	3	3	1
1/1/00	1	1	2	1	2
	40	3	2	3	3
	50	2	3	3	1
2/1/00	1	1	1	1	3
	40	3	3	3	2
	50	2	2	3	1
3/1/00	1	1	2	1	3
	40	3	3	3	2
	50	2	1	3	1
4/1/00	1	1	1	1	2
	40	3	2	3	3
	50	2	3	3	1
5/1/00	1	1	2	1	3
	40	3	3	3	2
	50	2	1	3	1
6/1/00	1	3	1	1	2
	40	3	3	3	3
	50	1	2	3	1

Date	HRU	SWE Rank	Precipitation Rank	Wind Speed Rank	Air Temperature Rank
11/1/00	1	1	2	1	3
	40	3	3	3	2
	50	2	1	3	1
12/1/00	1	1	2	1	3
	40	3	3	3	2
	50	2	1	3	1
1/1/01	1	1	1	1	2
	40	3	3	3	3
	50	2	2	3	1
2/1/01	1	1	2	1	3
	40	3	3	3	2
	50	2	1	3	1
3/1/01	1	2	2	1	3
	40	3	3	3	2
	50	1	1	3	1
4/1/01	1	2	3	1	2
	40	3	1	3	3
	50	1	2	3	1
5/1/01	1	2	2	1	2
	40	3	3	3	3
	50	1	1	3	1
6/1/01	1	2	1	1	2
	40	3	3	3	3
	50	1	2	3	1

REFERENCES

Anderson, Eric A., 1973. National Weather Service River Forecast System - Snow Accumulation and Ablation Model. NOAA Technical Memorandum NWS HYDRO-17, U.S. Dept. Of Commerce, Silver Spring, Maryland, 217 pp.

Armstrong, B.A. and Williams, K., 1986. The Avalanche Book, Fulcrum Incorporated, Golden, Colorado.

Bloschl, G., 1998. "Scaling Issues in Snow Hydrology", Hydrologic Processes, Vol. 23, 1 - 43.

Brubaker, K., Rango, A. and Kustas, W. 1996. "Incorporating Radiation Inputs into the Snowmelt Runoff Model", Hydrological Processes, Vol. 10, 1329 - 1343.

Buttle, J.M. and McDonnell, J.J., 1987. "Modeling the Areal Depletion of Snow Cover in a Forested Catchment", Journal of Hydrology, Vol. 90, 43 - 60.

California Department of Water Resources (CDWR), 2003. "Precipitation/Snow Information." http://cdec.water.ca.gov/snow_rain.html (accessed October 2001).

Castruccio, P.A., et al., 1980. "Cost/Benefit Analysis for the Operational Applications of Satellite Snow Cover Observations", NASA CP - 2116, 185 -200.

Cline, D.W., Bales, R.C. and Dozier, J., 1998. "Estimating the Spatial Distribution of Snow in Mountain Basins Using Remote Sensing and Energy Balance Modeling", Water Resources Research, Vol. 34, No. 5, 1275 - 1285.

Copland, L., 1998. "The Use of Terrain Analysis in the Evaluation of Snow Cover Over an Alpine Glacier", Landform Monitoring, Modeling and Analysis, John Wiley and Sons Ltd., 385 - 403.

Davis, F.W., et. al., 1992. "Covariance of Biophysical Data With Digital Topographic and Land Use Maps Over the FIFE Site", Journal of Geophysical Research, Vol. 97, No. D17, 19009 - 19021.

Davis, R.E., et. al., 1997. "Spatially-Distributing Modeling of Snow in the Boreal Forest: A Simple Approach", 54th Eastern Snow Conference, 20 - 28.

Derksen, C., Ledrew, E., Walker, A. and Goodison, B., 1999. "Associations Between the Principal Spatial Modes of North American Prairie Snow Water Equivalent and Low-Frequency Atmospheric Circulation", 56th Eastern Snow Conference, 199 - 210.

Dingman, S. L., 1994. Physical Hydrology, Macmillan Publishing Co., New York, New York.

Dingman, S.L., et al., 1988. "Application of Kriging to Estimating Mean Annual Precipitation in a Region of Orographic Influence", American Water Resources Association, Vol. 24, No.2, 329 - 339.

Donald, J.R., Kouwen, N., Soulis, E.D. and Pietroniro, A., 1995. "A Land Cover-Based Snow Cover Representation for Distributed Hydrologic Models", Water Resources Research, Vol. 31, No. 4, 995 -1009.

Dubayah, R. and Rich, P.M., 1995. "Topographic Solar Radiation Models for GIS", International Journal of Geographical Information Systems, Vol. 9, No. 4, 405 - 419.

Dubayah, R., 1994. "Modeling a Solar Radiation Topoclimatology for the Rio Grande River Basin", Journal of Vegetation Science, Vol 5, 627 - 640.

Dunne, T., and Leopold, L.B., 1978. Water In Environmental Planning, W.H. Freeman and Company, San Francisco, California, 467 p.

Elder, K., Dozier, J. and Michaelsen, J., 1989. "Spatial and Temporal Variation of Net Snow Accumulation in a Small Alpine Watershed, Emerald Lake Basin, Sierra Nevada, California, USA", International Glaciological Society, Vol. 21, 56 - 63.

Evans, B.M., et. al., 1989. "Spatial Interrelationships Between Terrain, Snow Distribution and Vegetation Patterns at an Arctic Foothills in Alaska", Holarctic Ecology, Vol. 12, 270 - 278.

Ferris, J.S. and Congalton, R.G., 1989. "Satellite and GIS Estimates of Colorado River Basin Snowpack", Photogrammetric Engineering and Remote Sensing, Vol. 55, No. 11, 1629 - 1635.

Fohn, P., et al., 1977. "Evaluation and Comparison of Statistical and Conventional Methods of Forecasting Avalanche Hazard", Journal of Glaciology, Vol. 19, 375 - 387.

Foster, J., et al., 1996. "Snow Cover and Snow Mass Intercomparisons of General Circulation Models and Remotely Sensed Datasets", Journal of Climate, Vol. 9, 409 - 425.

Gorokhovich,Y., et al., 2000. "Spatially Distributed Modeling of Stream Flow During Storm Events", American Water Resources Association, Vol. 36, No. 3, 523 - 539.

Gray, D. M. and Male, D. H., 1981. Handbook of Snow: Principles, Processes, Management and Use, Pergamon Press, New York, New York.

Haan, C.T., 1977. Statistical Methods in Hydrology, Iowa State University Press, Ames, Iowa, 327 p.

Hedstrom, N.R. and Pomeroy, J.W., 1998. "Measurements and Modelling of Snow Interception in the Boreal Forest", Hydrological Processes, Vol. 12, 1611 - 1625.

Hellstrom, R.A., 1999. "Representation in Forest Cover in a Physically Based Snowmelt Model, Phase I", 56th Eastern Snow Conference, 215 - 231.

Hopfinger, E.J. and Tochon-Danguy, J, 1991. "A Model Study of Powder-Snow Avalanches", Journal of Glaciology, Vol. 19, 343 - 356.

Jeton, A.E. and Smith, J.L., 1994. "Development of Watershed Models for Two Sierra Nevada Basins Using a Geographic Information System", American Water Resources Association, Vol. 29, No.6, 923 - 932.

Kirnbauer, R., Bloschl, G. and Gutknecht, D., 1993. "Entering the Era of Distributed Snow Models", Nordic Hydrology, Vol. 25, 1 - 24.

Konig, M. and Sturm, M., 1998. "Mapping Snow Distribution in the Alaskan Arctic Using Aerial Photography and Topographic Relationships", Water Resources Research, Vol. 34, No. 12, 3471 - 3483.

Kouwen, N., et al., 1993. "Grouped Response Units for Distributed Hydrologic Modeling", Journal of Water Resources Planning and Management, Vol. 119, No. 3, 289 - 305.

Leydecker, A. And Sickman, J., 1999. "Distribution of Snow in the Upper Marble Fork Basin, California", presented as poster at the 1999 AGU fall meeting, San Francisco, California.

Li, L. and Pomeroy, J.W., 1997. "Probability of Occurrence of Blowing Snow", Journal of Geophysical Research, Vol. 102, No. D18, 21955 - 21964.

Li, L. and Pomeroy, J.W., 1997. "Estimates of Threshold Wind Speeds for Snow Transport Using Meteorological Data", American Meteorological Society, Vol. 36, 205 - 213.

Liston, G. E., 1999. "Interrelationships among Snow Distribution, Snowmelt, and Snow Cover Depletion: Implications for Atmospheric, Hydrologic, and Ecologic Modeling", Journal of Applied Meteorology, Vol. 38, 1474 -1487.

Liston, G. E. and Sturm, M., 1998. "A Snow-Transport Model for Complex Terrain", Journal of Glaciology, Vol. 48, 498 - 516.

Luce, C.H., Tarboton, D.G. and Cooley, K.R., 1998. "Subgrid Parameterization of Snow Distribution for an Energy and Mass Balance Snow Cover Model", Hydrological Processes, Vol. 14, 1054 -1071.

Luce, C.H. and Tarboton, D.G., 2000. "Scaling Up Snowpack Accumulation and Melt Models", submitted to Water Resources Research.

Lundberg, A., Calder, I. and Harding, R., 1998. "Evaporation of Intercepted Snow: Measurement and Modeling", Journal of Hydrology, Vol. 206, 151 - 163.

Maidment, D.R., 1993. Handbook of Hydrology, McGraw-Hill Inc., New York, New York.

Martinec, J. and Rango, A., 1981. "Areal Distribution of Snow Water Equivalent Evaluated by Snow Cover Monitoring", Water Resources Research, Vol. 17, 1480 - 1488.

Mashriqui, H.S. and Cruise, J.F., 1997. "Sediment Yield Modeling by Grouped Response Units", Journal of Water Resources Planning and Management, 95 - 104.

McCuen, R.H., 2000. "Lessons from the Classics of Hydrologic Modeling". Unpublished report of the Civil and Environmental Engineering Department of the University of Maryland.

McCuen, R.H., 1989. Hydrologic Analysis and Design, Prentice-Hall, Englewood Cliffs, New Jersey, 867 p.

McClung, D. and Schaerer, P., 1993. The Avalanche Handbook, The Mountaineers, Seattle, Washington.

Meister, R., 1985. "Density of New Snow and its Dependence on Air Temperature and Wind", Workshop on the Correction of Precipitation Measurements, April 1 - 3, Zurich, 73 - 80.

Melloh, R.A., U.S. Army Corps of Engineers, 1999. "A Synopsis and Comparison of Selected Snowmelt Algorithms", CRREL Report 99 - 8. Cold Regions Research and Engineering Laboratory, Hanover, New Hampshire.

National Climatic Data Center (NCDC), 2003. "Climate - Radar Data Inventories." http://www.ncdc.noaa.gov/oa/climate/stationlocator.html (accessed April 2001).

National Weather Service - National Operational Hydrological Remote Sensing Center (NOHRSC), 2003. "GIS Data Sets." http://www.nohrsc.nws.gov/gis_datasets.html (accessed April 2001).

Pomeroy, J.W. and Essery, R.L., 1999. "Turbulent Fluxes During Blowing Snow: Field Tests of Model Sublimation Predictions", Hydrologic Processes, Vol. 13, 2963 - 2975.

Pomeroy, J.W., et al., 1998. "Coupled Modeling of Forest Snow Interception and Sublimation", Hydrological Processes, Vol. 12, 2317 - 2337.

Pratap, S. and Pratap, V.P., 2001. Snow and Glacier Hydrology, Kluwer Academic Publishers, Boston, Massachusetts.

Rango, A., 1996. "Spaceborne Remote Sensing for Snow Hydrology Applications", Hydrological Sciences, Vol. 4, 477 - 494.

Rango, A., 1998. "Operational Applications of Remote Sensing in Hydrology: Success, Prospects and Problems", Hydrological Science, Vol. 43, 947 - 968.

Schmidt, R.A., 1980. "Threshold Wind Speeds and Elastic Impact in Snow Transport", Journal of Glaciology, Vol. 26, No. 94, 453 - 467.

Schmidt, R.A., 1984. "Transport Rate of Drifting Snow and the Mean Wind Speed Profile", Journal of Meteorology, Vol. 34, 213 - 241.

Sierra Nevada Watershed Group, 1999. "Emerald Lake Watershed" http://www.icess.ucsb.edu/swg/sites/emerald_desc.html (accessed December 2001).

Sevruk, B., 1985. "Conversion of Snowfall Depths to Water Equivalents in the Swiss Alps", Workshop on the Correction of Precipitation Measurements, April 1 - 3, Zurich, 81 - 88.

Shook, K., Gray, D.M. and Pomeroy, J.W., 1993. "Temporal Variation in Snowcover Area During Melt in Prairie and Alpine Environments", Nordic Hydrology, Vol 24, 183 - 198.

Skaugen, T., 1999. "Estimating the Mean Areal Snow Water Equivalent by Integration in Time and Space", Hydrological Processes, Vol. 13, 2051 - 2066.

Slaughter, C.W., et al., 1998. "Research Data Collection at the Reynolds Creek Experimental Watershed, Idaho, USA", USDA-ARS Northwest Watershed Research Center, Boise, Idaho

Sulakvelidze, G. K. and Dolov, M. A., 1973. Physics of Snow Avalanches and Glaciers, Indian National Scientific Documentation Center, New Delhi, India.

Swamy, A.N. and Brivio P.A., 1997. "Modeling Runoff Using Optical Satellite Remote Sensing Data in a High Mountainous Alpine Catchment of Italy", Hydrological Processes, Vol. 11, 1475 -1491.

Tarboton, D.G. and Luce, C.H., 1996."Utah Energy Balance Snow Accumulation and Melt Model", Computer Model Technical Description and User Guide. USDA Forest Service.

Thornton, P.E., Running, S.W. and White, M.A., 1997. "Generating Surfaces of Daily Meteorological Variables Over Large Regions of Complex Terrain", Journal of Hydrology, Vol. 190, 214 - 251.

U.S. Army Corps of Engineers, 1956. "Snow Hydrology, Summary Report of the Snow Investigations", U.S. Army Corps of Engineers, North Pacific Division, Portland, Oregon.

U. S. Department of Agriculture - Agricultural Research Services (USDA - ARS), 2003. "ARS Project: Climate, Watershed, and Streamflow Processess." http://www.ars.usda.gov/research/projects/projects.html (accessed July 2001).

U.S. Environmental Protection Agency (USEPA), 2003. "Environmental Information Management System". http://www.epa.gov/eims (accessed May 2001).

U.S. Geological Survey (USGS), 2003. "USGS Geography Information: Home Page." http://mapping.usgs.gov (accessed February 2001).

Walland, D.J. and Simmonds, I., 1996. "Sub-Grid-Scale Topography and the Simulation of Northern Hemisphere Snow Cover", International Journal of Climatology, Vol. 16, 961 - 982.

Williams, K.S. and Tarboton, D.G., 1998. "The ABCs of Snowmelt: A Topographically Factorized Energy Component Snowmelt Model", Hydrological Processes, Vol. 13, 1905 -1920.

Yamazaki, T. and Kondo, J., 1992. "The Snowmelt and Heat Balance in Snow-Covered Forested Areas", Journal of Applied Meteorology, Vol. 31, 1322 - 1327.

Zuzel, J.F. and Cox, L.M., 1975. "Relative Importance of Meteorological Variables in Snowmelt", Water Resources Research, Vol. 11, No. 1, 174 - 176.